

Norwegian University of Life Sciences
Faculty of Biosciences
Department of Animal and Aquacultural Sciences (IHA)

Philosophiae Doctor (PhD)
Thesis 2023:67

Focal dark spots in the skeletal muscle of Atlantic salmon – involvement of rib abnormalities, environmental factors, and local immune responses

Mørke filétflekker i atlantisk laks - betydningen av ribbeinsavvik, miljøfaktorer og lokale immunresponser

Raúl Jiménez-Guerrero

Focal dark spots in the skeletal muscle of Atlantic salmon – involvement of rib abnormalities, environmental factors, and local immune responses

Mørke filétflekker i atlantisk laks -
betydningen av ribbeinsavvik, miljøfaktorer og lokale immunresponser

Philosophiae Doctor (PhD) Thesis

Raúl Jiménez-Guerrero

Norwegian University of Life Sciences
Faculty of Biosciences
Department of Animal and Aquacultural Sciences (IHA)

Ås (2023)



Thesis number 2023:67

ISSN 1894-6402

ISBN 978-82-575-2097-7

Supervisors and Evaluation Committee

Supervisors

Prof. Turid Mørkøre

Department of Animal and Aquacultural Sciences

Faculty of Biosciences

Norwegian University of Life Sciences

P.O. Box 5003 NMBU, 1432 Ås, Norway

Dr. Grete Bæverfjord

Department of Nutrition and feed technology

Nofima AS

Sjølsengvegen 22, 6600 Sunndalsøra, Norway

Prof. Øystein Evensen

Department of Paraclinical Sciences

Faculty of Veterinary Medicine

Norwegian University of Life Sciences

P.O. Box 5003 NMBU, 1433 Ås, Norway

Evaluation committee

Dr. Hamish Rodger

PatoGen Fish Health Services Ltd.

Courthouse Road, Kinvara, Co. Galway, H91N9CT, Ireland

Ass. Prof. Marit Bjørnevik

Faculty of Biosciences and Aquaculture

Nord University

Universitetsalléen 11, 8026 Bodø, Norway

Committee coordinator

Ass. Prof. Matthew Petter Kent

Department of Animal and Aquacultural Sciences

Centre for Integrative Genetics

Faculty of Biosciences

Norwegian University of Life Sciences

P.O. Box 5003 NMBU, 1432 Ås, Norway

Acknowledgements

The enigma of dark spots - "*melaninflekke*" or "*melanosis*" - represents perhaps the most profound puzzle in salmon farming. It is the kind of mystery that would ignite the imagination and fuel any researcher's determination. Like a cosmic black hole, as dark and beautiful as dangerous and enigmatic, but with the potential to harbor answers to numerous pivotal questions. Just as astronomers delve into the depths of the universe, we probe into the darkness of these events, seeking to illuminate the unknown. On the 12th of October 2019, after intense training, the rocket called "Ph. D." ignited its engines, setting a course towards a supermassive black hole. Only such a journey, taking us to the very edge of its event horizon, would let us to better understand the heart of this mystery.

It was a 4-year journey at light speed. During the mission, we got an impact from an asteroid carrying an unknown virus - we called it "COVID-19" - that infected the entire crew, losing critical personnel and instruments. Yet, the pandemic was not the only adversary we faced. The tense atmosphere on board led to multiple instances of sabotage. The situation became so critical that the spaceship almost burned by its own fire. We had to fix a broken airplane in the middle of a flight. Your presence here, reading this thesis, is a testament to our unwavering determination and resilience in preserving the mission, though we had to sacrifice a lot: time, samples, analysis, stays abroad, personal beliefs, and trust.

I want to express my gratitude and acknowledge the effort that everyone has put together in this endeavor. First, to my supervisors, the captains. Each of you has provided me with an unbailable set of tools and skills in many different levels of aquaculture science, from fish nutrition to health and product quality. I am the fish veterinarian that I am because of you. Prof. Turid Mørkøre, you have been my mentor and boss for the last eight years. Your passion and enthusiasm for aquaculture and attitude with the students are admirable. You have taught me enormous amounts of valuable knowledge and shown what "skin in the game" means. If that knowledge was money, I think I would be one of the wealthiest people in Norway. You have also taught me to doubt and question the big dogmas in science and swim against the current because that is what salmon do. Crazy problems require crazy ideas. Besides the bad weather, you always acted positive and full of hope, taking care of me, and helping me to stand when my body could continue. Thank

you for allowing me to meet the Norwegian salmon industry. Thank you for your blind trust in me, and sorry for being your most stubborn student. Dr. Grete Bæverfjord, you have given me superpowers by letting me see the world through your X-ray glasses, which is probably the dream of any veterinarian. This Ph. D. was extremely complicated and required the best fish orthopedics and nutrition expertise. Without your trained eyes, it could not have been possible. I am fortunate to have you as a supervisor. Because of your help and guidance, I can now appreciate bones' beauty and potential. You managed to be an excellent supervisor from a distance (which is not easy), always there to answer my questions. Thank you. Prof. Øystein Evensen, you have been following me since my master's thesis exploring the unknown of melanin. You have drastically improved my histology and pathology skills and terminology, something that I did not fully control at the beginning of this journey. Although COVID-19 made part of our experimental part more complicated, you managed to surf the tsunami! You have given me excellent tools that I will need in the future. All of you have been outstanding supervisors, guiding me through the cold and dark winter, and staunchly maintaining publishing quality and academic integrity in situations when research ethics were poor. This thesis and my skills are the averages of yours. Thank you.

I want also to express my immense gratitude to the coauthors of this work. Dr. Aleksei Krasnov, Dr. Pierre Boudinot, Dr. Christian Karlsen, Dr. Sergey Afanasyev, Dr. Thomas Larsson, Dr. Kristind Hamre, Dr. Jens-Erik Dessen and Kjellrun-Hoås Gannestad. Special mention to Dr. Aleksei Krasnov and Dr. Pierre Boudinot; you have shown me the beauty of B cells through unique techniques and have always provided support and feedback to many of my naïve questions. Prof. Øivind Andersen for helping to review some manuscripts. Similarly, I would like to thank the entire technical support for the excellent work and all the research partners. Thanks to Lerøy Midt AS, with special mention to Helge Endresen. Kjellrun-Hoås Gannestad from Nofima, you made X-ray of hundreds of salmon possible. The excellent quality of the images in this work is thanks to your work. I want to remark on the excellent work during sampling provided by Dr. Thomas Larsson, and Dr. Jens-Erik Dessen from Nofima and Håkon Torsvik from NMBU. Thank you, Vibeke Voldvik and Marianne Hansen from Nofima, for your RT-qPCR and Ig sequencing expertise. Miroslava Hansen from the Norwegian Veterinary Institute, you are the “Michelangelo” of histology preparation.

To my colleges at NMBU, Sumeng Galdat, Julia Formanowicz, Marte Røsvik, Dr. Byron Maximiliano Morales Lange, Dr. Sérgio Rocha, Øystein W. Milvang and many more. To the experts (also friends) at Nofima. My head (but also this thesis) is a mosaic with pieces of all of you. Special mention to Dr. Thomas Larsson. You were my first college at Nofima, always there to help me like an older brother. Some of you had to share office space/coffee breaks with me and listen to my student dramas with always a smile and supportive words. You always were there when I needed it, which was very often. So many wise words and good moments. To my friends in Norway and Spain. You were the non-academic support of this work. Great moments before and during the Ph. D. It has been great luck to share part of the journey with you. Truly amazing people. Thank you.

To my family, the spectators of this adventure. You have suffered and enjoyed with me from a distance. You have always been my true reference. You taught me great human values and never limited my ambitions, though that meant being far from home. You made up the air when the wind didn't blow. You are an example of strength and passion. You taught me a love for animals. I could not have managed through the most challenging moments without your support. I love you Mom, I love you Dad, I love you sister, I love you grandpas. This work is also yours.

Lastly, I want to thank my younger self, Raúl, whose dreams took me from a small fish tank with guppies at my grandparent's home to this vast and incredible journey. He always wanted to have magic superpowers and understood that being a scientist was the best way. After all, magic is a science we do not yet understand. Your creativity and passion fueled this engine, put off the fire, and saved the mission several times. This Ph. D. thesis proves what you can achieve and become. **We did it.**

Thank you all!

I hope you enjoy the reading,

From wherever there is water, November 2023

Raúl,

<'')))))-{

Table of contents

Supervisors and Evaluation Committee	i
Acknowledgements	iii
Table of contents	vii
1 Abbreviations and definitions	1
2 Abstract	5
3 Sammendrag.....	7
4 List of publications.....	11
5 Synopsis.....	13
5.1 General introduction	13
5.1.1 Focal dark spots.....	14
5.1.2 The anatomy of the abdominal wall.....	18
5.1.3 Skeletal pathology in salmonids.....	22
5.1.4 Regeneration and repair in the musculoskeletal system.....	22
5.1.5 Melanin.....	29
5.1.6 Knowledge gaps.....	30
5.1.7 Objectives and hypothesis	31
5.2 Experimental overview	31
5.3 Methodological considerations	32
5.4 Main results and general discussion	42
5.4.1 Atlantic salmon ribs	43
5.4.2 Understanding rib abnormalities.....	47
5.4.3 Relationship between rib abnormalities and focal dark spots.....	53
5.4.4 The effects of the environment on focal dark spots.....	57
5.4.5 The role of B cells on focal dark spot development.....	62

5.4.6	Implications for the aquaculture industry	66
5.5	Identified gaps for future studies	68
5.6	Conclusions	69
6	References	71
7	Appendices	85
7.1	Appendix – 1: Supplementary table.....	85
7.2	Appendix – 2: Supplementary table.....	86
7.3	Appendix – 3: Supplementary table.....	87
7.4	Appendix – 4: Supplementary figure.....	88
7.5	Appendix – 5: Papers I – III	89

1 Abbreviations and definitions

Abs	Antibodies
APCs	Antigen-processing and presentation cells
arg2	Arginase-2
BCR	B cell receptor
blimp1	Lymphocyte-induced maturation protein 1
blk	B cell lymphocyte kinase
BM-MSCs	Bone marrow-derived mesenchymal stromal cells
btla	B and T lymphocyte attenuator
Ca	Calcium
CCPs	Critical control points
CD	Cluster of differentiation
cd28	Cluster of differentiation 28
cd40	Cluster of differentiation 40
CD40L	Cluster of differentiation 40 ligand
cd79	Cluster of differentiation 79
cd83	Cluster of differentiation 83
CDR3	Complementarity determining region 3
CF	Cumulative frequencies
C_H	Constant regions of the heavy chain
C_L	Constant regions of the light chain
col1a1a	Collagen type I alpha 1a chain
col1a1b	Collagen type I alpha 1b chain
col1a2	Collagen type I alpha 2 chain
col2a1	Collagen type II alpha 1 chain
csfr	Colony-stimulating factor receptor
ctla	Cytotoxic T-lymphocyte-associated antigen
Cu	Copper

DAMPs	Damage-associated molecular patterns
DCs	Dendritic cells
DHA	Docosahexaenoic acid
DS	Focal dark spots
EDTA	Ethylenediaminetetraacetic acid
ef1a	Elongation factor 1-alpha
EPA	Eicosapentaenoic acid
Fe	Iron
GzmA	Granzyme A
ICP-MS	Inductively coupled plasma-mass spectrometry
ICP-OES	Inductively coupled plasma mass spectrometry
IFN-γ	Interferon-gamma
Ig	Immunoglobulin
igd	Immunoglobulin D
Ig-seq	High-throughput sequencing of immunoglobulin genes
igt	Immunoglobulin T
IL-4	Interleukin 4
IL-6	Interleukin 6
IL-10	Interleukin 10
IL-12	Interleukin 12
IL-13	Interleukin 13
IL-1β	Interleukin 1 β
inos2	Nitric oxide synthase
K	Potassium
LPS	Lipopolysaccharide
MAMPs	Microbe-associated molecular patterns
MAMPs	Microbe-associated molecular patterns
marco	Macrophage receptor
MD-MSCs	Muscle-derived mesenchymal stromal cells
Mg	Magnesium
M-group	Marine-based diet

MHC	Major histocompatibility complex
mhc2	Major histocompatibility complex II
migm	Membrane-bound immunoglobulin M
MMCs	Melanomacrophage centers
Mn	Manganese
MP-AES	Agilent microwave plasma atomic emission spectrometers
MSCs	Mesenchymal stromal cells
Na	Sodium
NF-κB	Nuclear factor kappa-light-chain-enhancer
NQC	Norwegian quality cut
P	Phosphorus
PAMPs	Pathogen-associated molecular patterns
pax5	Paired box protein 5
P-group	Plant-based diet
PMCV	Piscine myocarditis virus
PRV-1	Piscine orthoreovirus-1
PUFAs	Polyunsaturated fatty acids
R&D	Research and development
RAS	Recirculating aquaculture systems
RNS	Nitrogen reactive species
ROS	Reactive oxygen species
RT-qPCR	Real-time quantitative reverse transcription polymerase chain reaction
SAV	Salmonid alphavirus
SAV-3	Salmonid alphavirus-3
Se	Selenium
sigm	Secretory immunoglobulin M
SPC	Soy protein concentrate
SPV	Segmental parietal veins
TCR	T cell receptor
TD	T cell-dependent
TGF-β	Transforming growth factor-beta

TI	T cell-independent
TNF-α	Tumor necrosis factor-alpha
VDJ	Variable-diversity-joining
VEGF	Vascular endothelial growth factor
V_H	Variable regions of the heavy chain
V_L	Variable regions of the light chain
Zn	Zinc

2 Abstract

Focal dark spots (DS) represent a major fillet quality issue, leading to significant economic losses in farmed Atlantic salmon (*Salmo salar* L.). DS typically appear as discoloured red/black areas in the anterior hypaxial skeletal muscle, with unknown aetiology. This thesis aims to investigate rib abnormalities and to study their potential association with DS. The thesis also aims to further understand the local immune response in DS by exploring the B cell traffic across different tissues and DS.

In **Paper I**, a classification system for rib abnormalities was developed, based on X-ray images of wild and salmon farmed in a commercial smolt farm, small experimental land-based tanks or commercial sea-cages. Rib cage explorations showed that the number of rib abnormalities doubled after transfer to sea-cages, primarily attributed to resorptive rib morphologies: generalized radiolucent and shorter ribs. Over time, the abnormalities gradually shifted towards fracture-like types, but the total number was maintained. Black DS were only found in salmon farmed in commercial sea-cages, coinciding with the environment with the highest prevalence of rib abnormalities. DS and rib abnormalities shared anatomical location (ribs 11 - 14). Although, rib abnormalities were more concentrated in distal parts, DS were more severe in mid-proximal parts. Black DS exhibited twice as many rib abnormalities as unstained tissue, primarily as various forms of bent and broken ribs, especially of flatter DS shapes. However, DS were also found without any sign of abnormal ribs or fractures. There were signs of recurrent injury processes and pathological interconnections in DS with rib fractures and mechanical deformations. It is concluded that there is an association between rib abnormalities and DS, but additional factors are involved in the DS development.

In **Paper II**, different methods were used to assess morphological rib abnormalities of salmon within the broader musculoskeletal framework. The study focused on harvest-sized salmon (3 kg) reared in experimental tanks on land and fed either marine- or plant-based ingredients during smoltification. Histology showed that 29 % of sampled ribs presented radiolucency without nearby tissue inflammation. The changes involved cartilage core transformation and osteolysis, disorganized appositional growth, collagen and osteoid deposits in compact bone, and increased external collagen layer – resulting in 18 – 20 % increased rib diameter. Salmon fed plant ingredients showed more generalized

radiolucency and axis deviations, cooccurring with softer ribs with decreased phosphorus content, and softer skeletal muscle. Rib morphology was more sensitive to dietary composition during smoltification than vertebrae. Small DS were equally found in both dietary groups. The research expands the understanding of the two most prevalent rib abnormalities in Atlantic salmon, axis deviations and especially generalized radiolucency, linking these changes to altered rib development, degeneration, and likely osteomalacia.

Paper III combined RT-qPCR of 16 immune genes and Ig-seq of IgM CDR3 sequences in eight fish from **Paper I** with different DS morphologies. The flatter the DS, the higher the cumulative frequency (CF) of shared B cell clonotypes within DS, gene expression for macrophage, activation of CD4⁺ and CD8⁺ cells, and B cell maturation and activity. However, the flatter the DS, the lower the expression of dendritic cells and lymphocyte attenuator genes. Expression of immune genes was generally lower in DS than in the lymphatic organs, head kidney, and spleen, but higher than in normal skeletal muscle. At the earliest stage (increased *migm* and *sigm* ratio and minor CF with other tissues), naïve B cells likely migrated from visceral peritoneum fat and skeletal muscle to DS after injury. In further differentiation stages (decreased *migm* and *sigm* ratio and high expression of *pax5* and *cd79*), activated B cells from DS were disseminated to the head kidney, visceral peritoneum fat, and spleen. Traffic and expression of immune genes decreased at later stages. B cells differentiation and traffic could be due to a local infectious process, but no bacterial RNA or DNA were detected in DS. Viruses like SAV (7:8), and PRV-1 (2:8) were found in DS, but without correlation to DS morphology, CF, or immune gene expression.

In summary, this thesis demonstrates that rib or muscle damage are likely the primary cause of DS. The rearing environment significantly impacts DS aetiology as more severe rib abnormalities and higher DS prevalence are observed in commercial sea-cages than in land-based tanks. Environmentally unspecific immunostimulants common in commercial sea-cages/practices may also affect melanogenesis of injuries. The composition of the diet during smoltification does not influence the development of DS, though it has modulatory effects on long-term musculoskeletal health, manifested by abnormal rib morphology and softer muscle. The location of the injury in the rib cage and local adaptive immune responses are important in developing the condition. B cells primarily migrate from the visceral peritoneum fat and skeletal muscle to DS initiated by unidentified antigens.

The thesis highlights the need to create optimized farming conditions to prevent musculoskeletal damage and mitigate the development of DS.

3 Sammendrag

Mørke filétflekker (DS) er en kvalitetsutfordring som fører til betydelige økonomiske tap for oppdrettet atlantisk laks (*Salmo salar* L.). DS kan være røde eller svarte/grå og de sitter oftest i den fremre delen av bukområdet av fileten. Årsaken til at flekkene oppstår er ukjent. Formålet med denne avhandlingen var å undersøke morfologiske ribbeinsavvik i laks og deres mulige sammenheng med forekomsten av DS. Avhandlingen tok også sikte på å forstå den lokale immunresponsen i DS ved å utforske B-celletrafikken mellom ulike vev og DS.

I **Paper I** ble det utviklet et klassifiseringssystem for ribbeinsavvik, basert på røntgenbilder av villaks og laks oppdrettet i ferskvann og i sjø. Forekomsten av morfologiske ribbeinsavvik dobles seg etter overføring fra ferskvann til kommersielle merder i sjø, men ikke for laks overført til små forsøkskar på land med sjøvann. Ribbeinsavvikene var primært resorptive: ribbein med sentrale oppklaringer og forkortede ribbein. Over tid endret de morfologiske avvikene seg gradvis mot bruddlignende typer, men det totale antallet avvik ble opprettholdt. Svarte DS ble bare funnet i laks oppdrettet i sjømerder, sammenfallende med økt forekomst av ribbeinsavvik. Den høyeste forekomsten av både DS og ribbeinsavvik var på samme anatomiske område, ved ribbein 11 – 14. Selv om forekomsten av ribbeinsavvik var høyest i distale delen av ribbeina, var DS mer alvorlig i midt-proximale delen. Svarte DS hadde dobbelt så mange ribbeinsavvik som normalt vev, primært bøyde og brukne ribbein og særlig for flate DS. Imidlertid ble det også funnet DS uten tegn til ribbeinsavvik. I de mørke flekkene var det tegn til gjentatte skadeprosesser og patologi i form av ribbeinsbrudd og mekaniske deformasjoner. Det konkluderes med at det er en sammenheng mellom ribbeinsavvik og DS, men at ytterligere faktorer påvirker DS-utviklingen.

I **Paper II** ble morfologiske ribbeinsavvik av laks analysert ved histologiske og mekaniske metoder. Laksen som ble undersøkt veide 3 kg og var oppdrettet i små forsøkskar med sjøvann på land. Laksen ble føret med et standard kommersielt fôr, bortsett fra under smoltifiseringen i ferskvannsfasen da den fikk fôr med enten marine eller plantebaserte ingredienser. Histologiske undersøkelser viste at 29 % av de analyserte ribbeinene hadde sentral oppklaring, uten nærliggende vevsbetennelse. Kjennetegn for ribbein med sentral

oppklaring var bruskkjerne-transformasjon og osteolyse, uorganisert apposisjonell vekst, kollagen- og osteoidavsetninger i kompakt bein og økt ytre kollagenlag - noe som resulterte i 18 - 20 % økt ribbeinsdiameter. Laks fôret med plantebaserte ingredienser hadde generelt mer sentral oppklaring og akseavvik i ribbein, samtidig som ribbeina var mykere med redusert fosforinnhold, og filetene var bløtere. Ribbeinsmorfologien var mer sensitiv for fôrsammensetningen under smoltifisering enn ryggvirvlene. Små DS ble funnet i begge fôrgrupper. Resultatene fra dette forskningsarbeidet gir økt forståelse for akseavvik og fenomenet sentral oppklaring, som er de mest utbredte ribbeinsavvikene i atlantisk laks. De morfologiske avvikene knyttes til endret ribbeinsutvikling, degenerasjon og sannsynligvis tilstanden *osteomalasia*.

Paper III kombinerte RT-qPCR av 16 immungener og Ig-seq av IgM CDR3-sekvenser i åtte fisk fra **Paper I** som hadde DS med ulike morfologier. Jo flatere DS var, jo høyere var den kumulative frekvensen (CF) av delte klonotyper av B-celler. Det ble samtidig observert uttrykk av markørgener for makrofager, aktivering av CD4⁺ og CD8⁺ celler, og for B-cellemodning og aktivitet. Imidlertid, jo flatere DS, jo lavere uttrykk av markører til dendritiske celler og lymfocytthemmere. Uttrykk av immungener var generelt lavere i DS enn i nyre og milt, men høyere enn i normal skjelettmuskulatur. På det tidligste stadiet (en økt *migm/sigm*-ratio og en lavere CF til andre vev), migrerte sannsynligvis naive B-celler fra innvollsfett og skjelettmuskulatur til DS etter skade. I senere differensieringsstadier (en redusert *migm/sigm*-ratio og økt uttrykk av *pax5* og *cd79*), ble aktiverte B-celler fra DS spredt til nyre, innvollsfett og milt. Bevegelse mellom vev og uttrykk av immungener avtok i senere stadier. Differensiering av B-celler og bevegelse kan skyldes en lokal infeksjonsprosess, men hverken bakterielt RNA eller DNA ble påvist i DS. Virus som SAV (7:8), og PRV-1 (2:8) ble funnet i DS, men uten korrelasjon til DS-morfologi, CF, eller genuttrykk.

Oppsummert viser denne avhandlingen at skader på ribbein eller muskel sannsynligvis er årsaker til DS. Oppdrettsmiljøet påvirker DS-etologien betydelig ettersom mer alvorlige ribbeinavvik og høyere DS-prevalens ble observert i kommersielle merder i sjø enn i små forsøkskar på land. Uspesifikke immunstimulerende faktorer som kan finnes i oppdrettsmiljøet øker sannsynligvis graden av melanisering. Sammensetningen av dietten under smoltifisering påvirket ikke utviklingen av DS, selv om den hadde modulerende effekter på langsiktig muskel- og skjeletthelse, manifestert som ribbeinsavvik og bløt filet. Hvor skaden oppstår, samt lokale, adaptive immunresponser

har betydning for utviklingen av tilstanden. B-celler migrerer primært fra fettete i visceral peritoneum og skjelettmuskulaturen til DS, initiert av uidentifiserte antigener.

Avhandlingen understreker behovet for å skape optimale forhold i lakseoppdrett som kan forebygge muskel- og skjelettskader, og slik også redusere risikoen for utvikling av DS.

4 List of publications

The present thesis is built on the following publications (see Appendix 5), which are referenced in the text using Roman numbers:

Paper I

Jiménez-Guerrero, R. Baeverfjord, G., Evensen, Ø., Hamre, K., Larsson, T., Dessen, J.-E., Gannestad, K.-H., Mørkøre, T., 2022. **Rib abnormalities and their association with focal dark spots in Atlantic salmon filets.** *Aquaculture* 561, 738697. <https://doi.org/10.1016/j.aquaculture.2022.738697>

Paper II

Jiménez-Guerrero, R. Baeverfjord, G., Evensen, Ø., Mørkøre, T., 2023. **Understanding morphological rib abnormalities in Atlantic salmon.** (Submitted to *Aquaculture*).

Paper III

Jiménez-Guerrero, R. Karlsen, C., Boudinot, P., Afanasyev, S., Mørkøre, T., Krasnov, A. 2023. **Differentiation and traffic of IgM⁺ B cells between focal dark spots in skeletal muscle of Atlantic salmon, lymphoid and adipose tissues.** *Fish and Shellfish Immunology* 139, 108858. <https://doi.org/10.1016/j.fsi.2023.108858>

5 Synopsis

5.1 General introduction

Currently, aquaculture contributes to 49 % of the global production of aquatic animals ([FAO, 2022](#)). Atlantic salmon (*Salmo salar* L.) is dominant among all marine species, with 2.7 million tons and 32.6 % of farmed volume. The increasing demand and elevated prices for salmon have transformed the industry into one of the most profitable and technologically sophisticated farming sectors ([FAO, 2022](#)). Norway is the largest producer (1.6 million tons) ([Fiskeridirektoratet, 2021a](#)), with farmed salmon being a significant contributor to the national economy ([Fiskeridirektoratet, 2021b](#)).

Atlantic salmon production has evolved through genetic selection programs and changes of the farming systems and dietary composition. From the genetic side, growth, health, and quality traits have been the focus ([Næve et al., 2022](#)). However, faster growth may lead to metabolic changes and altered nutritional demands that may impact fish welfare. Regarding the environment, salmon have experienced modifications of their farming systems in the freshwater phase to expand the harvest seasons, such as hatching conditions ([Ojanguren, Reyes-Gavilán, & Muñoz, 1999](#)), parr growth, and time of smoltification ([Mørkøre & Rørvik, 2001](#); [Ytrestøyl et al., 2023](#)). Although most salmon are currently farmed in open net pens fully exposed to the environment, there is interest in expanding salmon farming in land-based systems due to environmental and health limitations. However, to minimize energy and water expenses in these novel systems, fish are raised at higher densities than in sea-cages, and water needs to be recirculated using recirculating aquaculture systems (RAS) ([Colt et al., 2008](#)). These factors can potentially impact water quality and fish welfare ([Calabrese et al., 2017](#)). Intensive systems can bring large amounts of physical stress in freshwater and seawater operations ([Noble et al., 2018](#)).

To make more sustainable and affordable diets, the composition of the salmon feed has drastically changed over the last decades from a very high inclusion of marine-based (in the form of fish oil and meal) to plant-based ingredients (principally rapeseed oil and soy protein concentrate (SPC)) ([Aas, Ytrestøyl, & Åsgård, 2019](#)). Marine ingredients are naturally rich in micronutrients ([Lall, 1995](#)), many of them essential and absent in plant sources; for instance, choline ([Hansen et al., 2020](#)) and polyunsaturated fatty acids

(PUFAs), such as eicosapentaenoic acid (EPA), and docosahexaenoic acid (DHA) ([Bou et al., 2017](#)). Plant-based ingredients may also lack balanced amino acids ([Hua & Bureau, 2019](#)) and mineral profiles ([Baeverfjord et al., 2018](#)), and contain higher levels of antinutrients that can impact health and induce low digestibility ([Hansen et al., 2020](#); [Krogdahl et al., 2010](#); [Lall, 2022](#)). Although the industry has fulfilled these known unbalances through supplementation, some micronutrients may be unknown and required in such small amounts that they are difficult to formulate in commercial diets.

5.1.1 Focal dark spots

Focal dark spots (DS) are the main quality problem in farmed Atlantic salmon, affecting ~16 % of the market's sized fillets ([Nordberg, 2018](#)). DS are presented as either fillet red- or black DS discolorations, as illustrated in Figure 1. Peritoneum DS of black/greyish appearance can also be observed, but they do not seem to impact fillet quality directly.

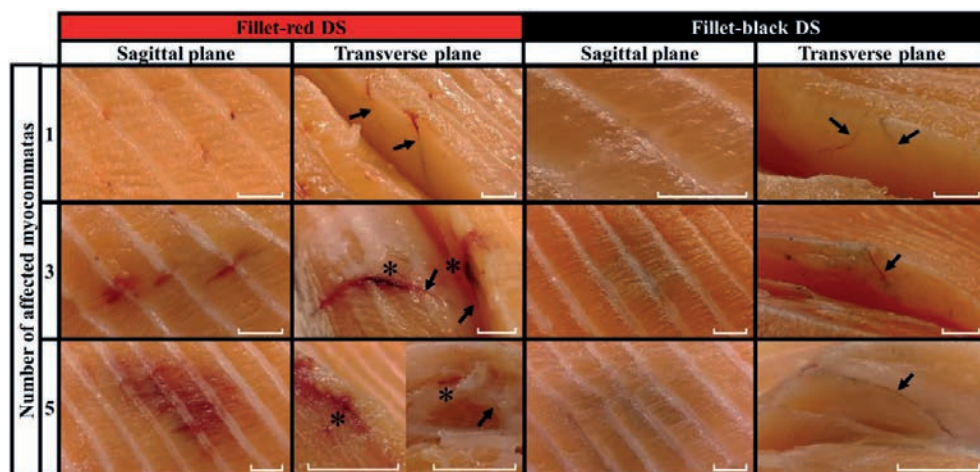


Figure 1. Haemorrhages/fillet-red and black focal dark spots (DS) of adult Atlantic salmon. Black asterisks indicate intramuscular haemorrhage. Black arrows indicate the position of blood vessels. White restricted bars on the bottom right corner of each picture show the scale, set to 1 cm. Unpublished material. Images from Raúl Jiménez-Guerrero.

DS are histologically identified as a chronic-active inflammatory process with infiltration of inflammatory cells, such as lymphocytes (B and T cells), major histocompatibility complex (MHC) class II positive cells (melanomacrophages), fibrosis, myocyte necrosis, fat infiltration, and or endo- and perimysial haemorrhage ([Bjørngen et al., 2019](#); [Krasnov et al., 2016](#); [Larsen et al., 2012](#)). On one hand, fillet-red DS (likely haemorrhages; early

stages) are characterized as a pro-inflammatory environment with M1 macrophages, downregulation of interleukin 10 (IL-10), upregulation of inducible nitric oxide synthase (*inos2*), MHC class I and II, with cluster of differentiation (CD) CD3⁺ and CD8⁺ cells, and granzyme A (GzmA) revealing targeted cytotoxic responses. On the other hand, fillet-black DS (later stages) are characterized as an anti-inflammatory environment with M2 melanomacrophages, where IL-10 and arginase-2 (*arg2*) are found to be upregulated ([Bjørngen et al., 2020](#); [Malik et al., 2021](#)). However, the same focal event may combine both fillet-red and black DS forms simultaneously, making its characterization difficult.

Individual factors such as gender (male) and sexual maturation have shown an increase in the prevalence of DS ([Mørkøre et al., 2015](#)), probably due to induced myocyte degeneration ([Salem et al., 2006, 2010](#)) caused by hormonal regulation. On the other hand, DS prevalence is challenging to control through genetic selection ([Mørkøre et al., 2015](#)).

The environment seems to be an important factor with large modulatory capacities in the development of DS. Indeed, DS have only been found so far in farmed salmon ([Bjørngen et al., 2015](#); [Mørkøre, 2012](#)). Four groups of environmental factors are found to affect DS: pathogens, farming practices, farming conditions, and diet.

Pathogens such as viruses and bacteria are colocalized with targeted immune responses in DS. *Piscine orthoreovirus-1* (PRV-1) has notably been the focus as it has been proposed as the aetiological factor ([Bjørngen et al., 2015](#); [Nylund et al., 2011](#)). However, the virus is not detected in all fish with DS, and fish do not develop DS after experimental inoculation ([Bjørngen et al., 2019](#); [Mørkøre et al., 2016](#)), but PRV-1 possibly enhances the local pro-inflammatory environment ([Malik et al., 2021](#)), which may explain why PRV-1 is especially prevalent in histologically severe DS ([Bjørngen et al., 2019](#)). *Salmonid alphavirus-3* (SAV-3) infections are associated with increased DS prevalence ([Mørkøre et al., 2016](#)). [Krasnov et al. \(2016\)](#) detected prokaryotic rRNA in DS. Though only in cardiac muscle, piscine myocarditis virus (PMCV) is associated with pathological pigmentation ([Fagerland et al., 2013](#)).

Farming practices such as immunoprophylaxis - intraperitoneal vaccines - has been discussed as a cause since the first DS reports. Vaccine adjuvants have been shown to produce melanised granulomas at the injection site ([Haugarvoll et al., 2010](#); [Koppang et al., 2005](#)). However, this is not a common reaction in the skeletal muscle of vaccinated fish, and DS can be found in either vaccinated or unvaccinated fish ([Berg et al., 2012](#);

[Larsen et al., 2014](#); [Mørkøre, 2012](#); [Mørkøre et al., 2015](#)). Impact injuries generate local haemorrhages that also increase the incidence of black DS in the long-term ([Mørkøre et al., 2022](#); [Mørkøre et al., 2015](#)). In organic farming, where fish are raised in lower densities (10 vs. 25 kg/m³), synthetic ingredients and chemicals such as copper impregnations are not used, and diets contain higher amounts of EPA and DHA, it is observed a reduction in the prevalence of DS ([Mørkøre, 2012](#); [Mørkøre, 2017](#)). The time in seawater increases the prevalence ([Bjørgen et al., 2019](#)). Handling large body weights at seawater transfer ([Lund et al., 2018](#)), transportation, and a long waiting time in the resting cages before slaughter may also increase DS prevalence ([Mørkøre, 2012](#)). This might be explained by proteolytic mechanisms in muscle after long-term stress ([Valenzuela et al., 2020](#); [Valenzuela et al., 2018](#)). Prolonged fasting also increases DS prevalence ([Mørkøre, 2012](#)), probably due to the switch to a catabolic metabolism producing cellular stress and degeneration ([Karatas, Onalan, & Yildirim, 2021](#)), which may be especially relevant in muscle pathologies.

The farming conditions have also proven to have significant effects. During freshwater, a less intense photoperiod (12:12 vs. 24:00; light:dark) and lower temperatures (8 vs. 16 °C) increase the size and prevalence of DS ([Mørkøre et al., 2022](#); [Mørkøre et al., 2015](#)). The lower the water temperature at the transfer to seawater, the higher the prevalence of DS ([Mørkøre et al., 2022](#)). This relationship may be the result of the suppressive effects of suboptimal temperature exposure on the immune system, particularly on adaptive immunity ([Abram, Dixon, & Katzenback, 2017](#)). During seawater, it was found that acute low oxygen exposure also increased DS prevalence ([Mørkøre et al., 2015](#)). Northern parts of Norway, where the water temperature and UV intensity are lower, and photoperiods closer to 24:00 (in summer), exhibit lower DS prevalence ([Mørkøre, 2012](#)).

The appearance of DS can also be modulated through the diet. The increasing trend of DS prevalence coincides with the gradual increase of plant-based ingredients in commercial salmon diets during the last two decades ([Aas et al., 2019](#)). This shift may result in low ratios of n-3:n-6 fatty acids and lack of EPA and DHA (< 3.5 %), which likely promotes a local pro-inflammatory environment in the skeletal muscle under infectious or physical stressors and, therefore, increasing DS development ([Lutfi et al., 2022](#); [Mørkøre, 2018](#); [Sissener et al., 2016](#)). The protein:fat ratio in the diets seems also to impact the development of DS ([Dessen et al., 2019](#); [Mørkøre et al., 2022](#)), likely by reducing the amount of pro-inflammatory n-6 fatty acids or the concentration of fat in the hypaxial musculature. Moreover, DS decreases in prevalence and size when supplementing diets

with antioxidants such as vitamin C, E, and selenium (Se) ([Mørkøre et al., 2015](#); [Rafiq, 2015](#); [Weizhi, 2016](#)), likely in response to a reduced oxidative microenvironment. The stabilization of DS prevalence in the last years ([Lund et al., 2018](#); [Mørkøre, 2017](#)) may be due to the implementation of these nutritional strategies by feeding companies and farmers.

Fillet DS are primarily (90 – 94 %) located at the anterior hypaxial skeletal muscle, the abdominal wall, especially in ventral mycommatas from vertebra number 12 to 20 ([Mørkøre, 2012](#); [Mørkøre et al., 2015](#)). Moreover, the highest concentration of DS cores is found approximately 3.5 cm below the horizontal transversal septum of the fillet ([Weizhi, 2016](#)). Unpublished data showed that dissecting petechial and focal red-fillet DS on the myocommata plane (*epimysium* in mammals), connects the discoloration to blood vessels. Similarly, the dissection of fillet-black DS also revealed blood vessels connecting to the core of the discoloration (Figure 1). In fact, there seems to be a cooccurrence between the anatomical location of these vessels and the concentration of DS (Figure 2). Moreover, most DS are located under the parietal peritoneum beneath the ribs (*costae* or *pleurapophysis*). As suggested in humans, this anatomical location might not have evolved for physical stress resilience ([McDonnell, Hume, & Nolte, 2011](#)). The hypothesis of a traumatic event as part of DS aetiology has been previously discussed ([Mørkøre, 2017](#); [Mørkøre et al., 2022](#); [Mørkøre et al., 2015](#)), but no literature has investigated this association using the impact of rib fractures or deformations as a model.

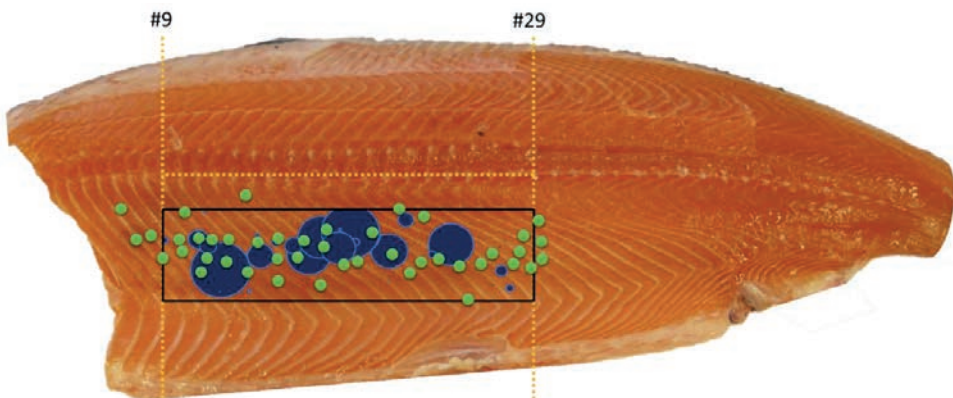


Figure 2. Cooccurrence of segmental parietal veins and focal dark spots (DS) in adult Atlantic salmon fillet. Green circles illustrate the position of segmental parietal veins after myocommata (*epimysium* in mammals) dissection of one salmon. Dark blue circles illustrate the position of DS within the study region (black box) of a salmon population (n = 90). The study region ranges between vertebrae numbers 9 and 29. The size of the circles indicates the relative area of DS. Unpublished material. Image from Raúl Jiménez-Guerrero.

5.1.2 The anatomy of the abdominal wall

Understanding the anatomy of the area where DS are concentrated is essential for interpretation, and for developing possible solutions to the problem. The abdominal wall is the anatomical boundary between the aquatic habitat and the visceral cavity in fish. In Atlantic salmon, it ranges longitudinally from the pericardial cavity to the anus while vertically from the linea alba to the kidney ([Kryvi & Poppe, 2016](#)). It is structured in different layers (medial-lateral): parietal peritoneum (serosa, subserosa, and transverse fascia), rib bones and adjacent blood vessels and nerves, skeletal muscle, hypodermis, dermis, and epidermis ([Kryvi & Poppe, 2016](#); [Smith & Bell, 1975](#)).

Rib bones

In teleost, ribs give structural support and protection of viscera in the abdominal cavity, presenting regional changes in their length and morphology ([Bird & Mabee, 2003](#)). In salmonids, ribs are intersegmental long bones located at the abdominal and transitional regions of the axial skeleton ([De Clercq et al., 2017](#)). While ribs of the abdominal region form the rib cage (*cavea thoracis*), ribs of the transitional region are vestigial. The proximal end of non-vestigial ribs (rib head), is predominantly cartilaginous and is attached to the vertebra *parapophyses* by a joint made of different types of cartilage; elastic/cell-rich connecting the hyaline cartilage of the rib to the hyaline cartilage of the *parapophyses* ventrally in the center of the joint, while fibro/cell-rich cartilage and Sharpley's fibers connect adjacent ossified margins of *parapophyses* and rib head around the hyaline union core, giving joint stability and serving as a bridge for connecting periosteum of both independent structures ([De Clercq et al., 2017](#)).

Teleost ribs develop independently by specific centers close to the axial skeleton. They appear as elongated cartilages that chondrify following a cranio-caudal sequence along the abdomen. During early development, the rib cartilage elongates and grows in a posteroventral manner ([Britz & Bartsch, 2003](#); [Emelianov, 1935](#)), following the intersection between the myocommata plane and the parietal peritoneum ([Goette, 1879](#); [Göppert, 1895](#)). Later, as shown in silver carp (*Hypophthalmichthys molitrix*) ([Soliman, 2018](#)), ribs undergo perichondral ossification and appositional growth with minimal endochondral ossification, but they may still experience longitudinal development by linear expansion of growth plate at the rib head. Here, resting chondrocytes enter differentiation into a proliferative phase with active cell replication. In salmonids, mature rib cartilage core is believed to be hyaline ([De Clercq et al., 2017](#)), but according to

[Soliman \(2018\)](#), after reaching a certain distance from the resting zone, chondrocytes undertake a hypertrophic phase where an abundant cartilage matrix (*pars cartilaginea*) is produced. Later, the hypertrophic zone undergoes extensive degradation and erosion by chondroclasts. This leaves an empty medullary area (rib cavity), although remnants of the hypertrophic zone may be seen. Distal rib parts are found to follow typical cartilage growth as in the proximal side, with perichondral ossification and without medullary bone formation ([Soliman, 2018](#)). At the beginning of the appositional growth, matured peri- and endochondrium leaves peri- and endosteum with differentiated osteogenic cells (osteoblasts) ([Huysseune & Sire, 1992](#)). Osteoblasts produce perichondral compact bone (*substantia compacta; pars ossea*) at both periosteum and endosteum, where osteoclasts may be found in an active (oval) or resting (flattened) phase. Slight projections of ossified tissue may extend to the cartilage matrix ([Soliman, 2018](#)). Appositional growth and remodelling may occur even after the animal fully develops in response to mechanical stress ([Ofer et al., 2019](#)). Although many of these features are common in teleost species, there is no available literature targeting Atlantic salmon ribs.

Bone composition and cellularity vary broadly among different fish species, as shown by [Cohen et al. \(2012\)](#). Lower teleosts, such as Atlantic salmon or common carp (*Cyprinus carpio* L.), have naturally more cellular-rich bones than higher teleost like tilapia (*Oreochromis aureus*), whose bones are considered acellular ([Cohen et al., 2012](#); [Moss, 1963](#)). However, cellularity may also vary according to the structural organization of bone. For example, the osteocyte density is ten times higher in the trabecular than in the compact bone of Atlantic salmon vertebrae ([Nordvik et al., 2005](#)).

Blood vessels

In salmon ([Smith & Bell, 1975](#)), the heart pumps blood through the ventral aorta to the gills. Although part of this blood supplies cranial structures, most of the flow is distributed to the body through the dorsal aorta. The subclavian artery supplies the pectoral girdle, the coeliacomesenteric artery supplies blood to the intestinal organs, and the renal arteries supply the kidney and segmental arteries trunk muscles. The circle is repeated where blood is transported to the heart by the abdominal, hepatic, and common cardinal veins. When it comes to the abdominal wall, blood is collected by the segmental parietal veins (SPV) into the abdominal and common cardinal veins ([Smith & Bell, 1975](#)). Although [Kryvi and Poppe \(2016\)](#) described the most superficial vessel to the parietal peritoneum as segmental arteries, unpublished histological evaluations reveal tunica externa and

media with typical vein features (Figure 3). Thus, lateral cutaneous branches would collect blood from the abdominal wall to SPV (Figure 3. B) (Smith & Bell, 1975).

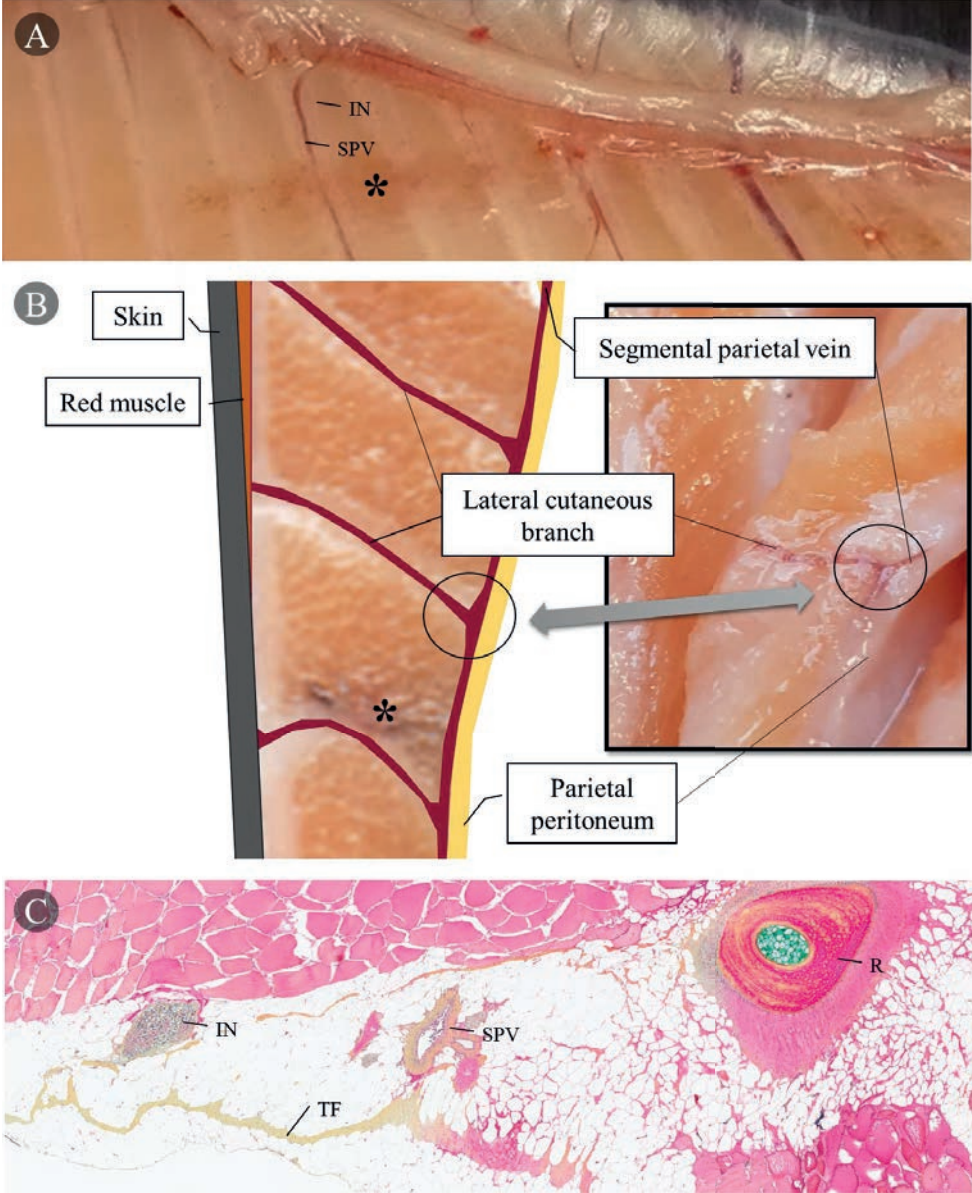


Figure 3. Anatomy of the rib cage (*cavea thoracis*) of Atlantic salmon. A) Macroscopic view of the parietal peritoneum. B) Illustration of transversal rib cage anatomy. Black asterisks indicate the presence of focal dark spots. C) Histological anatomy of the rib cage; horizontal cut. Movat pentachrome staining. IN, intercostal nerve; SPV, segmental parietal vein; TF, transverse fascia; R, rib. Unpublished material. Images from Raúl Jiménez-Guerrero.

Skeletal muscle

The largest functional unit of the skeletal muscle is the myotome, which corresponds to the number of vertebrae ([Kryvi & Poppe, 2016](#)). The myotome consists of myomere (muscle and intramuscular adipose tissue) and myocommata or intermyotomal fascia/myosepta ([Turnbull, 2006](#)). The myocommata comprise adipose and connective tissue, a network of tendons connecting the skeletal muscle fibers to bones and skin ([Kryvi & Poppe, 2016](#)). The interface between two myotomes is symmetrically conformed by the sarcolemma membrane, followed by the basal lamina (limit of the muscle fiber), myocommat's adipose, and connective tissue ([Fletcher et al., 1997](#)). Salmon myotome follows a “W” shape with the side with three peaks (anterior cones) pointing towards the head. This structural organization changes progressively from head to tail ([Kryvi & Poppe, 2016](#)). Additionally, as shown in other species, there may be local muscle groups (*obliquus superioris*) ([Allen, Ladin, & Rowell, 2020](#)) providing controlled movements of ribs.

Muscle growth (myogenesis) is contributed by hyperplasia (increase in myofiber number) as well as hypertrophy (increase in myofiber size). In teleost, the dominance of hyperplasia over hypertrophy depends on species and life stage ([Froehlich et al., 2013](#); [Galloway, Kjørsvik, & Kryvi, 1999](#); [Manneken, Dauer, & Currie, 2022](#)). There are three different types of skeletal muscle fibers: red (*muscularis lateralis superficialis*), white (*muscularis lateralis profundus*) ([Kryvi & Poppe, 2016](#)), and an intermediate type (pink) ([Wang et al., 2021](#)). In salmonids, red fibers (~15 % of muscle mass), localized laterally under the skin, are well vascularized and specialized in aerobic metabolism. This makes them suitable for slow and repetitive contractions, such as during regular swimming. White fibers (~85 % of muscle mass) are placed medially under the red fibers and have less vascularization, specialized in anaerobic metabolism. Thus, white fibers are more suitable for spontaneous, fast, and powerful contractions ([Grunow et al., 2021](#); [Kryvi & Poppe, 2016](#)).

The abdominal wall of Atlantic salmon has a higher muscle fat content versus posterior and epaxial areas ([Aursand et al., 1994](#)). Morphologically, this region is thinner than other axial areas, and its overall vertical length varies with the condition factor, which is highly dependent on the viscera that fluctuates according to fish size, diet, and season in farmed salmon ([Dessen et al., 2017](#); [Rørvik et al., 2018](#)).

5.1.3 Skeletal pathology in salmonids

Deteriorated skeletal health impacts fish welfare ([Noble et al., 2018](#)) and business profitability derived from reduced growth ([Hansen et al., 2010](#)), fillet quality ([Haugarvoll et al., 2010](#); [Sullivan et al., 2007](#)), and technology difficulties due to uniformities (e.g., malformations and fractures) affecting filleting and processing at the slaughterhouse ([Currey, 2003](#)). Several factors may impact skeletal health, from individual-dependent such as ploidy ([Fraser et al., 2015](#)) to environmental factors: farming practices such as vaccines ([Aunsmo et al., 2008](#); [Holm et al., 2020](#); [Trangerud et al., 2020](#)), farming conditions such as egg incubation temperature ([Fraser et al., 2015](#)), light regime ([Fjellidal et al., 2012](#)), water speed/exercise ([Solstorm et al., 2016](#)), and diet ([Baeverfjord et al., 2018](#)).

Currently, salmon bone research focuses on vertebrae ([Drábiková et al., 2021, 2022](#); [Witten et al., 2019](#)), but little is known about other skeletal parts, such as salmon ribs. More than two decades ago, [Baeverfjord, Asgard and Shearer \(1998\)](#) reported axis deviations in the form of wrinkly malformations and mechanical deterioration in ribs in response to a phosphorus (P) deficient diet during fresh and seawater phases. Later, [Roberts, Hardy and Sugiura \(2001\)](#) observed similar findings associated with dietary P and vitamin C deficiency during early life stages. Axis deviations of the ribs have also been associated with myocommata injury during the early life stages in other teleost species, such as zebrafish (*Danio rerio*) ([Akama et al., 2020](#)). Other forms of rib abnormalities in the form of supernumerary ribs associated with a dominant mutation mechanism have been described in rainbow trout (*Oncorhynchus mykiss*) ([Gislason et al., 2010](#)). Here, supernumerary ribs appeared as flouting segments on the distal rib area and partially inserted on the myocommata plane, but with deep lateral muscle intrusion, and in severe cases, they gave skin erosion or even perforations. In addition, compatible morphologies with fractures and the subsequent healing process have also been identified in neural spines of salmon ([Fjellidal et al., 2004](#)) and neural, haemal and ribs bones from wild and farmed non-salmonid species ([Fjellidal et al., 2020](#); [Fjellidal et al., 2018](#); [Horton & Summers, 2009](#)).

5.1.4 Regeneration and repair in the musculoskeletal system

The healing process is a complex and dynamic mechanism whose goal is to limit injury, restore tissue homeostasis, protect against infections, regenerate the damaged tissue, and

restore its function, if possible ([Velnar, Bailey, & Smrkolj, 2009](#)). This process can be realized by either regeneration or repair, depending on whether the original tissue is fully restored or replaced with connective tissue. In teleosts, the healing of the musculoskeletal system is poorly understood, where most of the previous literature has focused on fin skeleton injuries in zebrafish ([Sousa, Valerio, & Jacinto, 2012](#); [Tomecka et al., 2019](#)). However, in mammals, the healing process has been extensively studied, where there is a consensus for dividing healing into several overlapping phases: the inflammatory, the fibrovascular, and remodelling ([Bahney et al., 2019](#); [Khurana, 2009](#); [Maruyama et al., 2020](#); [Sciorati et al., 2016](#)). Besides their evolutionary distance - meaningful at the immunological level - the healing process occurs in teleosts similar as in mammals.

Inflammatory phase - From innate to adaptative immunity

The initial phase of the healing process following a musculoskeletal injury (haemorrhage, acute inflammation, and degeneration) is crucial as it establishes the foundation for the subsequent development steps ([Eming, Martin, & Tomic-Canic, 2014](#)). The haemorrhage is a temporary hypoxic source of essential growth factors and stem cells for healing ([Guo & Dipietro, 2010](#)). Here, tissue-resident innate immune cells respond to damage-associated molecular patterns (DAMPs), and/or microbe-/pathogen-associated molecular patterns (MAMPs/PAMPs) ([Soliman & Barreda, 2023](#)), which results in swelling, redness, and pain in higher vertebrates ([Tang et al., 2012](#)). MAMPs/PAMPs induce the migration of myeloid leukocytes (e.g., monocytes, neutrophils), typically the first immune cells to react. Leukocytes generate both intracellularly and extracellularly reactive species of oxygen (ROS) and nitrogen (RNS), antimicrobial peptides, and pro-inflammatory cytokines such as tumor necrosis factor-alpha (TNF- α), interleukin 1 β (IL-1 β) and interleukin 6 (IL-6), which intensify local inflammation and damage ([Havixbeck & Barreda, 2015](#)). Eventually, extracellular release of ROS and RNS also leads to local collateral tissue damage ([Havixbeck & Barreda, 2015](#)).

Across vertebrates, DAMPs, and MAMPs/PAMPs also drive the migration of professional antigen-presenting cells (APCs; e.g., dendritic-like cells (DCs), and resident macrophages) to the injury ([Soliman & Barreda, 2023](#)). Macrophages and their M1/M2 dichotomy profiles are evolutionarily conserved cells that evolved more than 500 million years ago ([Wiegertjes & Elks, 2022](#)). During a pro-inflammatory environment, macrophages become polarized to the M1 (pro-inflammatory) type. M1 produces an intracellular release of ROS and RNS in their attempt to help remove damaged tissue and debris, as

well as additional pro-inflammatory cytokines such as TNF- α , IL1- β , IL-6, and interleukin 12 (IL-12) ([Soliman & Barreda, 2023](#); [Wiegertjes & Elks, 2022](#)). The result further amplifies the pro-inflammatory environment and recruitment of other immune cells. In addition, M1 cytokines are also responsible for the activation and non-differentiated proliferation of satellite cells in the injury in higher vertebrates ([Manneken et al., 2022](#)). There are two main different types of antigen presentation, either displaying intracellular (MHC type I; all nucleated cells) or extracellular proteins (MHC type II; DCs, macrophages, and B cells) ([Wieczorek et al., 2017](#); [Wu et al., 2020](#); [Wu et al., 2022](#)). In teleosts, under regulatory cytokines such as IL-10 ([Wu et al., 2020](#)), B cells display robust phagocytic capacity similar to mammalian B1 cells, increasing their APCs capabilities and role in innate responses. Both teleosts B and B1 cells arise early during ontogeny, stay in the head kidney, or migrate and reside in tissues, such as the peritoneal cavity, mucosal surfaces, and spleen, where they reside as immature or naïve ([Abós, Bailey, & Tafalla, 2022](#)). After antigen processing, APCs migrate to lymphoid organs, presenting the antigen to lymphocytes, beginning the transition from an innate to an adaptive immune response. B and T lymphocytes are responsible for the specific adaptive immune responses. After differentiation, lymphocytes mature into either effector or memory cells ([Son et al., 2021](#)). Effector lymphocytes are well-described in teleosts ([Abós et al., 2022](#)). However, the existence of lymphocytes with memory capabilities in teleosts similar to the mammalian homolog systems is unclear. There is a debate on whether the innate immune system in teleost fish primarily carries immune memory functions, termed trained immunity ([Stosik, Tokarz-Deptuła, & Deptuła, 2021](#); [T. Yamaguchi et al., 2019](#)).

Before proliferation and differentiation, naïve B cells must enter activation by two main mechanisms depending on whether CD4⁺ T (helper T) cells intervene or not. In the T cell-independent (TI), direct activation occurs through the exposition by APCs of specific antigens to an IgM B cell receptor (BCR) expressed in the surface of naïve and memory-like B cells ([Abós et al., 2022](#); [Jones et al., 2020](#)). When an antigen binds to the BCR, it initiates a signal transduction pathway that leads to effector B cell activation, proliferation, and differentiation into mature antibodies (Abs) or immunoglobulins (Ig)-secreting B cells (plasma cells) with both membrane IgM and IgD expression at the same time ([Abós et al., 2022](#); [Wu et al., 2019](#); [Wu et al., 2022](#)).

On the other hand, APCs can also present antigens to T cell receptors (TCR) of effector CD4⁺ T cells ([Tang et al., 2021](#)), which enter activation capable of co-stimulating naïve B

cells in a T cell-dependent (TD) manner. The TD pathway requires the co-stimulation of the BRC (signal 1), the cluster of differentiation 40 and its ligand (CD40/CD40L) (signal 2) ([Granja et al., 2019](#)), and the production of pro-inflammatory cytokines by the cognate-activated CD4⁺ T cell (signal 3) that stimulate B cell proliferation and differentiation (interleukin 2 (IL-2), interleukin 4/13B (IL-4/13B), and IL-10) ([Maruyama et al., 2020](#); [Sciorati et al., 2016](#)). T and B cells must be specific for the same antigen in the TD pathway. As DCs may also express CD40L, innate cells may simulate naïve B cells by using some of the TD signals ([Abós et al., 2022](#)).

Activated CD4⁺ T cell cytokines can also activate M1 macrophages (TNF- α and interferon-gamma (IFN- γ)) and CD8⁺ (cytotoxic T) cells maturation (IL-2 and IFN- γ) ([Maruyama et al., 2020](#); [Sciorati et al., 2016](#)). Effector CD8⁺ T cells, recognize aberrant antigens presented by MHC class I, typical of infected or cancerous cells, where they induce apoptosis by releasing cytotoxic granules containing perforin and granzyme ([Takuya Yamaguchi et al., 2019](#)). CD8⁺ cells also produce pro-inflammatory cytokines, principally IFN- γ ([Abós et al., 2022](#)), that polarize M1 and activate other immune cells, while inhibiting tissue regeneration - at least in mammals - ([Maruyama et al., 2020](#); [Sciorati et al., 2016](#)).

TI activation plays a role in maintaining homeostasis by contributing to the natural Ig repertoire, which is present in the body even without prior exposure to specific pathogens. This is crucial for providing a first line of defense against pathogens ([Abós et al., 2022](#)). In mammals, though relatively slower, TD is usually more efficient than TI activation as it promotes more differentiation into memory B cells ([Cerutti, Puga, & Cols, 2011](#)). However, this dichotomy between TI and TD responses does not seem to be clear in teleosts, as the degree of B cell activation can be reached through the accumulation of signals or respond much more to certain co-stimulatory DCs signals (e.g., lipopolysaccharide (LPS)) in TI than TD ([Granja et al., 2019](#)).

In teleosts, there are “two different waves” of Abs responses. The primary wave occurs principally in the spleen, while in the head kidney during the secondary repose ([Abós et al., 2022](#)). In the first wave, upon TI and TD exposure ([Abós et al., 2022](#); [Sunyer & Boudinot, 2022](#)), multiple naïve B cells with different specificities are activated. On one hand, a group of these activated B cells proliferate and matures into plasmablast and plasma cells. Then, each plasma cell produces Abs (IgM; polyclonal) with slightly different low-affinity for different antigen parts or epitopes. On the other hand, activated naïve B

cells also differentiate through somatic hypermutation affinity maturation. During somatic hypermutation, the genes encoding their BCRs mutate rapidly. This results in a pool of B cells with BCRs (thus, Abs, once they differentiate into plasma cells) of varying affinities. Later, during affinity maturation, mutated B cells producing higher-affinity Abs are preferentially selected to survive and further proliferate upon future activation of specific clonotypes, producing more specific Abs (monoclonal) in the second wave. Affinity maturation in teleosts is much less efficient than in mammals in terms of potential specificity and quantity, taking several months to reach a 100-fold increase in IgM affinity ([Abós et al., 2022](#)). In mammals, in addition to Abs, plasma cells can also produce pro-inflammatory cytokines (IL-6, TNF- α , IL1- β , IFN- γ) ([de Gruijter, Jebson, & Rosser, 2022](#)). Although these cytokines are described in teleosts, no studies have reported their production by plasma cells.

Fibrovascular phase

At some point, initial pro-inflammatory stimuli (by DAMPs and MAMPs/PAMPs) must be controlled, reducing the production of pro-inflammatory mediators and inducing the apoptosis of leukocytes. This will mark the beginning of the fibrovascular phase ([Feehan & Gilroy, 2019](#); [Maruyama et al., 2020](#)), which is poorly understood in teleosts.

Generally, in response to transforming growth factor-beta (TGF- β), and IL-10, M1 macrophages polarize to the M2 phenotype (anti-inflammatory) ([Wiegertjes & Elks, 2022](#)). In Atlantic salmon, M2 macrophages have been associated with the production and accumulation of melanin pigments ([Malik et al., 2021](#)). M2 macrophages play a crucial role in promoting musculoskeletal injury healing through the resolution of inflammation by phagocytosing remaining apoptotic cells (efferocytosis) and debris, which clears the inflammatory environment and prevents the pro-inflammatory stimuli from dead or dying cells ([Mills & Ley, 2014](#)). M2 also contributes to tissue regeneration by secretion of anti-inflammatory cytokines (TGF- β , IL-4, IL-10, and IL-13) ([Abós et al., 2022](#)), which promote tissue repair by leading the differentiation and fusion of proliferated satellite cells ([Manneken et al., 2022](#); [Soliman & Barreda, 2023](#)).

In mammals, where the fibrovascular phase is extensively studied, M2 macrophages, satellite cells, and mesenchymal stromal cells (MSCs) play a crucial role in local inter-cellular communication. MSCs are recruited during the late inflammatory phase in response to pro-inflammatory cytokines, such as TNF- α and IL-6 ([Maruyama et al., 2020](#)). Cross-talk between secreted anti-inflammatory cytokines by M2 and MSCs such as IL-10,

TGF- β , bone morphogenetic proteins, and growth factors initiate angiogenesis and a transitory reparative granuloma, which serves as a template for the subsequent formation of muscle and callus. These cytokines and most characteristic growth factors, such as vascular endothelial growth factor (VEGF), platelet-derived growth factor, insulin-like growth factor-1, and fibroblast growth factor-2, are present in teleosts ([Cao et al., 2023](#)). This process ensures the delivery of oxygen and nutrients to the healing tissues, at least in mammals ([Maruyama et al., 2020](#); [Sciorati et al., 2016](#)). Growth factors such as VEGF and an increase in lactate production (hypoxia) promote the polarization of M2 macrophages which accelerates the process ([Colegio et al., 2014](#)). Local hypoxia also stimulates MSCs migration and tissue regeneration in mammals ([Lin et al., 2017](#)). Although MSCs are also reported in teleosts ([Lund et al., 2014](#)), their osteogenic precursors are mainly derived from dedifferentiated mature osteoblasts rather than MSCs ([Geurtzen et al., 2014](#)). Osteogenic precursors may also be derived from adipocytes, as shown in Atlantic salmon ([Ytteborg et al., 2015](#)).

In mammals, there are two types of MSCs; muscle-derived (MD-MSCs), and bone marrow-derived (BM-MSCs). In muscle lesions, satellite and MSCs synthesize and secrete an infiltrate of extracellular matrix components, such as collagen and fibronectin, which provide structural support for the newly formed tissue ([Csapo, Gumpenberger, & Wessner, 2020](#)). In bone healing, this process is dominated by BM-MSCs that create a fibrovascular bud. This is followed by two different ossification strategies: intramembranous ossification and endochondral ossification. Intramembranous ossification occurs at the periosteum and directly forms a hard callus from differentiated BM-MSCs into osteoblast that synthesizes and mineralizes bone matrix, where they mature as osteocytes. On the other hand, in endochondral ossification, BM-MSCs differentiate into chondroblasts followed by hyaline- and hypertrophic chondrocytes, which create a cartilaginous template that undergoes mineralization to form a cartilaginous callus (soft callus) ([Maruyama et al., 2020](#)).

During early phases of the fibrovascular phase, pro-inflammatory cytokines such as IL-1 β , IL-6, and TNF- α are absent. However, TNF- α increases in late healing phases to facilitate chondrocyte apoptosis, cartilage resorption, and vascular invasion, leading to osteoblast migration and osteocyte differentiation ([Maruyama et al., 2020](#)). This process converts the cartilage matrix into a bone matrix (hard callus). The organic components of the bone matrix are predominantly collagen, as well as other proteins like osteocalcin,

osteopontin, and bone sialoprotein ([Lin et al., 2020](#)). These components create the foundation for mineralization, the incorporation process of calcium (Ca) and P ions to form hydroxyapatite crystals (the primary mineral component of bone) into the surrounding collagen matrix.

During post-resolution in mammals, the successful completion of the fibrovascular phase results in restoring tissue integrity and function (adapted homeostasis) through different remodelling mechanisms. However, an imbalance in these physiological immune mechanisms can lead to the failure of healing with chronic inflammation and fibrosis (maladapted homeostasis) that may occur at clinical and subclinical levels after resolution ([Feehan & Gilroy, 2019](#)).

Remodelling phase

Little is known about the remodelling phase in teleosts. As reviewed in mammals, the new tissue is remodelled to restore its original structure, shape, and mechanical properties to resist stress and strain. A local secondary increase of pro-inflammatory cytokines such as IL-1 β , IL-6, and TNF- α drives this process ([Maruyama et al., 2020](#)). In muscle, M2 macrophages produce matrix metalloproteinases, enzymes involved in the degradation of damaged and granular extracellular matrix (excess fibrotic tissue or scar tissue) ([Nagase, Visse, & Murphy, 2006](#); [Sciorati et al., 2016](#)). Thus, the extracellular matrix is reorganized with the realignment of collagen fibers to optimize muscle function. Then, newly formed muscle fibers mature, increase in size, and develop functional contractile properties. In bone, the balance between the osteoblast and osteoclast activity of the hard callus gradually results in a lamellar bone deposition (appositional growth), which gives stronger tissue ([Maruyama et al., 2020](#)). This process is highly regulated by osteomacs (not described in teleosts). Osteomacs are specialized local macrophages that support bone remodelling and homeostasis by regulating osteoblasts and osteoclasts activity.

Failure of healing - Chronic inflammation

Understanding the implications of inadequate musculoskeletal healing is important for DS as they are chronic inflammatory processes. However, DS have not been characterized under this perspective, and there is a lack of studies exploring the failure of healing in musculoskeletal injuries of teleosts. In mammals, excess of acute inflammatory stimuli (e.g., infection, defective apoptotic cell clearance) induces TNF- α overexpression by neutrophils which leads to more pro-inflammatory cytokines and chemokines (TNF- α , IL-1 β , and IL-6) by differentiated M1 macrophages ([Epsley et al., 2021](#)). This stimulates

differentiation and activation of osteoclast while inhibiting osteogenesis as it interferes BM-MSD differentiation to osteoblast, producing net bone resorption. Targeted immune activity with a high CD4⁺:CD8⁺ ratio and more effector B and T cells in response to the pro-inflammatory environment also inhibits osteogenesis ([Maruyama et al., 2020](#)). Continuous upregulation of TNF- α and persistent activation of the nuclear factor kappa-light-chain-enhancer (NF- κ B) of activated B cells pathway is a common feature of chronic inflammation. Interestingly, the NF- κ B signalling appears well conserved in teleosts ([Soliman & Barreda, 2023](#)). The erosion/resorption of bone surfaces due to the pro-inflammatory environment is typical of human inflammatory diseases ([Maruyama et al., 2020](#)). In muscle, continuously proliferating satellite cells and MD-MSDs in persistently inflamed tissue generates self-perpetuating matrix deposition, fibrosis, and adipose tissue infiltration ([Sciorati et al., 2016](#)). Consequently, as the tissue cannot recover homeostasis, this may lead to defective healing with loss of tissue properties and function, which resembles the typical histological features of DS ([BjØrger et al., 2019](#)).

5.1.5 Melanin

Melanin is an inert and highly stable molecule produced in various tissues of mammals ([Boissy & Hornyak, 2006](#)), lower vertebrates ([Agius, 1980](#)), plants, and certain microorganisms ([El-Naggar & Saber, 2022](#)). The process of melanin formation is termed melanogenesis. Melanin is synthesized and stored inside cells in specialized organelles called melanosomes ([Raposo & Marks, 2007](#)). The type of melanin produced relies on available enzymes such as tyrosinase, and substrates such as tyrosine ([Boissy & Hornyak, 2006](#); [Hearing, 1993](#)). Disturbances in its function lead to albinism. The synthesis pathway involves multiple steps and intermediate compounds, with the presence or absence of certain molecules determining the melanin type produced, either eumelanin (black-brown) or pheomelanin (yellow-red) ([Hennessy et al., 2005](#); [Ito, Wakamatsu, & Ozeki, 2000](#); [Yamaguchi, Brenner, & Hearing, 2007](#)). In fish, pheomelanin synthesis has not yet been reported ([Kottler, K¼nstner, & Schartl, 2015](#)).

During its biosynthesis, melanin generates a small number of ROS ([Sealy, 1984](#)), while absorbing and neutralizing ROS when polymerizing ([de C¼ssia & Pombeiro-Sponchiado, 2005](#); [Dunford et al., 1995](#); [R¼zanowska et al., 1999](#); [Sarna, Menon, & Sealy, 1985](#); [Sealy et al., 1984](#); [Wang, Dillon, & Gaillard, 2006](#); [Wu et al., 2008](#)). This (net redox) duality allows melanin to regulate ROS production in favor of cellular functions. Together with

other molecular properties, melanin can bind, oxidize, and neutralize molecules efficiently, making it the preferred agent for various biological processes. In unicellular organisms like bacteria and fungi, melanin provides resistance to environmental factors such as UV light, high temperatures, desiccation, polysaccharide lytic enzymes, encapsulating or isolating oxidizing chemicals, pesticides, and infectious organisms, as well as reinforcing cell walls ([Hullo et al., 2001](#); [Kollias et al., 1991](#); [Kuo & Alexander, 1967](#); [Kuznetsov, Filippova, & Rybakova, 1984](#); [Patel et al., 2013](#)). These properties also make melanin an exceptional tool for the immune response of more complex organisms. Macrophages synthesizing melanin (melanomacrophages) are essential for the innate immune system of invertebrates, lower vertebrates ([Blazer, 1991](#)), and poorly vascularized areas like adipose tissue where the function of the adaptive immune system is limited ([Randhawa et al., 2009](#))

In Atlantic salmon, melanomacrophages are cells found in the anterior kidney as aggregated structures called melanomacrophage centers (MMCs) ([Agius, 1985](#); [Agius & Roberts, 2003](#); [Reimschuessel & Ferguson, 1989](#)), although adventitious forms may also be found within chronic inflammatory processes ([Roberts, 1975](#)). It has been suggested that MMCs are structurally like the germinal center in mammals and that MMCs play a role in the humoral adaptive immune response serving as “primitive germinal centers”. However, this designation may be premature ([Steinel & Bolnick, 2017](#)).

5.1.6 Knowledge gaps

- The potential traumatic causes of DS have not been explored using rib morphology as a model.
- There is a lack of basic knowledge and diagnostic techniques for ribs.
- No studies have investigated the influence of environmental factors, such as the growing conditions on DS.
- The effects of environmental factors, such as the growing conditions and the composition of the diet, on rib morphology in the general musculoskeletal framework are poorly understood.
- The population of B cells in DS has not been studied, nor has their traffic between lymphoid tissues and DS.

5.1.7 Objectives and hypothesis

The objective was to investigate the aetiology of DS in Atlantic salmon fillets through the following sub-goals:

- Explore the association between rib abnormalities and the occurrence of DS using salmon reared in different environments (**Paper I**).
- Understand long-term morphological rib abnormalities within the general musculoskeletal framework using salmon fed either marine- or plant-based ingredients during smoltification (**Paper II**).
- Understand the local immune response in DS by investigating B cells and their traffic between lymphoid tissues and DS (**Paper III**).

The initial hypothesis were:

- H_{0a}: There is an association between abnormal rib morphology and DS.
- H_{0b}: The rearing/farming environment is an aetiological factor for DS.
- H_{0c}: The composition of the diet during smoltification is an aetiological factor for rib abnormalities and DS in the long-term.
- H_{0d}: B cells in DS primarily migrate from the head kidney and spleen.

5.2 Experimental overview

This work is based on two experiments (Experiment I and II) (Figure 4). In the Experiment I (**Papers I and III**), farmed salmon from the same smolt population were fed the same commercial feed from the start feeding to slaughter. Fish were farmed in different environments and sampled in different life stages, starting in the smolt farm (0.1 kg), followed by either small experimental flow-through land-based tanks (non-vaccinated; 0.3 – 3.2 kg; 3 m³) or large commercial sea-cages (vaccinated; 0.5 – 4.5 kg; 120 m circumference, 40 m depth). Wild-caught seawater (2.2 kg) and freshwater (5.1 kg) salmon were used as additional materials. **Paper III** only used fish from the seacage environment at the slaughterhouse (4.5 kg) (Figure 4).

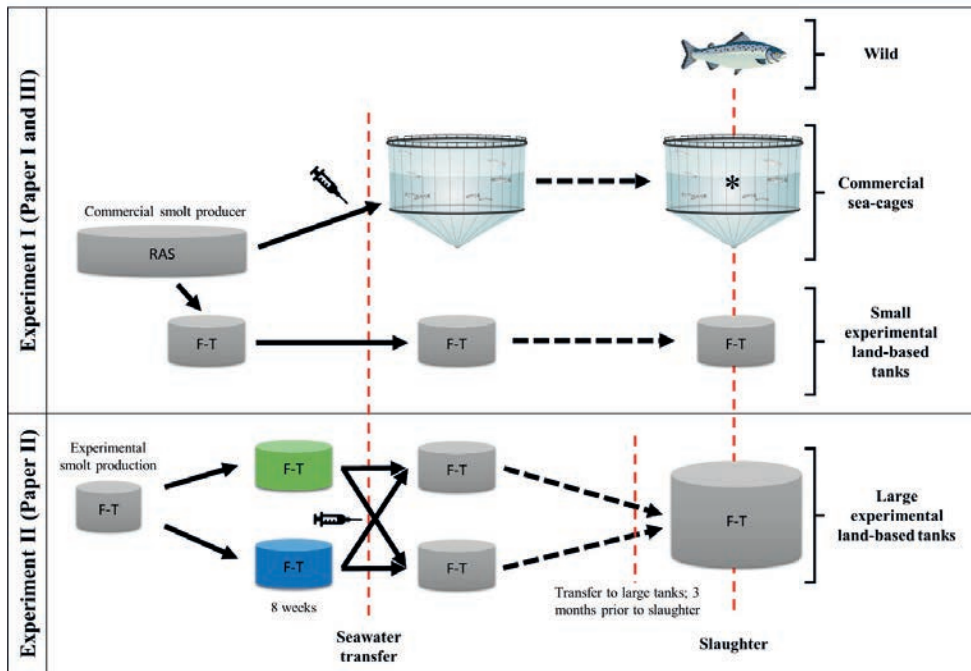


Figure 4. Experimental overview of the thesis. Two experiments (Experiment I and II). Fish were fed standard commercial diets adjusted to the life stage, except for fish prior to seawater transfer in Experiment II. Green color indicates fish fed a plant-based diet. Blue color indicates fish feed a marine-based diet. Intraperitoneal vaccination was performed in fish prior to transfer to sea-cages in the Experiment I and all fish groups in Experiment II. F-T, flow-through. The asterisk indicates the fish material used for **Paper III**. RAS, recirculated aquaculture system.

In Experiment II (**Paper II**), farmed salmon derived from a common commercial genetic lineage. Here, fish were fed two different diets during the smoltification phase: marine-based (M-group) or plant-based (P-group) (Appendix – 1 to 4). Fish were sampled in different life stages. Prior to seawater transfer, fish were vaccinated. Then, fish were fed a standard commercial diet from the time of seawater transfer to small experimental flow-through land-based tanks (similar to **Paper I**) for 10 months and then to a large common experimental land-based tank from the same research facility for 11 weeks until slaughter (3.1 kg) (Figure 4).

5.3 Methodological considerations

A broad selection of morphological, mechanical, chemical, and molecular methods were chosen to accomplish the objectives. When the study of salmon ribs was initiated, there were no established methods to evaluate their health. To address this gap, morphological

(X-ray and histology), mechanical, and chemical methods were either custom-developed or adapted.

X-ray

X-rays can simultaneously provide non-invasive, inexpensive 2D data from many bone units (rib and vertebra) and individuals. Thus, allowing morphological evaluation and relative estimation of mineral density. However, (in some cases) 2D assessment may not be sufficient, requiring the use of 3D techniques such as micro-CT. X-ray imaging performs well with bone but poorly with soft tissues. In contrast to higher vertebrates, teleost bones are less mineralized. This feature, combined with small sizes, limits the image quality when using conventional equipment. Therefore, studying the rib cage in small fish may benefit from equipment with better resolution and sensitivity.

Every rib number 1 to 22 was divided into three regions (proximal, mid, and distal) where the evaluations were taken. A classification system was developed (**Paper I**) based on the type of rib abnormalities observed in fish from different sampling points, environments (salmon, n = 176), and existing literature ([Fjellidal et al., 2020](#); [Gislason et al., 2010](#); [Khurana, 2009](#); [Tomecka et al., 2019](#)), aiming to identify abnormality prevalence's and its potential relation to DS development. Assuming a post-traumatic mechanical disturbance of local tissue after a potential fracture, rib abnormalities were classified into two categories: those with no relation to fractures (Category I) and ribs in different phases of the healing process after fracture, with or without existing continuity breaks (Category II). Category I was further divided into two sub-categories: generalized radiolucent – normally at mid-distal parts - with increased rib diameter, and axis deviations. These abnormalities could be linked to either mechanical stress or potential nutritional deficiencies. Category II was divided into six sub-categories, represented in Figure 5. Hypothetically, if A) a fracture occurs, the healing process might take three different directions (B, C, or D). As part of the normal healing responses in long bones, B₁) a soft radiolucent callus is formed, followed by B₂) a hard radiopaque callus and further stages of B₃) bone remodelling. On the other hand, the failure of callus formation would lead to C₁) radiolucent non-unions, as atrophic non-unions in different stages C₂ to C₃) with resorption of free fragments C₄), followed by C₅) shorter or missing rib parts once free fragments are fully reabsorbed. Free terminal rib fragments could continue their longitudinal growth independently after rib fracture, giving D) supernumerary ribs (Figure 5).

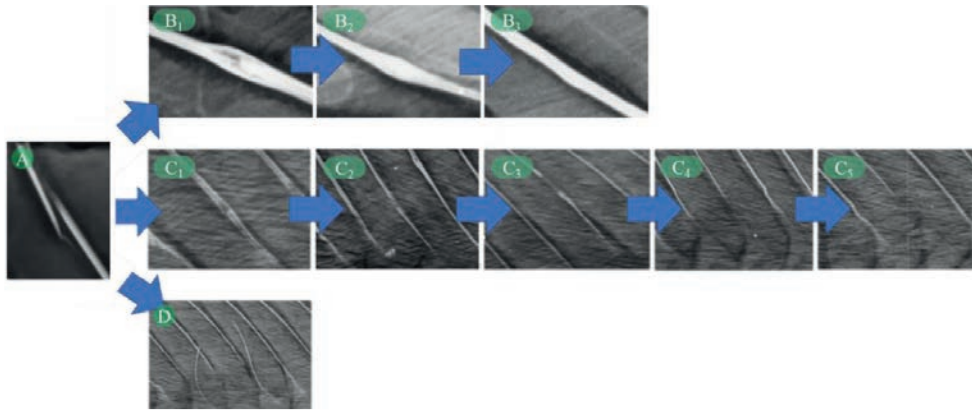


Figure 5. Rib (*costae*) morphological abnormalities related to continuity breaks in Atlantic salmon organized according to their potential healing process after a A) fracture. B₁) Soft radiolucent callus is formed, followed by B₂) hard radiopaque callus, and further B₃) bone remodelling stages. Failure of callus formation could lead to C₁), radiolucent non-unions, as atrophic non-unions with resorption of free fragments in different stages from C₁ to C₃), followed by C₄) shorter or missing rib parts once free fragments are mostly or fully reabsorbed C₅). Free terminal rib fragments may continue their longitudinal growth independently, giving D) supernumerary ribs. Lateral X-ray. Raw material, **Paper I**.

Although **Papers I** and **II** focused on rib cages, X-ray evaluations in **Paper II** were also carried out on vertebrae as it is a well established evaluation system for skeletal health, and would allow to understand rib morphology in the general skeletal framework. The evaluation of vertebral morphology was done similarly to [Bou et al. \(2017\)](#) and [Fjelldal, Nordgarden and Hansen \(2007\)](#), though separating major morphological abnormalities (e.g., compression, fusion, and cross-stitch) from deviations in vertebral width or length (X) versus height (Y) (X:Y ratio) ([Bou et al. 2017](#)) and internal structural malformation of the vertebral body ([Witten et al. 2019](#)).

Histology

Histology allows for detailed analysis of tissue microstructure and can identify subtle changes in tissue health or organization. However, its main weakness lies in its subjective nature and potential for artifacts during tissue preparation. This is especially critical in small mineralized structures, such as ribs, that are surrounded by soft tissues. Furthermore, conventional histology offers only a 2D perspective of tissues, which may not fully capture the complexity of specific structures or processes, as it poorly explores the “Z” plane. However, advanced image analysis can improve objectiveness and its diagnostic capabilities.

Tissue samples from the abdominal wall (parietal peritoneum, ribs and skeletal muscle) preserved in formalin (10 % phosphate-buffered formalin, pH 7.0, >3 days at 4 °C) were examined for pathological changes. Decalcification was performed by incubating the samples in 10 and 14 % ethylenediaminetetraacetic acid (EDTA) at pH 7 for up to 48 hours and two weeks in **Paper I** and **II**, respectively. Samples were then embedded in paraffin wax and sectioned at 1.5 – 2 µm. The stains included: Haematoxylin and Eosin for standard morphology and histopathology; Periodic acid–Schiff for detecting glycogen accumulation in muscle; Movat Pentachrome for morphology and structural composition; and Picro Sirius Red for highlighting collagen. In addition to light microscopy, samples with Picro Sirius Red were inspected under polarized light at 90 ° (cross-polarization) and for confocal microscopy (emission bandwidth, 496 nm – 554 nm and 574 nm – 644 nm). Subjective morphological image analysis was done using the ImageJ software (v1.52s, U. S. National Institutes of Health, Bethesda, USA).

Mechanical properties

Revealing a potential relationship between rib fractures, deformations, and DS requires an understanding of the mechanical properties. Mechanical testing provides critical data on structural integrity and physical properties of biological tissues ([Mørkøre & Einem, 2003](#)). Yet, these techniques can be invasive, potentially destructive, and may not accurately reflect *in vivo* conditions (e.g., isolated bones). Variability in sample preparation and testing conditions (temperature and moisture) can also introduce inconsistency of the results. These issues might be magnified in smaller or more delicate specimens, like fish ribs and vertebrae. Although the original focus was the rib cage, potential challenges in repeatability and sample collection were anticipated. As a result, the mechanical properties of vertebrae were also investigated.

In **Paper II**, techniques were developed to assess the mechanical properties of fish ribs and vertebrae, specifically designed for large-scale sampling and practicality in salmon research. Parameters recorded from the stress-strain curves included the elastic modulus (N/mm), breaking force/load (N), and area (graph area, N*mm) at a given point (Figure 6).

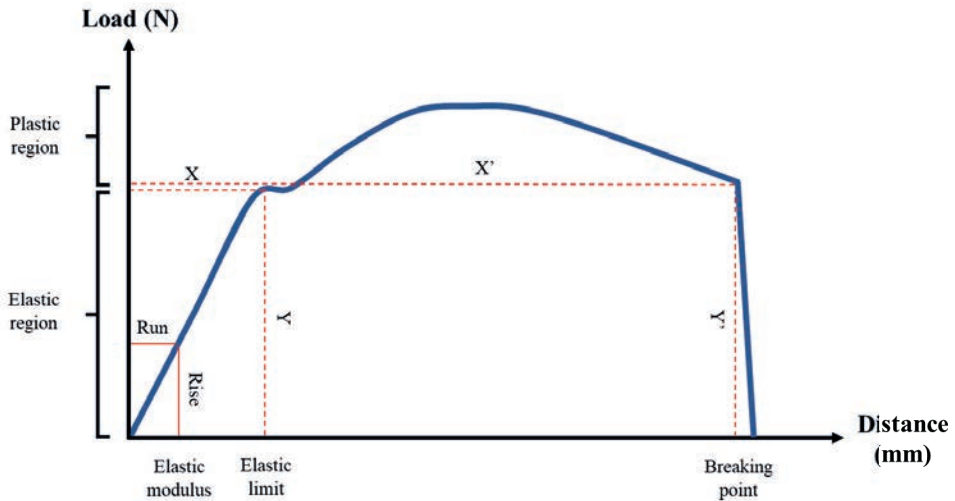


Figure 6. Load/distance graph. The elastic modulus or slope of the stress-strain curve is calculated based on rise/run at a given point within the elastic region. The elastic limit [X, Y] is the termination of the elastic and the beginning of the plastic region of the material. The breaking point [X', Y'] is the fast failure of material resistance. In certain materials, the elastic limit coincides with the breaking point.

The trigger force was adjusted to either rib (N) or vertebra (N), the traveling speed of the probe (guillotine knife; 70 mm width, 3 mm thickness) was set to 2 mm/s, and anatomical regions of focus were chosen according to an unpublished experiment (Figure 7). Further method development could include a thinner knife with a shaper edge to improve the quality of the measurements. Mechanical tests were performed on every second rib from numbers 2 to 22 and every fifth vertebra from number 11 to 55, starting from the head after cleaning for surrounding soft tissue and trimming vertebrae for haemal and neural spines. For the rib, the region of interest was set to ribs number 12 to 14, where there was relatively high variation between proximal, mid, and distal rib parts and proximity to the anatomical region with the highest prevalence of DS ([Mørkøre, 2012](#); [Mørkøre et al., 2015](#)) (Figure 7. A). For vertebrae, every vertebra was latero-laterally compressed until the knife reached up to 50 % of the vertebral thickness to emphasize the trabecular fraction as it is naturally more active than compact bone ([Gil Martens et al., 2006](#); [Nordvik et al., 2005](#)), and it resembles the laminar structure of the rib. The region of interest was established within the anatomical region corresponding to the Norwegian quality cut (NQC) because values collected at various depths indicated that it was a mechanically

stable vertebrae region, allowing measurements to be taken regardless of the selected vertebra (Figure 7. B). Moreover, this easy-to-access region during sampling would allow for multiple measurements of different vertebrae.

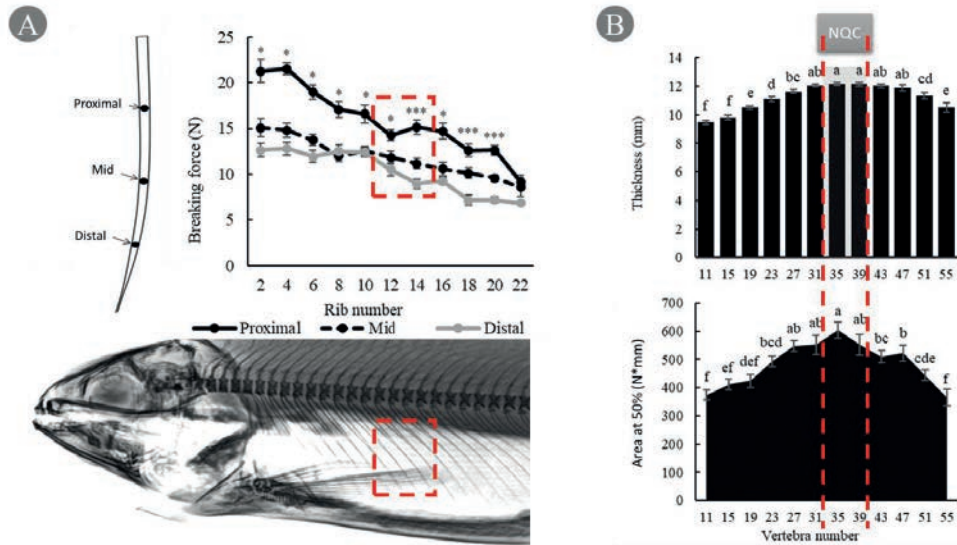


Figure 7. Overview of mechanical properties of ribs (*costae*) and vertebrae of 5 kg Atlantic salmon used for mechanical method design. A) Rib method. Red lines indicate the location of the rib cage (*cavea thoracis*), subjected to mechanical test. Red box shows the region of interest (**Paper I** and **II**) with the highest prevalence of focal dark spots and relatively high variation between proximal, mid, and distal rib parts. Significant differences between breaking force of proximal, mid and distal rib parts of the same rib are indicated with * ($p \leq 0.05$), ** ($p \leq 0.01$), and *** ($p \leq 0.001$) over the top error bars. B) Vertebrae method. Data is collected as thickness and area at 50 % of compression depth. Red lines indicate the anatomical location of interest for **Paper II**, the Norwegian quality cut (NQC). Significant differences between anatomical locations are indicated by different letters over the top error bars ($p \leq 0.05$). Least Squares Means, ANOVA. Data are presented as mean \pm SEM, n = 10. Unpublished material. Images from Raúl Jiménez-Guerrero.

Chemical analysis

Obtaining vital information on biological tissues' elemental composition contributes to understanding pathological and physiological states. Chemical analysis can elucidate key details such as mineral content and distribution, which are crucial in musculoskeletal research. However, they require invasive sampling and extensive sample preparation. Additionally, they typically focus on a targeted set of compounds or elements, potentially missing other relevant aspects of the tissue's chemical profile. In the case of smaller or less mineralized tissues, like teleost rib bones, the minimum amount of homogenized material, sensitivity and resolution of the analysis can be limiting factors. In fact, the low

volume of rib material would limit sampling and other analyses that had to be prioritized in **Paper I**. Therefore, NQC vertebrae were chosen, expecting that if there were major bone mineralization differences, they would also have been detected at the vertebrae level.

Rib samples were cleaned for surrounding soft tissue before homogenization per rearing unit. **Paper II** had enough rib material to analyze the total concentration of three elements (Ca, P, and magnesium (Mg)). Ca and Mg concentrations were assessed using inductively coupled plasma mass spectrometry (ICP-OES) after microwaved digestion, while total P concentration was estimated through an individual spectrophotometrically method ([ISO6491, 1998](#)). Regarding vertebrae, analyses were carried out using either gutted fish (small fish size) or trimmed vertebrae for soft tissue, neural and haemal arches (large fish size). In **Paper I**, the concentrations of major macrominerals of vertebrae (Ca; K, potassium; Mg; P) were performed using acid digestion, extraction, and inductively coupled plasma-mass spectrometry (ICP-MS), according to [Liaset, Julshamn and Espe \(2003\)](#). In **Paper II**, gutted bodies and vertebrae were homogenized per original reading unit, and heated for dry matter ([ISO6496, 1999](#)), and ash content ([ISO5984, 2002](#)) determination. Then, concentrations of Ca, P, Mg, K, sodium (Na), zinc (Zn), iron (Fe), manganese (Mn), and copper (Cu) were determined spectrophotometrically after digestion with acid using an agilent microwave plasma atomic emission spectrometers (MP-AES).

Molecular

In **Paper III**, eight fish with visible DS through the peritoneum from the same fish material as **Paper I** (sea-cages) at the processing line were sampled for head kidney, spleen, and visceral peritoneum fat, with one tissue sample taken from each fish. The peritoneum and ribs were removed, and additional samples were collected from three different locations of each DS. Samples from three different locations of normal skeletal muscle were also obtained from the same anatomical region on the opposite fillet side to the DS. All samples were preserved in RNAlater (Thermo Fisher Scientific, Waltham, MA, USA), and subsequently used for high-throughput sequencing of the complementarity determining region 3 (CDR3) of the IgM heavy chains (Ig-seq). Additionally, Real-Time Quantitative Reverse Transcription Polymerase Chain Reaction (RT-qPCR) was used to quantify the expression of gene markers associated with B/T and antigen-presenting cells.

Ig-seq of MmIgM

IgM exists in two forms, membrane-bound (mIgM) and secreted (sIgM). IgM can be found in several structural states, such as monomer, hexamer, and pentamer (the most naturally occurring sIgM) (Jones et al., 2020) (Figure 8). The IgM monomer consists of two heavy chains with five domains (V_H , C_{H1} , C_{H2} , C_{H3} , and C_{H4}) and two light chains with two domains (V_L and C_L) (Davis, Roux, & Shulman, 1988). The variable regions of the light (V_L) and the heavy chain (V_H) conform to the antigen binding region (Figure 8. A). Generally, the diversity and specificity of Ig are mainly determined by the variable region produced during B cell development through insertions and deletions following the somatic recombination of V and J genes in the V_L and V, D, and J genes in the V_H , which form a variable-diversity-joining (VDJ) region or CDR3 (Figure 8. A). Recombination and enzymatic modification of VDJ represent the major source of variation in Ig (Bassing, Swat, & Alt, 2002; Jung et al., 2006; Schlissel, 2003). As the probability of independent production of two identical CDR3 sequences is low, a specific combination of V, D, and J genes is referred to as a clonotype, a “barcode” for a B cell clone – cells having a common ancestor.

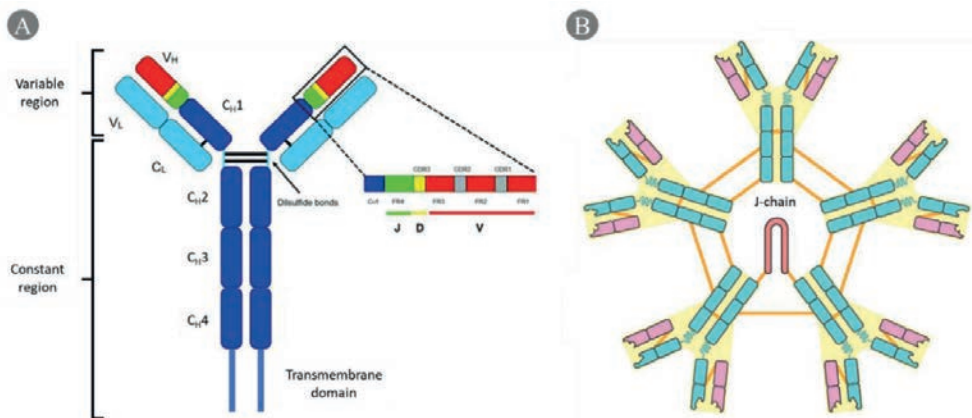


Figure 8. Structure of immunoglobulin M (IgM). A) Monomer structure of membrane IgM (mIgM) is made up of two heavy chains with five domains (V_H , C_{H1} , C_{H2} , C_{H3} , and C_{H4}) and two light chains with two domains (V_L and C_L). The variable-diversity-joining (VDJ) region is located in the variable region of the heavy chains (V_H). VDJ can be regarded as a clonotype “barcode”. The variable regions of light (V_L) and V_H shape the antigen-binding region. The constant regions of the heavy chains are attached to the B cell surface by a transmembrane signalling domain. B) Secreted form of IgM as a pentamer structure (sIgM) of five monomers held together by a J-chain. Diffusive bonds connect chains intramolecularly and heavy chains of different monomers intermolecularly. Modified from Lee et al. (2019) and Britannica (2023). Based on Davis et al. (1988).

High-throughput sequencing of the variable region or Ig-seq is a powerful technique for studying the adaptive immune system ([Sunyer & Boudinot, 2022](#)). Ig-seq is unable to identify the antigen-specific Ig, but it is a comprehensive overview of the immunoglobulin repertoire. Regarding Atlantic salmon, Ig-seq was initially developed to evaluate the complexity and diversity of IgM and detect responses to immunization ([Krasnov, Jørgensen and Afanasyev \(2017\)](#)). The cooccurrence of CDR3 sequences in different tissues of the same individual indicates the migration of B cells, which is stimulated by immunization, such as vaccination or infection with pathogens.

Paper III compared the IgM repertoire in DS and other tissues: head kidney, spleen, visceral peritoneum fat, and normal skeletal muscle (opposite fillet side). The numbers and percentage of clonotypes detected in different tissues of the same fish were assessed, and their cumulative frequencies (CF; sums of frequencies) were calculated (Figure 9. A and B). CF depends on the phase of B cells migration between the source and recipient tissues, as shown in the model (Figure 9. C). CF of clonotypes co-expressed in several samples of a tissue reflects homogeneity of the local B cell population, such as DS or normal skeletal muscle.

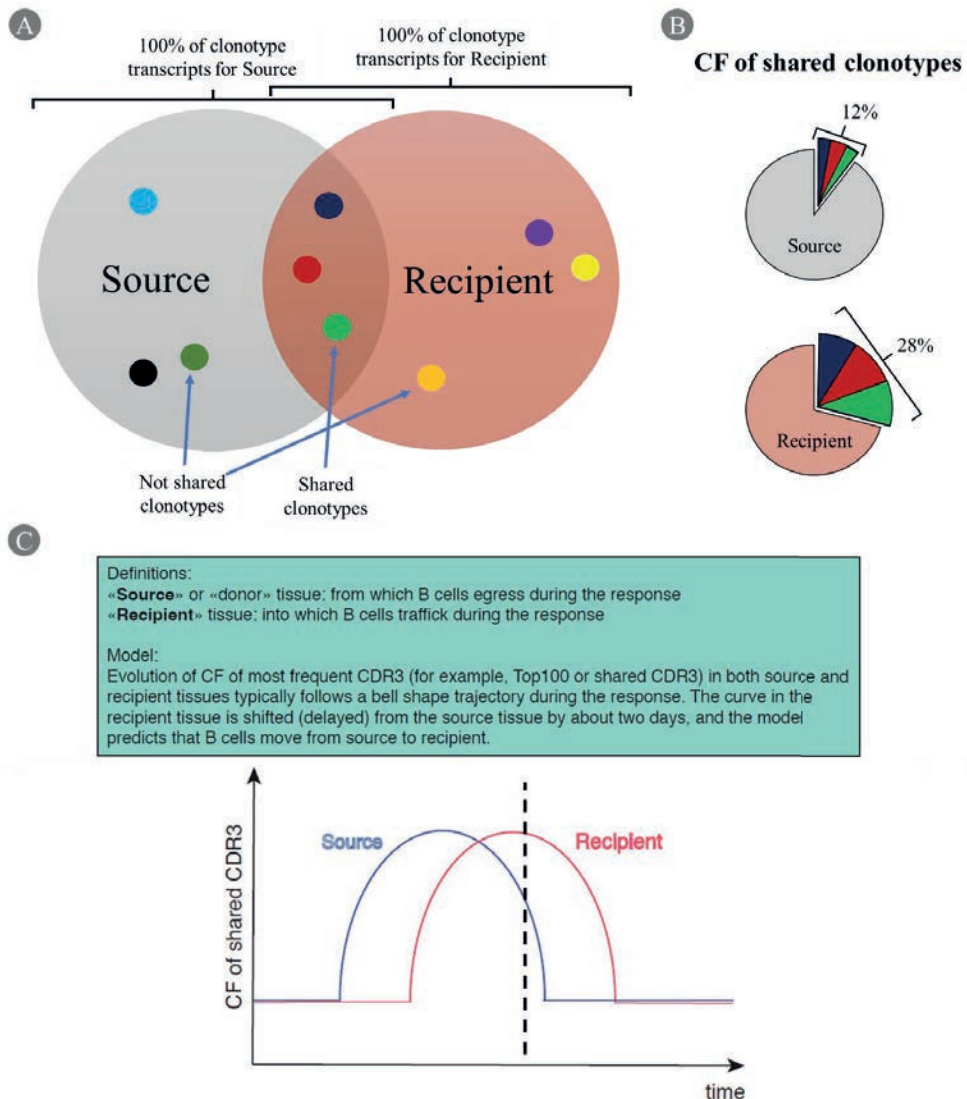


Figure 9. Example of the cooccurrence of complementarities determining region 3 (CDR3) of IgM within samples using Ig-seq results. A) Clonotype repertoire in Source and Recipient tissues. The overlapping region indicates those clonotypes transcripts shared/expressed in both samples. B) Example of the cumulative frequencies (CF) of shared clonotypes from A). The relative fraction of shared transcripts (dark blue, red, and light green clonotypes) is compared to not shared transcripts in each sample. In this case, shared clonotypes take a larger relative fraction of the total number of clonotype transcripts in Recipient than in Source. C) Approximate phase (discontinuous line) of the B cell response in A) and B) according to the model. Based on **Paper III**.

RT-qPCR

RT-qPCR is a reliable method for quantifying gene expression, providing precise and sensitive results. However, it only simultaneously measures a selected number of genes and has a limiting scope as it may not capture the complexity of biological systems. Additionally, gene expression does not always correlate with protein synthesis, making interpretation of the result more difficult if not combined with other methods such as Ig-seq, histology, or gross macroscopy.

RT-qPCR was used to understand better the adaptive immune response phase in each fish used in Ig-seq. A reference gene, elongation factor 1-alpha (*ef1a*) ([Julin, Johansen, & Sommer, 2009](#)), and several markers of immune cells and phases of their development were selected. Antigen presentation: cluster of differentiation 83 (*cd83*) as a marker of dendritic cells ([Steinman, Pack, & Inaba, 1997](#)), colony-stimulating factor receptor (*csfr*) ([Peñaranda et al., 2019](#)), macrophage receptor (*marco*) as markers for macrophages ([van der Wal et al., 2021](#)), and cluster of differentiation 40 (*cd40*) and major histocompatibility complex II (*mhc2*) as markers for antigen presentation ([Lagos et al., 2012](#)). Master regulators of B cell differentiation: membrane IgM (*migm*) as a marker of undifferentiated B cells ([Tadiso, Lie, & Hordvik, 2011](#)), cluster of differentiation 79 (*cd79*) as signalling for binding of antigen to B cell receptor ([Chu & Arber, 2001](#)), paired box protein 5 (*pax5*) as a marker for regulation of expansion and differentiation of progenitors B cells ([Cobaleda et al., 2007](#)), lymphocyte-induced maturation protein 1 (*blimp1*) as a marker for terminal differentiation ([Nutt, Fairfax, & Kallies, 2007](#)), B cell lymphocyte tyrosine kinase (*blk*) expressed in differentiating and mature B cells, but not in plasma cells ([Dymecki et al., 1992](#)). Three Ig isotypes: Secretory IgM (*sigm*), IgT (*igt*), and IgD (*igd*) as markers of Ig-producing (plasma cells) B cells ([Tadiso et al., 2011](#)). Markers of T cells: cluster of differentiation 28 (*cd28*) as a contact stimulator marker for naïve CD4⁺ and CD8⁺ cells with APCs ([Vallejo et al., 1999](#)), cytotoxic T-lymphocyte-associated antigen (*ctla*) as a marker for activated cytotoxic T cells ([Bernard et al., 2006](#)), and B and T lymphocyte attenuator (*btl*) as a marker for inhibitory regulation of B and T cells ([Zeng et al., 2005](#)).

5.4 Main results and general discussion

In our attempt to understand DS aetiology, the potential relationship between musculoskeletal damage in the abdominal wall and DS was explored. Furthermore, the influence of environmental factors and local immune responses driven by secondary

infections on the following healing process was examined. The focus was placed on the rib cage since bone fractures in this area would be a determinant link to mechanical stress in the abdominal wall.

Before exploring the relationship between rib morphology and DS and its healing process, a detailed anatomical study of normal ribs from farmed and wild salmon is provided using the knowledge from **Papers I** (X-ray and histology) and **II** (histology, and mechanical properties). This is followed by a study and classification of the most typical abnormal morphologies. In **Paper I**, different types of rib abnormalities in many different forms and numbers were observed in virtually all explored fish, independently of the presence of DS, including wild salmon. This fact largely complicated the study of the association.

5.4.1 Atlantic salmon ribs

Paper I showed that the typical rib cage of Atlantic salmon presented ribs following a ventro-caudal orientation with a progressively decreasing angle towards the tail (Figure 10). There was a gradual change in rib length in the caudal direction. Starting from the 3rd vertebra, where the shortest rib - often missing - is usually found, ribs generally increased in length until they reach the 9th to 12th vertebra. The total number of non-vestigial ribs attached to vertebrae basiventral typically ranges between 21 and 23 (Figure 10).

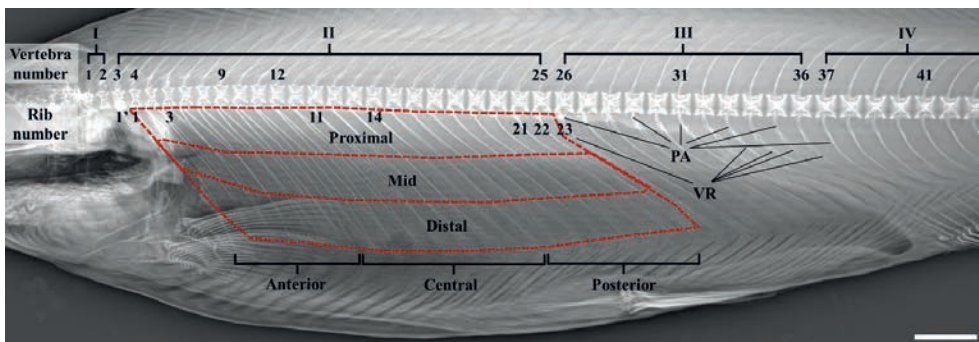


Figure 10. Overview of the Atlantic salmon rib cage (*cavea thoracis*). Vertebrae and rib (*costae*) reference numbers for **Paper I** and **II** are indicated. The original first rib (1') which corresponds to the 3rd vertebra, is the shortest and is often missing. As a result, it is not included in rib cage evaluations (indicated by red dashed selections; proximal, mid, and distal areas). The rib cage is divided into three regions: anterior (ribs 1 - 7), central (ribs 8 - 15), and posterior (ribs 16 - 22). The Norwegian quality cut ranges from vertebra number 31 to 41. I, Postcranial vertebrae; II, Abdominal vertebrae; III, Transitional vertebrae; IV, Caudal vertebrae; PA, Parapophyses starting from vertebrae number 26; VR, vestigial ribs from vertebra number 26 to 36. The white bar on the bottom right corner shows the image scale, set to 12 mm. Lateral X-ray. Based on [De Clercq et al. \(2017\)](#), and **Paper I**.

According to their morphology, ribs were longitudinally divided into proximal, mid, and distal parts (Figure 10 and Figure 11). Micro-CT scans in **Paper I** revealed that ribs present a tubular structure, where sometimes bone processes ventrally oriented on the exterior surface of proximal parts could be seen. The cross-sectional morphology of proximal parts was flattened and laterally oriented, reaching into deeper layers of the muscle wall, becoming increasingly rod-like and less integrated into the muscle wall at distal parts (Figure 11), similar to zebrafish ([Bird & Mabee, 2003](#)). Distal rib parts seemed to have high motility within their periosteal sheath. Histological examinations from **Paper I** and **II** showed that ribs (core and compact bone), and their associated tissues (cellular and fibrous periosteum) (Figure 11. A), were separated from the abdominal cavity by different tissue layers (medial-lateral): serosa, subserosa (where melanomacrophages were seen) and transverse fascia (Figure 11. B and C). Rib cores at proximal and distal parts were usually abundant in cell-rich hyaline cartilage (immature-like) ([Witten, Huysseune, & Hall, 2010](#)). At mid rib parts (rib numbers 11 – 14), 71 % of rib cores featured hyaline-cell cartilage (hypertrophic-like) ([Witten et al., 2010](#)) with a matrix rich in collagen with perpendicular type III collagen fibers (thin fibers) of trabeculae formation (slight radiolucency) (Figure 11. A, B, and C, and Figure 12). More detailed histological characterization featured appositional growth of compact bone with multiple concentric layers of osteocytes (Figure 12). Here, osteocyte density was around 0.003 cells/ μm^2 . Compared to the cartilage core, the bone matrix contained a relatively lower amount of collagen with mainly perpendicular type III fibers, and non-collagen proteins organized around the rib core. The rib periosteum presented an irregular thickness on the fibrous fraction (internal and external). Radial glycoproteins and collagen type I (thick fibers) and III seemed to connect the fibrous periosteum to the outermost compact bone, sometimes forming a layer of perpendicular type I collagen fibers under the osteoblasts (Figure 12. B and C). The external fibrous periosteum layer, which perpendicularly surrounds the rib, had the richest content of collagen, presenting abundant perpendicular type I and III fibers (Figure 12. B and D). The polarized signal near the compact bone and the external fibrous periosteum layer was stronger than in the internal fibrous periosteum, suggesting that some fibers may run back into the bone (Sharpey's fibers) (Figure 12. C and D). Osteoblasts were mainly found in the cellular periosteum (Figure 12).

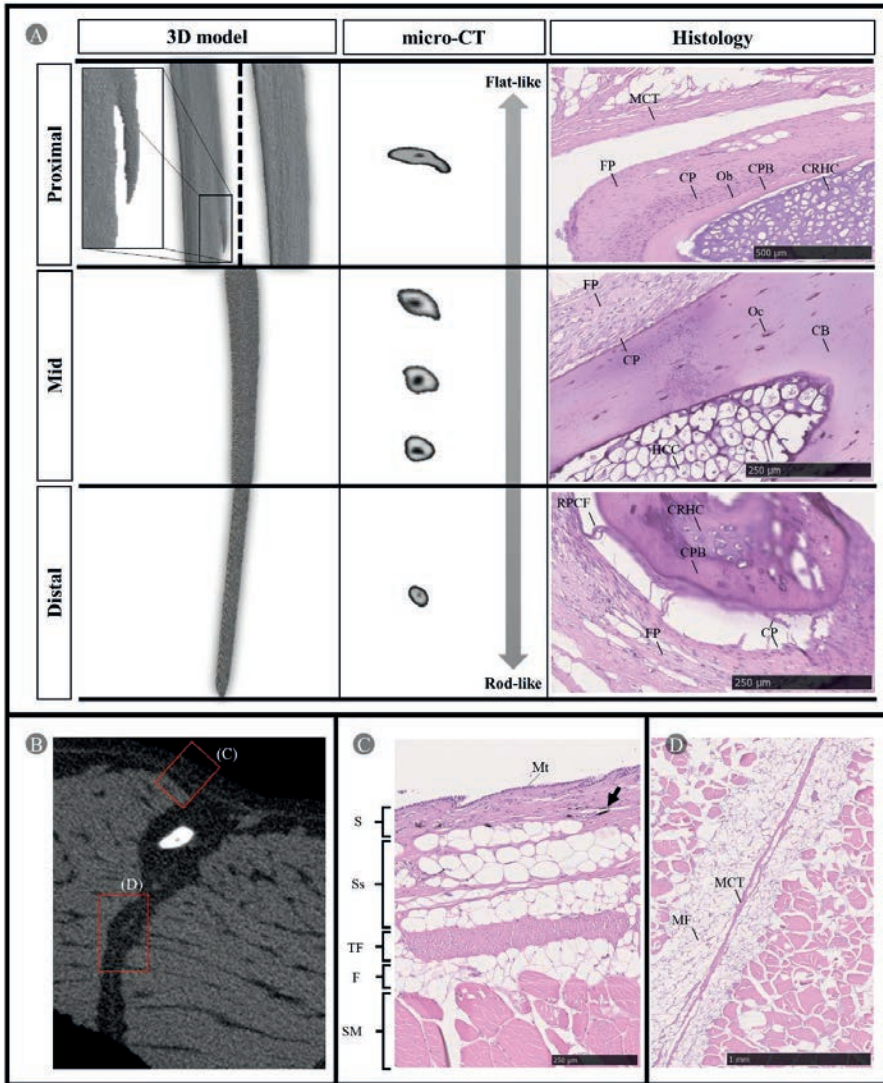


Figure 11. General anatomical overview of adult Atlantic salmon rib (*costae*) and adjacent structures. A) Anatomical description combining 3D model, transversal micro-CT slices, and histology at the proximal, mid, and distal rib parts. The box at the proximal area of the 3D model shows a magnified view of the rib process on the external rib side. B) Cross-section micro-CT slice for rib mid part and adjacent structures. Boxes with letters indicate histological illustrations of corresponding anatomical regions. C) and D) Anatomical description of adjacent rib structures, both peritoneum and myocommata (*epimysium* in mammals), respectively, combining transversal micro-CT slice and histology. The black arrow points to melanomachrophages. Haematoxylin and eosin staining. CPB, Compact perichondral bone; Oc, Osteocytes; HCC, Hyaline-cell cartilage (hypertrophic-like) of the rib core (*pars cartilaginea*); CRHC, Cell-rich hyaline cartilage (immature-like); RPCF, Radial periosteal collagen/Sharpey's fibers; Ob, Osteoblast; CP, Cellular periosteum with Ob; FP, Fibrous periosteum; MCT, Myocommata connective tissue; MF, Myocommata fat; Mt, Mesothelium; S, Serosa; Ss, Subserosa; TF, transverse fascia; F, fat; SM, Skeletal muscle. Figure from **Paper I**.

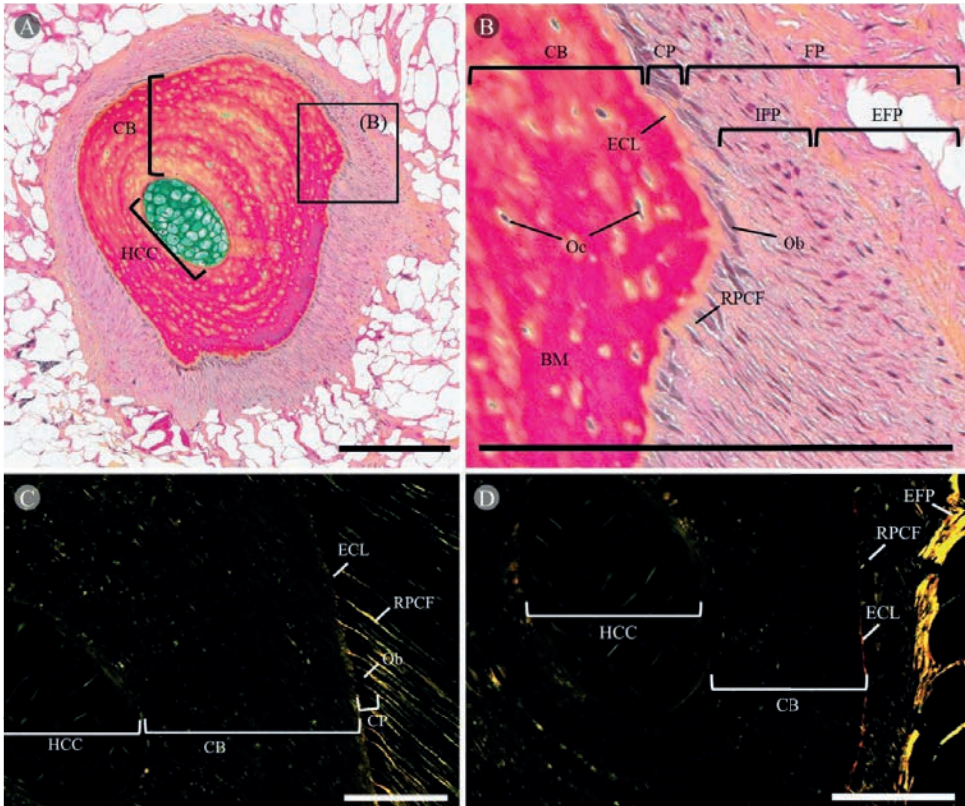


Figure 12. Cross-sectional anatomy of normal mid ribs (*costae*) number 11 - 14 of adult Atlantic salmon. Box with letters indicates the region of zoom of image B). Movat pentachrome staining for proteoglycans and mucins (blue), collagen/reticular fibers (yellow), colocalization of collagen/reticular fibers and proteoglycans (green), muscle and osteoid (or decalcified bone matrix) (reddish-brown), nuclei and elastin (black) and active nucleus (osteoblast in cellular periosteum) (violet/purple). C) and D) rib cross-sections under polarized light. Yellow-orange birefringence in polarized images stands for perpendicular collagen type I (thick fibers), while green birefringence perpendicular type III (thin fibers). Picro Sirius red staining. CB, Compact bone (*substantia compacta; pars ossea*); Oc, Osteocytes; BM, Bone matrix; HCC, Hyaline-cell cartilage (hypertrophic-like) of the rib core (*pars cartilaginea*); ECL, External collagen layer of the CB; Ob, Osteoblast; CP, Cellular periosteum with Ob; FP, Fibrous periosteum; IFP, Internal fibrous periosteum; EFP, External fibrous periosteum; RPCF, Radial periosteal collagen/Sharpey's fibers. Black bars on the bottom right corners show the image scale, set to 250 μm . White bars on the bottom right corners show the image scale, set to 100 μm . Based on **Paper II**.

No blood vessels were observed in the periosteum. The external fibrous periosteum fuses with the myocommata's connective tissue (Figure 11. B and D). Mechanical testing in **Paper II** showed that the breaking load of the ribs consistently tends to decrease from proximal to distal parts, similar to Figure 7. A. The elasticity showed a similar pattern, with lower values at the proximal than the mid and distal parts.

5.4.2 Understanding rib abnormalities

X-ray explorations of rib cages revealed up to eight types of morphological rib abnormalities. Some rib abnormalities (generalized radiolucency and axis deviations) were not classified as continuity breaks, in contrast to others (fracture, supernumerary ribs, radiolucent callus, radiopaque callus, radiolucent non-unions, and shorter or missing rib parts) (**Paper I**). Except from radiolucent non-unions in wild fish, all rib abnormalities were found in all environments and most life stages (Table 1). The most prevalent abnormalities across different experiments, environments, and live stages were axis deviations followed by generalized radiolucency and shorter or missing rib parts (**Papers I and II**). X-ray evaluations in **Paper I** showed that the number of axis deviations was vulnerable to post-mortem handling and filleting, and its degree varied with fish size. As a result, axis deviations were not included in the total sums of the time-based study of rib cages to minimize the influence of artifacts. However, this problem was later addressed in **Paper II** and therefore considered in total sums of abnormalities in rib cages.

Table 1. Number of different rib (*costae*) abnormalities per rib cage (*cavea thoracis*) side for wild and farmed Atlantic salmon before and after seawater transfer in Sep.2018 to land-based tanks and sea-cages until harvest in Nov.2019 (Land-based tanks, 3.2 kg; Sea-cages, 4.5 kg).

Abnormality group	n	Wild	Smolt farm	Land-based tank			Sea-cage				
		Jun. 2020	Aug. 2018	Nov. 2018	Feb. 2019	May. 2019	Nov. 2019	Nov. 2018	Feb. 2019	May. 2019	Nov. 2019
Category I - No continuity break		15	20	15	15	15	23	10	30	10	23
Generalized radiolucent		1.3 ± 0.5 ^{bcd}	0.1 ± 0.1 ^d	1.7 ± 0.5 ^{bc}	0.7 ± 0.2 ^{bcd}	1.1 ± 0.5 ^{bc}	0.3 ± 0.1 ^{cd}	5.2 ± 1.4 ^a	1.7 ± 0.4 ^{bc}	2.2 ± 0.7 ^b	1.3 ± 0.3 ^{bcd}
Axis deviation		5.7 ± 1.1 ^{cdk}	6.7 ± 0.8 ^{bc}	6.5 ± 1.2 ^{bcd}	4.8 ± 0.8 ^{dk}	4.2 ± 0.9 ^c	12.9 ± 1 ^a	7.1 ± 1.4 ^{bc}	1.2 ± 0.4 ^f	1.8 ± 0.6 ^f	8.2 ± 0.9 ^b
Any Category I		7 ± 1.2 ^{bcd}	6.8 ± 0.8 ^{bcd}	8.2 ± 1.3 ^{abcd}	5.5 ± 0.8 ^{cdk}	5.3 ± 0.9 ^{cdk}	13.1 ± 1.1 ^a	12.3 ± 2.1 ^{ab}	2.9 ± 0.6 ^c	4 ± 1 ^{bc}	9.5 ± 0.9 ^{abc}
Category II - Continuity break											
Fracture		0.3 ± 0.3	0.3 ± 0.1	0 ± 0	0 ± 0	0.1 ± 0.1	0.3 ± 0.2	0.3 ± 0.2	0.5 ± 0.2	0 ± 0	0 ± 0
Supernumerary		0.1 ± 0.1	0.1 ± 0.1	0.1 ± 0.1	0.1 ± 0.1	0.1 ± 0.1	0.2 ± 0.1	0.1 ± 0.1	0.6 ± 0.3	0.3 ± 0.3	0.2 ± 0.1
Radiolucent callus		1.1 ± 0.4 ^{ab}	0.1 ± 0.1 ^b	0.1 ± 0.1 ^b	0.1 ± 0.1 ^b	0.1 ± 0.1 ^b	1.4 ± 0.3 ^a	0.2 ± 0.2 ^b	0.1 ± 0.1 ^b	0.7 ± 0.4 ^{ab}	0.7 ± 0.2 ^{ab}
Radiopaque callus		0.5 ± 0.3 ^b	1.7 ± 0.3 ^{ab}	0.9 ± 0.4 ^b	0.5 ± 0.2 ^b	0.4 ± 0.2 ^b	0.7 ± 0.2 ^b	0.9 ± 0.4 ^b	1.2 ± 0.4 ^b	1.7 ± 0.5 ^{ab}	3 ± 0.5 ^a
Radiolucent non-union		0 ± 0	0.1 ± 0.1	0 ± 0	0.1 ± 0.1	0 ± 0	0 ± 0	0 ± 0	0.1 ± 0	0 ± 0	0 ± 0
Shorter or missing part		0.7 ± 0.3 ^c	1.5 ± 0.3 ^{bc}	1.4 ± 0.3 ^{bc}	1.2 ± 0.3 ^{bc}	1.3 ± 0.3 ^{bc}	1.5 ± 0.3 ^{bc}	3.4 ± 0.8 ^a	3.2 ± 0.4 ^a	2.7 ± 0.9 ^{ab}	2.6 ± 0.6 ^{ab}
Any Category II		2.7 ± 0.6 ^b	3.7 ± 0.5 ^{ab}	2.6 ± 0.7 ^b	2 ± 0.4 ^b	1.9 ± 0.4 ^b	4.1 ± 0.6 ^{ab}	4.9 ± 1.3 ^{ab}	5.7 ± 0.9 ^{ab}	5.4 ± 1.8 ^{ab}	6.5 ± 0.8 ^a

Values shown as mean ± SEM in the same row between environments and life stages with different letters are significantly different ($p \leq 0.05$). Most frequent variables were analysed using linear model and Tukey's honest significant difference using squared root-transformed data. Less frequent variables (from fracture to shorter or missing rib parts) were analysed using a generalized linear model adjusted for Poisson distributions, and Wilcoxon signed rank test using non-transformed data. Table from **Paper I**.

There seems to be a consistent number of four rib abnormalities in wild and farmed salmon in land-based tanks of **Paper I** during the seawater phase, which could be considered basal or "normal" for future comparisons (e.g., **Paper II**). The number was found to increase in salmon farmed in sea-cages, principally contributed by generalized

radiolucent ribs, shorter or missing rib parts in a time-decreasing trend, and radiopaque callus in a time-increasing trend (Figure 13 and Table 1). The results proved the influence of the growing environment on rib morphology and suggested a switch in the potential aetiology of rib abnormalities between early (potentially vaccine side effects and nutritional deficiencies) and late life phases (e.g., higher mechanical stress). Though not necessarily reflected in the rib cage, there were indications of mechanical stress in the form of intramuscular haemorrhages after grading in freshwater. At laughter, there were more radiopaque calluses in rib cages of sea-cage fish than land-based tanks, presenting evidence of a higher incidence of rib fractures when fish grow in sea-cages.

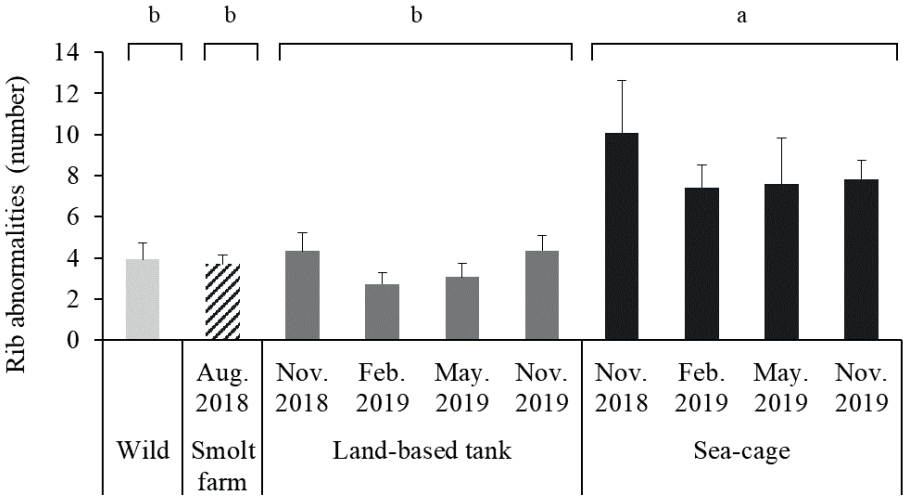


Figure 13. Life stage and growing environment effects in the number of rib (*costae*) abnormalities per rib cage (*cavea thoracis*) side for wild and farmed Atlantic salmon before (0.1 kg) and after seawater transfer in Sep.2018 to land-based tanks and sea-cages until harvest in Nov.2019 (Land-based tanks, 3.2 kg; Sea-cages, 4.5 kg). Significant differences between groups are indicated by different letters over the top brackets ($p \leq 0.05$). Linear model and Tukey’s honest significant difference using squared root-transformed data. Data are presented as non-transformed mean \pm SEM, $n = 15, 20, 68, 73$, for wild, smolt farm, land-based tank, and sea-cage groups, respectively. Figure from **Paper I**.

The abrupt increase from four to 10 rib abnormalities when transferring fish to seawater in sea-cages observed in **Paper I** was mainly attributed to resorptive-like rib morphologies, such as shorter or missing rib parts and generalized radiolucent ribs. This justifies future studies focusing on any source/form of stress in this period (partially explored in **Paper II**). The increase in the number of shorter or missing rib parts was characteristic of the transfer to seawater in sea-cages, which highlights factors affecting

exclusively the sea-cage group in this period (Figure 14 and Table 1). The resorptive morphology and location of these abnormalities (distal parts of rib numbers 11 - 19), near the vaccination site might suggest vaccine-induced rib defects that have not been observed before. Side effects of vaccines in the skeleton are documented in the form of spinal deformities, sometimes cooccurring with melanomacrophage infiltration as part of the inflammatory process ([Holm et al., 2020](#); [Trangerud et al., 2020](#)). Here, the local inflammatory process in the rib cage possibly induced osteolysis and disruption of myocommata stem cells in the short-term, followed by abnormal rib development in later stages ([Akama et al., 2020](#)), as the presence of supernumerary ribs in the exact location indicates. Therefore, in addition to the mutation mechanism presented by [Gislason et al. \(2010\)](#), new potential causes for the occurrence of supernumerary ribs are presented.

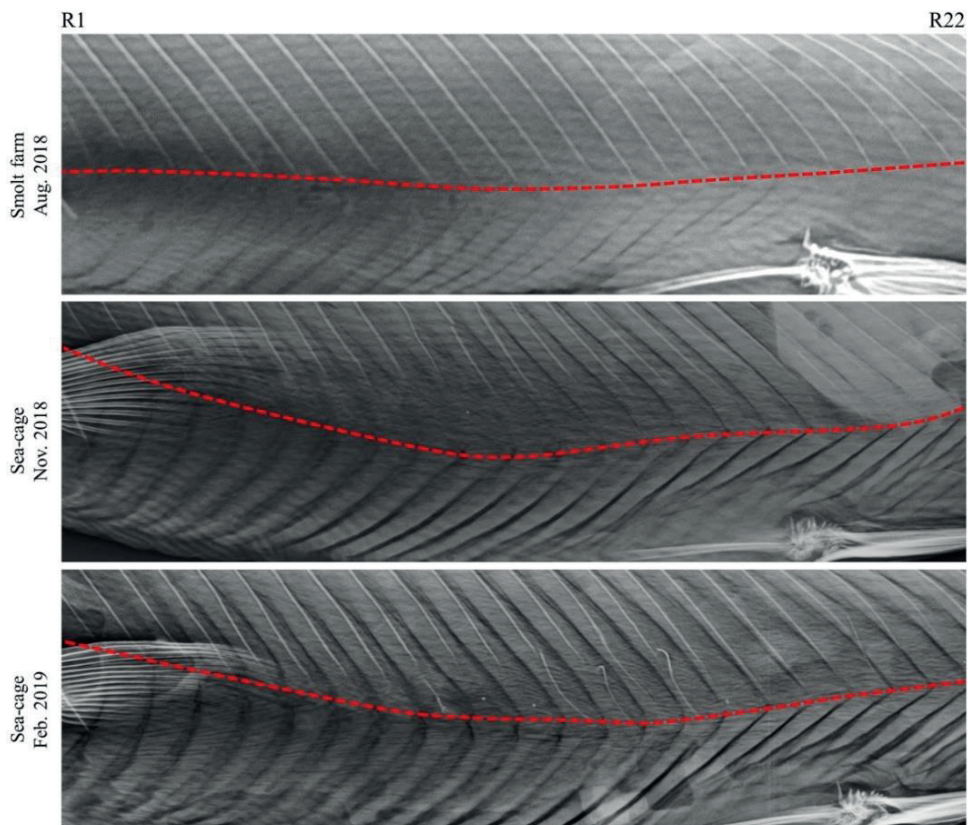


Figure 14. Example of distal rib (*costae*) changes of Atlantic salmon from commercial smolt farm (Aug. 2018, 0.1 kg) to sea-cages (Nov. 2018, 0.5 kg; Feb. 2019, 1.2 kg). Discontinuous red lines highlight ventral angle change in myomere as reference from rib number 1 - 22. Lateral X-ray. Supplementary 1 in **Paper I**.

Although the number of generalized radiolucent ribs increased in both farmed groups in **Paper I** after seawater transfer, the magnitude of the increase at seawater transfer to sea-cages was 3.1 times higher than transfer to land-based tanks. Therefore, there seem to be common factors acting at different magnitudes, but higher for commercial seawater transfer (e.g., more mechanically intensive practices, environmentally dependent dietary requirements). This difference was also manifested in the distribution of rib abnormalities along the rib cage. Here, farmed salmon groups showed a tendency for rib abnormalities to concentrate in the central and distal parts of the rib cage (more pronounced in sea-cages than land-based tanks) than wild fish.

The abrupt increase of the generalized radiolucent rib morphology in **Paper I** coincided with a known period - seawater transfer - with a high risk of mineralization imbalance ([Fjelldal et al., 2006](#); [Fjelldal et al., 2007](#)). It is near seawater transfer when the first DS are reported. Reduced structural integrity of the abdominal wall due to weaker ribs may be a risk factor for more severe mechanical deformations of the abdominal wall and, therefore, damage. To further understand the predominant morphological changes in ribs after seawater transfer, rib morphology was examined within the general musculoskeletal framework using two different diets during smoltification (**Paper II**).

Paper II confirmed that the dominant rib abnormalities in farmed salmon were axis deviations and generalized radiolucency. There were two subtypes of axis deviations: parallel bending of several mid rib parts probably resulting from mechanical deformations of the abdominal wall, as observed in **Paper I**; and wrinkly malformations in mid-distal ribs mainly concentrated in the anterior areas of the rib cage due to alterations in bone development in response to a suboptimal diet ([Baeverfjord et al., 1998](#)).

Paper II showed that generalized radiolucent ribs were primarily localized in the central regions of the rib cage. Histologically, these rib abnormalities typically lacked a surrounding local inflammatory process and featured a degenerated hyaline-cell cartilage core followed by an enlarged osteolytic and fibrotic cavity (high radiolucency) with internal lipid vacuoles and vascularization. Additionally, there was an increased rib diameter, possibly as a compensatory mechanism to maintain mechanical properties. Rib cartilage core degradation and internal vascularization were also reported by [Brimsholm et al. \(2023\)](#), who suggested that these changes could be mere anatomical variations in salmon ribs because of the aquatic environment, similar to other marine species where

this bone erosion may be normal in late growth phases ([Soliman, 2018](#)). **Paper II** showed that these changes potentially represent the degradation and transformation of hyaline-cell cartilage to mesenchymal-like cells in the central core of the rib ([de la Fuente et al., 2004](#); [Witten et al., 2010](#)). Here, the newly formed blood vessels resulting from remodelling would facilitate osteoclasts to enter rib cavities ([Veis & O'Brien, 2023](#)), which could be an essential step for the progression of generalized radiolucency if osteoclasts are naturally absent in salmon rib cores. Vascularization was also observed in the metaplastic periosteum at the site of the advancing osteolytic cavity.

This thesis finds evidence for pathology in generalized radiolucent ribs when they are not associated with local inflammation, especially in higher grades where the morphological changes clearly correspond with detectable X-ray changes:

- Generalized radiolucency is not a common morphology as only ≤ 29 % of ribs in a defined anatomical area present an osteolytic and fibrotic cavity instead of a hyaline-cell cartilage core (**Paper II**).
- The prevalence of generalized radiolucency was very low in adult wild fish (5.1 kg; 2.6 rib abnormalities per rib cage) (**Paper I**).
- There was no increase in prevalence in later growth phases in farmed fish, but there was a response to environmental (**Paper I**) and dietary factors (**Paper II**).
- The concentric appositional growth pattern was altered, with abnormal deposition of disorganized type I and III collagen islands (slight radiolucency) (**Paper II**).
- The osteolysis of the compact bone around the rib cavity was irregular (**Paper II**).
- New osteoid deposits were present at the inner layers of osteolytic cavities with the invasion of cellular periosteum (**Paper II**).

Altogether, altered rib development, degeneration, and possibly osteomalacia seemed to be the likely diagnosis of generalized radiolucent ribs when there was no associated local inflammatory process. Osteomalacia in the ribs was indicated by increased periosteal collagen, likely compensating for deteriorated mechanical strength, and was further confirmed by the link between increased elasticity, lower P levels, and morphological changes (generalized radiolucency and axis deviations). However, the increased elasticity of the ribs could also be due to the relative enlargement of the cavity, osteoid deposits, altered concentric mineralized layers, or the presence of collagen-rich islands in the compact bone. As our data shows, these features could elevate the likelihood of rib

deformities, making it clinically significant. When choosing ribs to evaluate elasticity and P deficiencies, differentiating between normal and abnormal ribs through visual inspection proved challenging. This resulted in an increased standard deviation that impacted significance levels between dietary groups.

Papers I and II show that distal rib parts concentrate most rib abnormalities, probably due to their anatomical features and higher mechanical vulnerability than proximal parts. In **Paper II**, the deteriorated rib health was associated with long-term deterioration of the mechanical properties of the trabecular fraction of vertebrae, but this did not correspond with vertebral morphological deviations, indicating subclinical vertebral effects. Thus, rib morphology appeared more sensitive to the smoltification diet than vertebrae. In addition to bone, dietary differences influenced fillet firmness. This marks the first evidence of the long-term effects of the smoltification diet on muscle integrity in salmonids. Consequently, these results highlight the importance of including rib bones and final fillet firmness for future musculoskeletal evaluations when planning early stage nutrition-related experiments.

The parallel long-term effects on bone strength and skeletal muscle fiber integrity in the P-group (**Paper II**) point to a generalized alteration of the extracellular collagen matrix (essential for bone and muscle). This has not been reported earlier in nutritional deficiency studies. The extracellular collagen matrix is known to be mediated by collagen type I ([Aubin, 1998](#)) and collagen type II alpha 1 chain (*col2a1*) ([Dale & Topczewski, 2011](#)) among other genes. In teleost, there are three type I collagens, alpha 1a (*col1a1a*), 1b (*col1a1b*) and 2 (*col1a2*) chains ([Gistelinck et al., 2016](#); [Morvan-Dubois et al., 2003](#)). Although, little literature is available, while *col1a1* can be upregulated by n-3 PUFAs ([Abshirini, Ilesanmi-Oyelere, & Kruger, 2021](#); [Aubin, 1998](#); [Ytteborg et al., 2015](#)), *col2a1* may be downregulated by plant-based protein concentrates ([Dhanasiri et al., 2020](#)). Transformation of rib cartilage can relate to dietary-dependent components or be induced through mechanical factors ([Hall, 2015](#)). For example, n-3 PUFAs can suppress collagen matrix degradation in cartilage ([Abshirini et al., 2021](#)), one of the characteristic histological changes in generalized radiolucent rib. Therefore, combining fish oil and non-plant-based proteins might have a positive synergic effect on musculoskeletal health in the long-term, at least during the smoltification phase.

Interestingly, there were high rib morphological similarities between fish fed marine ingredients in **Paper II** and the wild fish investigated in **Paper I**. Moreover, sustained

higher Na concentrations in the P-group salmon than in the M-group was found. This establishes an association between Na levels in bone and long-term deterioration of the strength of vertebral trabeculae and ribs' strength, morphology, and composition. Such association could be due to the stimulatory effects of Na-based hydroxyapatite on bone osteolysis and remodelling of compact bone ([Yoo et al., 2021](#)), which are histological features of generalized radiolucent ribs.

5.4.3 Relationship between rib abnormalities and focal dark spots

An association between rib abnormalities and DS was found in **Paper I**. Sea-cages, the only environment developing DS, exhibited the largest number of rib abnormalities per rib cage. Analyses of these DS by X-ray revealed a higher prevalence of rib abnormalities in fillet-black DS (72 %) and peritoneum DS (87 %) compared to haemorrhages (33 %) and control samples (40 %). Although generalized radiolucency was present, mainly different forms of bent and broken ribs numerically contributed to increased fillet-black DS and peritoneum DS compared to haemorrhages and control samples. Control samples belonged to the ribs that usually concentrate most rib abnormalities (number 11 - 14); therefore, it shows a maximum prevalence that is not representative of the entire rib cage. Generalized radiolucency explained most of the abnormalities in control samples (63 %), which agrees with the findings in targeted samples from **Paper II**.

The anatomical location of fillet DS's followed a similar symmetric distribution as rib abnormalities along the rib cage's horizontal plane. However, this spatial association was not consistent in the vertical plane. While most rib abnormalities were concentrated towards distal areas of the rib cage, most fillet DS were located in mid rib parts. Moreover, the severity of DS increased towards the proximal rib parts (Figure 15). Thus, those (less frequent) rib abnormalities occurring in mid and proximal parts were associated with most fillet-black DS and most severe forms (larger area and intensity level). The association also depended on DS morphology; the flattest DS forms were concentrated in mid and distal rib parts, while they were rounder towards proximal parts. Generally, rounder forms, typically of larger relative DS size and intensity level, were less associated with rib abnormalities, although generalized radiolucent if occurring, which gave an osteolytic porotic appearance (Figure 16). On the other hand, flatter forms, typically of relatively small DS size and intensity level, were more associated with mechanical

deformations of rib abnormalities, with axis deviations as principal contributors (Figure 15).

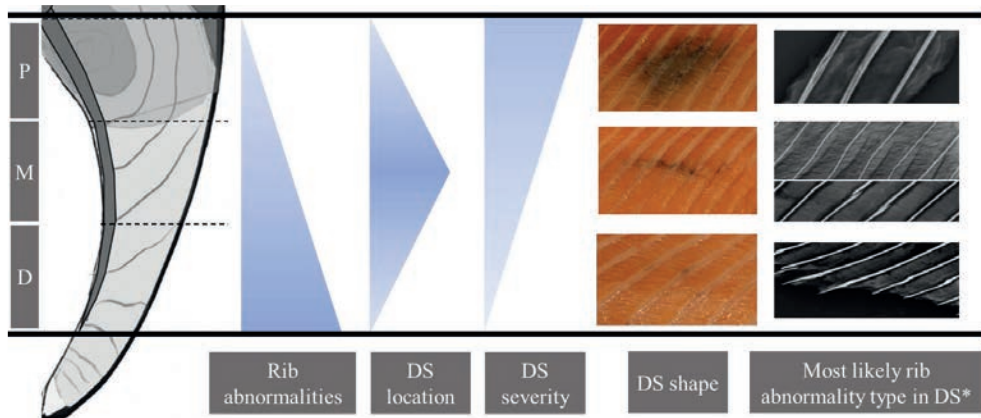


Figure 15. Model for the association between the number of rib (*costae*) abnormalities and focal dark spot (DS) location, severity and shape in each rib part: proximal (P), mid (M), and distal (D). DS severity = DS area*Focal color. The asterisk indicates that the association is based on the DS severity and shape but not the rib position. Lateral X-ray. Based on **Paper I**.

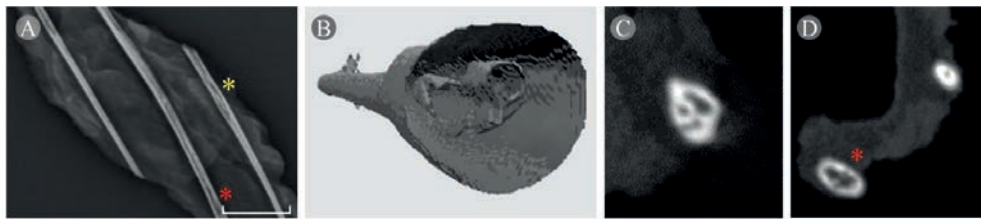


Figure 16. Generalized radiolucent ribs (*costae*) in a focal dark spot. A) Lateral X-ray. B) 3D model from micro-CT. C) and D) micro-CT slice. The yellow asterisk in A) indicates the rib of interest in B and C). Red asterisks in A) indicate the rib of interest in D). Based on **Paper I**.

Similar fracture-like rib abnormalities could be found in DS of different severity levels and locations of the rib cage in **Paper I**, suggesting the implications of additional factors involved in developing the DS besides a rib abnormality. This was also supported by the presence of similar abnormality types in fish and abdominal wall areas without DS development. One of these factors could be the location of the injured muscle/rib. The cross-sectional rib shape, orientation, and depth in the muscle wall suggest more support for musculature and natural endurance to continuous latero-lateral flexion at mid-proximal than mid-distal rib parts ([Van Leeuwen, 1999](#)). Latero-lateral forces would be derived from internal organ pressure ([Jiao et al., 2020](#)), but also from oblique and radial

forces of the anterior cones (between mid-proximal rib parts and the horizontal septum) ([Van Leeuwen, 1999](#)). At the muscular level, continuous mechanical stress can lead to recurrent injuries, adversely affecting normal healing and remodelling. This could result in chronic-active inflammation and fibrosis, typical features of DS ([Bjørngen et al., 2019](#); [Larsen et al., 2012](#); [Nikolaou et al., 1987](#)). In mammals, fibrosis can lead to pathological interconnections (myofascial adhesions) that increase local stiffness and elevate re-injury risk ([Bernabei, van Dieën, & Maas, 2017](#)). In the case of a rib injury, recurrent mechanical stress could lead to conditions ranging from atrophic to hypertrophic non-union or pseudarthrosis. Although this condition has not been described in salmon, it has been reported in terrestrial animals, where factors such as inadequate stabilization can directly delay the union of bone segments ([Kumar, Abbas, & Aster, 2018](#); [Miclau et al., 2007](#)).

Paper I reported all these features typical of recurrent muscle and bone injuries. In mammals, myofascial adhesions are associated with varying degrees of musculoskeletal pain and abnormal proprioception ([Langevin, 2021](#)). If this is the case in salmon, DS might be a source of acute and chronic pain and, therefore, a persistent welfare problem.

Accordingly, three scenarios can be proposed for DS pathophysiology after a traumatic event in the abdominal wall (Figure 15). A first scenario, where trauma in proximal parts of the rib cage primarily results in muscle haemorrhages, with occasional rib deformation/fractures. Here, the injured tissue would evolve into severe outcomes attributed to these areas experiencing high mechanical stress due to their anatomical location. These events would be difficult to detect by X-ray due to the lack of initial bone damage, but the intense pro-inflammatory microenvironment may generate secondary rib changes, such as osteomyelitis with different levels of osteolysis ([Mbalaviele et al., 2017](#)). In a second scenario, trauma affecting mid parts causing muscle haemorrhages and rib damage, principally manifested as rib deformations (but also fractures) in a linear pattern involving several ribs, which would be easily detected by X-ray and visible through the peritoneum. Traumas located in the mid parts would still be subjected to continuous mechanical stress from the anterior cones. However, this stress would be relatively lower than experienced in the proximal parts. Therefore, it could result in a lower pro-inflammatory microenvironment and, subsequently, the intensity of DS development. A third scenario, where traumatic events occurring in distal rib parts generate rib deformations/fractures with minor muscle haemorrhage. Here, an injury would be possible to detect by X-ray. However, it would be unable to create an intense

pro-inflammatory microenvironment and, subsequently, DS due to the residual mechanical stress of the hypaxial musculature in this anatomical location. Haemorrhages in these three scenarios would most likely result from the rupture of muscle fibers and/or major local vessels, such as lateral cutaneous branches and their union to SPV (Figure 1 and Figure 3. B) ([Smith & Bell, 1975](#)).

In addition to the location in the abdominal wall, the association between rib abnormalities and DS also depends on the life stage. In **Paper I**, the prevalence from the first observed black DS (five months after seawater transfer) to those last recorded (14 months after seawater transfer; slaughter) increased from 41 to 72 % in fillet-black DS, and from 68 to 87 % in peritoneum DS. Therefore, the life stage or body weight could also be an essential factor in the pathophysiology. On one hand, typical handling practices with pre- and post-smolts could generate rounder DS principally because of muscle haemorrhages with no significant rib damage. This would be possible due to relatively lower body weight and softer ribs ([Cohen et al., 2012](#); [Fiedler et al., 2021](#); [Jiao et al., 2020](#)), which would prevent larger structural bone damage after a traumatic event. On the other hand, typical practices in late phases near slaughter would cause more flattened DS due to a higher number of rib deformations or fractures after a traumatic event. Here, as fish gain weight, the force exerted on the rib cage may proportionally increase, especially during out-of-water situations where the rib cage would likely be subjected to abnormal forces of varying direction and intensity.

On the contrary, in the unlikely scenario where all DS forms have a common pathophysiology, the data from **Paper I** might be used to propose a model for the time-based morphological changes of DS (Figure 17). Here, the model predicts a relative size and intensity decrease in fillet-black DS while transitioning from a round to a flat-like shape with time. Thus, the first fillet-black DS in seawater would not appear before three months after the first haemorrhage's registration. Moreover, over the following nine months, black DS would experience a series of morphological changes derived from healing. Unfortunately, the age of these DS could not be determined and, therefore, verify the model.

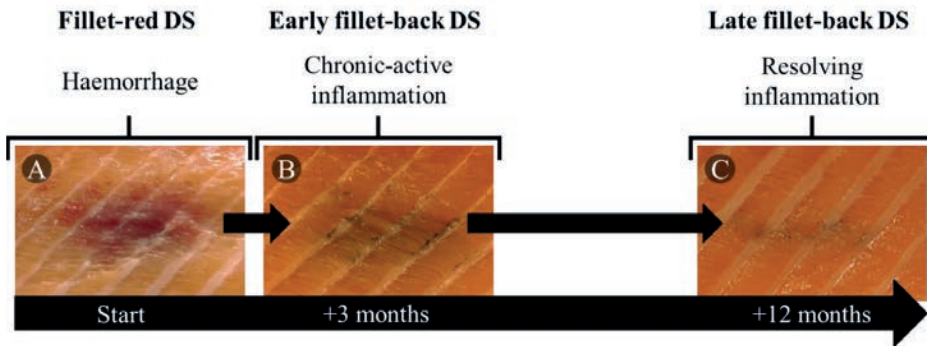


Figure 17. Proposed model for time-based morphological changes of focal dark spots (DS) assuming common pathophysiology and healing. A) Start the process as muscle haemorrhage, round haemorrhages/fillet-red DS. B) Inflammatory process with melanin pigment deposition in the focal area, round fillet-black DS. C) Possible pigment dilution and relative size reduction due to fish growth and dorso-ventral compression of DS as a result of contraction after scar formation, flat fillet-black DS. Based on **Paper I**.

5.4.4 The effects of the environment on focal dark spots

It was hypothesized that environmental factors directly influence DS development (traumatic events, **Paper I**) or indirectly (diet, **Paper II**; and secondary infections, **Paper III**). An overview of the salmon groups is given in Figure 18. In **Paper I**, haemorrhages were found in all farmed environments, starting from the smolt farm. However, fish over 0.3 kg in small land-based tanks did not exhibit these haemorrhages, and only those in sea-cages developed fillet-black DS (43 – 45 %). Accordingly, muscle haemorrhages are more prevalent in farming than in experimental environments. Moreover, these haemorrhages in fish farmed in small flow-through land-based tanks did not evolve into melanised chronic processes/fillet-back DS. Therefore, it is concluded that the presence of black DS is environmentally dependent.



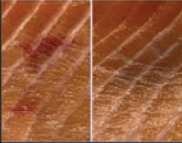
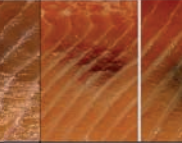







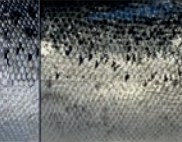
	Paper I	Paper I	Paper II	Paper I
Farming system	Wild	In-door flow-through (3m ²)	In-door flow-through (103 m ²)	Commercial sea-cage
Vaccinated	No	No	Yes	Yes
Viral infection	.	No	No	Yes*
Immunostimulants exposition	Low	Low	Medium	High
Fillet DS				
	No	No	Yes (up to 17% of fish)	Yes (up to 45% of fish)
Fillet DS type		Petequeal and focal haemorrhages only in earlier stages (≤ 0.3 kg)	Petequeal and focal haemorrhages plus mild black DS (low economic impact)	Focal haemorrhages and black DS
Rostral view				
Mechanical stress in snout	No	Yes	Yes	Yes
Snout melanisation in response to mechanical stress	No	No	Yes (low)	Yes (intense)
Skin appearance				
	Low pigmentation	Low pigmentation	Medium pigmentation	High pigmentation

Figure 18. Summary of farmed Atlantic salmon material at slaughter from **Paper I** and **II**. Pigment deposition in skeletal muscle, as dark spots (DS), and rostral and lateral skin. * While the fish population tested positive for PRV-1 and SAV, DS were mostly negative for PRV-1 in **Paper III**.

Among all the different environmental factors in Experiment I (**Paper I**), the diet composition was excluded as a primary contributor to DS development as all farmed fish were fed the same commercial diet. However, the parallel deterioration of rib health (rib strength, mineralization, and morphology) and skeletal muscle strength in **Paper II** pointed to a theoretically increased susceptibility to musculoskeletal damage. Although fish from **Paper II** developed DS with a lower prevalence and economic relevance than reported in sea-cages in **Paper I** (Figure 18), the presented musculoskeletal deterioration did not impact DS. Regardless of this lack of effects, the possibility that smoltification feeding modulates DS in more challenging environments, such as sea-cages, can not be

excluded. Here, better musculoskeletal health could be a protective factor. Regarding healing, there was enough evidence in **Paper II** suggesting that the composition of the diet during smoltification would not modulate the focal inflammatory response of musculoskeletal injuries in the long-term, in contrast to other studies where the dietary treatment was applied in later life stages and longer duration than eight weeks ([Dessen et al., 2019](#); [Lutfi et al., 2022](#); [Sissener et al., 2016](#)).

Paper II showed that haemorrhages from vaccinated fish farmed in small- but transferred to large flow-through land-based tanks in the last 11 farming weeks can evolve into fillet-black DS, in contrast to non-vaccinated fish in small experimental tanks in **Paper I** (Figure 18). Such a pattern also agrees with the absence of melanisation in skin areas exposed to high mechanical stress (e.g., snout) and the amount of melanin pigmentation and macroscopically healthy skin. The results were consistent throughout fish from **Papers I** and **II**. Though on a low level, the association of melanisation between skin and muscle seems to exist even between salmon from a specific farming environment. In an unpublished study from a commercial R&D farm (n = 90), a weak positive correlation was identified between the relative length of DS and both the darkness of the skin and the number of melanin dots ($r = 0.23$ and 0.25 ; $p = 0.03$ and 0.02 , respectively) ([Jiménez-Guerrero, 2018](#)). These findings suggest that melanisation of injured tissue appears to be a systemic feature in fish that can be modulated with environmental factors. Moreover, the snout could be a cheap and efficient external indicator of melanizing capabilities between Atlantic salmon of different populations, as shown in Figure 18.

This thesis identifies several critical differentiating environmental factors that could regulate melanogenesis between the conditions described in **Papers I** and **II** experiments. These were intraperitoneal vaccination, farming system (in-door flow-through vs. commercial sea-cage), and infection pressure/presence (Figure 18).

Regarding immunoprophylaxis, only vaccinated fish developed fillet-black DS, though in different degrees. The land-based experiments in controlled conditions from **Papers I** and **II** were conducted in the same research facility, utilizing flow-through with UV-treated water inlets, and underwent comparable handling conditions by the same team of technicians and personnel. Thus, intraperitoneal vaccination remained the main differential melanogenic factor between both experiments under controlled conditions in **Papers I** and **II**. Tank size was also different during the 11 weeks before harvesting, but it seems unlikely that an increase in tank size may modulate melanogenesis to that extent.

Although the vaccination is not a determinant for DS ([Berg et al., 2012](#); [Mørkøre, 2012](#)), several DS samples with chronic musculoskeletal damage at slaughter from **Paper I** presented histiocytic-like granuloma and large lipid vacuoles under the peritoneum in the hypaxial musculature (Figure 19). These pathological changes were similar to foreign body reactions, as the mineral oil adjuvant used in intraperitoneal salmon vaccines ([Carlton et al., 2001](#); [Hwang et al., 2012](#); [Larsen et al., 2012](#)). Although the hypothesis needs to be proven, in a very likely scenario, the local inflammatory stimuli in the musculoskeletal injury after a traumatic event and the ongoing recurrent processes, well documented in **Paper I**, might cause the migration of loaded macrophages with vaccine compounds from parietal peritoneum layers to the adjacent skeletal muscle. Thus, it would enhance the chronification of the process.

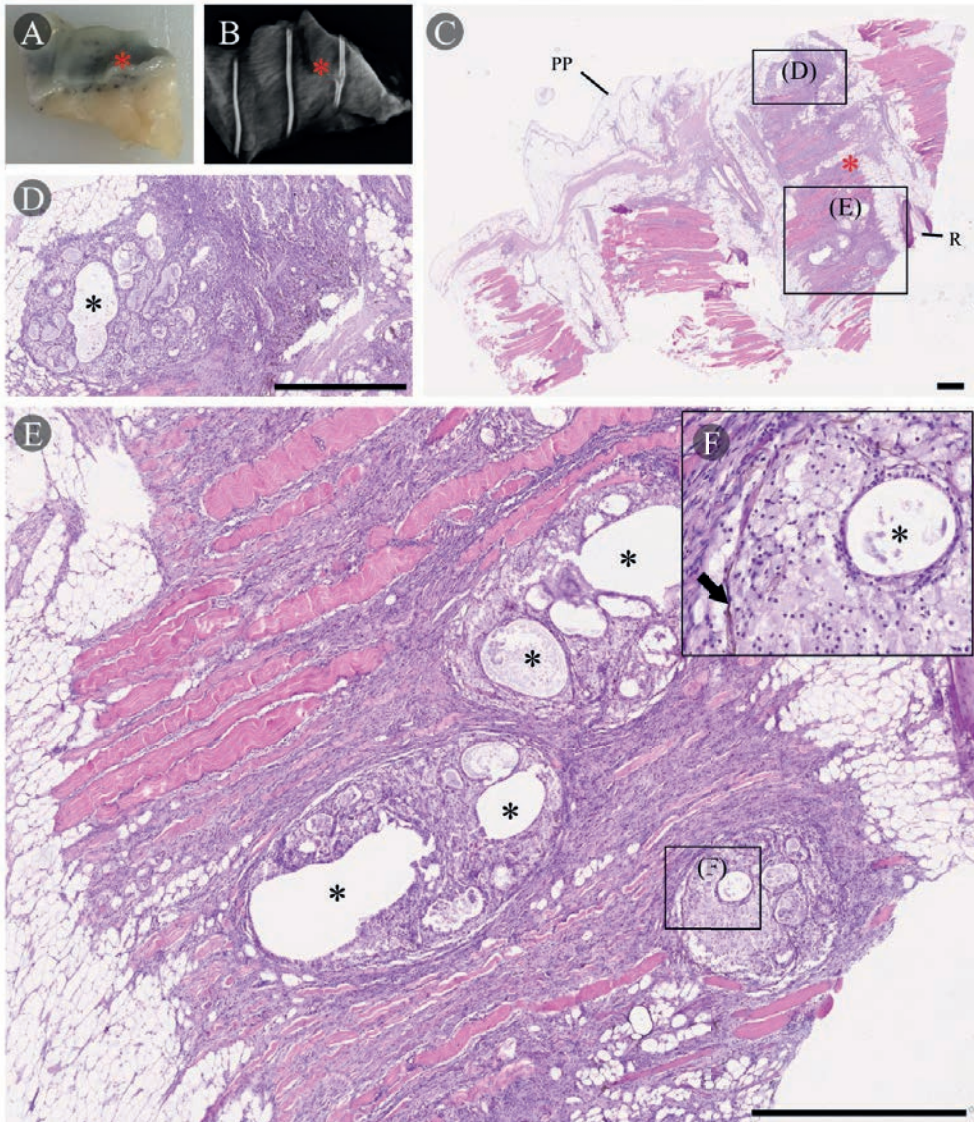


Figure 19. Characterization of focal dark spots granuloma of a sample with chronic musculoskeletal pathology. A) Image, B) lateral X-ray, and C) D) E) histology. Boxes with letters indicate the region of histology of D), E), and F). Red asterisks indicate the reference across different images from A) to C). Black asterisks indicate areas of large lipid vacuoles in histiocytic-like granulomas. The black arrow highlights melanomacrophages infiltrate. Black bars on the bottom right corner from C) to E) images show the image scale, set to 1mm. Haematoxylin and eosin. R, Rib (*costae*); PP, Parietal peritoneum. Sample from **Paper I**.

Intraperitoneal vaccination, farming system, and infection pressure/presence share a common feature; they determined different exposition levels to environmental

immunostimulants that seemed the most plausible candidate to explain the melanisation model of Figure 18. As melanisation is a very unspecific response, according to the model, fish farmed in land-based tanks of **Paper I** were exposed to a lower concentration of immune-stimulating factors (e.g., no vaccination, lower antigen concentration in UV-treated flow-through water) than in sea-cages (e.g., vaccinated, circulating antigens, infections) ([Bateman et al., 2021](#); [Lund et al., 2022](#)). Such immune-stimulating factors might have increased systemic melanin production to enhance immunocompetence to a disease threat - an important component of the innate immune system of insects and teleosts ([Gagnaire et al., 2013](#); [Wilson et al., 2001](#)). This could be especially evident in recurrent local inflammatory processes such as DS. In mammals ([Fu et al., 2020](#)), pro-inflammatory cytokines such as IL-18, IL-33, and granulocyte-macrophage colony-stimulating factors are known to stimulate melanogenesis by stimulating the protein kinase A pathway. IL-4 also stimulates melanogenesis by stimulating the signal transducer and activator of the transcription pathway. Prostaglandin E2 and F2 alpha, IL-1 α , and IL-6 also stimulate melanogenesis through unidentified signaling pathways. These pathways can be activated in response to several environmental factors (e.g., LPS and allergens), while individual factors like autoimmune diseases can trigger the release of several cytokines, including IL-1 α , IL-4, IL-6, and IL-18 ([Fu et al., 2020](#); [Page, Kell, & Pretorius, 2022](#)). Some of these cytokines are used as adjuvants in fish vaccines ([Guo & Li, 2021](#)). Thus, if fish are vaccinated, they could be artificially exposed to a similar activation as given in commercial sea-cage environments. The smaller potential immune stimulation in **Paper II** (vaccination) compared to sea-cages of **Paper I** (vaccination, more environmental antigens, and pathogens), might explain why DS of smaller size and pigmentation levels were found after transferring fish to a large tank compared to sea-cages (Figure 18). However, this difference could also be attributed to potential differences in the age of musculoskeletal damage.

5.4.5 The role of B cells on focal dark spot development

Immune-stimulating factors, such as environmental antigens, may impact DS development. The cause-relationship between viruses or bacteria infection and DS has been previously hypothesized ([Bjørngen et al., 2015](#); [Krasnov et al., 2016](#)), but not confirmed in [Bjørngen et al. \(2019\)](#) and our work (Figure 18).

The results of **Paper III** indicated a strong local antigenic stimulation in DS. However, no universal bacterial DNA/RNA and muscle-specific viral RNA, like PRV-1 and PMCV, that might influence the antigenic response in various DS phases were detected. On the other hand, RT-qPCR consistently detected the presence of SAV in most DS and control skeletal muscle. Virtually all fish were infected with either SAV (7:8) or PRV-1 (2:8), with slightly higher expression of SAV in DS (Ct = 29.7) than in control skeletal muscle from the opposite side of the fish (Ct = 33.5). As these fish were not vaccinated with SAV-inactivated whole virus or plasmids vaccines, one may suspect that these exogenous antigens could be the main driver for the Ab response. On the other hand, though the viral load was higher in DS than in control skeletal muscle, its presence was not restricted to DS. Moreover, viral Ct-values were not aligned with the phase of the inflammatory process or DS morphology. This discrepancy suggests a lack of direct causal association between the viral antigenic activity and these DS. Factors such as a potential higher tropism for myoblasts during the regenerative process or the anti-inflammatory local environment due to increased IL-10 levels might provide more direct mechanisms for increased viral loads in DS than in control samples ([Bjørger et al., 2020](#); [Dahle & Jørgensen, 2019](#)). The exact contribution of these factors and their interplay leading to higher viral loads in DS would likely require further research.

Consequently, in the most likely scenario, opportunistic bacteria, SAV, and other muscle-infecting viruses are not causative agents, but they may be one of the predisposing factors to the development of fillet-black DS in some instances ([Malik et al., 2021](#)). This may explain the previously reported association with bacteria [Krasnov et al. \(2016\)](#) or PRV-1 [Bjørger et al. \(2019\)](#). Nevertheless, it is possible that the material was degraded in chronic DS forms (bacterial especially) or that there may be too few samples to draw a determinant conclusion.

The molecular characterization of DS in **Paper III** showed that larger and more intense DS were associated with higher expression of all analysed innate and adaptive immune genes, especially *mhc2*, *cd83*, and *igt*. Here, the flatter the DS (high probability of a trauma involving rib damage and recurrent injury; **Paper I**), the higher the Spot-Spot CF and the expression of *csfr*, *cd28*, *ctla*, *igt*, and particularly *sigm*, but lower of *cd83* and *btla*. These findings suggest that trauma and recurrent injury processes are associated with a higher presence of macrophage, CD4⁺ and CD8⁺ cells activation, and B cell maturation and activity, but lower dendritic cells and lymphocyte attenuators. Alternatively, the DS

appearance might be associated with different stages of immune responses, which would invalidate the model proposed in Figure 17. Unfortunately, the events' duration could not be estimated because all DS in **Paper III** were sampled simultaneously at the end of the commercial-scale experiment.

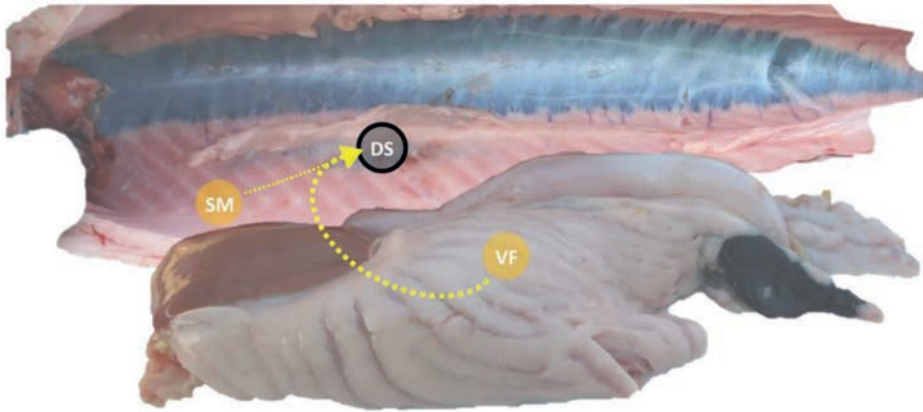
In mammals, local recurrent injuries can create a reactive immune microenvironment with persistent endogenous alarm signals from necrotic, distressed, injured cells, neutrophils, and APCs such as TNF- α , IL1- β , IL-6, and IL-12. Such a reactive immune microenvironment would contribute to a maladaptive repair ([Soliman & Barreda, 2023](#); [Wiegertjes & Elks, 2022](#)). Such immune microenvironments could also generate disrupted cytokine and cell balance ([Farini et al., 2021](#); [Sciorati et al., 2016](#)). The DS cytokine microenvironment seems to be especially rich in IL-10 in most chronic forms ([BjØrgen et al., 2020](#)). This is consistent with its role as a natural mechanism to control excessive inflammation and facilitate tissue regeneration. However, if the inflammatory stimuli persists, as seen in recurrent injuries, the anti-inflammatory effects of increased levels of IL-10 might be insufficient. This is a common finding in chronic inflammatory conditions, such as rheumatoid arthritis ([Cush et al., 1995](#); [Hernández-Bello et al., 2017](#)). In addition to endogenous alarm signals, as shown in mammals, the continuous cell damage in recurrent injuries may expose lymphocytes to a constant source of autoantigens ([Kimura et al., 2015](#); [Madaro & Bouché, 2014](#); [Sciorati et al., 2016](#)) that in a pro-inflammatory context would activate lymphocytes. A trauma and recurrent injury scenario could also induce tissue regeneration with myoblasts expressing high levels of myositis autoantigens ([Casciola-Rosen et al., 2005](#); [Kimura et al., 2015](#); [Suber, Casciola-Rosen, & Rosen, 2008](#)). Consequently, if neither bacterial nor viral antigens were responsible for the local maturation of early ontogeny B cells in **Paper III**, in the most likely scenario, the antigenic stimulation and transition from haemorrhages to melanised chronic processes/fillet-back DS could be contributed by an autoimmune inflammatory myopathy driven by autoantigens ([Farini et al., 2021](#)), an endogenous pathway. Similar studies addressing the clonotype repertoire in autoimmune processes in humans mirror a local maturation of B cells - also of early ontogeny - that could play a role in developing chronic inflammatory conditions, such as inflammatory myopathies ([Salajegheh et al., 2010](#)) and rheumatoid arthritis ([Cowan et al., 2020](#)). Unfortunately, due to a lack of time and resources, the presence of autoantibodies in the serum from these fish, as undertaken

by [Koppang et al. \(2008\)](#), was not investigated, which would have helped reinforce the hypothesis.

Activation and maintenance of the immune response in DS in the absence of pathogens align with the "danger model" proposed by [Matzinger \(1994\)](#) or now the "damage theory" as reviewed by [Pradeu and Cooper \(2012\)](#). The model suggests that the immune response has evolved mainly to be triggered by "alarm or damage signals" produced by the body's own cells, rather than foreign entities (e.g., bacteria and viruses). However, if the endogenous antigens model is correct, what is the reason for the failure of some fish groups to develop chronification and melanisation of musculoskeletal injuries? A possible scenario would be that these fish may lack or still develop chronic inflammation with endogenous antigenic stimulation where melanogenesis as a part of the innate immune system is disabled/downregulated, as described in Chapter 5.4.4.

According to the current views on the teleost immune system ([Abós et al., 2022](#)), preferential migration of B cells from the head kidney and spleen to peripheral tissues such as DS was expected. However, our analyses in **Paper III** suggested that an antigen-stimulated proliferation and differentiation of naïve to mature B cells was instead initiated in DS followed by subsequent migration. Thus, the first wave of naïve B cells most likely migrated from visceral peritoneum fat (principally) and/or locally by resident B cells in normal skeletal muscle. The process in Figure 20. A was possibly mediated in a TI way as Fish #4 had the lowest expression of *cd28* and *ctla*, but the highest *pax5* and *cd79* expression. This may be potentially interpreted as a significant binding of antigens to B cell receptors. However, there was insufficient gene expression data to support a TI in this first wave. Later, B cells either stayed at the site of antigen deposition (DS; MMCs) or migrated to other tissues, such as the head kidney, visceral peritoneum fat, and spleen (likely in this order), causing a systemic immunization to the target antigen (Figure 20. B). These B cell dynamics provide new insights into teleost immunity as they reveal the maturation of B cells in DS and a preferential implication of naïve B cells from serous areas as the visceral peritoneum fat, and skeletal muscle in the first stages of the adaptive immune response of musculoskeletal injuries of the abdominal wall.

A B cell traffic from tissues to DS



B B cell traffic from DS to other tissues

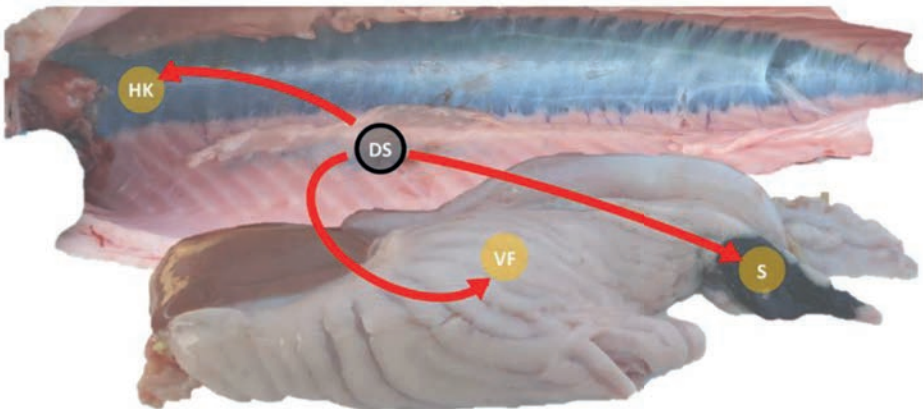


Figure 20. Model of B cell traffic in Atlantic salmon between focal dark spots (DS) and other tissues based on cumulative frequencies (CF) and expression of *migm* and *sigm*. A) After stimulation by local antigens in the musculoskeletal injury, B cells likely migrate from visceral peritoneum fat (VF) and skeletal muscle (SM) to DS, as illustrated by discontinuous yellow arrows. Then, B) B cells migrate from DS to other tissues, including head kidney (HK), VF, and spleen (S), indicating systemic immunization, as illustrated by continuous red arrows between DS and B cell resident organs or tissues. The thickness of the arrows indicates the order of shared CF. Based on **Paper III**.

5.4.6 Implications for the aquaculture industry

Before this work, DS were principally considered the result of PRV-1 infection, and there was little focus on the anatomic relationship with other structures of the hypaxial skeletal muscle, such as rib bones. The present thesis demonstrated that DS most likely originated

from damaging incidents affecting the abdominal wall of salmon, and that their transition from haemorrhages/fillet-red DS to melanised chronic processes/fillet-back DS was probably regulated by a series of factors in a cascade. This can represent a turning point in the approach and aetiological focus of the problem, offering numerous critical control points (CCPs) of significant interest for future research that will help to control the prevalence of DS in farmed salmon (Figure 21). The model predicts a significant reduction in the prevalence of DS by blocking or controlling one or several of these CCPs. Moreover, this work provides evidence of important production-related musculoskeletal issues concerning fish health, welfare, and product quality.

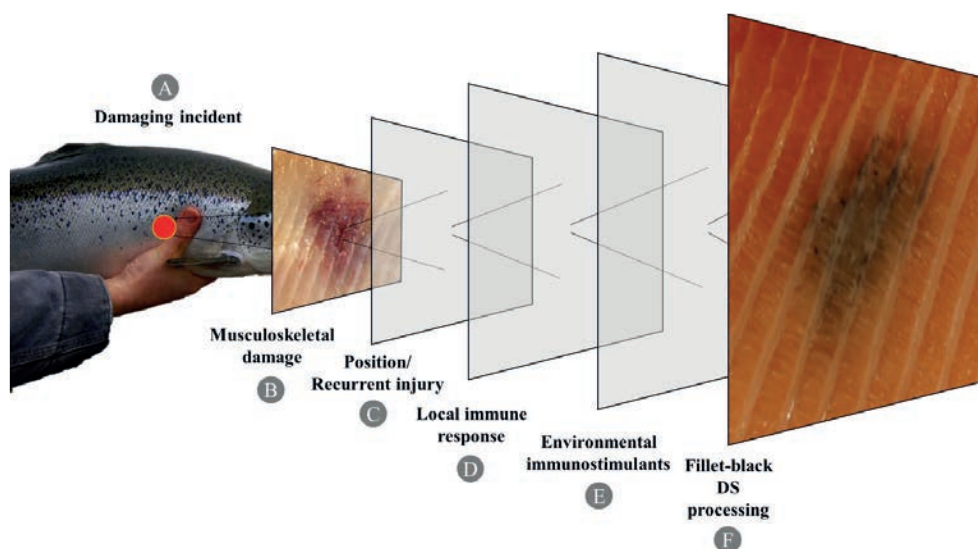


Figure 21. Critical control points (CCPs) for focal dark spots (DS). The model predicts six CCPs: A) Environmental factors generating damaging incidents; B) Individual factors influencing the degree of musculoskeletal damage; C) The position and the formation of a recurrent injury, which might influence the development of the healing process; D) The local immune response; E) Environmental factors modulating the melanogenesis as part of the immune response, and F) Post-mortem processing of DS (trimming). Based on **Papers I, II, III** and literature in Chapter 5.1.1.

Complementary, methods that can be the basis for future research on the rib cage of Atlantic salmon were developed. These methods included a novel approach for DS morphology evaluation (molecularly validated), a rib classification system (X-ray and histology), histological protocols for rib pathology, bone strength methods (ribs and vertebrae), a cheap and efficient potential external indicator of melanizing capabilities in

an Atlantic salmon population (melanisation of the rostral area of the mouth). General dietary insight that could potentially build the basis of future nutritional strategies to improve salmon musculoskeletal health were also provided.

5.5 Identified gaps for future studies

The shift to focus on mechanical stress as a main aetiological factor for DS brings new possibilities that must be explored in future research. Thus, focusing on **any source of mechanical stress during the fresh and seawater phases** of commercial salmon farming should be further explored to evaluate their impact on the abdominal wall. Precisely, the lack of related available information, the presence of relatively larger haemorrhages in freshwater fish, and the abrupt increase of rib abnormalities after seawater transfer to sea-cages, are evidence that more research in these stages should be done.

Smoltification diet is an important factor for rib morphology and general musculoskeletal traits, and that ribs are more sensitive than vertebrae in the long-term. Therefore, **ribs should be included in bone health evaluations in future dietary experiments** to improve fish welfare and fillet quality. Positive effects when using high percentages of marine ingredients were also observed. Hence, **high inclusion of marine ingredients** during smoltification and factors **modulating Na-based hydroxyapatite** concentrations in fish bones and their **impact on musculoskeletal health** should be a focus in future salmon nutrition research.

There is potential evidence of vaccination's impact on rib morphology and the chronification process of musculoskeletal injuries. Thus, **the reactivity of vaccine components** in the parietal peritoneum and ribs, and targeted studies exploring the possible **migration of loaded macrophages with vaccine compounds** from parietal peritoneum layers to the adjacent skeletal muscle in response to a traumatic event and the ongoing recurrent injury processes stimuli, should be considered.

There is evidence that some forms of salmon production can potentially limit the development of DS, suggesting a potential for developing specially designed solutions. Therefore, the **impact of the production systems** on the development of DS should be further understood in future studies, particularly the **interaction of the host-environmental immunostimulants on melanogenesis**.

The source of the antigenic responses in DS remains unidentified, and more studies in this direction should be planned. The thesis suggests focussing on **autoantigens generated in the recurrent injury** as a possible candidate for an autoimmune disease driving DS development.

Salmon farmers should consider the **development and implementation of a CCP plan for DS** adjusted to their production system based on the conclusions of this thesis.

5.6 Conclusions

This thesis concludes that rib and muscle damage, which may develop into recurring injury processes, are the primary cause of DS in Atlantic salmon fillets. The rearing environment has a significant impact on the aetiology of DS as the severity of the rib abnormalities and DS prevalence was larger in commercial sea-cages than in land-based tanks. The rearing environment also affected DS development as it may influence systemic immune-mediated melanin synthesis during healing, likely through unspecific immunostimulants common in commercial sea-cages/practices.

The composition of the diet during smoltification does not influence the development of DS but can have modulatory effects on long-term musculoskeletal health by inducing altered rib development, degeneration, possibly osteomalacia, and softer muscle. The development of DS is significantly influenced by factors such as the degree and location of the musculoskeletal injury (higher in mid and proximal rib parts), and local adaptive immune responses. The study highlights a local differentiation and maturation of naïve B and their migration, primarily from the visceral peritoneum fat and skeletal muscle to DS in response to unidentified local antigens (most likely endogenous). These B cells later migrate to other tissues, implying systemic immunization.

The findings highlight the need to create optimized farming conditions to prevent musculoskeletal damage and mitigate the development of DS.

6 References

- Abós, B., Bailey, C., & Tafalla, C. (2022). Adaptive immunity. In K. Buchmann & C. J. Secombes (Eds.), *Principles of fish immunology: From cells and molecules to host protection* (pp. 105-140). Springer International Publishing. https://doi.org/10.1007/978-3-030-85420-1_3
- Abram, Q. H., Dixon, B., & Katzenback, B. A. (2017). Impacts of low temperature on the teleost immune system. *Biology (Basel)*, 6(4), 39. <https://doi.org/10.3390/biology6040039>
- Abshirini, M., Hesanmi-Oyelere, B. L., & Kruger, M. C. (2021). Potential modulatory mechanisms of action by long-chain polyunsaturated fatty acids on bone cell and chondrocyte metabolism. *Prog. Lipid Res.*, 83, 101113. <https://doi.org/10.1016/j.plipres.2021.101113>
- Agius, C. (1980). Phylogenetic development of melano-macrophage centres in fish. *J. Zool.*, 191(1), 11-31. <https://doi.org/10.1111/j.1469-7998.1980.tb01446.x>
- Agius, C. (1985). The melano-macrophage centres in fish: a review. In M. J. Manning & M. F. Tatner (Eds.), *Fish Immunology* (pp. 85-105). Academic Press. <https://doi.org/10.1016/B978-0-12-469230-5.50011-8>
- Agius, C., & Roberts, R. J. (2003). Melano-macrophage centres and their role in fish pathology. *J. Fish Dis.*, 26(9), 499-509. <https://doi.org/10.1046/j.1365-2761.2003.00485.x>
- Akama, K., Ebata, K., Maeno, A., Taminato, T., Otsuka, S., Gengyo-Ando, K., Nakai, J., Yamasu, K., & Kawamura, A. (2020). Role of somite patterning in the formation of Weberian apparatus and pleural rib in zebrafish. *J. Anat.*, 236(4), 622-629. <https://doi.org/10.1111/joa.13135>
- Allen, L. G., Ladin, E. S., & Rowell, T. J. (2020). Sound production and mechanism in the giant sea bass, *Stereolepis gigas* (Polyprionidae). *Copeia*, 108(4), 809-814. <https://doi.org/10.1643/ci2020041>
- Aubin, J. E. (1998). Bone stem cells. *J. Cell. Biochem. Suppl.*, 30-31, 73-82. <https://pubmed.ncbi.nlm.nih.gov/9893258/>
- Aunsmo, A., Guttvik, A., Midtlyng, P. J., Larssen, R. B., Evensen, Ø., & Skjerve, E. (2008). Association of spinal deformity and vaccine-induced abdominal lesions in harvest-sized Atlantic salmon, *Salmo salar* L. *J. Fish Dis.*, 31(7), 515-524. <https://doi.org/10.1111/j.1365-2761.2007.00899.x>
- Aursand, M., Bleivik, B., Rainuzzo, J. R., Leif, J., & Mohr, V. (1994). Lipid distribution and composition of commercially farmed atlantic salmon (*Salmo salar*). *J. Sci. Food Agric.*, 64(2), 239-248. <https://doi.org/10.1002/jsfa.2740640214>
- Baeverfjord, G., Antony Jesu Prabhu, P., Fjellidal, P. G., Albrektsen, S., Hatlen, B., Denstadli, V., Ytteborg, E., Takle, H., Lock, E.-J., Berntssen, M. H. G., Lundebye, A.-K., Åsgård, T., & Waagbø, R. (2018). Mineral nutrition and bone health in salmonids. *Rev. Aquac.*, 11(3), 740-765. <https://doi.org/10.1111/raq.12255>
- Baeverfjord, G., Asgard, T., & Shearer, K. D. (1998). Development and detection of phosphorus deficiency in Atlantic salmon, *Salmo salar* L., parr and post-smolts. *Aquacult. Nutr.*, 4(1), 1-11. <https://doi.org/10.1046/j.1365-2095.1998.00095.x>
- Bahney, C. S., Zondervan, R. L., Allison, P., Theologis, A., Ashley, J. W., Ahn, J., Miclau, T., Marcucio, R. S., & Hankenson, K. D. (2019). Cellular biology of fracture healing. *J. Orthop. Res.*, 37(1), 35-50. <https://doi.org/10.1002/jor.24170>
- Bassing, C. H., Swat, W., & Alt, F. W. (2002). The mechanism and regulation of chromosomal V(D)J recombination. *Cell*, 109 Suppl, S45-55. [https://doi.org/10.1016/s0092-8674\(02\)00675-x](https://doi.org/10.1016/s0092-8674(02)00675-x)
- Bateman, A. W., Teffer, A. K., Bass, A., Ming, T., Hunt, B. P. V., Krkošek, M., & Miller, K. M. (2021). Atlantic salmon farms are a likely source of *Tenacibaculum maritimum* infection in migratory Fraser River sockeye salmon. *Can. J. Fish. Aquat. Sci.*, 00, 1-16. <https://doi.org/10.1101/2021.06.15.448581>
- Berg, A., Yurtseva, A., Hansen, T., Lajus, D., & Fjellidal, P. G. (2012). Vaccinated farmed Atlantic salmon are susceptible to spinal and skull deformities. *J. Appl. Ichthyol.*, 28(3), 446-452. <https://doi.org/10.1111/j.1439-0426.2012.01988.x>

- Bernabei, M., van Dieën, J. H., & Maas, H. (2017). Altered mechanical interaction between rat plantar flexors due to changes in intermuscular connectivity. *Scand. J. Med. Sci. Sports*, 27(2), 177-187. <https://doi.org/10.1111/sms.12644>
- Bernard, D., Six, A., Rigottier-Gois, L., Messiaen, S., Chilmonczyk, S., Quillet, E., Boudinot, P., & Benmansour, A. (2006). Phenotypic and functional similarity of gut intraepithelial and systemic T cells in a teleost fish. *J. Immunol.*, 176(7), 3942-3949. <https://doi.org/10.4049/jimmunol.176.7.3942>
- Bird, N. C., & Mabee, P. M. (2003). Developmental morphology of the axial skeleton of the zebrafish, *Danio rerio* (Ostariophysi: Cyprinidae). *Dev. Dyn.*, 228(3), 337-357. <https://doi.org/10.1002/dvdy.10387>
- Bjørngen, H., Haldorsen, R., Oaland, Ø., Kvellestad, A., Kannimuthu, D., Rimstad, E., & Koppang, E. O. (2019). Melanized focal changes in skeletal muscle in farmed Atlantic salmon after natural infection with *Piscine orthoreovirus* (PRV). *J. Fish Dis.*, 42(6), 935-945. <https://doi.org/10.1111/jfd.12995>
- Bjørngen, H., Kumar, S., Gunnes, G., Press, C. M., Rimstad, E., & Koppang, E. O. (2020). Immunopathological characterization of red focal changes in Atlantic salmon (*Salmo salar*) white muscle. *Vet. Immunol. Immunopathol.*, 222, 110035. <https://doi.org/10.1016/j.vetimm.2020.110035>
- Bjørngen, H., Wessel, Ø., Fjellidal, P. G., Hansen, T., Sveier, H., Sæbø, H. R., Enger, K. B., Monsen, E., Kvellestad, A., Rimstad, E., & Koppang, E. O. (2015). *Piscine orthoreovirus* (PRV) in red and melanised foci in white muscle of Atlantic salmon (*Salmo salar*). *Vet. Res.*, 46(1), 89. <https://doi.org/10.1186/s13567-015-0244-6>
- Blazer, V. S. (1991). Piscine macrophage function and nutritional influences: A review. *Journal of Aquatic Animal Health*, 3(2), 77-86. <https://afspubs.onlinelibrary.wiley.com/doi/abs/10.1577/1548-8667%281991%29003%3C0077%3APMFANI%3E2.3.CO%3B2>
- Boissy, R. E., & Hornyak, T. J. (2006). Extracutaneous melanocytes. In *The pigmentary system* (pp. 91-107). <https://doi.org/10.1002/9780470987100.ch4>
- Bou, M., Berge, G. M., Baeverfjord, G., Sigholt, T., Østbye, T. K., & Ruyter, B. (2017). Low levels of very-long-chain n-3 PUFA in Atlantic salmon (*Salmo salar*) diet reduce fish robustness under challenging conditions in sea cages. *J. Nutr. Sci.*, 6, e32. <https://doi.org/10.1017/jns.2017.28>
- Brimsholm, M., Fjellidal, P. G., Hansen, T., Trangerud, C., Knutsen, G. M., Asserson, C. F., Koppang, E. O., & Bjørngen, H. (2023). Anatomical and pathological characteristics of ribs in the Atlantic salmon (*Salmo salar* L.) and its relevance to soft tissue changes. *Anat. Histol. Embryol.* <https://doi.org/10.1111/ahc.12900>
- Britannica, E. (2023). *Classes of antibodies*. Encyclopædia Britannica. <https://www.britannica.com/science/immune-system/Classes-of-immunoglobulins#/media/1/283636/17661>
- Britz, R., & Bartsch, P. (2003). The myth of dorsal ribs in gnathostome vertebrates. *Proceedings: Biological Sciences*, 270, S1-S4. <http://www.jstor.org/stable/3592244>
- Calabrese, S., Nilsen, T. O., Kolarevic, J., Ebbesson, L. O. E., Pedrosa, C., Fivelstad, S., Hosfeld, C., Stefansson, S. O., Terjesen, B. F., Takle, H., Martins, C. I. M., Sveier, H., Mathisen, F., Imsland, A. K., & Handeland, S. O. (2017). Stocking density limits for post-smolt Atlantic salmon (*Salmo salar* L.) with emphasis on production performance and welfare. *Aquac.*, 468, 363-370. <https://doi.org/10.1016/j.aquaculture.2016.10.041>
- Cao, J., Xu, H., Yu, Y., & Xu, Z. (2023). Regulatory roles of cytokines in T and B lymphocytes-mediated immunity in teleost fish. *Dev. Comp. Immunol.*, 144, 104621. <https://doi.org/10.1016/j.dci.2022.104621>
- Carlton, W. W., Boitnott, J. K., Dungworth, D. L., Ernst, H., Hayashi, Y., Mohr, U., Parodi, A. L., Pattengale, P. K., Rittinghausen, S., & Ward, J. M. (2001). Assessment of the morphology and significance of the lymph nodal and hepatic lesions produced in rats by the feeding of certain mineral oils and waxes. *Exp. Toxicol. Pathol.*, 53(4), 247-255. <https://doi.org/10.1078/0940-2993-00198>

- Casciola-Rosen, L., Nagaraju, K., Plotz, P., Wang, K., Levine, S., Gabrielson, E., Corse, A., & Rosen, A. (2005). Enhanced autoantigen expression in regenerating muscle cells in idiopathic inflammatory myopathy. *J. Exp. Med.*, *201*(4), 591-601. <https://doi.org/10.1084/jem.20041367>
- Cerutti, A., Puga, I., & Cols, M. (2011). Innate control of B cell responses. *Trends Immunol.*, *32*(5), 202-211. <https://doi.org/10.1016/j.it.2011.02.004>
- Chu, P. G., & Arber, D. A. (2001). CD79: a review. *Appl. Immunohistochem. Mol. Morphol.*, *9*(2), 97-106. <https://doi.org/10.1097/00129039-200106000-00001>
- Cobaleda, C., Schebesta, A., Delogu, A., & Busslinger, M. (2007). Pax5: the guardian of B cell identity and function. *Nat. Immunol.*, *8*(5), 463-470. <https://doi.org/10.1038/ni1454>
- Cohen, L., Dean, M., Shipov, A., Atkins, A., Monsonego-Ornan, E., & Shahar, R. (2012). Comparison of structural, architectural and mechanical aspects of cellular and acellular bone in two teleost fish. *J. Exp. Biol.*, *215*(11), 1983-1993. <https://doi.org/10.1242/jeb.064790>
- Colegio, O. R., Chu, N.-Q., Szabo, A. L., Chu, T., Rhebergen, A. M., Jairam, V., Cyrus, N., Brokowski, C. E., Eisenbarth, S. C., Phillips, G. M., Cline, G. W., Phillips, A. J., & Medzhitov, R. (2014). Functional polarization of tumour-associated macrophages by tumour-derived lactic acid. *Nature*, *513*(7519), 559-563. <https://doi.org/10.1038/nature13490>
- Colt, J., Summerfelt, S., Pfeiffer, T., Fivelstad, S., & Rust, M. (2008). Energy and resource consumption of land-based Atlantic salmon smolt hatcheries in the Pacific Northwest (USA). *Aquac.*, *280*(1), 94-108. <https://doi.org/10.1016/j.aquaculture.2008.05.014>
- Cowan, G. J. M., Miles, K., Capitani, L., Giguere, S. S. B., Johnsson, H., Goodyear, C., McInnes, I. B., Breusch, S., Gray, D., & Gray, M. (2020). In human autoimmunity, a substantial component of the B cell repertoire consists of polyclonal, barely mutated IgG+ve B cells. *Front. Immunol.*, *11*. <https://doi.org/10.3389/fimmu.2020.00395>
- Csapo, R., Gumpenberger, M., & Wessner, B. (2020). Skeletal muscle extracellular matrix - What do we know about its composition, regulation, and physiological roles? A narrative review. *Front. physiol.*, *11*, 253. <https://doi.org/10.3389/fphys.2020.00253>
- Currey, J. D. (2003). The many adaptations of bone. *J. Biomech.*, *36*(10), 1487-1495. [https://doi.org/10.1016/s0021-9290\(03\)00124-6](https://doi.org/10.1016/s0021-9290(03)00124-6)
- Cush, J. J., Splawski, J. B., Thomas, R., McFarlin, J. E., Schulze-Koops, H., Davis, L. S., Fujita, K., & Lipsky, P. E. (1995). Elevated interleukin-10 levels in patients with rheumatoid arthritis. *Arthritis Rheumatol.*, *38*(1), 96-104. <https://doi.org/10.1002/art.1780380115>
- Dahle, M. K., & Jørgensen, J. B. (2019). Antiviral defense in salmonids – Mission made possible? *Fish Shellfish Immunol.*, *87*, 421-437. <https://doi.org/10.1016/j.fsi.2019.01.043>
- Dale, R. M., & Topczewski, J. (2011). Identification of an evolutionarily conserved regulatory element of the zebrafish *col2a1a* gene. *Dev. Biol.*, *357*(2), 518-531. <https://doi.org/10.1016/j.ydbio.2011.06.020>
- Davis, A. C., Roux, K. H., & Shulman, M. J. (1988). On the structure of polymeric IgM. *Eur. J. Immunol.*, *18*(7), 1001-1008. <https://doi.org/10.1002/eji.1830180705>
- de Cássia, R. G. R., & Pombeiro-Sponchiado, S. R. (2005). Antioxidant activity of the melanin pigment extracted from *Aspergillus nidulans*. *Biol. Pharm. Bull.*, *28*(6), 1129-1131. <https://doi.org/10.1248/bpb.28.1129>
- De Clercq, A., Perrott, M. R., Davie, P. S., Preece, M. A., Wybourne, B., Ruff, N., Huysseune, A., & Witten, P. E. (2017). Vertebral column regionalisation in Chinook salmon, *Oncorhynchus tshawytscha*. *J. Anat.*, *231*(4), 500-514. <https://doi.org/10.1111/joa.12655>
- de Gruijter, N. M., Jebson, B., & Rosser, E. C. (2022). Cytokine production by human B cells: role in health and autoimmune disease. *Clin. Exp. Immunol.*, *210*(3), 253-262. <https://doi.org/10.1093/cei/uxac090>
- de la Fuente, R., Abad, J. L., García-Castro, J., Fernández-Miguel, G., Petriz, J., Rubio, D., Vicario-Abejón, C., Guillén, P., González, M. A., & Bernad, A. (2004). Dedifferentiated adult articular chondrocytes: a population of human multipotent primitive cells. *Exp. Cell Res.*, *297*(2), 313-328. <https://doi.org/10.1016/j.yexcr.2004.02.026>
- Dessen, J.-E., Weihe, R., Hatlen, B., Thomassen, M. S., & Rørvik, K.-A. (2017). Different growth performance, lipid deposition, and nutrient utilization in in-season (S1) Atlantic salmon post-

- smolt fed isoenergetic diets differing in protein-to-lipid ratio. *Aquac.*, 473, 345-354. <https://doi.org/10.1016/j.aquaculture.2017.02.006>
- Dessen, J. E., Mørkøre, T., Bildøy, J. I., Johnsen, S. N., Poppe, L. T., Hatlen, B., Thomassen, M. S., & Rørvik, K. A. (2019). Increased dietary protein-to-lipid ratio improves survival during naturally occurring pancreas disease in Atlantic salmon, *Salmo salar* L. *J. Fish. Dis.*, 42(1), 21-34. <https://doi.org/10.1111/jfd.12904>
- Dhanasiri, A. K. S., Johny, A., Xue, X., Berge, G. M., Bøgevik, A. S., Rise, M. L., Fæste, C. K., & Fernandes, J. M. O. (2020). Plant-Based Diets Induce Transcriptomic Changes in Muscle of Zebrafish and Atlantic Salmon. *Front. Genet.*, 11. <https://doi.org/10.3389/fgene.2020.575237>
- Drábiková, L., Fjellidal, P. G., De Clercq, A., Yousaf, M. N., Morken, T., McGurk, C., & Witten, P. E. (2021). Vertebral column adaptations in juvenile Atlantic salmon *Salmo salar*, L. as a response to dietary phosphorus. *Aquac.*, 541, 736-776. <https://doi.org/10.1016/j.aquaculture.2021.736776>
- Drábiková, L., Fjellidal, P. G., De Clercq, A., Yousaf, M. N., Morken, T., McGurk, C., & Witten, P. E. (2022). What will happen to my smolt at harvest? Individually tagged Atlantic salmon help to understand possible progression and regression of vertebral deformities. *Aquac.*, 559, 738430. <https://doi.org/10.1016/j.aquaculture.2022.738430>
- Dunford, R., Land, E. J., Rozanowska, M., Sarna, T., & Truscott, T. G. (1995). Interaction of melanin with carbon- and oxygen-centered radicals from methanol and ethanol. *Free Radic. Biol. Med.*, 19(6), 735-740. [https://doi.org/10.1016/0891-5849\(95\)00059-7](https://doi.org/10.1016/0891-5849(95)00059-7)
- Dymecki, S. M., Zwollo, P., Zeller, K., Kuhajda, F. P., & Desiderio, S. V. (1992). Structure and developmental regulation of the B-lymphoid tyrosine kinase gene *blk*. *J. Biol. Chem.*, 267(7), 4815-4823. <https://pubmed.ncbi.nlm.nih.gov/1537861/>
- El-Naggar, N. E.-A., & Saber, W. I. A. (2022). Natural melanin: Current trends, and future approaches, with especial reference to microbial source. *Polymers*, 14(7), 1339. <https://www.mdpi.com/2073-4360/14/7/1339>
- Emelianov, S. W. (1935). *Die morphologie der fischrippen*. G. Fischer. Link not available
- Eming, S. A., Martin, P., & Tomic-Canic, M. (2014). Wound repair and regeneration: Mechanisms, signaling, and translation. *Sci. Transl. Med.*, 6(265), 265sr266-265sr266. <https://doi.org/doi:10.1126/scitranslmed.3009337>
- Epsley, S., Tadros, S., Farid, A., Kargilis, D., Mehta, S., & Rajapakse, C. S. (2021). The Effect of Inflammation on Bone. *Front. physiol.*, 11. <https://doi.org/10.3389/fphys.2020.511799>
- Fagerland, H. A. S., Austbø, L., Fritsvold, C., Alarcon, M., Rimstad, E., Falk, K., Taksdal, T., & Koppang, E. O. (2013). Pathological pigmentation in cardiac tissues of Atlantic salmon (*Salmo salar* L.) with cardiomyopathy syndrome. *Vet. Res.*, 44(1), 107. <https://doi.org/10.1186/1297-9716-44-107>
- FAO. (2022). *The state of world fisheries and aquaculture (SOFIA). Towards blue transformation*. FAO. <https://doi.org/10.4060/cc0461en>
- Farini, A., Villa, C., Tripodi, L., Legato, M., & Torrente, Y. (2021). Role of immunoglobulins in muscular dystrophies and inflammatory myopathies. *Front. Immunol.*, 12. <https://doi.org/10.3389/fimmu.2021.666879>
- Feehan, K. T., & Gilroy, D. W. (2019). Is resolution the end of inflammation? *Trends Mol. Med.*, 25(3), 198-214. <https://doi.org/10.1016/j.molmed.2019.01.006>
- Fiedler, I. A. K., Elmogazy, O., Courtemanche, G., Cardoso, L., & Berteau, J. P. (2021). Bones of teleost fish demonstrate high fracture strain. *J. Biomech.*, 120, 110341. <https://doi.org/10.1016/j.jbiomech.2021.110341>
- Fiskeridirektoratet. (2021a). *Biomassestatistikk*. Retrieved from <https://www.fiskeridir.no/English/Aquaculture/Statistics/Atlantic-salmon-and-rainbow-trout>
- Fiskeridirektoratet. (2021b). *Nøkkeltall fra norsk havbruksnæring*. Retrieved from <https://www.fiskeridir.no/Akvakultur/Tall-og-analyse/Statistiske-publikasjoner/Noekkeltall-for-norsk-havbruksnaering>
- Fjellidal, P. G., Grotmol, S., Kryvi, H., Gjerdet, N. R., Taranger, G. L., Hansen, T., Porter, M. J., & Totland, G. K. (2004). Pinealectomy induces malformation of the spine and reduces the

- mechanical strength of the vertebrae in Atlantic salmon, *Salmo salar*. *J. Pineal Res.*, 36(2), 132-139. <https://doi.org/10.1046/j.1600-079x.2003.00109.x>
- Fjellidal, P. G., Lock, E.-J., Grotmol, S., Totland, G. K., Nordgarden, U., Flik, G., & Hansen, T. (2006). Impact of smolt production strategy on vertebral growth and mineralisation during smoltification and the early seawater phase in Atlantic salmon (*Salmo salar*, L.). *Aquac.*, 261(2), 715-728. <https://doi.org/10.1016/j.aquaculture.2006.08.008>
- Fjellidal, P. G., Lock, E.-J., Hansen, T., Waagbø, R., Wargelius, A., Gil Martens, L., El-Mowafi, A., & Ørnsrud, R. (2012). Continuous light induces bone resorption and affects vertebral morphology in Atlantic salmon (*Salmo salar* L.) fed a phosphorous deficient diet. *Aquac. Nutr.*, 18(6), 610-619. <https://doi.org/10.1111/j.1365-2095.2011.00918.x>
- Fjellidal, P. G., Madaro, A., Hvas, M., Stien, L. H., Oppedal, F., & Fraser, T. W. K. (2020). Skeletal deformities in wild and farmed cleaner fish species used in Atlantic salmon *Salmo salar* aquaculture. *J. Fish Biol.*, 98(4), 1049-1058. <https://doi.org/10.1111/jfb.14337>
- Fjellidal, P. G., Nordgarden, U., & Hansen, T. (2007). The mineral content affects vertebral morphology in underyearling smolt of Atlantic salmon (*Salmo salar* L.). *Aquac.*, 270(1), 231-239. <https://doi.org/10.1016/j.aquaculture.2007.03.008>
- Fjellidal, P. G., van der Meeren, T., Fraser, T. W. K., Sambraus, F., Jawad, L., & Hansen, T. J. (2018). Radiological changes during fracture and repair in neural and haemal spines of Atlantic cod (*Gadus morhua*). *J. Fish Dis.*, 41(12), 1871-1875. <https://doi.org/10.1111/jfd.12899>
- Fletcher, G. C., Hallett, I. C., Jerrett, A. R., & Holland, A. J. (1997). Changes in the fine structure of the myocommata-muscle fibre junction related to gaping in rested and exercised muscle from king salmon (*Oncorhynchus tshawytscha*). *LWT - Food Sci. Technol.*, 30(3), 246-252. <https://doi.org/10.1006/fstl.1996.0175>
- Fraser, T. W., Hansen, T., Fleming, M. S., & Fjellidal, P. G. (2015). The prevalence of vertebral deformities is increased with higher egg incubation temperatures and triploidy in Atlantic salmon *Salmo salar* L. *J. Fish Dis.*, 38(1), 75-89. <https://doi.org/10.1111/jfd.12206>
- Froehlich, J., Fowler, Z., Galt, N., Smith, D., & Biga, P. (2013). Sarcopenia and piscines: the case for indeterminate-growing fish as unique genetic model organisms in aging and longevity research [Hypothesis and Theory]. *Front. Genet.*, 4. <https://doi.org/10.3389/fgene.2013.00159>
- Fu, C., Chen, J., Lu, J., Yi, L., Tong, X., Kang, L., Pei, S., Ouyang, Y., Jiang, L., Ding, Y., Zhao, X., Li, S., Yang, Y., Huang, J., & Zeng, Q. (2020). Roles of inflammation factors in melanogenesis (Review). *Mol. Med. Rep.*, 21(3), 1421-1430. <https://doi.org/10.3892/mmr.2020.10950>
- Gagnaire, B., Cavalie, I., Camilleri, V., & Adam-Guillermin, C. (2013). Effects of depleted uranium on oxidative stress, detoxification, and defence parameters of zebrafish *Danio rerio*. *Arch. Environ. Contam. Toxicol.*, 64(1), 140-150. <https://doi.org/10.1007/s00244-012-9814-z>
- Galloway, T. F., Kjørsvik, E., & Kryvi, H. (1999). Muscle growth and development in Atlantic cod larvae (*Gadus morhua* L.), related to different somatic growth rates. *J. Exp. Biol.*, 202(Pt 15), 2111-2120. <https://doi.org/10.1242/jeb.202.15.2111>
- Geurtzen, K., Knopf, F., Wehner, D., Huitema, L. F. A., Schulte-Merker, S., & Weidinger, G. (2014). Mature osteoblasts dedifferentiate in response to traumatic bone injury in the zebrafish fin and skull. *Development*, 141(11), 2225-2234. <https://doi.org/10.1242/dev.105817>
- Gil Martens, L., Witten, P. E., Fivelstad, S., Huysseune, A., Sævareid, B., Vikeså, V., & Obach, A. (2006). Impact of high water carbon dioxide levels on Atlantic salmon smolts (*Salmo salar* L.): Effects on fish performance, vertebrae composition and structure. *Aquac.*, 261(1), 80-88. <https://doi.org/10.1016/j.aquaculture.2006.06.031>
- Gislason, H., Karstensen, H., Christiansen, D., Hjelde, K., Helland, S., & Bæverfjord, G. (2010). Rib and vertebral deformities in rainbow trout (*Oncorhynchus mykiss*) explained by a dominant-mutation mechanism. *Aquac.*, 309(1), 86-95. <https://doi.org/10.1016/j.aquaculture.2010.09.016>
- Gistelink, C., Gioia, R., Gagliardi, A., Tonelli, F., Marchese, L., Bianchi, L., Landi, C., Bini, L., Huysseune, A., Witten, P. E., Staes, A., Gevaert, K., De Rucker, N., Menten, B., Malfait, F., Leikin, S., Carra, S., Tenni, R., Rossi, A., . . . Forlino, A. (2016). Zebrafish collagen type I: Molecular and biochemical characterization of the major structural protein in bone and skin. *Sci. Rep.*, 6(1), 21540. <https://doi.org/10.1038/srep21540>

- Goette, A. (1879). Beiträge zur vergleichenden morphologie des skeletsystems der wirbelthiere. *Archiv für mikroskopische Anatomie*, 16(1), 117-152. <https://doi.org/10.1007/BF02956382>
- Granja, A. G., Perdiguerro, P., Martín-Martín, A., Díaz-Rosales, P., Soletto, I., & Tafalla, C. (2019). Rainbow trout IgM+ B cells preferentially respond to thymus-independent antigens but are activated by CD40L. *Front. Immunol.*, 10. <https://doi.org/10.3389/fimmu.2019.02902>
- Grunow, B., Stange, K., Bochert, R., & Tönißen, K. (2021). Histological and biochemical evaluation of skeletal muscle in the two salmonid species *Coregonus maraena* and *Oncorhynchus mykiss*. *PLOS ONE*, 16(8), e0255062. <https://doi.org/10.1371/journal.pone.0255062>
- Guo, M., & Li, C. (2021). An overview of cytokine used as adjuvants in fish: current state and future trends. *Rev. Aquac.*, 13(2), 996-1014. <https://doi.org/10.1111/raq.12509>
- Guo, S., & Dipietro, L. A. (2010). Factors affecting wound healing. *J. Dent. Res.*, 89(3), 219-229. <https://doi.org/10.1177/0022034509359125>
- Göppert, E. (1895). Untersuchungen zur morphologie der fischrippen. *Morph. Jahrbuch*(23), 145-217. <https://www.regensburger-katalog.de/s/ubr/de/2/1035/BV007162937>
- Hall, B. K. (2015). Chapter 30 - Initiating skeletal growth. In B. K. Hall (Ed.), *Bones and cartilage* (Second Edition ed., pp. 475-486). Academic Press. <https://doi.org/10.1016/B978-0-12-416678-3.00030-6>
- Hansen, A. K. G., Kortner, T. M., Krasnov, A., Björkhem, I., Penn, M., & Krogdahl, Å. (2020). Choline supplementation prevents diet induced gut mucosa lipid accumulation in post-smolt Atlantic salmon (*Salmo salar* L.). *BMC Vet. Res.*, 16(1), 32. <https://doi.org/10.1186/s12917-020-2252-7>
- Hansen, T., Fjellidal, P. G., Yurtseva, A., & Berg, A. (2010). A possible relation between growth and number of deformed vertebrae in Atlantic salmon (*Salmo salar* L.). *J. Appl. Ichthyol.*, 26(2), 355-359. <https://doi.org/10.1111/j.1439-0426.2010.01434.x>
- Haugarvoll, E., Bjerkas, I., Szabo, N. J., Satoh, M., & Koppang, E. O. (2010). Manifestations of systemic autoimmunity in vaccinated salmon. *Vaccine*, 28(31), 4961-4969. <https://doi.org/10.1016/j.vaccine.2010.05.032>
- Havixbeck, J. J., & Barreda, D. R. (2015). Neutrophil development, migration, and function in teleost fish. *Biology*, 4(4), 715-734. <https://www.mdpi.com/2079-7737/4/4/715>
- Hearing, V. J. (1993). Unraveling the melanocyte. *Am. J. Hum. Genet.*, 52(1), 1-7. <https://www.ncbi.nlm.nih.gov/pmc/articles/PMC1682135/>
- Hennessy, A., Oh, C., Diffey, B., Wakamatsu, K., Ito, S., & Rees, J. (2005). Eumelanin and pheomelanin concentrations in human epidermis before and after UVB irradiation. *Pigment Cell Res.*, 18(3), 220-223. <https://doi.org/10.1111/j.1600-0749.2005.00233.x>
- Hernández-Bello, J., Oregón-Romero, E., Vázquez-Villamar, M., García-Arellano, S., Valle, Y., Padilla-Gutiérrez, J. R., Román-Fernández, I. V., Palafox-Sánchez, C. A., Martínez-Bonilla, G. E., & Muñoz-Valle, J. F. (2017). Aberrant expression of interleukin-10 in rheumatoid arthritis: Relationship with IL10 haplotypes and autoantibodies. *Cytokine*, 95, 88-96. <https://doi.org/10.1016/j.cyto.2017.02.022>
- Holm, H., Ytteborg, E., Høst, V., Reed, A. K., Dalum, A. S., & Bæverfjord, G. (2020). A pathomorphological description of cross-stitch vertebrae in farmed Atlantic salmon (*Salmo salar* L.). *Aquac.*, 526, 735382. <https://doi.org/10.1016/j.aquaculture.2020.735382>
- Horton, J. M., & Summers, A. P. (2009). The material properties of acellular bone in a teleost fish. *J. Exp. Biol.*, 212(9), 1413-1420. <https://doi.org/10.1242/jeb.020636>
- Hua, K., & Bureau, D. P. (2019). Estimating changes in essential amino acid requirements of rainbow trout and Atlantic salmon as a function of body weight or diet composition using a novel factorial requirement model. *Aquac.*, 513, 734440. <https://doi.org/10.1016/j.aquaculture.2019.734440>
- Hullo, M. F., Moszer, I., Danchin, A., & Martin-Verstraete, I. (2001). CotA of *Bacillus subtilis* is a copper-dependent laccase. *J. Bacteriol.*, 183(18), 5426-5430. <https://doi.org/10.1128/jb.183.18.5426-5430.2001>
- Huysseune, A., & Sire, J. Y. (1992). Development of cartilage and bone tissues of the anterior part of the mandible in cichlid fish: a light and TEM study. *Anat. Rec.*, 233(3), 357-375. <https://doi.org/10.1002/ar.1092330304>

- Hwang, S. H., Kim, H. H., Park, D. J., Jee, Y. S., Lee, K. H., Kim, Y. H., Lee, H. S., Lee, H. J., & Yang, H. K. (2012). Local tissue reaction after injection of contrast media on gastric wall of mouse: Experimental study for application of contrast media to computed tomography lymphography. *J. Korean Surg. Soc.*, 82(2), 70-78. <https://doi.org/10.4174/jkss.2012.82.2.70>
- ISO5984. (2002). Animal feeding stuffs - Specifies a method for the determination of crude ash of animal feeding stuffs. 6. <https://www.iso.org/standard/37272.html>
- ISO6491. (1998). Animal feeding stuffs - Determination of phosphorus content - Spectrometric method. 7. <https://www.iso.org/standard/12864.html>
- ISO6496. (1999). Animal feeding stuffs - Preparation of test samples - Determination of moisture and other volatile matter content. 7. <https://www.iso.org/obp/ui/en/#iso:std:iso:6496:ed-2:v1:en>
- Ito, S., Wakamatsu, K., & Ozeki, H. (2000). Chemical analysis of melanins and its application to the study of the regulation of melanogenesis. *Pigment Cell Res.*, 13(s8), 103-109. <https://doi.org/10.1034/j.1600-0749.13.s8.19.x>
- Jiao, Y. Y., Okada, M., Hara, E. S., Xie, S. C., Nagaoka, N., Nakano, T., & Matsumoto, T. (2020). Micro-architectural investigation of teleost fish rib inducing pliant mechanical property. *Materials*, 13(22), 5099. <https://doi.org/10.3390/ma13225099>
- Jiménez-Guerrero, R. (2018). *In vivo and in vitro study of dark pigment development in Atlantic salmon using novel methods based on image analysis* [Master thesis]. Norwegian University of Life Sciences. <https://nmbu.brage.unit.no/nmbu-xmlui/handle/11250/2569790>
- Jones, K., Savulescu, A. F., Brombacher, F., & Hadebe, S. (2020). Immunoglobulin M in health and diseases: How far have we come and what next? *Front. Immunol.*, 11. <https://doi.org/10.3389/fimmu.2020.595535>
- Julin, K., Johansen, L. H., & Sommer, A. I. (2009). Reference genes evaluated for use in infectious pancreatic necrosis virus real-time RT-qPCR assay applied during different stages of an infection. *J. Virol. Methods*, 162(1-2), 30-39. <https://doi.org/10.1016/j.jviromet.2009.07.003>
- Jung, D., Giallourakis, C., Mostoslavsky, R., & Alt, F. W. (2006). Mechanism and control of v(d)j recombination at the immunoglobulin heavy chain locus. *Annu. Rev. Immunol.*, 24(1), 541-570. <https://doi.org/10.1146/annurev.immunol.23.021704.115830>
- Karatas, T., Onalan, S., & Yildirim, S. (2021). Effects of prolonged fasting on levels of metabolites, oxidative stress, immune-related gene expression, histopathology, and DNA damage in the liver and muscle tissues of rainbow trout (*Oncorhynchus mykiss*). *Fish Physiol. Biochem.*, 47(4), 1119-1132. <https://doi.org/10.1007/s10695-021-00949-2>
- Khurana, J. S. (2009). *Bone pathology* (Second ed., Vol. Temple University Hospital). Humana Press, Springer. <https://doi.org/10.1007/978-1-59745-347-9>
- Kimura, N., Hirata, S., Miyasaka, N., Kawahata, K., & Kohsaka, H. (2015). Injury and subsequent regeneration of muscles for activation of local innate immunity to facilitate the development and relapse of autoimmune myositis in C57BL/6 mice. *Arthritis Rheumatol.*, 67(4), 1107-1116. <https://doi.org/10.1002/art.39017>
- Kollias, N., Sayre, R. M., Zeise, L., & Chedekel, M. R. (1991). New trends in photobiology: Photoprotection by melanin. *J. Photochem. Photobiol. B, Biol.*, 9(2), 135-160. [https://doi.org/10.1016/1011-1344\(91\)80147-A](https://doi.org/10.1016/1011-1344(91)80147-A)
- Koppang, E. O., Bjerkås, I., Haugarvoll, E., Chan, E. K., Szabo, N. J., Ono, N., Akikusa, B., Jirillo, E., Poppe, T. T., Sveier, H., Tørud, B., & Satoh, M. (2008). Vaccination-induced systemic autoimmunity in farmed Atlantic salmon. *J. Immunol.*, 181(7), 4807-4814. <https://doi.org/10.4049/jimmunol.181.7.4807>
- Koppang, E. O., Haugarvoll, E., Hordvik, I., Aune, L., & Poppe, T. T. (2005). Vaccine-associated granulomatous inflammation and melanin accumulation in Atlantic salmon, *Salmo salar* L., white muscle. *J. Fish Dis.*, 28(1), 13-22. <https://doi.org/10.1111/j.1365-2761.2004.00583.x>
- Kottler, V. A., Künstner, A., & Schartl, M. (2015). Pheomelanin in fish? *Pigment Cell Melanoma Res.*, 28(3), 355-356. <https://doi.org/10.1111/pcmr.12359>
- Krasnov, A., Jørgensen, S. M., & Afanasyev, S. (2017). Ig-seq: Deep sequencing of the variable region of Atlantic salmon IgM heavy chain transcripts. *Mol. Immunol.*, 88, 99-105. <https://doi.org/10.1016/j.molimm.2017.06.022>

- Krasnov, A., Moghadam, H., Larsson, T., Afanasyev, S., & Mørkøre, T. (2016). Gene expression profiling in melanised sites of Atlantic salmon fillets. *Fish Shellfish Immunol.*, *55*, 56-63. <https://doi.org/10.1016/j.fsi.2016.05.012>
- Krogdahl, Å., Penn, M., Thorsen, J., Refstie, S., & Bakke, A. M. (2010). Important antinutrients in plant feedstuffs for aquaculture: an update on recent findings regarding responses in salmonids. *Aquac. Res.*, *41*(3), 333-344. <https://doi.org/10.1111/j.1365-2109.2009.02426.x>
- Kryvi, H., & Poppe, L. T. (2016). *Fiskeanatomi*. Fagbokforlaget. <https://www.fagbokforlaget.no/Fiskeanatomi/I9788245037333>
- Kumar, V., Abbas, A. K., & Aster, J. C. (2018). *Robbins basic pathology* (Tenth ed.). <https://shop.elsevier.com/books/robbins-basic-pathology/kumar/978-0-323-35317-5>
- Kuo, M. J., & Alexander, M. (1967). Inhibition of the lysis of fungi by melanins. *J. Bacteriol.*, *94*(3), 624-629. <https://doi.org/10.1128/jb.94.3.624-629.1967>
- Kuznetsov, V. D., Filippova, S. N., & Rybakova, A. M. (1984). Nature of the brown pigment and the composition of the phenol oxidases of *Streptomyces galbus*. *Mikrobiologiya*, *53*(2), 251-256. <http://europepmc.org/abstract/MED/6204187>
- Lagos, L. X., Iliiev, D. B., Helland, R., Roseblatt, M., & Jørgensen, J. B. (2012). CD40L--a costimulatory molecule involved in the maturation of antigen presenting cells in Atlantic salmon (*Salmo salar*). *Dev. Comp. Immunol.*, *38*(3), 416-430. <https://doi.org/10.1016/j.dci.2012.07.011>
- Lall, S. P. (1995). Macro and trace elements in fish and shellfish. In A. Ruiter (Ed.), *Fish and fishery products: Composition, nutritive properties and stability* (pp. 187-213). CAB International. <https://www.semanticscholar.org/paper/Fish-and-Fishery-Products-Composition%2C-Nutritive-Ruiter/d48575b43258c99f05191c8d1d7ad637b7425ade>
- Lall, S. P. (2022). The minerals. In R. W. Hardy & S. J. Kaushik (Eds.), *Fish nutrition* (Fourth ed., pp. 469-554). Charlotte Cackle. <https://doi.org/10.1016/B978-0-12-819587-1.00005-7>
- Langevin, H. M. (2021). Fascia Mobility, Proprioception, and Myofascial Pain. *Life*, *11*(7), 668. <https://www.mdpi.com/2075-1729/11/7/668>
- Larsen, H. A., Austbø, L., Mørkøre, T., Thorsen, J., Hordvik, I., Fischer, U., Jirillo, E., Rimstad, E., & Koppang, E. O. (2012). Pigment-producing granulomatous myopathy in Atlantic salmon: A novel inflammatory response. *Fish Shellfish Immunol.*, *33*(2), 277-285. <https://doi.org/10.1016/j.fsi.2012.05.012>
- Larsen, H. A., Austbø, L., Nødtvedt, A., Fraser, T. W., Rimstad, E., Fjelldal, P. G., Hansen, T., & Koppang, E. O. (2014). The effect of vaccination, ploidy and smolt production regime on pathological melanin depositions in muscle tissue of Atlantic salmon, *Salmo salar* L. *J. Fish. Dis.*, *37*(4), 327-340. <https://doi.org/10.1111/jfd.12106>
- Lee, A. Y. S., Chataway, T., Colella, A. D., Gordon, T. P., & Wang, J. J. (2019). Quantitative mass spectrometric analysis of autoantibodies as a paradigm shift in autoimmune serology. *Front. Immunol.*, *10*, 2845. <https://doi.org/10.3389/fimmu.2019.02845>
- Liaset, B., Julshamn, K., & Espe, M. (2003). Chemical composition and theoretical nutritional evaluation of the produced fractions from enzymic hydrolysis of salmon frames with Protamex™. *Process Biochem.*, *38*(12), 1747-1759. [https://doi.org/10.1016/S0032-9592\(02\)00251-0](https://doi.org/10.1016/S0032-9592(02)00251-0)
- Lin, W., Xu, L., Zwingenberger, S., Gibon, E., Goodman, S. B., & Li, G. (2017). Mesenchymal stem cells homing to improve bone healing. *J. Orthop. Translat.*, *9*, 19-27. <https://doi.org/10.1016/j.jot.2017.03.002>
- Lin, X., Patil, S., Gao, Y.-G., & Qian, A. (2020). The bone extracellular matrix in bone formation and regeneration. *Front. Pharmacol.*, *11*. <https://doi.org/10.3389/fphar.2020.00757>
- Lund, H., Bakke, A., Boysen, P., Afanasyev, S., Rebl, A., Manji, F., Ritchie, G., & Krasnov, A. (2022). Evaluation of immune status in two cohorts of Atlantic salmon raised in different aquaculture systems (case study). *Genes (Basel)*, *13*(5). <https://doi.org/10.3390/genes13050736>
- Lund, M., Skjerve, E., Qviller, L., Christiaan van Son, T., Lillehaug, A., Kristoffersen, A. B., & Brun, E. (2018). *Epidemiologisk studie av sammenhenger mellom melanin i filét hos laks og virusinfeksjoner og andre produksjonsvariabler* [Accademic report]. Veterinærinstituttet. <https://www.vetinst.no/rapporter-og-publikasjoner/rapporter/2018/epidemiologisk-studie-av->

[sammenhenger-mellom-melanin-i-filet-hos-laks-og-virusinfeksjoner-og-andre-produksjonsvariabler](#)

- Lund, T. C., Patrinostro, X., Kramer, A. C., Stadem, P., Higgins, L. A., Markowski, T. W., Wroblewski, M. S., Lidke, D. S., Tolar, J., & Blazar, B. R. (2014). sdf1 Expression reveals a source of perivascular-derived mesenchymal stem cells in zebrafish. *Stem Cells*, 32(10), 2767-2779. <https://doi.org/10.1002/stem.1758>
- Lutfi, E., Berge, G. M., Bæverfjord, G., Sigholt, T., Bou, M., Larsson, T., Mørkøre, T., Evensen, Ø., Sissener, N. H., Rosenlund, G., Sveen, L., Østbye, T.-K., & Ruyter, B. (2022). Increasing dietary levels of the n-3 long-chain PUFA, EPA and DHA, improves the growth, welfare, robustness and fillet quality of Atlantic salmon in sea cages. *Br. J. Nutr.*, 1-19. <https://doi.org/10.1017/S0007114522000642>
- Madaro, L., & Bouché, M. (2014). From innate to adaptive immune response in muscular dystrophies and skeletal muscle regeneration: the role of lymphocytes. *Biomed. Res. Int.*, 2014, 438675. <https://doi.org/10.1155/2014/438675>
- Malik, M. S., Bjørgen, H., Nyman, I. B., Wessel, Ø., Koppang, E. O., Dahle, M. K., & Rimstad, E. (2021). PRV-1 Infected macrophages in melanized focal changes in white muscle of Atlantic Salmon (*Salmo salar*) correlates with a pro-inflammatory environment. *Front. Immunol.*, 12, 664624. <https://doi.org/10.3389/fimmu.2021.664624>
- Manneken, J. D., Dauer, M. V. P., & Currie, P. D. (2022). Dynamics of muscle growth and regeneration: Lessons from the teleost. *Exp. Cell Res.*, 411(2), 112991. <https://doi.org/10.1016/j.yexcr.2021.112991>
- Maruyama, M., Rhee, C., Utsunomiya, T., Zhang, N., Ueno, M., Yao, Z., & Goodman, S. B. (2020). Modulation of the inflammatory response and bone healing. *Front. Endocrinol.*, 11. <https://doi.org/10.3389/fendo.2020.00386>
- Matzinger, P. (1994). Tolerance, danger, and the extended family. *Annu. Rev. Immunol.*, 12(1), 991-1045. <https://doi.org/10.1146/annurev.iv.12.040194.005015>
- Mbalaviele, G., Novack, D. V., Schett, G., & Teitelbaum, S. L. (2017). Inflammatory osteolysis: a conspiracy against bone. *J. Clin. Invest.*, 127(6), 2030-2039. <https://doi.org/10.1172/jci93356>
- McDonnell, L. K., Hume, P. A., & Nolte, V. (2011). Rib stress fractures among rowers: definition, epidemiology, mechanisms, risk factors and effectiveness of injury prevention strategies. *Sports Med.*, 41(11), 883-901. <https://doi.org/10.2165/11593170-000000000-00000>
- Miclau, T., Lu, C., Thompson, Z., Choi, P., Puttlitz, C., Marcucio, R., & Helms, J. A. (2007). Effects of delayed stabilization on fracture healing. *J. Orthop. Res.*, 25(12), 1552-1558. <https://doi.org/10.1002/jor.20435>
- Mills, C. D., & Ley, K. (2014). M1 and M2 macrophages: The chicken and the egg of immunity. *J. Innate Immun.*, 6(6), 716-726. <https://doi.org/10.1159/000364945>
- Morvan-Dubois, G., Le Guellec, D., Garrone, R., Zylberberg, L., & Bonnaud, L. (2003). Phylogenetic analysis of vertebrate fibrillar collagen locates the position of zebrafish $\alpha 3(I)$ and suggests an evolutionary link between collagen α chains and hox clusters. *J. Mol. Evol.*, 57(5), 501-514. <https://doi.org/10.1007/s00239-003-2502-x>
- Moss, M. L. (1963). The biology of acellular teleost bone. *Ann. N. Y. Acad. Sci.*, 109, 337-350. <https://doi.org/10.1111/j.1749-6632.1963.tb13475.x>
- Mørkøre, T. (2012). *Filet av oppdrettslaks: Kvalitetsavvik og årsakssammenhenger* (Vol. 12) [Accademic report]. Nofima. <https://nofima.no/publikasjon/1154001/>
- Mørkøre, T. (2017). *Mørke flekker i laksefilet - kunnskapsstatus* [Accademic report]. Nofima. <https://doi.org/10.13140/RG.2.2.12843.13608>
- Mørkøre, T., Dessen, J.-E., Larsson, T., Jiménez-Guerrero, R., & Rørvik, K.-A. (2016). *Effekt av fôr på melaninflekker i laks infisert med både PRV og SAV* (Vol. 31) [Accademic report]. Nofima. <https://nofima.no/publikasjon/1391570/>
- Mørkøre, T., & Einen, O. (2003). Relating sensory and instrumental texture analyses of Atlantic salmon. *J. Food Sci.*, 68(4), 1492-1497. <https://doi.org/10.1111/j.1365-2621.2003.tb09672.x>
- Mørkøre, T., Larsson, T., Jiménez-Guerrero, R., Moreno, H. M., Borderias, J., Ruyter, B., Standal, I. B., Sarno, A., Evensen, Ø., Dessen, J.-E., Rørvik, K.-A., Hamre, K., Andersen, Ø., Wakamatsu, K., Ito, S., Gannestad, K. H., Xu, C., Østbye, T.-K., Hillestad, B., . . . Bæverfjord, G. (2022). *EX-*

- spot: *Mørke flekker i laksefilet* (Vol. 27) [Accademic report]. Nofima. <https://nofima.no/publikasjon/2087763/>
- Mørkøre, T., Larsson, T., Kvellestad, A. S., Koppang, E. O., Åsli, M., Krasnov, A., Dessen, J.-E., Moreno, H. M., Valen, E., Gannestad, K. H., Gjerde, B., Taksdal, T., Bæverfjord, G., Meng, Y., Heia, K., Wold, J. P., Borderias, A. J., Moghamad, H., Romarheim, O. H., & Rørvik, K. A. (2015). *Mørke flekker i laksefilet – Kunnskapsstatus og tiltak for å begrense omfanget* (Vol. 34) [Accademic report]. Nofima. <https://nofima.no/publikasjon/1289894/>
- Mørkøre, T., & Rørvik, K.-A. (2001). Seasonal variations in growth, feed utilisation and product quality of farmed Atlantic salmon (*Salmo salar*) transferred to seawater as 0+smolts or 1+smolts. *Aquac.*, 199(1), 145-157. [https://doi.org/10.1016/S0044-8486\(01\)00524-5](https://doi.org/10.1016/S0044-8486(01)00524-5)
- Mørkøre, T. M., Yuqiong; Larsson, Thomas; Rørvik, Kjell-Arne; Kousoulaki, Katerina; Berge, Gerd M.; Ruyter, Bente. (2018). Nutritional effects on dark fillet spots of Atlantic salmon (*Salmo salar* L.) [Conference paper]. *18th International Symposium on Fish Nutrition and Feeding*. <https://doi.org/10.13140/RG.2.2.15540.40322>
- Nagase, H., Visse, R., & Murphy, G. (2006). Structure and function of matrix metalloproteinases and TIMPs. *Cardiovasc. Res.*, 69(3), 562-573. <https://doi.org/10.1016/j.cardiores.2005.12.002>
- Nikolaou, P. K., Macdonald, B. L., Glisson, R. R., Seaber, A. V., & Garrett Jr., W. E. (1987). Biomechanical and histological evaluation of muscle after controlled strain injury. *Am. J. Sports Med.*, 15(1), 9-14. <https://doi.org/10.1177/036354658701500102>
- Noble, C., Gismervik, K., Iversen, M. H., Kolarevic, J., Nilsson, J., Stien, L. H., & Turnbull, J. F. (2018). *Welfare Indicators for farmed Atlantic salmon: tools for assessing fish welfare* (C. Noble, K. Gismervik, M. H. Iversen, J. Kolarevic, J. Nilsson, L. H. Stien, & J. F. Turnbull, Eds.). <https://nofima.com/publication/1636395/>
- Nordberg, M. (2018). *Seasonal variation in fillet quality of Atlantic salmon (Salmo salar)* [Master thesis]. Norwegian University of Life Sciences. <https://nmbu.brage.unit.no/nmbu-xmlui/handle/11250/2569081>
- Nordvik, K., Kryvi, H., Totland, G. K., & Grotmol, S. (2005). The salmon vertebral body develops through mineralization of two preformed tissues that are encompassed by two layers of bone. *J. Anat.*, 206(2), 103-114. <https://doi.org/10.1111/j.1469-7580.2005.00372.x>
- Nutt, S. L., Fairfax, K. A., & Kallies, A. (2007). BLIMP1 guides the fate of effector B and T cells. *Nat. Rev. Immunol.*, 7(12), 923-927. <https://doi.org/10.1038/nri2204>
- Nylund, S., Andersen, L., Saevareid, I., Plarre, H., Watanabe, K., Arnesen, C. E., Karlsbakk, E., & Nylund, A. (2011). Diseases of farmed Atlantic salmon *Salmo salar* associated with infections by the microsporidian *Paramucleospora theridion*. *Dis. Aquat. Organ.*, 94(1), 41-57. <https://doi.org/10.3354/dao02313>
- Næve, I., Korsvoll, S. A., Santi, N., Medina, M., & Aunsmo, A. (2022). The power of genetics: Past and future contribution of balanced genetic selection to sustainable growth and productivity of the Norwegian Atlantic salmon (*Salmo salar*) industry. *Aquac.*, 553, 738061. <https://doi.org/10.1016/j.aquaculture.2022.738061>
- Ofer, L., Dean, M. N., Zaslansky, P., Kult, S., Shwartz, Y., Zaretsky, J., Griess-Fishheimer, S., Monsonego-Ornan, E., Zelzer, E., & Shahar, R. (2019). A novel nonosteocytic regulatory mechanism of bone modeling. *PLOS Biology*, 17(2), e3000140. <https://doi.org/10.1371/journal.pbio.3000140>
- Ojanguren, A. F., Reyes-Gavilán, F. G., & Muñoz, R. R. (1999). Effects of temperature on growth and efficiency of yolk utilisation in eggs and pre-feeding larval stages of Atlantic salmon. *Aquac. Int.*, 7(2), 81-87. <https://doi.org/10.1023/A:1009214804949>
- Page, M. J., Kell, D. B., & Pretorius, E. (2022). The role of lipopolysaccharide-induced cell signalling in chronic inflammation. *Chronic Stress (Thousand Oaks)*, 6, 24705470221076390. <https://doi.org/10.1177/24705470221076390>
- Patel, S. S., Molnar, M. Z., Tayek, J. A., Ix, J. H., Noori, N., Benner, D., Heymsfield, S., Kopple, J. D., Kovesdy, C. P., & Kalantar-Zadeh, K. (2013). Serum creatinine as a marker of muscle mass in chronic kidney disease: results of a cross-sectional study and review of literature. *J. Cachexia Sarcopenia Muscle*, 4(1), 19-29. <https://doi.org/10.1007/s13539-012-0079-1>

- Peñaranda, M. M. D., Jensen, I., Tollersrud, L. G., Bruun, J. A., & Jørgensen, J. B. (2019). Profiling the Atlantic salmon IgM(+) B cell surface proteome: Novel information on teleost fish B cell protein repertoire and identification of potential B cell markers. *Front. Immunol.*, *10*, 37. <https://doi.org/10.3389/fimmu.2019.00037>
- Pradeu, T., & Cooper, E. L. (2012). The danger theory: 20 years later. *Front. Immunol.*, *3*, 287. <https://doi.org/10.3389/fimmu.2012.00287>
- Rafiq, M. B. (2015). *Dietary impact of feed on performance, health and tissue melanization of Atlantic salmon (Salmo salar L.)* [Master thesis]. Norwegian University of Life Sciences. <https://nmbu.brage.unit.no/nmbu-xmlui/handle/11250/2391641>
- Randhawa, M., Huff, T., Valencia, J. C., Younossi, Z., Chandhoke, V., Hearing, V. J., & Baranova, A. (2009). Evidence for the ectopic synthesis of melanin in human adipose tissue. *FASEB J.*, *23*(3), 835-843. <https://doi.org/10.1096/fj.08-116327>
- Raposo, G., & Marks, M. S. (2007). Melanosomes--dark organelles enlighten endosomal membrane transport. *Nat. Rev. Mol. Cell. Biol.*, *8*(10), 786-797. <https://doi.org/10.1038/nrm2258>
- Reimschuessel, R., & Ferguson, H. W. (1989). Kidney. In H. W. Ferguson (Ed.), *Systemic pathology of fish: A text and atlas comparative tissue response in diseases of teleost* (Second ed., pp. 91-139). Taylor & Francis. <https://api.semanticscholar.org/CorpusID:85114540>
- Roberts, R. J. (1975). Melanin-containing cells of the teleost fish and their relation to disease. In W. E. Ribelin & G. Migaki (Eds.), *The Pathology of Fishes* (pp. 399-428). University of Wisconsin Press. <https://www.abebooks.co.uk/9780299065201/Pathology-Fishes-Ribelin-William-E-0299065200/plp>
- Roberts, R. J., Hardy, R. W., & Sugiura, S. H. (2001). Screamer disease in Atlantic salmon, *Salmo salar* L., in Chile. *J. Fish Dis.*, *24*(9), 543-549. <https://doi.org/10.1046/j.1365-2761.2001.00328.x>
- Rózanowska, M., Sarna, T., Land, E. J., & Truscott, T. G. (1999). Free radical scavenging properties of melanin interaction of eu- and pheo-melanin models with reducing and oxidising radicals. *Free Radic. Biol. Med.*, *26*(5-6), 518-525. [https://doi.org/10.1016/s0891-5849\(98\)00234-2](https://doi.org/10.1016/s0891-5849(98)00234-2)
- Rørvik, K.-A., Dessen, J.-E., Åsli, M., Thomassen, M. S., Hoås, K. G., & Mørkøre, T. (2018). Low body fat content prior to declining day length in the autumn significantly increased growth and reduced weight dispersion in farmed Atlantic salmon *Salmo salar* L. *Aquac. Res.*, *49*(5), 1944-1956. <https://doi.org/10.1111/are.13650>
- Salajegheh, M., Pinkus, J. L., Amato, A. A., Morehouse, C., Jallal, B., Yao, Y., & Greenberg, S. A. (2010). Permissive environment for B-cell maturation in myositis muscle in the absence of B-cell follicles. *Muscle Nerve*, *42*(4), 576-583. <https://doi.org/10.1002/mus.21739>
- Salem, M., Kenney, P. B., Rexroad, C. E., 3rd, & Yao, J. (2006). Microarray gene expression analysis in atrophying rainbow trout muscle: a unique nonmammalian muscle degradation model. *Physiol. Genom.*, *28*(1), 33-45. <https://doi.org/10.1152/physiolgenomics.00114.2006>
- Salem, M., Kenney, P. B., Rexroad, C. E., 3rd, & Yao, J. (2010). Proteomic signature of muscle atrophy in rainbow trout. *J. Proteom.*, *73*(4), 778-789. <https://doi.org/10.1016/j.jprot.2009.10.014>
- Sarna, T., Menon, I. A., & Sealy, R. C. (1985). Photosensitization of melanins: a comparative study. *Photochem. Photobiol.*, *42*(5), 529-532. <https://doi.org/10.1111/j.1751-1097.1985.tb01605.x>
- Schlissel, M. S. (2003). Regulating antigen-receptor gene assembly. *Nat. Rev. Immunol.*, *3*(11), 890-899. <https://doi.org/10.1038/nri1225>
- Sciorati, C., Rigamonti, E., Manfredi, A. A., & Rovere-Querini, P. (2016). Cell death, clearance and immunity in the skeletal muscle. *Cell Death Differ.*, *23*(6), 927-937. <https://doi.org/10.1038/cdd.2015.171>
- Sealy, R. C. (1984). Free radicals in melanin formation, structure and reactions. In *Free radicals in molecular biology, aging and disease* (pp. 67-75). Raven Press. https://books.google.hn/books/about/Free_radicals_in_molecular_biology_aging.html?id=oOJqAAAAMAAJ&hl=es-419&output=html_text
- Sealy, R. C., Sarna, T., Wanner, E. J., & Reszka, K. (1984). Photosensitization of melanin: An electron spin resonance study of sensitized radical production and oxygen consumption. *Photochem. Photobiol.*, *40*(4), 453-459. <https://doi.org/10.1111/j.1751-1097.1984.tb04617.x>
- Sissener, N. H., Waagbø, R., Rosenlund, G., Tvenning, L., Susort, S., Lea, T. B., Oaland, Ø., Chen, L., & Breck, O. (2016). Reduced n-3 long chain fatty acid levels in feed for Atlantic salmon (*Salmo*

- salar* L.) do not reduce growth, robustness or product quality through an entire full scale commercial production cycle in seawater. *Aquac.*, 464, 236-245. <https://doi.org/10.1016/j.aquaculture.2016.06.034>
- Smith, L. S., & Bell, G. R. (1975). *A practical guide to the anatomy and physiology of Pacific salmon*. Dept. of the Environment Fisheries and Marine Service. <https://waves-vagues.dfo-mpo.gc.ca/library-bibliotheque/14918.pdf>
- Soliman, A. M., & Barreda, D. R. (2023). The acute inflammatory response of teleost fish. *Dev. Comp. Immunol.*, 146, 104731. <https://doi.org/10.1016/j.dci.2023.104731>
- Soliman, A. S. (2018). The growth cartilage and beyond: Absence of medullary bone in silver carp ribs. *Mathews j. cytol. histol.*, 2(1). <https://www.mathewsopenaccess.com/full-text/the-growth-cartilage-and-beyond-absence-of-medullary-bone-in-silver-carp-ribs>
- Solstorm, F., Solstorm, D., Oppedal, F., & Fjellidal, P. G. (2016). The vertebral column and exercise in Atlantic salmon — Regional effects. *Aquac.*, 461, 9-16. <https://doi.org/10.1016/j.aquaculture.2016.04.019>
- Son, Y. M., Cheon, I. S., Wu, Y., Li, C., Wang, Z., Gao, X., Chen, Y., Takahashi, Y., Fu, Y. X., Dent, A. L., Kaplan, M. H., Taylor, J. J., Cui, W., & Sun, J. (2021). Tissue-resident CD4(+) T helper cells assist the development of protective respiratory B and CD8(+) T cell memory responses. *Sci. Immunol.*, 6(55). <https://doi.org/10.1126/sciimmunol.abb6852>
- Sousa, S., Valerio, F., & Jacinto, A. (2012). A new zebrafish bone crush injury model. *Biol. Open*, 1(9), 915-921. <https://doi.org/10.1242/bio.2012877>
- Steinel, N. C., & Bolnick, D. I. (2017). Melanomacrophage centers as a histological indicator of immune function in fish and other poikilotherms [Mini Review]. *Front. Immunol.*, 8. <https://doi.org/10.3389/fimmu.2017.00827>
- Steinman, R. M., Pack, M., & Inaba, K. (1997). Dendritic cells in the T-cell areas of lymphoid organs. *Immunol. Rev.*, 156, 25-37. <https://doi.org/10.1111/j.1600-065x.1997.tb00956.x>
- Stosik, M., Tokarz-Deptuła, B., & Deptuła, W. (2021). Immunological memory in teleost fish. *Fish Shellfish Immunol.*, 115, 95-103. <https://doi.org/10.1016/j.fsi.2021.05.022>
- Suber, T. L., Casciola-Rosen, L., & Rosen, A. (2008). Mechanisms of disease: autoantigens as clues to the pathogenesis of myositis. *Nat. Clin. Pract. Rheumatol.*, 4(4), 201-209. <https://doi.org/10.1038/ncprheum0760>
- Sullivan, M., Hammond, G., Roberts, R. J., & Manchester, N. J. (2007). Spinal deformation in commercially cultured Atlantic salmon, *Salmo salar* L.: a clinical and radiological study. *J. Fish Dis.*, 30(12), 745-752. <https://doi.org/10.1111/j.1365-2761.2007.00889.x>
- Sunyer, J. O., & Boudinot, P. (2022). B-cell responses and antibody repertoires in teleost fish: From Ag receptor diversity to immune memory and vaccine development. In K. Buchmann & C. J. Secombes (Eds.), *Principles of fish immunology: From cells and molecules to host protection* (pp. 253-278). Springer International Publishing. https://doi.org/10.1007/978-3-030-85420-1_8
- Tadiso, T. M., Lie, K. K., & Hordvik, I. (2011). Molecular cloning of IgT from Atlantic salmon, and analysis of the relative expression of τ , μ , and δ in different tissues. *Vet. Immunol. Immunopathol.*, 139(1), 17-26. <https://doi.org/10.1016/j.vetimm.2010.07.024>
- Tang, D., Kang, R., Coyne, C. B., Zeh, H. J., & Lotze, M. T. (2012). PAMPs and DAMPs: signal 0s that spur autophagy and immunity. *Immunol. Rev.*, 249(1), 158-175. <https://doi.org/10.1111/j.1600-065X.2012.01146.x>
- Tang, H., Jiang, X., Zhang, J., Pei, C., Zhao, X., Li, L., & Kong, X. (2021). Teleost CD4(+) helper T cells: Molecular characteristics and functions and comparison with mammalian counterparts. *Vet. Immunol. Immunopathol.*, 240, 110316. <https://doi.org/10.1016/j.vetimm.2021.110316>
- Tomecka, M. J., Ethiraj, L. P., Sánchez, L. M., Roehl, H. H., & Carney, T. J. (2019). Clinical pathologies of bone fracture modelled in zebrafish. *Dis. Models Mech.*, 12(9), dmm037630. <https://doi.org/10.1242/dmm.037630>
- Trangerud, C., Bjørgen, H., Koppang, E. O., Grøntvedt, R. N., Skogmo, H. K., Ottesen, N., & Kvellestad, A. (2020). Vertebral column deformity with curved cross-stitch vertebrae in Norwegian seawater-farmed Atlantic salmon, *Salmo salar* L. *J. Fish Dis.*, 43(3), 379-389. <https://doi.org/10.1111/jfd.13136>

- Turnbull, J. (2006). Musculoskeletal system. In H. W. Ferguson (Ed.), *Systemic pathology of fish: A text and atlas of normal tissues in teleosts and their responses in disease* (Second ed., pp. 289-313). Scotian Press. https://books.google.es/books/about/Systemic_Pathology_of_Fish.html?id=FWTAAAACAAJ&redir_esc=y
- Valenzuela, C. A., Ponce, C., Zuloaga, R., González, P., Avendaño-Herrera, R., Valdés, J. A., & Molina, A. (2020). Effects of crowding on the three main proteolytic mechanisms of skeletal muscle in rainbow trout (*Oncorhynchus mykiss*). *BMC Vet. Res.*, 16(1), 294. <https://doi.org/10.1186/s12917-020-02518-w>
- Valenzuela, C. A., Zuloaga, R., Mercado, L., Einarsdottir, I. E., Björnsson, B. T., Valdés, J. A., & Molina, A. (2018). Chronic stress inhibits growth and induces proteolytic mechanisms through two different nonoverlapping pathways in the skeletal muscle of a teleost fish. *Am. J. Physiol. - Regul. Integr. Comp. Physiol.*, 314(1), R102-R113. <https://doi.org/10.1152/ajpregu.00009.2017>
- Vallejo, A. N., Brandes, J. C., Weyand, C. M., & Goronzy, J. J. (1999). Modulation of CD28 expression: distinct regulatory pathways during activation and replicative senescence. *J. Immunol.*, 162(11), 6572-6579. <https://pubmed.ncbi.nlm.nih.gov/10352273/>
- van der Wal, Y. A., Jenberie, S., Nordli, H., Greiner-Tollersrud, L., Kool, J., Jensen, I., & Jørgensen, J. B. (2021). The importance of the Atlantic salmon peritoneal cavity B cell response: Local IgM secreting cells are predominant upon *Piscirickettsia salmonis* infection. *Dev. Comp. Immunol.*, 123, 104125. <https://doi.org/10.1016/j.dci.2021.104125>
- Van Leeuwen, J. L. (1999). A mechanical analysis of myomere shape in fish. *J. Exp. Biol.*, 202(23), 3405-3414. <https://doi.org/10.1242/jeb.202.23.3405>
- Weis, D. J., & O'Brien, C. A. (2023). Osteoclasts, master sculptors of bone. *Annu. Rev. Pathol.: Mech. Dis.*, 18(1), 257-281. <https://doi.org/10.1146/annurev-pathmechdis-031521-040919>
- Velnar, T., Bailey, T., & Smrkolj, V. (2009). The wound healing process: An overview of the cellular and molecular mechanisms. *J. Int. Med.*, 37(5), 1528-1542. <https://doi.org/10.1177/147323000903700531>
- Wang, Y., Liang, J., Miyazaki, R., Sun, H., Zhao, X., Hirasaka, K., Hamada, Y., Tachibana, K., Liu, B., & Taniyama, S. (2021). Influence of the interposition of pink muscle fibers in the dorsal ordinary muscle on the postmortem hardness of meat in various fishes. *J. Texture Stud.*, 52(3), 358-367. <https://doi.org/10.1111/jtxs.12587>
- Wang, Z., Dillon, J., & Gaillard, E. R. (2006). Antioxidant properties of melanin in retinal pigment epithelial cells. *Photochem. Photobiol.*, 82(2), 474-479. <https://doi.org/10.1562/2005-10-21-ra-725>
- Weizhi, W. (2016). *The effect of dietary antioxidants on hyperpigmented fillet spots of Atlantic salmon (Salmo salar L.)* [Master thesis]. Norwegian University of Life Sciences. <https://brage.bibsys.no/xmlui/bitstream/handle/11250/2399825/Weizhi%20Wang.pdf?sequence=1&isAllowed=y>
- Wieczorek, M., Abualrous, E. T., Sticht, J., Álvaro-Benito, M., Stolzenberg, S., Noé, F., & Freund, C. (2017). Major histocompatibility complex (MHC) class I and MHC class II proteins: Conformational plasticity in antigen presentation. *Front. Immunol.*, 8. <https://doi.org/10.3389/fimmu.2017.00292>
- Wiegertjes, G. F., & Elks, P. M. (2022). Fish macrophages. In K. Buchmann & C. J. Secombes (Eds.), *Principles of fish immunology: From cells and molecules to host protection* (pp. 203-227). Springer International Publishing. https://doi.org/10.1007/978-3-030-85420-1_6
- Wilson, K., Cotter, S. C., Reeson, A. F., & Pell, J. K. (2001). Melanin and disease resistance in insects. *Ecol.*, 4(6), 637-649. <https://doi.org/10.1046/j.1461-0248.2001.00279.x>
- Witten, P. E., Fjellidal, P. G., Huysseune, A., McGurk, C., Obach, A., & Owen, M. A. G. (2019). Bone without minerals and its secondary mineralization in Atlantic salmon (*Salmo salar*): the recovery from phosphorus deficiency. *J. Exp. Biol.*, 222(3). <https://doi.org/10.1242/jeb.188763>
- Witten, P. E., Huysseune, A., & Hall, B. K. (2010). A practical approach for the identification of the many cartilaginous tissues in teleost fish. *J. Appl. Ichthyol.*, 26(2), 257-262. <https://doi.org/10.1111/j.1439-0426.2010.01416.x>

- Wu, L., Fu, S., Yin, X., Guo, Z., Wang, A., & Ye, J. (2019). Long-lived plasma cells secrete high-affinity antibodies responding to a T-dependent immunization in a teleost fish. *Front. Immunol.*, *10*. <https://doi.org/10.3389/fimmu.2019.02324>
- Wu, L., Qin, Z., Liu, H., Lin, L., Ye, J., & Li, J. (2020). Recent advances on phagocytic B cells in teleost fish. *Front. Immunol.*, *11*. <https://doi.org/10.3389/fimmu.2020.00824>
- Wu, L., Yang, Y., Gao, A., Li, J., & Ye, J. (2022). Teleost fish IgM+ plasma-like cells possess IgM-secreting, phagocytic, and antigen-presenting capacities. *Front. Immunol.*, *13*. <https://doi.org/10.3389/fimmu.2022.1016974>
- Wu, Y., Shan, L., Yang, S., & Ma, A. (2008). Identification and antioxidant activity of melanin isolated from *Hypoxylon archeri*, a companion fungus of *Tremella fuciformis*. *J. Basic Microbiol.*, *48*(3), 217-221. <https://doi.org/10.1002/jobm.200700366>
- Yamaguchi, T., Quillet, E., Boudinot, P., & Fischer, U. (2019). What could be the mechanisms of immunological memory in fish? *Fish Shellfish Immunol.*, *85*, 3-8. <https://doi.org/10.1016/j.fsi.2018.01.035>
- Yamaguchi, T., Takizawa, F., Furihata, M., Soto-Lampe, V., Dijkstra, J. M., & Fischer, U. (2019). Teleost cytotoxic T cells. *Fish Shellfish Immunol.*, *95*, 422-439. <https://doi.org/10.1016/j.fsi.2019.10.041>
- Yamaguchi, Y., Brenner, M., & Hearing, V. J. (2007). The regulation of skin pigmentation. *J. Biol. Chem.*, *282*(38), 27557-27561. <https://doi.org/10.1074/jbc.R700026200>
- Yoo, D. S., Cho, J. S., Chung, Y.-C., & Rhee, S.-H. (2021). Defect structures of sodium and chloride co-substituted hydroxyapatite and its osseointegration capacity. *J. Mater. Sci.*, *56*(9), 5493-5508. <https://doi.org/10.1007/s10853-020-05645-9>
- Ytrestøyl, T., Hjelle, E., Kolarevic, J., Takle, H., Rebl, A., Afanasyev, S., Krasnov, A., Brunsvik, P., & Terjesen, B. F. (2023). Photoperiod in recirculation aquaculture systems and timing of seawater transfer affect seawater growth performance of Atlantic salmon (*Salmo salar*). *J. World Aquac. Soc.*, *54*(1), 73-95. <https://doi.org/10.1111/jwas.12880>
- Ytteborg, E., Todorcevic, M., Krasnov, A., Takle, H., Kristiansen, I., & Ruyter, B. (2015). Precursor cells from Atlantic salmon (*Salmo salar*) visceral fat holds the plasticity to differentiate into the osteogenic lineage. *Biol. Open*, *4*(7), 783-791. <https://doi.org/10.1242/bio.201411338>
- Zeng, C., Wu, T., Zhen, Y., Xia, X. P., & Zhao, Y. (2005). BTLA, a new inhibitory B7 family receptor with a TNFR family ligand. *Cell Mol. Immunol.*, *2*(6), 427-432. <https://pubmed.ncbi.nlm.nih.gov/16426492/>
- Aas, T. S., Ytrestøyl, T., & Åsgård, T. (2019). Utilization of feed resources in the production of Atlantic salmon (*Salmo salar*) in Norway: An update for 2016. *Aquac. Rep.*, *15*, 100216. <https://doi.org/10.1016/j.aqrep.2019.100216>

7 Appendices

7.1 Appendix – 1: Supplementary table

Formulation and chemical composition of the marine- (M-group) and plant-based diet (P-group) of salmon fed during smoltification.

	M-group	P-group
Formulation		
Fish meal (%)	61.0	0.0
Wheat (%)	20.7	8.4
SPC (%)	0.0	34.6
Wheat gluten (%)	0.0	22.0
Corn gluten (%)	0.0	10.0
Fish oil (%)	15.4	0.0
Rapeseed oil (%)	0.0	20.4
MgSO ₄ (500 ppm extra) (%)	0.2	0.2
K ₂ CO ₃ (500 ppm extra) (%)	0.1	0.1
Vitamin premix (%)	0.5	0.5
Monosodium phosphate (%)	2.5	2.5
Astaxanthin (%)	0.1	0.1
Mineral premix (%)	0.5	0.5
Chemical composition		
Protein (%)	46.1	46.5
Lipids (%)	21.2	18.2
Starch (%)	12.6	9.3
Energy (MJ kg ⁻¹)	21.2	22.2

SPC, Soy protein concentrate.

7.2 Appendix – 2: Supplementary table

Amino acid and fatty acid composition of the marine- (M-group) and plant-based diet (P-group) of salmon fed during smoltification.

	M-group	P-group
Amino acid composition		
Aspartic acid (g g ⁻¹)	3.9	3.5
Glutamic acid (g g ⁻¹)	6.1	12.0
Hydroxyproline (g g ⁻¹)	0.4	< 0.1
Serine (g g ⁻¹)	1.9	2.4
Glycine (g g ⁻¹)	2.7	1.8
Histidine (g g ⁻¹)	1.0	1.0
Arginine (g g ⁻¹)	2.6	2.3
Treonine (g g ⁻¹)	1.8	1.5
Alanine (g g ⁻¹)	2.6	1.9
Proline (g g ⁻¹)	1.9	3.9
Tyrosine (g g ⁻¹)	1.3	1.4
Valine (g g ⁻¹)	2.2	2.0
Methionine (g g ⁻¹)	1.3	0.7
Isoleucine (g g ⁻¹)	1.8	1.9
Leucine (g g ⁻¹)	3.2	4.0
Phenylalanine (g g ⁻¹)	1.7	2.4
Lysine (g g ⁻¹)	3.4	1.8
Fatty acid composition		
14:0 (g 100g lipids ⁻¹)	6.3	0.1
16:0 (g 100g lipids ⁻¹)	13.3	4.9
18:0 (g 100g lipids ⁻¹)	1.6	1.8
20:0 (g 100g lipids ⁻¹)	0.2	0.5
16:1 n-7 (g 100g lipids ⁻¹)	4.1	0.2
18:1 (n-9)+(n-7)+(n-5) (g 100g lipids ⁻¹)	11.8	56.6
20:1 (n-9)+(n-7) (g 100g lipids ⁻¹)	8.7	1.5
22:1 (n-11)+(n-9)+(n-7) (g 100g lipids ⁻¹)	13.5	0.4
18:2 n-6 (g 100g lipids ⁻¹)	2.5	20.4
18:3 n-3 (g 100g lipids ⁻¹)	1.2	7.8
18:4 n-3 (g 100g lipids ⁻¹)	2.9	< 0.1
20:5 n-3 (EPA) (g 100g lipids ⁻¹)	7.0	0.1
22:6 n-3 (DHA) (g 100g lipids ⁻¹)	10.2	0.1
Sum of saturated fatty acids (g 100g lipids ⁻¹)	21.5	7.7
Sum of unsaturated fatty acids (g 100g lipids ⁻¹)	38.8	58.9
Sum of n-6 (g 100g lipids ⁻¹)	3.3	20.5
Sum of n-3 (g 100g lipids ⁻¹)	23.1	8.1
Sum of EPA + DHA (g 100g lipids ⁻¹)	17.2	0.2

Fatty acids results shown for values > 1 g 100g lipids-1 in both dietary groups.

EPA, eicosapentaenoic acid; DHA, docosahexaenoic acid

7.3 Appendix – 3: Supplementary table

Analysed chemical and mineral composition of the standard commercial diets during the seawater phase.

Feed	Skretting Nutra Olympic	Skretting Supreme Plus 75	Skretting Supreme Plus 150	Skretting Prime 300	Skretting Spirit Trout	Skretting Express 1200/2500-50A
Pellet size (mm)	3	3	4.5	5	6	9
Protein (%)	50.6	47.7	47.6	43.1	43.3	35.7
Drymatter (%)	93.8	92.1	91.8	92	92.1	92.6
Ash (%)	8.8	5.5	5.2	4.4	4.4	4.2
Mineral composition (ww)						
Total Ca (g kg ⁻¹)	19.5	7.3	6.4	3.5	3.4	3.5
Total Na (g kg ⁻¹)	6.8	2.1	2.0	1.7	1.7	1.4
Total Mg (g kg ⁻¹)	3.1	2.2	2.0	1.9	1.9	2.2
Total K (g kg ⁻¹)	11.1	10.1	8.9	7.9	7.9	7.3
Total P (g kg ⁻¹)	12.0	10.6	10.6	10.2	10.1	9.8
Soluble P (g kg ⁻¹)	2.5	5.2	5.3	5.9	6.0	4.9
Ca:P ratio	1.6	0.7	0.6	0.3	0.3	0.4
Total Fe (mg kg ⁻¹)	214	265	265	309	259	233
Total Mn (mg kg ⁻¹)	54	63	55	54	58	52
Total Cu (mg kg ⁻¹)	16	13	14	14	14	16
Total Zn (mg kg ⁻¹)	153	165	245	149	152	147
Fat (%)	22.8	24.5	26.5	27	27.7	36.2
Fiber (%)	2.1	2.1	1.8	2	2.2	2.4
Starch (%)	6.8	12.3	10.7	15.5	8.1	6.9
Free Astaxantin (mg kg ⁻¹)	7.2	58	61	49	42	41
Energy (MJ kg ⁻¹)	22.4	22.8	23.2	23.5	23.5	24.9

7.5 Appendix – 5: Papers I – III

Paper I



Rib abnormalities and their association with focal dark spots in Atlantic salmon filets

Raúl Jiménez-Guerrero^{a,*}, Grete Baeverfjord^b, Øystein Evensen^c, Kristin Hamre^d, Thomas Larsson^e, Jens-Erik Dessen^e, Kjellrun-Hoås Gannestad^b, Turid Mørkøre^{a,e}

^a Department of Animal and Aquacultural Sciences, Norwegian University of Life Sciences, NO-1432 Ås, Norway

^b Nofima, NO-6600 Sunndalsøra, Norway

^c Department of Paraclinical Sciences, Faculty of Veterinary Medicine, Norwegian University of Life Sciences, NO-1433 Ås, Norway

^d Department of Feed and Nutrition, Institute of Marine Research, NO-5005 Bergen, Norway

^e Nofima, NO-1432 Ås, Norway

ARTICLE INFO

Keywords:

Fish farming
Rib fracture
Rib morphology
Melanin spots
Welfare

ABSTRACT

Focal dark spots (DS) represent the most common quality problem in farmed Atlantic salmon (*Salmo salar* L.). DS are predominantly located in the cranio-ventral region of the fillet, that is characterized by the presence of ribs. The current study explores the possible association between abnormal rib morphology and DS types and the frequency of rib abnormalities in the rib cage by X-ray imaging. The fish used were salmon from a common smolt group that were sampled in freshwater (smolt farm) and subsequently two, five, eight and 14 months after sea transfer to small-scale land-based tanks or commercial sea-cages. Large size wild salmon were used as additive. Rib abnormalities were found in most fish, with a consistent number of four abnormalities per rib cage side of smolts, land-based and wild salmon. After transfer from freshwater to sea-cages, there was an abrupt increase from four to 10 abnormal ribs per rib cage side, mainly explained by low-density and shorter ribs. The number of abnormal ribs stabilized in further samplings at around eight abnormalities per rib cage side. In contrast to wild salmon, abnormalities in farmed salmon were symmetrically concentrated in the center of the rib cage in mid and distal parts of ribs, where also most DS were concentrated. No typical black DS were observed in smolts, salmon farmed in land-based tanks or wild salmon. Two months after transfer to sea-cages, 15% of the salmon had fillet-red DS, while fillet-black DS were observed five months after sea transfer (30%). The prevalence of fillet-red DS oscillated between 15 and 3% during the seawater phase, while fillet-black DS increased until the eighth month after seawater transfer, stabilizing in further samplings at 43–45%. The prevalence of rib abnormalities was 1.6 times higher in fillet-black DS than in control tissue, and 2 times higher for peritoneum DS, principally because of various forms of bent-, and broken ribs. There was an association between rib abnormalities and DS, although additional factors influenced the final DS phenotype. Preventing damaging incidents in the late smolt phase and sea-cage operations can likely reduce the prevalence of abnormal ribs and DS.

1. Introduction

Focal dark spots (DS) represent the most common fillet quality problem in all regions globally with significant farming of Atlantic salmon (Nordberg, 2018), affecting 16% of marketable sized fish, and causing 9–67% price losses, depending on the intensity and size of the discoloration (Färber, 2017). Most fillet DS are about 3 cm wide with brown/black discoloration, but spots can also be reddish, or diffuse grayish covering larger areas (Mørkøre, 2012). DS are principally

concentrated in the cranio-ventral region of the fillet, under the parietal peritoneum from ventral myocommata number 12 to 20 (Mørkøre, 2012; Mørkøre et al., 2015). Histological examination of DS has revealed degeneration and necrosis, fibrosis and granulomatous inflammation containing varying numbers of melano-macrophages (Larsen et al., 2012) of unclear etiology. Koppang et al. (2005), concluded that DS are an unpredictable side-effect of vaccination, while Bjørgen et al. (2015) proposed that *Piscine orthoreovirus* (PRV) is a premise for the development of DS. On the other hand, Krasnov et al. (2016) pointed to chronic

* Corresponding author at: Department of Animal and Aquacultural Sciences, Norwegian University of Life Sciences, NO-1430 Ås, Norway.
E-mail address: raul.jimenez.guerrero@nmbu.no (R. Jiménez-Guerrero).

<https://doi.org/10.1016/j.aquaculture.2022.738697>

Received 17 February 2022; Received in revised form 1 August 2022; Accepted 2 August 2022

Available online 6 August 2022

0044-8486/© 2022 The Authors. Published by Elsevier B.V. This is an open access article under the CC BY license (<http://creativecommons.org/licenses/by/4.0/>).

inflammation initiated by trauma without specific causative agents.

The anatomical region where the majority of DS are found is characterized by relatively high fat deposits (Aursand et al., 1994; Zhol et al., 1995), the presence of ribs (pleurapophysis) (De Clercq et al., 2017), and a thin muscle layer that may be susceptible to mechanical deformations. Long bone fractures and phases of the healing processes have been described in wild and farmed non-salmonid fish species (Fjellidal et al., 2020; Fjellidal et al., 2018; Horton and Summers, 2009; Tomecka et al., 2019). In farmed salmonids, rib abnormalities have been observed in form of sigmoid deviations associated with phosphorous deficiency (Baeverfjord et al., 1998). Gislason et al. (2010) reported supernumerary ribs due to dominant mutations. There is no literature investigating the association between ribs abnormalities and DS.

This study aimed to explore the association between rib abnormalities and DS of the abdominal wall of Atlantic salmon. This was done by characterizing normal and deviant rib bone morphology, and DS of salmon in freshwater and subsequently throughout the seawater grow-out phase in land-based tanks and commercial sea-cages until harvest (3.2–4.5 kg). Further, rib abnormalities and occurrence of DS were studied in large wild salmon as reference group.

2. Material and methods

2.1. Fish material

The fish material used were farmed and wild Atlantic salmon (*Salmo salar* L.). The farmed salmon (S0; Benchmark Genetics Norway, Bergen, Norway, line: trio QTL PD/IPN/Lice) were obtained from a commercial smolt producer making use of freshwater recirculation aquaculture technology (RAS) (Belsvik, Lerøy Midt, Hemne, Norway). The fish were farmed at the commercial RAS facility until smoltification and transferred to seawater in September 2018 (360,000 fish; 100 g), or they were transferred to flow-through land-based 0.7 m³ tanks at the Research Station for Sustainable Aquaculture (Nofima, Sunndalsøra, Møre and Romsdal, Norway) as 20 g pre-smolts (June 5th 2018; 2000 fish). The salmon at the RAS facility were vaccinated July 2018 using Alpha ERM® salar bath treatment, and Alpha JECT® micro 6 by machine injection (PHARMAQ AS, Overhalla, Norway). The fish kept in land-based tanks were not vaccinated. Smoltification was induced with artificial photoperiod regimes (6 weeks winter signal of 12:12 Light:Dark hours, post and prior to 24 L:0D) at both pre-smolt farming locations. The smoltification status was checked by conducting a seawater challenge test, followed by determination of plasma osmolality, chloride content, and gill Na⁺,K⁺-ATPase activity (Clarke et al., 1996) before sea transfer in September 2018 when the average weight was 100 g. The smolts at the land-based facility were transferred to 3.2 m³ tanks, supplied with UV-treated seawater from Tingvollfjorden (pumped from 40 m depth). The smolts from the commercial RAS facility were transported by a well-boat and distributed into four open commercial-sized sea-cages (120 m circumference, 40 m depth) with 80,000 fish in each cage at Nofima commercial-scale research and development (R&D) facility in Tingvollfjorden (Lerøy Midt AS, Gjemmes, Norway; 62° North, 8° 5' 0" East east). The distance between the farming locations was 45 km, i.e., the land-based tanks and sea-cages were supplied with seawater from the same fjord. The fish in sea-cages were mechanically deloused using the SkaMik 1.5 system (SkaMik AS, Ottersøy, Norway) in September and October 2019.

Both fish groups were fed the same standard grower feed, with pellet size and feed composition adjusted to fish size according to the recommendation from the feed producer (BioMar, Trondheim, Norway).

As additive material, wild Atlantic salmon by-caught in the sea outside Finnmark, Norway April 2018 and in the Namsen River, Trøndelag, Norway by net in June 2019 were purchased from a fish-monger and shipped frozen and on ice, respectively to Nofima AS, Ås, Norway for analyses.

2.2. Sampling of fish material

Farmed salmon were sampled for analyses prior to seawater transfer after vaccination at the commercial smolt farm and four times throughout the seawater rearing phase in land-based tanks and sea-cages (Table 1). At each sampling point, fish representing the average weight of the rearing units were anesthetized using MS-222 (Metacaine 0.1 g l⁻¹; Pharmaq Ltd., Hampshire, UK) or Benzoac (Benzoac® 2 ml × 150 10 L⁻¹, ACD Pharmaceuticals AS, Leknes, Norway) and killed by a lethal blow to the head before bleeding out, evisceration and filleting by hand. Left and right rib cages of each salmon (farmed and wild) were examined by X-ray.

In November 2019, the ventricle tip of 32 salmon farmed in land-based tanks and sea-cages were sampled in RNA later® for real-time RT-PCR analysis of *Piscine orthoreovirus-1* (PRV-1) (PatoGen AS, Ålesund, Norway).

2.3. Radiography

Rib morphology changes with growth were studied by X-ray of farmed salmon rib cages at each sampling timepoint (Table 1). Wild salmon caught in freshwater were additive, and not part of the time-based study. Left and right sides of rib cages were placed on trays before X-ray analyses using an IMS Giotto mammography equipment (Giotto, Pontecchio Marconi, BO, Italy) (Fig. 1A). The image resolution was 20 pixels per mm², with exposure at 22 kV and 100 mAs. X-ray images were recorded on coated photo-reactive phosphorous Fujifilm Computed Radiography (FCR) Imaging Plates (Fujifilm, Tokyo, Japan). Plates were read using FCR Profect Reader (Fujifilm, Tokyo, Japan).

General rib morphology and abnormalities were evaluated from the first fully developed rib (vertebra number 4) to 22nd rib at three different positions of each rib; proximal, mid, and distal (Fig. 1A). Before rib evaluation, a classification system was developed based on the type

Table 1
Fish material description and purpose.

Environment	Sampling time	Body weight (kg)	n	DS		
				prevalence	Rib cage X-ray	NQC bone analysis
Wild-Seawater	April 2019	2.2 ± 0.2	21			
Wild-Freshwater	June 2019	5.1 ± 0.2	15		15	15
Smolt farm - Freshwater	August 2018	0.1 ± 0	20		20	
Land-based tank - Seawater	November 2018	0.3 ± 0	15		15	
Land-based tank - Seawater	February 2019	0.8 ± 0	15		15	
Land-based tank - Seawater	May 2019	1.4 ± 0	15		15	
Land-based tank - Seawater	November 2019	3.2 ± 0	60		23	15
Sea-cage - Seawater	November 2018	0.5 ± 0	60		10	
Sea-cage - Seawater	February 2019	1.2 ± 0	60		30	
Sea-cage - Seawater	May 2019	2 ± 0	60		10	
Sea-cage - Seawater	November 2019	4.5 ± 0	113		23	10

DS, focal dark spots.

NQC, Norwegian quality cut.

Weight values are shown as mean ± SEM.

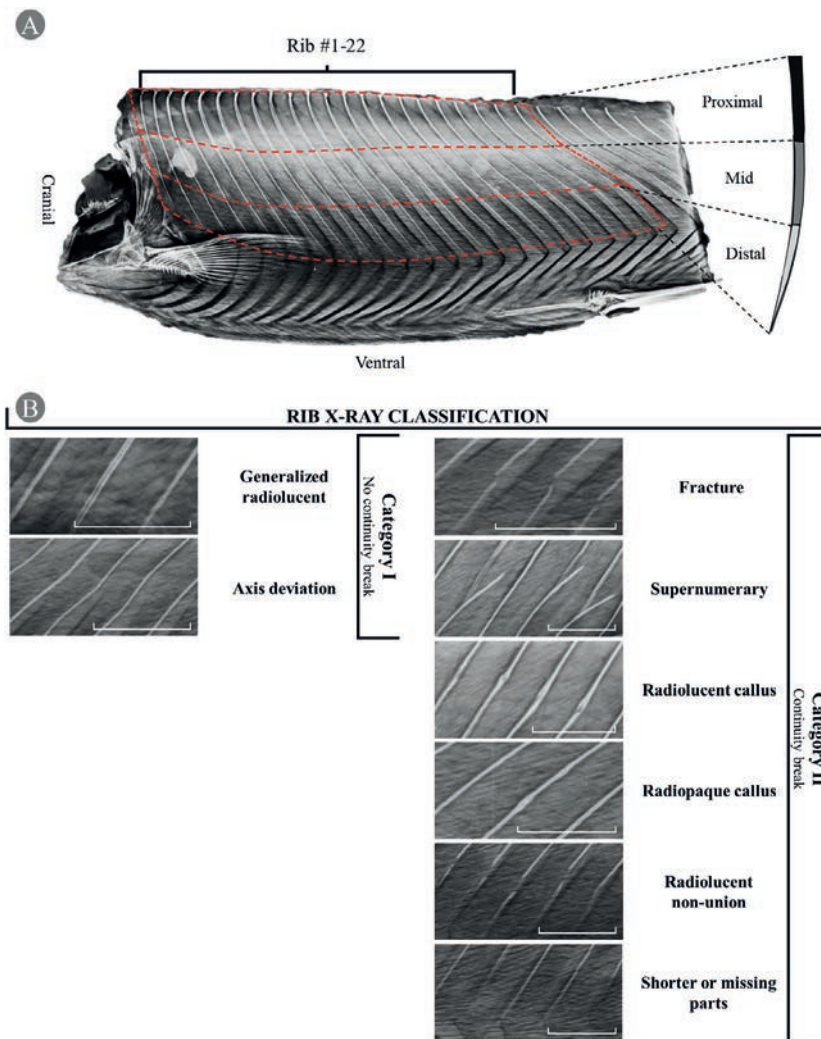


Fig. 1. Method for salmon rib morphology evaluation in rib cage of Atlantic salmon. A) Fillet map evaluation. B) Classification system for rib abnormalities. White restricted bars on the bottom right corner of each picture show the scale, set to 1 cm.

of abnormalities observed in rib cages from different sampling points and environments (salmon, $n = 176$) and existing literature (Fjellidal et al., 2020; Gislason et al., 2010; Khurana, 2009; Tomecka et al., 2019), aiming to identify different abnormality types and severity (Fig. 1B). Assuming a post-traumatic mechanical disturbance of local tissue in continuity breaks, abnormalities were classified into two distinct categories: rib abnormalities with no continuity break (Category I) and ribs with or related to continuity breaks (Category II). Category I was further divided into two sub-categories: 1) generalized radioluent at mid-distal parts with an increase of rib diameter and 2) axis deviations. Category II was divided into six sub-categories: 1) fracture, 2) supernumerary ribs, where free terminal rib fragments could continue their longitudinal growth independently, 3) radiolucent callus, 4) radiopaque callus as normal healing responses in long bones, 5) radiolucent non-unions, as atrophic non-unions with resorption of free fragments, and 6) shorter or missing rib parts. Rib axis deviations were not included in total sums of

the time-based study of rib cages to minimize artifacts given their vulnerability during handling and filleting different fish sizes. However, rib axis deviations were considered in the targeted study of DS and control areas, since the risk of artifacts is considered minimal for the dissected small DS areas.

Morphology of ribs attached to dark-stained skeletal muscle and peritoneum was characterized using the same classification system (Fig. 1) and compared to their non-pigmented surroundings.

2.4. Targeted study of DS

DS observed in left and right fillets of sea-cage farmed fish (Fig. 2) were macroscopically examined and categorized from seawater transfer to harvest (Lerøy processing plant, Hitra island, Norway) (fillet-red DS, $n = 23$; fillet-black DS, $n = 94$; peritoneum DS, $n = 63$). Due to the low number of detected fillet-red DS at the smolt farm and land-based tanks,

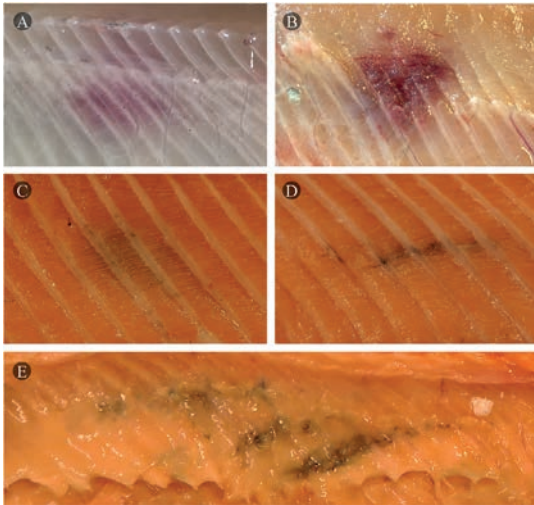


Fig. 2. Illustration of different focal dark spots (DS) of Atlantic salmon fillets. A) Fillet-red DS of salmon in freshwater (smolts), B) fillet-red DS after seawater transfer, C) fillet-black DS of salmon in seawater with low- and D) high aspect ratio, and E) peritoneum DS. (For interpretation of the references to color in this figure legend, the reader is referred to the web version of this article.)

they were not included in statistical analysis (Fig. 2), though they were evaluated and examined by X-ray. If the fish presented several DS (e.g., left and right fillet, or fillet and peritoneum), they were studied as independent focal discolorations. Randomly selected DS from sea-cage fish were chosen for X-ray examinations, (fillet-red DS, $n = 15$; fillet-black DS, $n = 76$; peritoneum DS, $n = 63$). From harvest size fish, randomly selected black DS with adjacent ribs and peritoneum ($n = 46$) were put in formalin (10% phosphate-buffered formalin, pH 7.0, >3 days at 4 °C). Rib and peritoneum samples without macroscopic evidence for DS were sampled as controls ($n = 20$) from the same fish between rib number 11 to 14 at the mid position of the rib and placed in formalin. Based on macroscopic appearance and X-ray examinations, formalin-fixed samples were selected for micro-CT (control, $n = 9$; black DS, $n = 21$), followed by histopathology. Additional ribs ($n = 5$) from adult wild fish were sampled and placed in formalin for complementing morphological descriptions.

2.5. Evaluation of fillet DS

A novel method for evaluating red and brown/black DS of the cranio-ventral fillet region was developed to facilitate objective continuous measurements of discoloration and area separately, while correcting for different fish sizes (Fig. 3). After filleting, the peritoneum and rib cage were carefully trimmed to visualize aberrant DS. Pictures of the cranio-ventral fillet region with visible DS were taken using a Canon PowerShot G7 X Mark II (Canon Inc., Tokyo, Japan), 5472 × 3648 resolution, using “Auto” mode with flash off, and ambient lighting. Images of skeletal muscle DS were further processed, and fillet-red DS were excluded at slaughter-exclusive explorations due to insufficient available X-rayed material ($n = 3$).

DS features based on the photographic images included: rib numbers corresponding to discolored myomeres, absolute distance from the horizontal septum (mid-line) to DS center (cm), absolute area (mm^2), maximum horizontal (X) and vertical length (Y) to estimate aspect ratio ($\text{AR} = X/Y$) as a scale-independent factor; number of affected myomeres, and color as darkness intensity (Fig. 3). Inputs for estimating aspect ratio were assessed using the ImageJ software (v1.52s, U. S. National

Institutes of Health, Bethesda, USA), and DS area was calculated assuming that most DS have an ellipse-like shape ($\text{DS area} = \pi * a * b$). The number of affected myomeres (starting from 0.2 when it affects only one myocommata) was transformed (times 5) to relative DS length to avoid values between 0 and 1, which might disturb area calculations. Thus, a equals $0.5 * \text{Relative DS length}$, while b equals $0.5 * \text{Relative DS length}/\text{AR}$. The relative DS area was transformed to DS area as myomere² units. Darkness intensity was determined at the DS core using a scale with five levels, from 0 (no visible dark pigmentation) to 4 (intense and homogeneous dark pigmentation with or without visible scar formation). DS level was calculated by multiplying the DS area by their DS darkness intensity (Fig. 3).

2.6. Micro computed tomography (micro-CT)

Samples were scanned at the Nofima center of nutrition and feed technology (Kjerreidviken, Bergen, Norway) using a Skyscan 1275 X-ray microtomograph (Bruker micro-CT, Kontich, Belgium) by a source voltage of 50 kV and 200 μA current, with exposure time set to 46 ms. 360-degree images, pixel size 20–28 μm , and rotation step of 0.3°. Image reconstruction was done using NRecon (v. 1.7.3.1, Bruker micro-CT, Kontich, Belgium), with the following parameters: 0 smoothing, 5 ring artifact reduction, 25 beam hardening correction, post alignment adjusted for every sample, and CS to 0.000000–0.030000. After scanning, 3D models for rib bones were made with CTAn (v.1.17.7.2, Bruker, Kontich, Belgium). Video files for each sample were created using CTVOx (v.3.3.0, Bruker, Kontich, Belgium). The bone tissue threshold was set manually for every sample.

2.7. Vertebra mineral analysis

Selected macrominerals in vertebrae of wild and slaughter size land-based and sea-cage farmed salmon were analyzed in the axial skeleton between the caudal end of the dorsal fin and the gut, commonly termed the Norwegian quality cut (NQC). The vertebrae were cleaned for surrounding soft tissue and trimmed for haemal and neural spines. Thereafter samples were pooled and homogenized in groups of five fish (per rearing unit farmed salmon). Analyses of the macrominerals (Ca, K, Mg, P) was performed using acid digestion, extraction, and inductive coupled plasma-mass spectrometry (ICP-MS) according to Liaset et al. (2003).

2.8. Statistics

Statistical analyses were conducted using R software (v. 4.0.3, R Core Team, Vienna, Austria). Figures were produced using Microsoft® Excel® software (v. 16.0.12527.21294, Microsoft Corporation, Redmond, United States). Parametric responses were modeled using the “lm()” R function, while “glm()” adjusted for Poisson or binomial distribution when dealing with non-parametric responses. The pair-wise comparison was made using the “HSD.test()” R function with square root normalization of the response if possible when dealing with non-parametric distributions, or Wilcoxon signed rank test using the “pairwise.wilcox.test()” R function when diagnostic plots revealed no optimum distribution of residuals after transformation. Models were adjusted for unbalanced design when required. Results from vertebral mineral analyses were evaluated with SAS® (V9.4, SAS Institute Inc., Cary, US). No random effects were considered in the models. The significance level was set at $p \leq 0.05$, and results are presented as mean \pm standard error (SEM).

2.9. Histopathology

Tissue samples in formalin were examined for pathological changes by light microscopy. Decalcification was performed by incubating the samples in 14% ethylenediaminetetraacetic acid (EDTA) for up to 48 h.

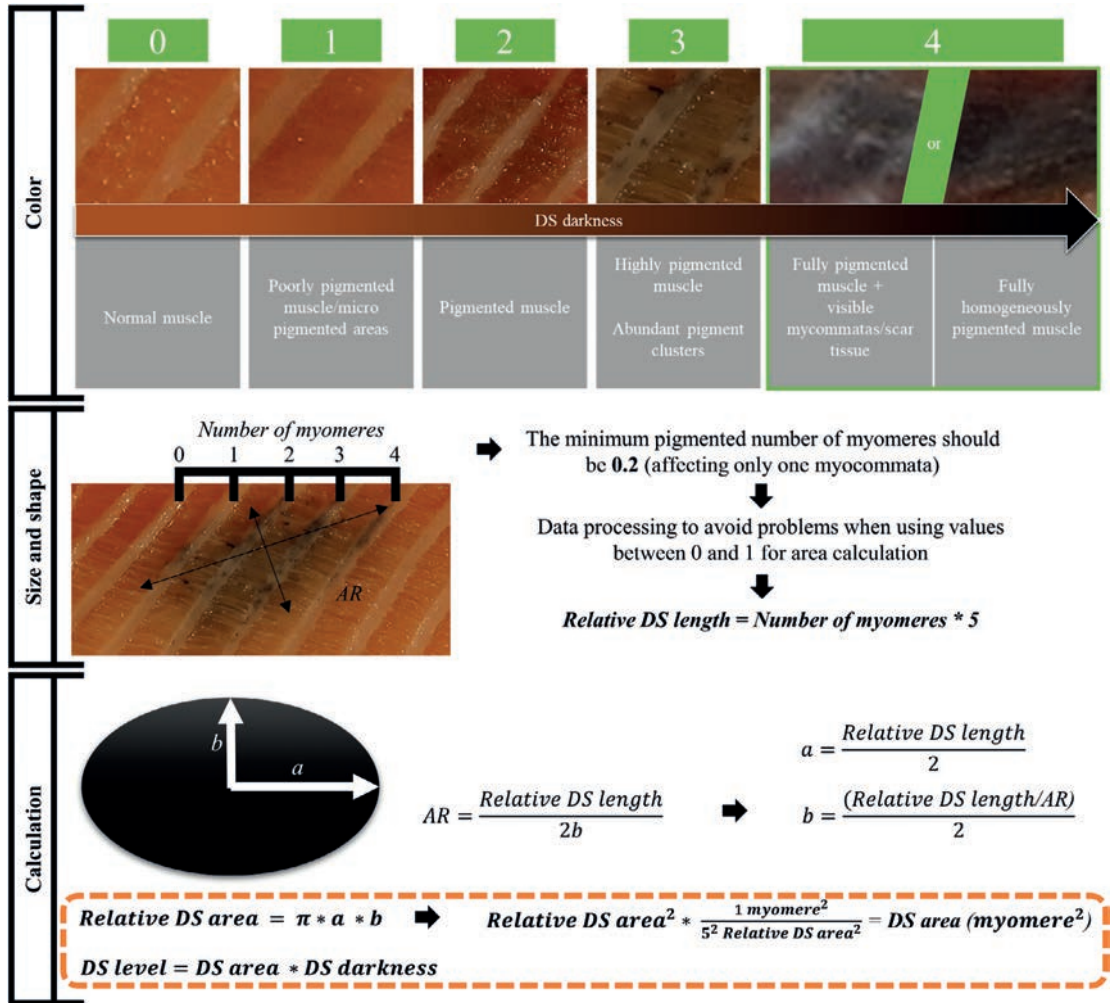


Fig. 3. Color scale and formula for quantification of targeted fillet DS area and DS level of Atlantic salmon fillets. Aspect ratio (AR) is calculated as the major horizontal axis's length divided by the DS minor vertical axis. The initial transformation for the number of myomeres to relative spot length, is corrected at the end of DS area calculation.

Samples were then embedded in paraffin wax and sectioned at 1.5–2 μm. Sections were mounted on glass slides and stained with haematoxylin and eosin. Slides were scanned at a resolution of 221 nm/pixel, with an image size of 126.720 × 87.296 pixels in a Nanosizer digital pathology image (ndpi) format, and created in a NDP.scan 3.2.15. Images were examined and sampled using NDP.view.2 (v.2.7.43, Hamamatsu Photonics K-K, Hamamatsu, Japan).

3. Results

3.1. Rib morphology of rib cages

X-ray evaluations showed ventro-caudally orientation of the ribs in a decreasing angle towards the tail. Ribs changed the length gradually along the rib cage. The shortest rib, usually the first one and frequently missing, was found at the 3rd vertebra. Generally, the length of the ribs

increased from vertebra number 3 to 9–12 counted from the head. The total number of ribs attached to the vertebra basiventral (non-vestigial ribs) was between 21 and 23.

X-ray evaluations showed all rib abnormality types in each studied environment, except for radiolucent non-unions, which were not found in wild fish (Table 2), and at least one rib abnormality was observed in every rib cage at any life stage and environment. The overall average rib abnormalities per rib cage side was four for wild salmon, salmon sampled at the smolt farm and land-based tanks. The salmon farmed in sea-cages had eight rib abnormalities per rib cage side on average, that was significantly higher from the other groups ($p \leq 0.01$). The abrupt increase in the number of rib abnormalities from the smolt farm (Aug. 2018) to two months after seawater transfer to sea-cages (Nov. 2018) ($p = 0.03$), was mainly due to an increased number of generalized radiolucent ribs (0.1 vs. 5.2; $p < 0.0001$) and shorter or missing rib parts (1.5 vs. 3.4; $p = 0.004$). The prevalence of generalized radiolucent ribs was

Table 2
Number of different rib abnormalities per rib cage side for wild and farmed Atlantic salmon before and after seawater transfer to land-based tanks and sea-cages.

Abnormality group n	Wild		Land-based tank				Sea-cage			
	Jun. 2020	Aug. 2018	Nov. 2018	Feb. 2019	May. 2019	Nov. 2019	Nov. 2018	Feb. 2019	May. 2019	Nov. 2019
	15	20	15	15	15	23	10	30	10	23
Category I - No continuity break										
Generalized radiolucent	1.3 ± 0.5 ^{bcd}	0.1 ± 0.1 ^d	1.7 ± 0.5 ^{bc}	0.7 ± 0.2 ^{bcd}	1.1 ± 0.5 ^{bc}	0.3 ± 0.1 ^{cd}	5.2 ± 1.4 ^a	1.7 ± 0.4 ^{bc}	2.2 ± 0.7 ^b	1.3 ± 0.3 ^{bcd}
Axis deviation	5.7 ± 1.1 ^{cde}	6.7 ± 0.8 ^{bc}	6.5 ± 1.2 ^{bcd}	4.8 ± 0.8 ^{de}	4.2 ± 0.9 ^e	12.9 ± 1 ^a	7.1 ± 1.4 ^{bc}	1.2 ± 0.4 ^f	1.8 ± 0.6 ^f	8.2 ± 0.9 ^b
Any Category I	7 ± 1.2 ^{bcd}	6.8 ± 0.8 ^{bcd}	8.2 ± 1.3 ^{abcd}	5.5 ± 0.8 ^{cde}	5.3 ± 0.9 ^{cde}	13.1 ± 1.1 ^a	12.3 ± 2.1 ^{ab}	2.9 ± 0.6 ^e	4 ± 1 ^{de}	9.5 ± 0.9 ^{abc}
Category II - Continuity break										
Fracture	0.3 ± 0.3	0.3 ± 0.1	0 ± 0	0 ± 0	0.1 ± 0.1	0.3 ± 0.2	0.3 ± 0.2	0.5 ± 0.2	0 ± 0	0 ± 0
Supernumerary	0.1 ± 0.1	0.1 ± 0.1	0.1 ± 0.1	0.1 ± 0.1	0.1 ± 0.1	0.2 ± 0.1	0.1 ± 0.1	0.6 ± 0.3	0.3 ± 0.3	0.2 ± 0.1
Radiolucent callus	1.1 ± 0.4 ^{ab}	0.1 ± 0.1 ^b	0.1 ± 0.1 ^b	0.1 ± 0.1 ^b	0.1 ± 0.1 ^b	1.4 ± 0.3 ^a	0.2 ± 0.2 ^b	0.1 ± 0.1 ^b	0.7 ± 0.4 ^{ab}	0.7 ± 0.2 ^{ab}
Radiopaque callus	0.5 ± 0.3 ^b	1.7 ± 0.3 ^{ab}	0.9 ± 0.4 ^b	0.5 ± 0.2 ^b	0.4 ± 0.2 ^b	0.7 ± 0.2 ^b	0.9 ± 0.4 ^b	1.2 ± 0.4 ^b	1.7 ± 0.5 ^{ab}	3 ± 0.5 ^a
Radiolucent non-union	0 ± 0	0.1 ± 0.1	0 ± 0	0.1 ± 0.1	0 ± 0	0 ± 0	0 ± 0	0.1 ± 0	0 ± 0	0 ± 0
Shorter or missing part	0.7 ± 0.3 ^e	1.5 ± 0.3 ^{bc}	1.4 ± 0.3 ^{bc}	1.2 ± 0.3 ^{bc}	1.3 ± 0.3 ^{bc}	1.5 ± 0.3 ^{bc}	3.4 ± 0.8 ^a	3.2 ± 0.4 ^a	2.7 ± 0.9 ^{ab}	2.6 ± 0.6 ^{ab}
Any Category II	2.7 ± 0.6 ^b	3.7 ± 0.5 ^{ab}	2.6 ± 0.7 ^b	2 ± 0.4 ^b	1.9 ± 0.4 ^b	4.1 ± 0.6 ^{ab}	4.9 ± 1.3 ^{ab}	5.7 ± 0.9 ^{ab}	5.4 ± 1.8 ^{ab}	6.5 ± 0.8 ^a

Values shown as mean ± SEM in the same row between environments and life stages with different letters are significantly different ($p \leq 0.05$).

the only abnormality type increasing two months after seawater transfer to land-based tanks (0.1 vs. 1.7; $p = 0.02$) (Table 2).

Time-based changes in seawater for the total number of rib abnormalities in fish from land-based tanks and sea-cages remained stable (Fig. 4). The main contributors for higher numbers in sea-cages were generalized radiolucent ribs and shorter or missing rib parts, although a decreasing tendency was observed from two months after seawater transfer to slaughter (5.2–1.4; $p < 0.0001$ and 3.4–2.6; $p = 0.8$, respectively). On the other hand, the prevalence of radiopaque callus increased during sweater phase (0.9–3; $p = 0.0005$) (Table 2). At harvesting, the number of shorter or missing rib parts and radiopaque callus were four and six times higher in farmed salmon in sea-cages than in wild salmon ($p = 0.002$ and $p < 0.0001$, respectively) (Table 2).

The total number of abnormalities per rib of salmon sampled at the smolt farm increased in the posterior direction to a maximum level of 0.4 at rib number 21 (Fig. 5A). The pattern changed two months after transfer to seawater to a consistent increasing tendency towards rib number 12–14, with a peak at each third rib. Thereafter, the prevalence

of rib abnormalities decreased posteriorly for the salmon farmed in land-based tanks, while the prevalence of rib abnormalities continued to be high towards rib 19 for sea-cage farmed salmon (Fig. 5A) (Supplementary 1). The number of abnormalities per rib of sea-cage farmed salmon was consistently higher compared with salmon farmed in land-based tanks, reaching a maximum level of 1 and 0.75 rib abnormalities per rib of the cage side, respectively. At slaughter (Nov. 2019) (Fig. 5B), the rib abnormality pattern was similar in salmon farmed in sea-cages and land-based tanks, with an increasing frequency up to rib number 12 for both farming environments while decreasing gradually in the posterior direction. The wild salmon showed a non-consistent longitudinal pattern. Abnormalities increased in the proximal-distal direction of the ribs for all fish groups, with significantly highest values for salmon farmed in sea-cages compared with wild ($p = 0.04$), and salmon farmed in land-based tanks ($p = 0.04$) (Fig. 6).

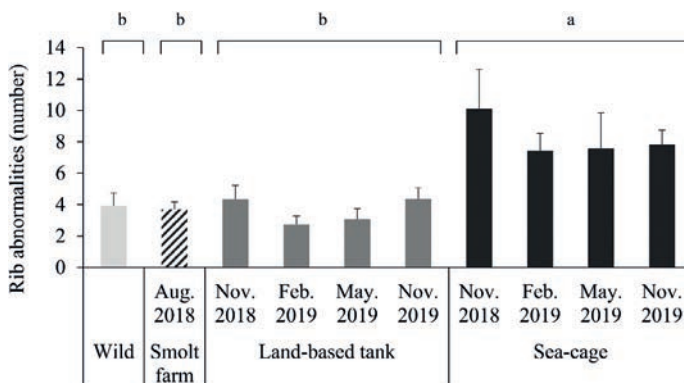


Fig. 4. Life stage and growing environment effects in the number of rib abnormalities per rib cage side for wild, and farmed Atlantic salmon before and after seawater transfer to land-based tanks and sea-cages. Significant differences between groups are indicated by different letters over the top brackets ($p \leq 0.05$). Data are presented as non-transformed mean ± SEM, $n = 15, 20, 68, 73$, for wild, smolt farm, land-based tank, and sea-cage groups, respectively.

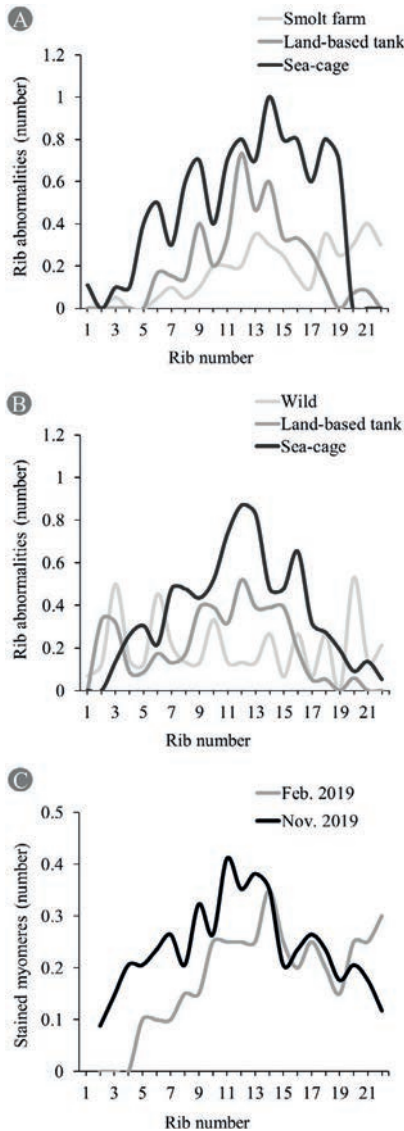


Fig. 5. Distribution of rib abnormalities and fillet DS along the rib cage of Atlantic salmon. A) farmed salmon in freshwater (smolts after vaccination, 80 g; $n = 20$) and two months after (Nov. 2018) seawater transfer to sea-cages (0.5 kg; $n = 10$) or land-based tanks (0.3 kg; $n = 15$). B) Slaughter size wild (5.1 kg; $n = 15$) and farmed salmon in land-based tank (3.2 kg; $n = 23$) and sea-cages (4.5 kg; $n = 23$). C) Mean values for the number of stained myomeres per fillet of salmon five months after transfer to sea-cages (Feb. 2019, 1.2 kg; $n = 20$), and slaughter (Nov. 2019, 4.5 kg; $n = 34$).

3.2. Targeted study of DS

3.2.1. DS prevalence, distribution, and morphology

Fillet-black DS were only observed in salmon farmed in sea-cages and only five months following sea transfer (30% of fish) and onwards (43–45% of fish). At the first sampling following seawater transfer (body

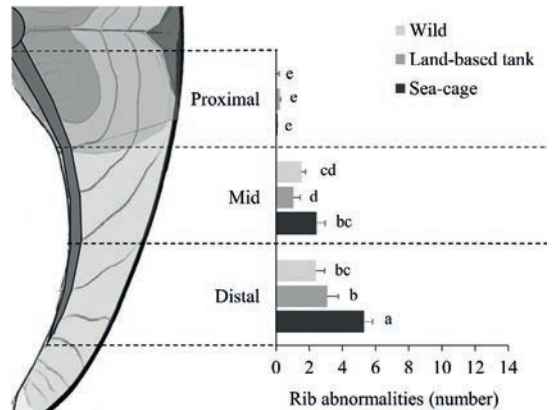


Fig. 6. Growing environment effects in the number of rib abnormalities at proximal, mid, and distal rib parts per rib cage side of slaughter size wild, and farmed Atlantic salmon using two rearing conditions after seawater transfer: land-based tank and sea-cage. Significant differences between groups and rib parts are indicated by different letters over the bars ($p \leq 0.05$). Data are presented as mean \pm SEM, $n = 15, 23$, and 23 for wild, land-based tank and sea-cage farmed salmon, respectively.

weight 0.5 kg), all fillet DS were red, but subsequently both fillet-red DS and fillet-black DS were observed (body weight 1.2–4.5 kg). Fillet-red DS in sea-cage fish followed a non-increasing prevalence ranging from 3 to 15% (Fig. 7). Fillet-red DS, determined as focal intramuscular hemorrhages, were detected at the smolt farm and land-based tanks only following seawater transfer. Focal peritonitis in the form of hyperemic areas was observed in some fish at the smolt farm near the vaccination site.

At slaughter, 73% of salmon showed some form of DS (peritoneum and/or fillet). Peritoneum DS prevalence was 52%, and 79% of fillet DS were visible through the overlying peritoneum ($n = 33$). Diffuse dark pigmentation was observed in some parietal peritoneum areas in contact with voluminous organs (e.g., liver). Dark pigmentation was also observed in the adjacent peritoneum of rib terminal regions, where there

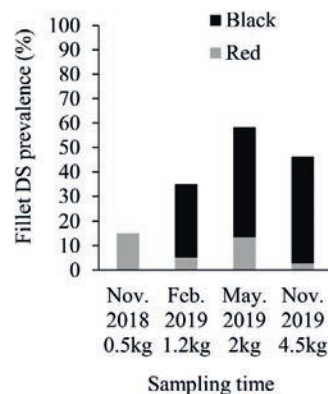


Fig. 7. Prevalence of focal black and red dark spots (DS) of fillets of Atlantic salmon farmed in sea-cages. The fish were sampled for analyses in Nov. 2018 ($n = 60$), Feb. 2019 ($n = 60$), May. 2019 ($n = 60$), and Nov. 2019 ($n = 113$). (For interpretation of the references to color in this figure legend, the reader is referred to the web version of this article.)

is a certain degree of rib motility.

The location of the DS in salmon fillets five months after seawater transfer to sea-cages (Feb. 2019) showed an increasing tendency towards rib number 14 where a maximum level of 0.34 stained myomeres was observed. Thereafter, the pattern oscillated between 0.15 and 0.3 myomeres in the posterior direction. At slaughter, the occurrence of fillet DS increased towards rib number 11–14 with 0.4 stained myomeres as maximum. The prevalence of fillet DS decreased gradually from rib 14–22 (Fig. 5C). Moreover, most of fillet DS were located at 3 cm below the horizontal septum, (mid rib parts), following a normal distribution from 0.9 cm (proximal rib parts) to 4.8 cm (distal rib parts).

Macroscopic evaluations revealed that fillet-red DS were consistently darker ($p = 0.0005$), relatively larger ($p = 0.04$), of higher level ($p < 0.0001$), and rounder ($p = 0.008$) than fillet-black DS (Table 3). Fillet-black DS area became larger in absolute terms (338 vs. 210 mm²; $p = 0.03$), smaller relative to the fish size (2.4 vs. 6.5 myomere²; $p < 0.0001$), flatter (4 vs. 1.7 aspect ratio; $p < 0.0001$), and lower intensity level (4.5 vs. 17.1 DS level; $p < 0.0001$) at harvesting than those first observed five months after seawater transfer. At harvesting, the appearance of fillet DS depended on where on the fillet the spot was located. The closer the DS was to the horizontal septum, the larger the relative DS area (myomere²; $p = 0.02$), intensity level (DS level; $p < 0.0001$), and the rounder the shape (lower aspect ratio; $p < 0.0001$).

3.2.2. Relationship between DS and rib abnormalities

Besides a few ribs with axis deviations, no major X-ray findings compatible with rib fractures or other abnormalities associated with continuity break were observed in fillet-red DS of fish from the smolt farm and land-based tanks.

X-ray analysis of DS from all sampling times in sea-cages showed that the prevalence of rib abnormalities was significantly higher in peritoneum DS (79%) compared with the control tissue (40%) ($p = 0.002$), and the prevalence of rib abnormalities also tended to be higher in fillet-black DS (63%) ($p = 0.07$). The prevalence of rib abnormalities was lower of fillet-red DS (33%) compared with fillet-black DS ($p = 0.04$), but similar with control tissue (Table 3). Rib abnormality prevalence of fillet-black DS was higher at slaughter (72%; $n = 46$) than those first detected in five months after seawater transfer (41%; $n = 17$) ($p = 0.03$), and rib abnormalities in peritoneum DS followed the same trend (87 and 68%; $p = 0.08$). No differences were observed in relative prevalence for individual rib abnormality types among DS, except from higher prevalence of shorter or missing rib parts in fillet-black DS (43% vs. 6% of DS with rib abnormalities; $p = 0.02$) and peritoneum DS (59% vs. 6% of DS with rib abnormalities; $p = 0.0004$) five months after seawater transfer than at slaughter.

At slaughter, the difference between rib abnormality prevalence of peritoneum DS and fillet-black DS was not significant, but both were

Table 3

Discoloration and morphological characteristics of focal dark spots (DS) of fillets and peritoneum of Atlantic salmon sampled during the seawater period, and their associated rib abnormality prevalence. Fillet DS parameters are presented as pigment intensity (darkness score), shape (aspect ratio), relative area (myomere²) and relative area times pigment intensity (DS level).

	Control ^a	Fillet-red DS	Fillet-black DS	Peritoneum DS
Darkness score	.	3.2 ± 0.2 ^a	1.8 ± 0.1 ^b	.
Aspect ratio	.	1.9 ± 0.4 ^b	3.1 ± 0.4 ^a	.
DS area (myomere ²)	.	5.5 ± 1.0 ^a	4.3 ± 0.5 ^b	.
DS level	.	19.2 ± 4.0 ^a	8.8 ± 1.2 ^b	.
Any rib abnormality (%)	40 ^{bc}	33 ^c	63 ^b	79 ^a

Values shown as prevalence or mean ± SEM in the same row with different letters are significantly different ($p \leq 0.05$).

^a Control samples exclusively from slaughter.

higher than control samples (40%) ($p = 0.0005$ and $p = 0.02$, respectively). Axis deviation was the most prevalent abnormality type in DS (76% of DS with rib abnormalities), followed by radiolucent callus and generalized radiolucent ribs (30–39% of DS with rib abnormalities). The relative prevalence for individual rib abnormality types between DS and control tissues did not differ significantly. Rib fractures, supernumerary ribs, radiolucent callus, and shorter or missing rib parts were not found in control tissues. These are called “DS-specific Category II” rib abnormalities, being present in 42% of DS samples with rib abnormalities at slaughter (Supplementary 2). Hence, the number of these most characteristic rib abnormalities in DS of the targeted study (either quantitatively, axis deviations; or qualitatively, DS-specific Category II), were found to be similar in general rib cage evaluations of fish with none or any form of DS.

At slaughter, rib X-ray morphology in targeted fillet-black DS was compared against their DS features. Fillet-black DS with larger intensity levels had fewer presence of rib abnormalities ($p = 0.002$), and larger presence of the generalized radiolucent type ($p = 0.0007$) than lower intensity levels. In contrast to rounder DS, flattened phenotypes showed smaller relative DS area ($p = 0.02$) and larger presence rib abnormalities ($p = 0.0003$), especially axis deviations ($p < 0.0001$). Generally, flattened phenotypes presented a series of rib abnormalities in a linear pattern perpendicular to the rib direction.

3.3. PRV status

Heart samples of slaughter size farmed salmon showed positive results for PRV in all sampled individuals from sea-cages, while fish sampled in land-based tanks were negative for PRV.

3.4. Micro-CT and 3D model

The morphology of salmon ribs presents a tubular structure with bone processes ventrally oriented in the exterior surface of some proximal parts (Fig. 8A). Proximal cross-sectional ribs parts were flattened and laterally oriented, reaching deeper layers into the muscle wall, becoming increasingly rod-like and less integrated into the muscle wall at distal parts (Fig. 8A and B).

The 3D model for bone density of rib abnormalities from the DS-specific Category II group at distal (radiolucent non-union), mid (radiolucent callus), and mid-proximal (fracture) rib parts, presented different degrees of bone callus formations (Fig. 9; Video 1, 2 and 3, respectively), and larger DS area and levels at mid-proximal than distal rib positions with dark pigments concentrated focally on the affected area (Fig. 9A). This morphological classification (Fig. 9A - C) was positively associated to the general homogeneous appearance of myomere (Fig. 9D - F). Samples showed similar features through micro-CT imaging; fusiform structure of similar radiodensity as near skeletal muscle with some radiopaque islands at continuity breaks (Fig. 9J and K). The sample at mid-proximal rib part showed two rib abnormalities (Fig. 9I); continuity break with no visible callus and diffuse non-mineralized radiolucent callus (Fig. 9L and O); radiopaque callus without visible non-mineralized callus (Fig. 9I and L). Radiolucent structures at the continuity break from inspected samples showed connections with near myomere and transverse fascia (Fig. 9M - O).

Micro-CT of axis deviations in ribs showed alterations of myocommata structure with a tissue of similar radiodensity as skeletal muscle irregularly infiltrated in the myocommata at the axis deviation (Fig. 10D).

Some undetected rib abnormalities from X-ray images were visualized by the 3D model, such as latero-lateral axis deviations, overlapping fractures (Fig. 9F), or bi-tubular rib morphology. Bi-tubular ribs were found to be linked to generalized radiolucent morphology in X-rayed ribs when oriented in the cranio-caudal plane. The generalized radiolucent morphology showed other different forms on the 3D model as thickening with irregular rib lumen, and thinner porotic compact bone

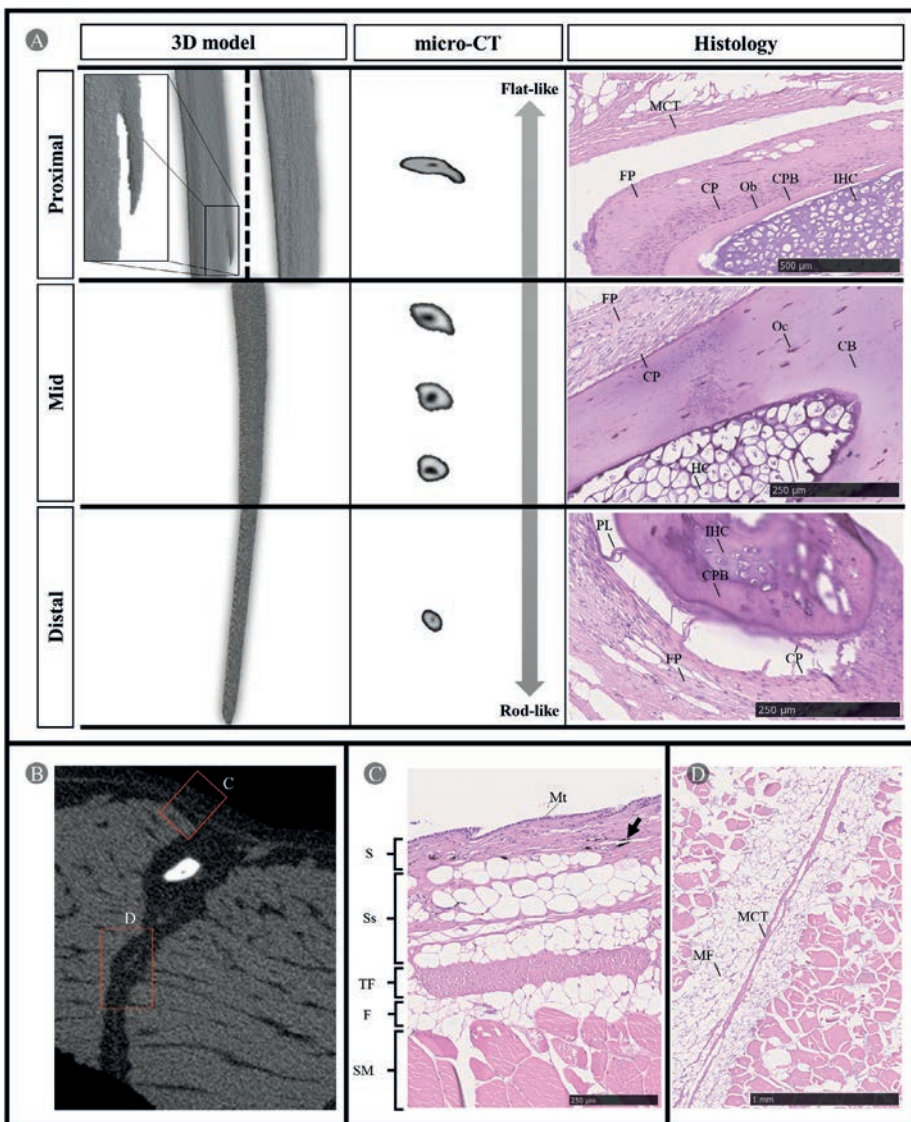


Fig. 8. Anatomical overview of adult Atlantic salmon rib and adjacent structures from targeted rib samples. A) Anatomical description combining 3D model, transversal micro-CT slices and histology at the proximal, mid, and distal rib parts. Box at the proximal area of the 3D model shows a magnified view of the rib process on the external rib side. CB, Compact bone; CP, cellular periosteum; CPB, compact perichondral bone; FP, fibrous periosteum; IHC, immature hyaline cartilage; HC, hypertrophic chondrocytes; Ob, osteoblast; Oc, osteocytes; PL, periosteal ligaments. B) Cross-section micro-CT slice for rib mid part and adjacent structures. Boxes with letters indicate histological illustration of corresponding anatomical regions. C) and D) Anatomical description of adjacent rib structures, both peritoneum and myocommata, respectively, combining transversal micro-CT slice and histology. MCT, myocommata connected tissue; MF, myocommata fat; Mt, mesothelium; S, serosa; SM, skeletal muscle; Ss, Subserosa; TF, transverse fascia; F, fat. Black arrow points to melanomacrophages. Haematoxylin and eosin staining.

cortex of osteolytic and resorptive appearance (Video 4).

3.5. Mineral composition of axial skeleton

Mineral composition of the axial skeleton of slaughter size salmon was similar for salmon farmed in land-based tanks or sea-cages. Wild salmon had significantly lower content than farmed groups for Ca

($80,409 \pm 3435$ vs. $104,165 \pm 1692$ mg kg^{-1} dw; $p = 0.0001$), P ($39,350 \pm 1702$ vs. $50,979 \pm 848$ mg kg^{-1} dw; $p = 0.0005$), and Mg (1198 ± 57 vs. 1578 ± 24 mg kg^{-1} dw; $p = 0.0002$). The Ca:P ratio was similar in all groups (2.04 ± 0.01).

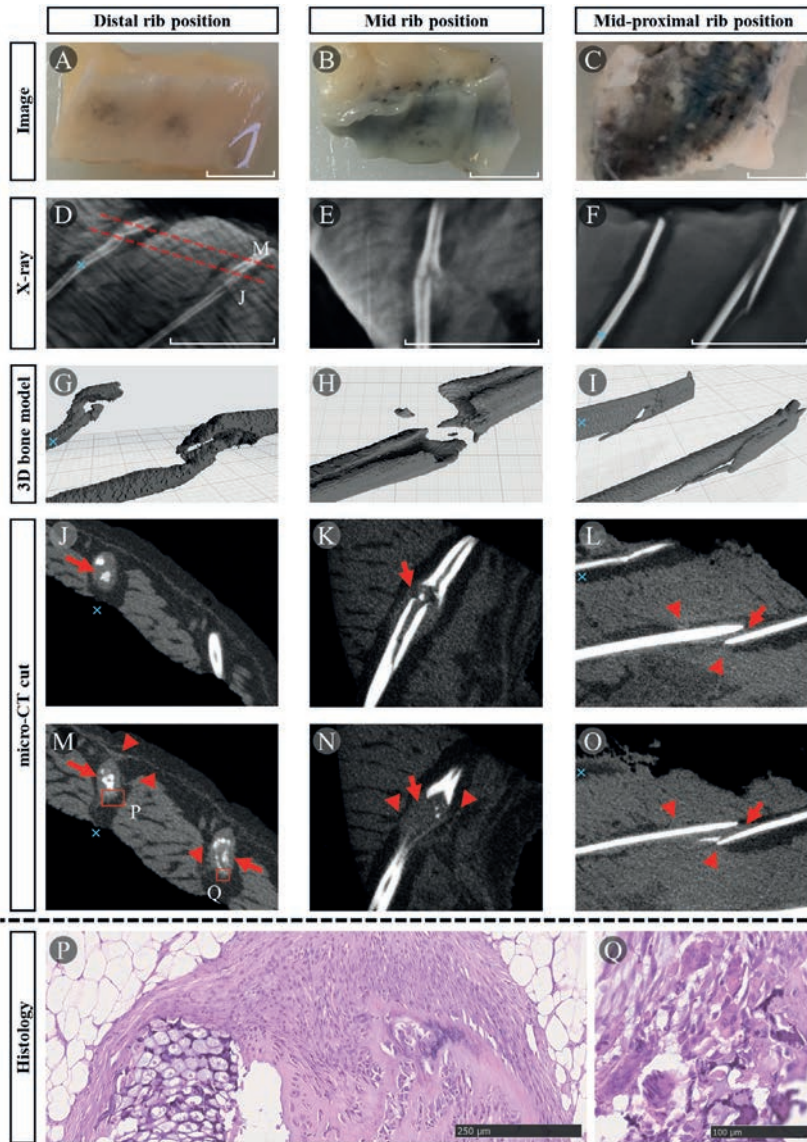


Fig. 9. Characterization of continuity break group abnormalities in targeted focal dark spots (DS) of fillets of farmed Atlantic salmon with different DS levels at different rib parts. Images A) to O) are organized by column. Image, X-ray, 3D model for bone density, and micro-CT cut are provided for each sample. Box with letters on image M) indicates the region of histology P) and Q) (haematoxylin and eosin staining). Parallel discontinuous red lines in X-ray images indicate micro-CT planes if transversal. Blue color marks connect X-ray with micro-CT images. Red arrows point to non-mineralized callus with similar radiodensity as muscle. Red arrowhead indicates the connection between non-mineralized callus and adjacent skeletal muscle or peritoneal transverse fascia. Restricted white bars on bottom right corners of A – F show the X-ray and ordinary image scale, set to 1 cm. Major squares in 3D models show the scale, set to 1 * 1 cm. (For interpretation of the references to color in this figure legend, the reader is referred to the web version of this article.)

3.6. Histopathology

The histological morphology of salmon ribs showed a core rich in immature hyaline cartilage in proximal parts, whereas the mid area contained hyaline cartilage in a hypertrophic phase with trabeculae formation. In more distal areas, ribs contained hyaline cartilage (Fig. 8A). Ribs were surrounded by myocommata's connective tissue and located adjacent to the parietal peritoneum, separated by different tissue layers; serosa, subserosa (with visible melanomacrophages), and transverse fascia (Fig. 8B - D). The periosteum presented a series of periosteal ligaments connecting cellular layers with compact rib bone (Fig. 8A).

Histological evaluations of radiolucent fusiform bodies showed signs of external callus formations with hyaline cartilage in several hypertrophic stages non-covered by a compact bone. Fibrous areas with different mineralization degrees were seen near hypertrophic cartilage, whereof trapped active osteoblasts and osteoclasts could be observed (Fig. 9P and Q). The near myomere of mid and mid-proximal DS presented muscle fibrosis and a chronic-active process with melanomacrophage, fat infiltration, and histiocytic-like granuloma formation.

Histology of ribs with axis deviations revealed muscle fibrosis in a chronic-active inflammatory process with melanomacrophage infiltration. Such fibrosis affected the totality of the length of near myocytes. Fat infiltration was observed between muscle fibrosis (Fig. 10E and H).

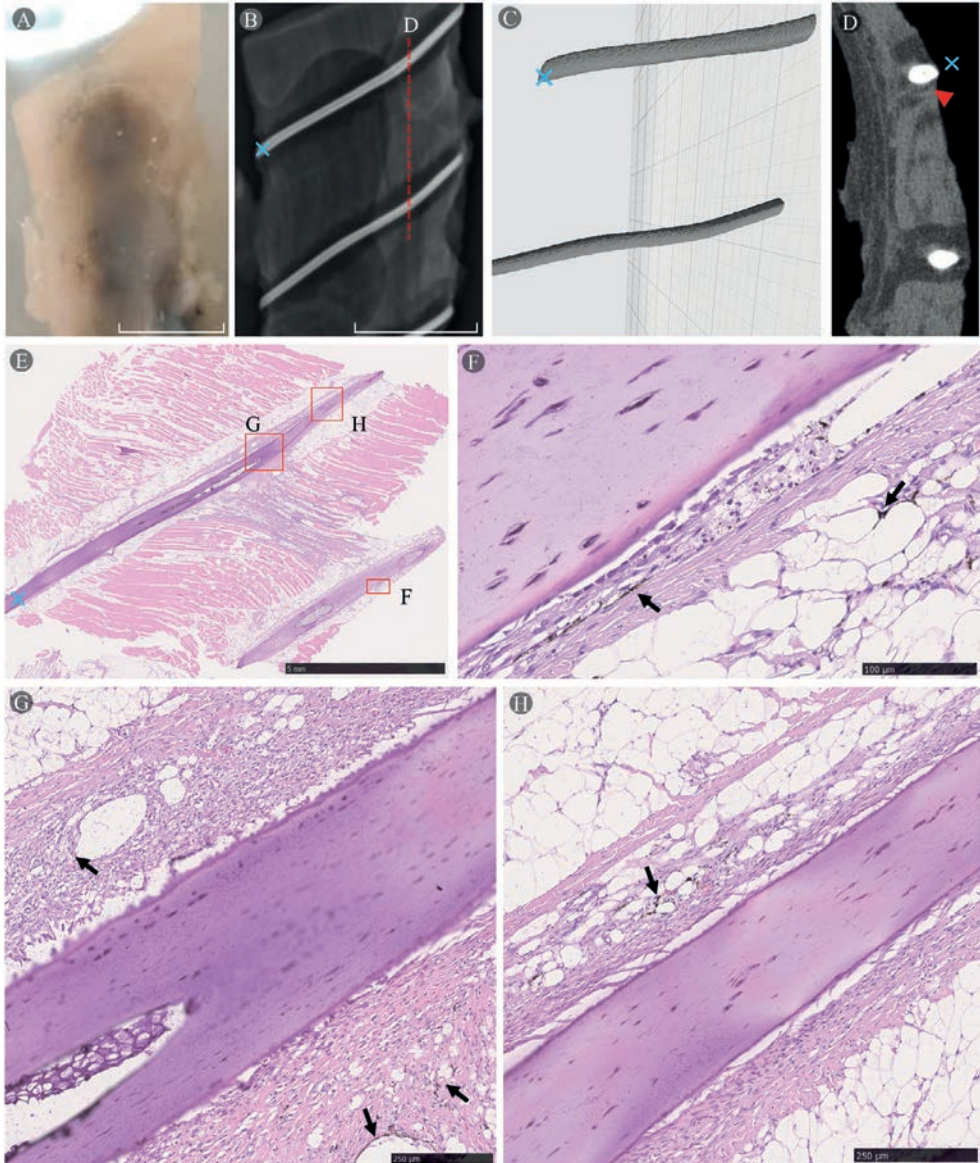


Fig. 10. Characterization of axis deviations in targeted focal dark spots (DS) of fillets of farmed Atlantic salmon shown by A) image, B) X-ray, C) 3D model for bone density, D) micro-CT cut, and E) F) G) H) histology. Blue color mark connects ribs from X-ray to histology images. Boxes with letters on image D) indicate the region of histology of F), G), and H). Discontinuous red line in image B) indicates the micro-CT plane in image D). Red arrowhead indicates the connection between non-mineralized connective tissue around the rib and adjacent structures. Black arrows point to melanomacrophages. The restricted white bar on the bottom right corner of image A) and B) shows the X-ray and ordinary image scale, set to 1 cm. Major squares in the 3D model show the scale, set to 1 * 1 cm. Haematoxylin and eosin staining. (For interpretation of the references to color in this figure legend, the reader is referred to the web version of this article.)

The fibrous periosteum and myocommatas entire architecture from axis deviations were found altered. Metaplastic periosteum with granuloma-like structures and melanomacrophages infiltration between fibrous and cellular layers was observed, giving the periosteum a relatively thicker appearance. Extended vacuolization of cells from the cellular periosteum was also observed, with necrotic melanomacrophage

infiltration in some affected areas (Fig. 10F). Periosteal ligaments were found altered (Fig. 10G).

4. Discussion

Fillet-red DS were present in sea-cage farmed salmon throughout the

whole seawater phase as expected (Bjørngen et al., 2019), but the present study is the first to report typical fillet-red DS of the cranio-ventral fillet region of smolts in freshwater. The occurrence of fillet-black DS after five months in seawater coincides with Bjørngen et al. (2019), who proposed that fillet-red DS are acute focal changes that develop into chronic melanized fillet-black DS (Bjørngen et al., 2015). The prevalence of fillet-black DS was 43% on average at harvesting, which is higher than former reports for harvest sized salmon (range 8–33%) (Bjørngen et al., 2019; Dessen et al., 2019; Lutfi et al., 2022; Sissener et al., 2016), though our evaluation method was more sensitive.

The study was initiated with no presumption of the magnitude of morphological rib abnormalities. Hence a consistent deviation from the expected rib morphology of all salmon groups, complicated the understanding of rib abnormality effects on fillet DS. Black DS (either fillet or peritoneum) only occurred in sea-cage farmed salmon, coinciding with twice as high rib abnormalities compared with smolts, salmon farmed in land-based tanks, and wild salmon, however, the association between rib abnormalities and DS is complex. Because all DS were located in the same anatomical area (cranio-ventral), shared healing responses, and rib abnormality types, we assume they share similar etiology with different pathophysiological scenarios. On one hand, muscle strains and hemorrhages (fillet-red DS) of generally round appearance without rib damage, result from either local myositis or traumatic events that exclusively affect soft tissues. Such processes would not be detected by X-ray of the ribs in acute forms, but secondary rib changes may evolve over time when transitioning to fillet-black DS (e.g., generalized radiolucent and shorter or missing rib parts), typically observed at early seawater phase. On the other hand, rib deformations or fractures that evolve into flattened focal lesions, resulting from multiple rib damage in a linear pattern. In this scenario, acute and chronic forms are normally detected by X-ray, unless they are produced in the latero-lateral plane or overlapped, being more typical near slaughter. The presence of ribs with primary and potential secondary changes suggests a combination of both pathophysiological processes.

Non-mechanical stress-related forms such as generalized radiolucent could indicate either osteomyelitis (Epsley et al., 2021; Gu et al., 2017), osteoporosis, or osteomalacia. Osteomalacia-derived changes may bring abnormal flexibility (Khurana, 2009), reducing the risk of rib fracture while increasing deformation. However, osteomyelitis and osteoporosis may increase fracture risk. As DS levels depend on the size of the lesion and melanomacrophages density, with a positive trend to muscle fibrosis (by X-ray), this parameter may be a good macroscopic indicator of the focal inflammatory degree, as proposed by Malik et al. (2021). Given the positive association between higher DS levels and the prevalence of generalized radiolucent ribs, focal osteomyelitis is a potential process, as micro-CT analyses suggest.

Similar numbers for most characteristic rib abnormalities in DS between farmed sea-cage salmon rib cages with or without DS, suggest implications of additional major factors than rib abnormalities influencing the development of DS.

Pigmentation of areas of the rib cage under a continuously high degree of motility suggests a natural melanizing response to mechanical stress. Pigmentation related to mechanical stress was likewise present in DS with radiolucent non-mineralized callus, where the chronicity of the histological study indicates abnormal healing responses with delayed mineralization and hypertrophic non-unions (pseudoarthrosis), typical of inadequate stabilization (Khurana, 2009; Kumar et al., 2018; Miclau et al., 2007). Mechanical stress might also cause metaplastic changes resulting in thicker periosteum with altered periosteal unions near axis rib deviation (Sakai et al., 2011). Thus, the degree of mechanical stress in near soft tissue should depend on the type of rib abnormality. On the other hand, distal rib parts, which concentrated most of rib abnormalities, did not coincide with the cranio-ventral fillet region with largest DS, and similar rib abnormalities did not produce the same degree and type of pigmentation at proximal and distal parts. Therefore, there must be other factors contributing to the melanizing response of the healing

process in injured tissue.

The flattened cross-sectional rib shape at mid-proximal parts and their deeper location in the muscle wall than in distal rib parts, suggest insertion support for musculature and natural endurance to latero-lateral flexion (Van Leeuwen, 1999). Ribs resist expansion and contraction of fish organs (Jiao et al., 2020), but also oblique and radial expansion of white muscle during explosive starts and turning maneuvers. This concentrates most of the tension at the anterior cones, between mid-proximal rib parts and the horizontal septum (Van Leeuwen, 1999). The association of the higher severity of the spots (larger, more intense, and rounder) at mid-proximal than mid-distal rib anatomical regions evidences such specific mechanical effect on injuries, evolving into more severe muscle fibrosis with recurrent injury, chronic-active inflammation (Bjørngen et al., 2019; Larsen et al., 2012; Nikolaou et al., 1987), hypertrophic non-unions (given a rib injury), and pathological interconnections (myofascial adhesions) that increases local stiffness (Bernabei et al., 2017).

While land-based tank smolts were carefully transferred to flow-through seawater tanks and no vaccination was performed, smolts in commercial sea-cages experienced more intensive production-related activities. Such procedures were pumping, grading, vaccination, transportation by well-boat, and mechanical delousing one- and two-months prior harvesting. Additionally, fish in sea-cages experienced different swimming activity, faster growth, and infections (e.g., PRV). There were similar fillet-red DS and rib abnormality types (though in different numbers) in fish from land-based tanks and sea-cages after seawater transfer. Therefore, the absence of melanin during healing in fish from land-based tanks, points to environmental factors as determinants for the final DS phenotype.

Teleost ribs are soft and flexible to sustain constant mechanical loads during swimming (Cohen et al., 2012; Fiedler et al., 2021; Jiao et al., 2020), but in out-of-the-water situations (e.g., grading, vaccination, crowding), fish may experience abnormal forces in either direction or intensity. This might be seen in the consistent concentration of rib abnormalities in central parts of the rib cage, which reveals a vulnerable area that coincides with the highest occurrence of DS in fillets (rib number 10–14). Nevertheless, no increase in DS and the total number of rib abnormalities after mechanical sea lice treatments was observed. Either delousing did not have an effect on the number of injuries, or there was efficient healing, as the increase of radiopaque callus shows. Although, we must consider a dilution effect of some abnormality types by appositional growth when comparing fish of different sizes.

In view of the abrupt increase in the number of rib abnormalities shortly after transfer to sea-cages, focus on any sources of stress during this period seems justified. The increased number of generalized radiolucent ribs from smolt farm to land-based tanks and sea-cages, suggests a common etiology acting at different magnitudes in both seawater environments. For example, seawater transfer might affect rib bone mineralization in the form of osteomalacia due to different nutritional requirements in response to standard stressful farming procedures (Iversen et al., 2005), not occurring in land-based tanks. Because the mineral composition of the vertebrae was similar for the farmed groups at slaughter and higher than wild salmon, we could exclude general alterations in bone mineralization at slaughter. On the other hand, we should also consider osteomyelitis as a result of inflammatory processes in the muscle wall derived from mechanical stress (e.g., traumatism) or immune stimulants (e.g., vaccine, infections).

Smolts sampled two weeks after vaccination did not show an increase in the number of rib abnormalities compared to non-vaccinated smolts, even though vaccinated smolts presented fillet-red DS in freshwater. However, the higher numbers of shorter and missing rib parts, and concentration in caudal and distal areas near the vaccination site after transfer to sea-cages, suggest a potential association with vaccination. This fact dissipates the acute effect of a mechanical disturbance of ribs during vaccination and related activities such as pumping and grading. Although, it suggests long-term effects such as alteration of the

path of rib ossification after myotome injury as Akama et al. (2020) reported, and osteomyelitis triggered by the vaccine component or traumatic events between late smolt operations and transfer to sea-cages. The decreasing tendency towards slaughter of shorter or missing and generalized radiolucent ribs highlights the possible effects of production-related factors shortly after transfer to sea-cages, which is considered a particularly critical period in farmed salmon (Borno, 2021).

Effects of farming operations, such as pumping, grading, and vaccinations on DS in salmon were found negative by Mørkøre (2012). Similarly, Berg et al. (2012) found no cause-effect relationship between vaccine components and DS, although side effects of vaccines on spinal deformities are observed, sometimes co-occurring with focal melanization as part of the inflammatory process (Holm et al., 2020; Trangerud et al., 2020). We found evidence for vaccine-induced rib defects and associated sparse pigmentation, but in line with previous studies, our results can not directly link vaccination component to the presence of DS. However, the presence of histiocytic-like granuloma in fillet-black DS at slaughter was similar to foreign body reactions, as the mineral oil adjuvant used in intraperitoneal salmon vaccines (Carlton et al., 2001; Hwang et al., 2012; Larsen et al., 2012). This might suggest migration of loaded macrophages with vaccine compounds from parietal peritoneum layers (Koppang et al., 2005) to the adjacent skeletal muscle after inflammatory stimuli (e.g., trauma).

Although the salmon farmed in sea-cages showed positive results for PRV, the presence of PRV in sea-cage fish is not considered as the primary cause for DS, since similar Ct-values of PRV were observed in unstained salmon muscle and DS by Mørkøre et al. (2016). Moreover, Bjørgen et al. (2019) did not find PRV in all DS, nor experimental inoculation of salmon muscle caused the development of DS. However, PRV may play a role in modulating the inflammatory response locally (Bjørgen et al., 2019; Krasnov et al., 2016; Malik et al., 2021), as well as other opportunistic pathogens (e.g., *Staphylococcus aureus*) (Tomecka et al., 2019).

The fact that fish farmed in land-based tanks could be exposed to a low concentration of antigenic compounds (no vaccination, UV-treated flow-through water) than in sea-cages (vaccinated, circulating antigens, infections) (Bateman et al., 2021), determines a differential factor for the melanization process in DS. This might be an effect of increased systemic melanin production to enhance immunocompetence to a disease threat, an important component of the innate immune system (Gagnaire et al., 2013; Wilson et al., 2001).

5. Conclusion

Rib abnormalities were common findings in both wild and farmed Atlantic salmon, seemingly a consequence of mechanical stress, and secondary changes due to an inflammatory process. The prevalence doubled after transferring farmed smolts to large commercial sea-cages, coinciding with the presence of fillet-red focal dark spots (DS) and subsequent development of fillet-black DS five months after sea transfer, as opposed to wild salmon and salmon reared in small land-based tanks, that did not develop black DS (either fillet or peritoneum). Rib abnormalities were more prevalent in black DS, and both co-occurred most frequently at the center of the rib cage. The black DS phenotype was associated with a higher presence of rib fractures and rib deformations in the injured area, but DS also occurred without any sign of abnormal ribs or fractures. Other factors such as the anatomical position of the injury contributed to the association. While feed and genetic origin were not primary causes, environmental factors such as damaging incidents in the commercial late smolt phase and sea-cage operations are more likely determinants for the presence of DS.

CRedit authorship contribution statement

Jiménez-Guerrero Raúl: Methodology, Validation, Formal analysis,

Investigation, Data curation, Visualization, Writing - original draft, Writing - review & editing. Baeverfjord Grete: Conceptualization, Methodology, Validation, Investigation, Resources, Visualization, Supervision, Project administration, Writing - review & editing. Evensen Øystein: Methodology, Investigation, Resources, Visualization, Supervision, Writing - review & editing. Hamre Kristin: Investigation, Resources, Writing - review & editing. Larsson Thomas: Methodology, Investigation, Resources, Data curation. Dessen Jens-Erik: Investigation, Resources. Gannestad Kjellrun-Hoås: Methodology, Investigation, Resources, Data curation. Mørkøre Turid: Conceptualization, Methodology, Validation, Formal analysis, Investigation, Resources, Visualization, Supervision, Project administration, Funding acquisition, Writing - review & editing.

Declaration of Competing Interest

The authors declare the following financial interests/personal relationships which may be considered as potential competing interests:

Turid Mørkøre reports financial support was provided by Norwegian Seafood Research Fund.

Data availability

Data will be made available on request.

Acknowledgments

The Norwegian Seafood Research Fund (FHF) and Norwegian University of Life Sciences (NMBU) supported this study. The study in sea-cages was carried out using Nofima's R&D licenses granted by the Norwegian Directorate of Fisheries for large-scale Industrial Research. The authors acknowledge the skillful assistance and dedicated fish management of the technicians at Lerøy Midt AS, with special thanks to Helge Endresen. The authors remark on the excellent work provided by staff at the Research Station for Sustainable Aquaculture (Nofima) and laboratories. Thanks to Dr. Elisabeth Ytteborg for helping to interpret some results. Thanks to M.Sc. Sumeng Galdat for your assistance processing part of the data. Thanks to Gunhild Haustveit for your help with micro-CT scans during COVID-19 restrictions. Thanks to Professor Øivind Andersen for valuable contributions to the manuscript.

Appendix A. Supplementary data

Supplementary data to this article can be found online at <https://doi.org/10.1016/j.aquaculture.2022.738697>.

References

- Akama, K., Ebata, K., Maeno, A., Taminato, T., Otosaka, S., Gengyo-Ando, K., Kawamura, A., 2020. Role of somite patterning in the formation of Weberian apparatus and pleural rib in zebrafish. *J. Anat.* 236 (4), 622–629. <https://doi.org/10.1111/joa.13135>.
- Aursand, M., Bleivik, B., Rainuzzo, J.R., Leif, J., Mohr, V., 1994. Lipid distribution and composition of commercially farmed Atlantic salmon (*Salmo salar*). *J. Sci. Food Agric.* 64 (2), 239–248. <https://doi.org/10.1002/jsfa.2740640214>.
- Baeverfjord, G., Asgard, T., Shearer, K.D., 1998. Development and detection of phosphorus deficiency in Atlantic salmon, *Salmo salar* L., parr and post-smolts. *Aquac. Nutr.* 4 (1), 1–11. <https://doi.org/10.1046/j.1365-2095.1998.00095.x>.
- Bateman, A.W., Teffer, A.K., Bass, A., Ming, T., Hunt, B.P.V., Krkosek, M., Miller, K.M., 2021. Atlantic salmon farms are a likely source of *Tenacibaculum maritimum* infection in migratory Fraser River sockeye salmon. *Can. J. Fish. Aquat. Sci.* 00, 1–16. <https://doi.org/10.1101/2021.06.15.448581>.
- Berg, A., Yurtseva, A., Hansen, T., Lajus, D., Fjellidal, P.G., 2012. Vaccinated farmed Atlantic salmon are susceptible to spinal and skull deformities. *J. Appl. Ichthyol.* 28 (3), 446–452. <https://doi.org/10.1111/j.1439-0426.2012.01988.x>.
- Bernabei, M., van Dieën, J.H., Maas, H., 2017. Altered mechanical interaction between rat plantar flexors due to changes in intermuscular connectivity. *Scand. J. Med. Sci. Sports* 27 (2), 177–187. <https://doi.org/10.1111/sms.12644>.
- Bjørgen, H., Wessel, Ø., Fjellidal, P.G., Hansen, T., Sveier, H., Saeba, H.R., Koppang, E.O., 2015. *Piscine orthoreovirus* (PRV) in red and melanised fish in white muscle of

- Atlantic salmon (*Salmo salar*). *Vet. Res.* 46 (1), 89. <https://doi.org/10.1186/s13567-015-0244-6>.
- Björge, H., Haldorsen, R., Oaland, Ø., Kveltestad, A., Kannimathu, D., Rimstad, E., Koppang, E.O., 2019. Melanized focal changes in skeletal muscle in farmed Atlantic salmon after natural infection with *Piscine orthoreovirus* (PRV). *J. Fish Dis.* 42 (6), 935–945. <https://doi.org/10.1111/jfd.12995>.
- Borno, G., 2021. Miscellaneous health problems in farmed salmonids. In: Sommerset, I., Bang Jensen, B., Børnø, B., Haukaas, A., Brun, E. (Eds.), *The Health Situation in Norwegian Aquaculture 2020*. Norwegian Veterinary Institute.
- Carlton, W.W., Boitnott, J.K., Dungworth, D.L., Ernst, H., Hayashi, Y., Mohr, U., Ward, J.M., 2001. Assessment of the morphology and significance of the lymph nodal and hepatic lesions produced in rats by the feeding of certain mineral oils and waxes. *Exp. Toxicol. Pathol.* 53 (4), 247–255. <https://doi.org/10.1078/0940-2993-00198>.
- Clarke, W.C., Saunders, R.L., McCormick, S.D., 1996. Smolt production. In: Pennel, W., Barton, B.A. (Eds.), *Principles of Salmonid Culture*. CRC Press, Elsevier, Amsterdam, The Netherlands, pp. 517–567.
- Cohen, L., Dean, M., Shipov, A., Atkins, A., Monsonejo-Ornan, E., Shahar, R., 2012. Comparison of structural, architectural and mechanical aspects of cellular and acellular bone in two teleost fish. *J. Exp. Biol.* 215 (11), 1983–1993. <https://doi.org/10.1242/jeb.064790>.
- De Clercq, A., Perrott, M.R., Davie, P.S., Preece, M.A., Wybourn, B., Ruff, N., Witten, P.E., 2017. Vertebral column regionalisation in Chinook salmon, *Oncorhynchus tshawytscha*. *J. Anat.* 231 (4), 500–514. <https://doi.org/10.1111/joa.12655>.
- Dessen, J.E., Mørkøre, T., Bildøy, J.L., Johnsen, S.N., Poppe, L.T., Hatlen, B., Rørvik, K.A., 2019. Increased dietary protein-to-lipid ratio improves survival during naturally occurring pancreas disease in Atlantic salmon, *Salmo salar* L. *J. Fish Dis.* 42 (1), 21–34. <https://doi.org/10.1111/jfd.12904>.
- Epsley, S., Tadros, S., Farid, A., Kargilis, D., Mehta, S., Rajapakse, C.S., 2021. The effect of inflammation on bone. *Front. Physiol.* 11 (1695) <https://doi.org/10.3389/fphys.2020.511799>.
- Färber, F., 2017. Melanin Spots in Atlantic Salmon Fillets – An Investigation of the General Problem, the Frequency and the Economic Implication Based on an Online Survey. Norwegian University of Life Sciences, Ås, Norway.
- Fiedler, I.A.K., Elmogazy, O., Courtemanche, G., Cardoso, L., Berteau, J.P., 2021. Bones of teleost fish demonstrate high fracture strain. *J. Biomech.* 120, 110341 <https://doi.org/10.1016/j.jbiomech.2021.110341>.
- Fjellidal, P.G., van der Meer, T., Fraser, T.W.K., Sambraus, F., Jawad, L., Hansen, T.J., 2018. Radiological changes during fracture and repair in neural and haemal spines of Atlantic cod (*Gadus morhua*). *J. Fish Dis.* 41 (12), 1871–1875. <https://doi.org/10.1111/jfd.12899>.
- Fjellidal, P.G., Madaro, A., Hvas, M., Stien, L.H., Oppedal, F., Fraser, T.W.K., 2020. Skeletal deformities in wild and farmed cleaner fish species used in Atlantic salmon *Salmo salar* aquaculture. *J. Fish Biol.* 98 (4), 1049–1058. <https://doi.org/10.1111/jfb.14337>.
- Gagnaire, B., Cavalie, I., Camilleri, V., Adam-Guillermin, C., 2013. Effects of depleted uranium on oxidative stress, detoxification, and defence parameters of zebrafish *Danio rerio*. *Arch. Environ. Contam. Toxicol.* 64 (1), 140–150. <https://doi.org/10.1007/s00244-012-9814-z>.
- Gislason, H., Karstensen, H., Christiansen, D., Hjelde, K., Helland, S., Bæverfjord, G., 2010. Rib and vertebral deformities in rainbow trout (*Oncorhynchus mykiss*) explained by a dominant-mutation mechanism. *Aquaculture* 309 (1), 86–95. <https://doi.org/10.1016/j.aquaculture.2010.09.016>.
- Gu, Q., Yang, H., Shi, Q., 2017. Macrophages and bone inflammation. *J. Orthop. Translat.* 10, 86–93. <https://doi.org/10.1016/j.jot.2017.05.002>.
- Holm, H., Ytteborg, E., Host, V., Reed, A.K., Dalum, A.S., Bæverfjord, G., 2020. A pathomorphological description of cross-stitch vertebrae in farmed Atlantic salmon (*Salmo salar* L.). *Aquaculture* 526, 735382. <https://doi.org/10.1016/j.aquaculture.2020.735382>.
- Horton, J.M., Summers, A.P., 2009. The material properties of acellular bone in a teleost fish. *J. Exp. Biol.* 212 (9), 1413–1420. <https://doi.org/10.1242/jeb.020636>.
- Hwang, S.H., Kim, H.H., Park, D.J., Jee, Y.S., Lee, K.H., Kim, Y.H., Yang, H.K., 2012. Local tissue reaction after injection of contrast media on gastric wall of mouse: experimental study for application of contrast media to computed tomography lymphography. *J. Korean Surg. Soc.* 82 (2), 70–78. <https://doi.org/10.4174/jks.2012.82.2.70>.
- Iversen, M., Finstad, B., McKinley, R.S., Eliassen, R.A., Carlsen, K.T., Evjen, T., 2005. Stress responses in Atlantic salmon (*Salmo salar* L.) smolts during commercial well boat transports, and effects on survival after transfer to sea. *Aquaculture* 243 (1), 373–382. <https://doi.org/10.1016/j.aquaculture.2004.10.019>.
- Jiao, Y.Y., Okada, M., Hara, E.S., Xie, S.C., Nagaoka, N., Nakano, T., Matsumoto, T., 2020. Micro-architectural investigation of teleost fish rib inducing pliant mechanical property. *Materials* 13 (22), 5099. <https://doi.org/10.3390/ma13225099>.
- Khurana, J.S., 2009. *Bone Pathology*, Second ed. Humana Press, Springer, New York, NY, USA.
- Koppang, E.O., Haugarvoll, E., Hordvik, I., Aune, L., Poppe, T.T., 2005. Vaccine-associated granulomatous inflammation and melanin accumulation in Atlantic salmon, *Salmo salar* L., white muscle. *J. Fish Dis.* 28 (1), 13–22. <https://doi.org/10.1111/j.1365-2761.2004.00583.x>.
- Krasnov, A., Moghadam, H., Larsson, T., Afanasyev, S., Mørkøre, T., 2016. Gene expression profiling in melanised sites of Atlantic salmon fillets. *Fish Shellfish Immunol.* 55, 56–63. <https://doi.org/10.1016/j.fsi.2016.05.012>.
- Kumar, V., Abbas, A.K., Aster, J.C., 2018. *Robbins Basic Pathology*, Tenth ed (Philadelphia, Pennsylvania, USA).
- Larsen, H.A., Austbo, L., Mørkøre, T., Thorsen, J., Hordvik, I., Fischer, U., Koppang, E.O., 2012. Pigment-producing granulomatous myopathy in Atlantic salmon: a novel inflammatory response. *Fish Shellfish Immunol.* 33 (2), 277–285. <https://doi.org/10.1016/j.fsi.2012.05.012>.
- Liaset, B., Julshamn, K., Espe, M., 2003. Chemical composition and theoretical nutritional evaluation of the produced fractions from enzymic hydrolysis of salmon frames with Protamex™. *Process Biochem.* 38 (12), 1747–1759. [https://doi.org/10.1016/S0032-9592\(02\)00251-0](https://doi.org/10.1016/S0032-9592(02)00251-0).
- Lutfi, E., Berge, G.M., Bæverfjord, G., Sigholt, T., Bou, M., Larsson, T., Ruyter, B., 2022. Increasing dietary levels of the n-3 long-chain PUFA, EPA and DHA, improves the growth, welfare, robustness and fillet quality of Atlantic salmon in sea cages. *Br. J. Nutr.* 1-19 <https://doi.org/10.1017/S0007114522000642>.
- Malik, M.S., Björge, H., Nyman, I.B., Wessel, Ø., Koppang, E.O., Dahle, M.K., Rimstad, E., 2021. PRV-1 infected macrophages in melanized focal changes in white muscle of Atlantic salmon (*Salmo salar*) correlates with a pro-inflammatory environment. *Front. Immunol.* 12, 664624 <https://doi.org/10.3389/fimmu.2021.664624>.
- Miclaui, T., Lu, C., Thompson, Z., Choi, P., Püttitz, C., Marcucio, R., Helms, J.A., 2007. Effects of delayed stabilization on fracture healing. *J. Orthop. Res.* 25 (12), 1552–1558. <https://doi.org/10.1002/jor.20435>.
- Mørkøre, T., 2012. Mørke flekker i laksefilet – Kunnskapstatus og tiltak for å begrense omfanget. *Nofima*. 17, 1–59.
- Mørkøre, T., Larsson, T., Kveltestad, A.S., Koppang, E.O., Åsli, M., Krasnov, A., Rørvik, K.A., 2015. Mørke flekker i laksefilet – Kunnskapstatus og tiltak for å begrense omfanget. *Nofima*. 34, 1–79.
- Mørkøre, T., Dessen, J.-E., Larsson, T., Jiménez-Guerrero, R., Rørvik, K.-A., 2016. Effekt av for på melaninflekker i laks infisert med både PRV og SAV. *Nofima*. 31, 1–23.
- Nikolaou, P.K., Macdonald, B.L., Glisson, R.R., Seaber, A.V., Garrett Jr., W.E., 1987. Biomechanical and histological evaluation of muscle after controlled strain injury. *Am. J. Sports Med.* 15 (1), 9–14. <https://doi.org/10.1177/036354658701500102>.
- Nordberg, M., 2018. Seasonal Variation in Fillet Quality of Atlantic Salmon (*Salmo salar*). Norwegian University of Life Sciences, Ås, Norway.
- Sakai, D., Kii, I., Nakagawa, K., Matsumoto, H.N., Takahashi, M., Yoshida, S., Kudo, A., 2011. Remodeling of actin cytoskeleton in mouse periosteal cells under mechanical loading induces periosteal cell proliferation during bone formation. *PLoS One* 6 (9), e24847. <https://doi.org/10.1371/journal.pone.0024847>.
- Sissener, N.H., Waagbø, R., Rosenlund, G., Tvenning, L., Susort, S., Lea, T.B., Breck, O., 2016. Reduced n-3 long chain fatty acid levels in feed for Atlantic salmon (*Salmo salar* L.) do not reduce growth, robustness or product quality through an entire full scale commercial production cycle in seawater. *Aquaculture* 464, 236–245. <https://doi.org/10.1016/j.aquaculture.2016.06.034>.
- Tomecka, M.J., Ethiraj, L.P., Sánchez, L.M., Roehl, H.H., Carney, T.J., 2019. Clinical pathologies of bone fracture modelled in zebrafish. *Dis. Model. Mech.* 12 (9), dmm037630. <https://doi.org/10.1242/dmm.037630>.
- Trangerud, C., Björge, H., Koppang, E.O., Grøntvedt, R.N., Skogmo, H.K., Ottesen, N., Kveltestad, A., 2020. Vertebral column deformity with curved cross-stitch vertebrae in Norwegian seawater-farmed Atlantic salmon, *Salmo salar* L. *J. Fish Dis.* 43 (3), 379–389. <https://doi.org/10.1111/jfd.13136>.
- Van Leeuwen, J.L., 1999. A mechanical analysis of myomere shape in fish. *J. Exp. Biol.* 202 (23), 3405–3414. <https://doi.org/10.1242/jeb.202.23.3405>.
- Wilson, K., Cotter, S.C., Reeson, A.F., Pell, J.K., 2001. Melanism and disease resistance in insects. *Ecol.* 4 (6), 637–649. <https://doi.org/10.1046/j.1461-0248.2001.00279.x>.
- Zhol, S., Ackman, R.G., Morrison, C., 1995. Storage of lipids in the myosepta of Atlantic salmon (*Salmo salar*). *Fish Physiol. Biochem.* 14 (2), 171–178. <https://doi.org/10.1007/BF00002460>.

Paper II

1 **Understanding morphological rib abnormalities in Atlantic salmon**

2
3 **Raúl Jiménez-Guerrero^{a*}, Grete Baeverfjord^b, Øystein Evensen^c, Turid Mørkøre^a**

4
5 ^a Department of Animal and Aquacultural Sciences, Faculty of Biosciences, Norwegian
6 University of Life Sciences, NO-1432 Ås, Norway

7 ^b Nofima, NO-6600 Sunndalsøra, Norway

8 ^c Department of Paraclinical Sciences, Faculty of Veterinary Medicine, Norwegian University
9 of Life Sciences, NO-1433 Ås, Norway

10
11 * Corresponding author: Raúl Jiménez-Guerrero; Department of Animal and Aquacultural
12 Sciences, Faculty of Biosciences, Norwegian University of Life Sciences, NO-1432 Ås,
13 Norway; Tel: +4767232638

14 Email: raul.jimenez.guerrero@nmbu.no

15
16 **Keywords: Rib deformity; Chondrocyte transformation; Osteomalacia; Farmed fish;**

17 **Fish welfare**

18
19 **Manuscript, intended peer review journal:**

- 20 • **Aquaculture (4.5) (Q1)**
21

22 **Abstract**

23 Poor rib health in Atlantic salmon (*Salmo salar* L.) can lead to negative effects on welfare
24 and fillet quality. The present research aimed to enhance the comprehension of long-term rib
25 morphology within a broader musculoskeletal framework of harvest-sized salmon (3 kg),
26 examining a population fed contrasting smoltification diets. Histological examination revealed
27 that 29 % of the sampled ribs exhibited abnormal morphologies, primarily characterized by
28 varying degree of generalized radiolucency (GR), unrelated to ongoing inflammatory processes
29 in adjacent tissues. Initial development of GR was potential transformation or dedifferentiation
30 of central core chondrocytes to mesenchymal-like cells and lumen osteolysis, progressing as
31 an expanded osteolytic lumen, reaching the periosteum. In parallel, there were progressive
32 alterations of the concentric appositional growth pattern of the compact bone, with an increase
33 of the external collagen layer under the cellular periosteum. Disorganized collagen-rich islands
34 were also seen in the compact bone, as were signs of new osteoid deposition in osteolytic
35 lumina. Due to the presence of GR, the cross-sectional diameter increased by 18 – 20 %. X-ray
36 examinations revealed the highest concentration of abnormalities in the anterior-central area of
37 the rib cage, and the mid-distal rib parts. The contrasting diets, based on either marine (M-
38 group) or plant (P-group) ingredients, modulated the morphology of the ribs in the central area.
39 The M-group had lower prevalence of GR (19 and 26 % of mid-distal rib parts) and axis
40 deviations (12 and 17 % of mid rib parts), and numerically lower mechanical rib strength and
41 phosphorus content ($p = 0.06$ and 0.07 , respectively). The sensitivity of rib morphology to
42 smoltification diet was higher than vertebrae in the long-term. This study enhances
43 understanding of the etiology of the primary morphological rib abnormalities in Atlantic
44 salmon, particularly in GR, by providing detailed histomorphology of pathological changes.
45 The study associates these changes with osteomalacia.

46 **1 Introduction**

47 Understanding the skeletal health of Atlantic salmon (*Salmo salar* L.), is of critical
48 importance, as it is essential for the shape and protection of soft tissues, structure support, and
49 swimming ([Gray, 1957](#); [Kryvi and Poppe, 2016](#)). Poor skeleton health directly impacts fish
50 welfare ([Noble et al., 2018](#)), but also business profitability as it negatively affects fish growth
51 ([Hansen et al., 2010](#)), product and technological quality of fillets ([Currey, 2003](#); [Haugarvoll et](#)
52 [al., 2010](#); [Sullivan et al., 2007](#)). Currently, salmon bone research is focused on vertebrae health
53 ([Drábiková et al., 2021, 2022](#); [Witten et al., 2019](#)), while there has been much less focus on the
54 rib cage (*cavea thoracis*). Rib (*costae* or *pleurapophysis*) morphology, mechanical properties
55 and chemical composition have already been studied in several fish species of cellular and
56 acellular bone ([Cohen et al., 2012](#); [Horton and Summers, 2009](#); [Jiao et al., 2020](#); [Soliman,](#)
57 [2018](#)). Although rib deformations have been described in zebrafish (*Danio rerio*) ([Akama et](#)
58 [al., 2020](#)), and rainbow trout (*Oncorhynchus mykiss*) ([Gislason et al., 2010](#)), to our knowledge,
59 only a few studies focus on Atlantic salmon.

60 Recently, [Jiménez-Guerrero et al. \(2022\)](#) and later [Brimsholm et al. \(2023\)](#) explored rib
61 morphology through X-ray and histopathology and its relationship with red (acute;
62 hemorrhages) and black (chronic) focal dark spots (DS) of fillets, the largest fillet quality
63 concern ([Nordberg, 2018](#)). They reported the presence of axis deviations, changes in
64 radiodensity, and rib fractures of farmed and wild salmon. [Jiménez-Guerrero et al. \(2022\)](#)
65 reported up to eight different types of morphological rib abnormalities can occur in the rib cage
66 and that the number of axis deviations, generalized radiolucency, shorter or missing rib parts,
67 radiolucent and radiopaque calluses may depend on the life stage and growing environment.
68 The transition from fresh- to seawater appeared to be critical, causing increasing generalized
69 radiolucency and shorter or missing ribs. Among different etiological factors, traumatic events

70 causing rib cage deformation/damage, local inflammatory processes, and time-specific dietary
71 deficiencies were suggested.

72 Skeletal deformities usually develop during early life stages ([Baeverfjord et al., 2018](#);
73 [Fjelldal et al., 2009](#); [Vielma and Lall, 1998](#)). Though [Brimsholm et al. \(2023\)](#) suggested that
74 generalized radiolucency and axis deviations are normal morphological variation, [Baeverfjord](#)
75 [et al. \(1998\)](#) already 25 years ago reported axis deviations in the form of wrinkly ribs and
76 mechanical deterioration in response to a phosphorus (P) deficient diet during fresh and
77 seawater phases. Later, [Roberts et al. \(2001\)](#) observed similar findings associated with dietary
78 P and vitamin C deficiency during early life stages. While many of these studies are primarily
79 descriptive, our understanding of salmon rib health remains nascent. Hence, the present study
80 aimed to improve the understanding of rib abnormalities of adults Atlantic salmon and to reveal
81 whether deviating rib morphology is anticipated or influenced by early feeding.

82

83 **2 Material and methods**

84 **2.1 Fish material**

85 Atlantic salmon eggs of common genetic origin (BO 1 - 20, AS Bolaks, Eikelandsosen,
86 Bjørnafjorden, Norway) were hatched at the Research Station for Sustainable Aquaculture
87 (Nofima, Sunndalsøra, Møre and Romsdal, Norway) December 6th 2019. On July 7th 2020 1600
88 fish averaging 30 g were PIT-tagged and fed either a marine-based diet (M-group) or a plant-
89 based diet (P-group) in quadruplicate tanks per dietary treatment (n = 200 per tank; flow-
90 through; tank volume, 0.5 m³) (Supplementary 1, Supplementary 2, and Supplementary 3).
91 Smoltification was induced following a 12:12 Light:Dark hours regime from July 13th 2020.
92 On August 26 – 27th 2020, all fish were vaccinated with Alpha JECT[®] micro 6 by hand injection
93 (PHARMAQ AS, Overhalla, Norway). Smoltification status was checked by challenge test,

94 plasma osmolality determination, chloride content, and gill Na⁺, K⁺-ATPase activity on
95 September 4th, 11th, and 15th 2020 (n = 12, 12, and 12) ([Clarke et al., 1996](#)). On September 16th
96 2020, 25 fish from each tank (n = 100 per dietary treatment) were mixed and randomly
97 transferred to two seawater tanks (flow-through; 3 m³). Fish were fed a standard commercial
98 diet with pellet size and composition were adjusted to fish size according to feed producer
99 recommendations (Skretting, Stavanger, Norway) during the entire seawater phase. The
100 Light:Dark hours regime was 24:00, tank biomass was kept under 30 kg/m³ by splitting the fish
101 into two to three (February 12th 2020) and four (June 1st 2020) tanks, and water flow was 100
102 l/m. On 22nd July 2021, 168 fish (n = 84 per dietary group; n = 21 per original quadruplicate
103 tank; 2.6 kg, individual body weight) were carefully transferred to a large common tank (flow-
104 through; 103 m³), where experience from the research station has shown that DS can develop.
105 The water flow gradually increased from 700 to 1200 l/min, and the Light:Dark hours regime
106 was kept at 24:00. On September 16th – 17th 2021 (body weight 3 kg), fish were slaughtered.
107 More details about the experiment can be found in Supplementary 4 and Supplementary 5.

108

109 **2.2 Diets**

110 The test diets were produced by extrusion at the Aquafeed Technology Centre (Nofima,
111 Bergen, Norway). Diets were qualitatively different, isoenergetic, and of similar particle size
112 (2 mm). While the M-group diet was formulated with exclusively fish meal and oil, and wheat
113 starch (binder), the P-group diet was formulated using soy protein concentrate, wheat gluten,
114 corn gluten, and rapeseed oil. The raw formulation and composition of the M- and P-group
115 diets are presented in Supplementary 1, Supplementary 2, and Supplementary 3. Pellet
116 properties are described in [Karki \(2022\)](#).

117 Test and standard feed samples were homogenized and analyzed for protein ([ISO5983-](#)
118 [2, 2009](#)), fat ([EC152, 2009](#)), dry matter ([ISO6496, 1999](#)), ash content ([ISO5984, 2002](#)), fiber
119 ([AOCSBa6a-05, 2017](#)), combustion value (energy) ([ISO9831, 1998](#)), total starch and free
120 astaxanthin (BioLab internal protocol, Nofima, Bergen, Norway), and the amino acid
121 composition was analyzed ([ISO13903, 2005](#)). The fatty acid composition was determined by
122 gas chromatography (GC) as fatty acids methyl esters using 23:0 as the internal standard. The
123 concentrations of calcium (Ca), P, magnesium (Mg), potassium (K), sodium (Na), zinc (Zn),
124 iron (Fe), manganese (Mn), and copper (Cu) were determined spectrophotometrically after
125 digestion with acid using an MP-AES (Microwave Plasma Atomic Emission Spectrometer)
126 (Agilent Technologies, Santa Clara, California, USA). Soluble P was indirectly estimated by
127 the colorimetric detection (880 nm absorption) of ascorbic acid-molybdate phosphate on a
128 spectrophotometer (Shimadzu UVmini 1210, Shimadzu Europe, Duisburg, Germany)
129 ([ISO6878, 2004](#)).

130

131 **2.3 Sampling**

132 Fish were sampled three times during the experimental period; September 16th 2020
133 (prior to seawater transfer), December 3rd 2020 (10 weeks after seawater transfer), and
134 September 16th – 17th 2021 (slaughter). Fish for analyses after seawater transfer were sampled
135 representing the original dietary tanks in freshwater based on PIT-tags readings. At sampling,
136 fish were euthanized by an overdose of MS-222 (Metacaine 0.1 g l⁻¹; Alpharma, Animal
137 Health Ltd., Hampshire, UK) before blood was collected from the caudal vessels. Thereafter,
138 fish were bled out by the gill section, and individual weight and length were recorded. On
139 September 16th 2020, randomly selected fish were sampled from three tanks per dietary
140 treatment (n = 15 per dietary group). All fish were sampled for blood, gutted and kept at -20
141 °C for X-ray and mineral analyses. On December 3rd 2020 (n = 50 per dietary group), blood

142 samples were taken from 10 fish per dietary group. The presence of DS was recorded (n = 40
143 per dietary group). A group of gutted fish (n = 10 per dietary group) was kept at -20 °C for X-
144 ray analyses. On September 16th – 17th 2021, at slaughter (n = 80 per dietary group), blood
145 samples were taken from 12 fish per dietary group. The abdominal right side wall (parietal
146 peritoneum, rib, and adjacent skeletal muscle) corresponding to rib numbers 11 to 14 at the
147 mid rib position of the ribs was sampled for histomorphology examinations of 12 fish per
148 dietary group. These samples and DS (red, n = 4; black, n = 3) were fixed in formalin (10 %
149 phosphate-buffered formalin, pH 7.0, 4 °C). Twenty fish were filleted pre-rigor and transported
150 in styrofoam boxes with ice to Nofima Ås laboratory for fillet quality analysis (color, firmness,
151 gaping, and DS) after five days, whereas a group of 40 gutted fish per dietary group was kept
152 at -20 °C for X-ray, mechanical properties and mineral analyses of ribs and vertebrae. Strength
153 and mineral analyses of the rib cage (n = 12 per dietary group) and vertebrae (n = 20 per dietary
154 group) were performed using selected fish with no vertebrae abnormalities.

155

156 **2.4 Histology**

157 Histological samples were decalcified (EDTA 10 %; pH 7) at room temperature for two
158 weeks, before they were dehydrated, embedded in paraffin wax, and sectioned at 2 - 2.5 µm.
159 Sections of the abdominal wall were performed horizontally at the center of the sample to
160 obtain a cross-sectional view of 3 - 4 ribs and adjacent tissues (Supplementary 6). DS were
161 sectioned parallel to the parietal peritoneum. Sections were mounted on glass slides, stained
162 with Haematoxylin and Eosin, Periodic acid–Schiff, Movat Pentachrome, and Picro Sirius Red,
163 scanned using NanoZoomer S360 (C13220-01, Hamamatsu Photonics K.K, Hamamatsu,
164 Japan), and visualized with NDP.view.2 (v.2.7.43, Hamamatsu Photonics K.K, Hamamatsu,
165 Japan). Picro Sirius Red-stained glasses were inspected under polarized light by a Leica DM6B
166 Light microscope with a DMC4500 Digital Camera (Leica Microsystems, Wetzlar, Germany)

167 at 90 ° (cross polarization), and for confocal microscopy with a Leica TCS SP5 Confocal laser
168 scanning microscope (Leica Microsystems, Wetzlar, Germany) using two channels (emission
169 bandwidth, 496 nm – 554 nm and 574 nm – 644 nm).

170 The morphometry of the ribs was evaluated using the transverse fascia as a reference
171 point. The parallel line, representing the combined thickness of the rib bone, periosteum, and
172 adjacent fat (referred to as the rib cluster), was collected at the rib's center (Supplementary 6).
173 The cross-sectional micro-organization of the compact bone (*substantia compacta*) from
174 normal (n = 4) and abnormal ribs (n = 6) was studied by gray level co-occurrence matrix texture
175 analysis, using the ImageJ software (v1.52s, U. S. National Institutes of Health, Bethesda,
176 USA), plug-in “GLCM Texture” on Picro Sirius Red-stained images. Prior to grayscale
177 transformation (8-bit images), images from individual ribs and adjacent soft tissues were
178 generated, and histogram equalized. Then, compact bone was manually selected
179 (Supplementary 7) to perform the gray level co-occurrence matrix texture analysis with the size
180 of the step-in pixels set to 1 using 0 and 90 ° directions. The following parameters were
181 extracted ([Zaletel et al., 2017](#)): angular second moment and inverse difference moment as
182 measures of image homogeneity; and contrast and entropy as a measure of heterogeneity.
183 Values for 0 and 90 ° direction were averaged since the aleatory position of ribs made it
184 impossible to study linear dependencies.

185 Osteocyte density was calculated by dividing the number of local maxima corresponding
186 to osteocytes or lacunae in compact bone (“Find Maxima” function; prominence > 25;
187 excluding edges maxima; light background) by the selected area (μm^2) (Supplementary 7).

188

189 **2.5 X-ray**

190 X-rays of frozen fish and formalin-fixed material were performed at the Nofima
191 radiography laboratory in Sunndalsøra. Samples of fish prior to and after seawater transfer, the
192 right and left sides of the rib cage of fish at slaughter, and targeted formalin-fixed samples of
193 fish at slaughter were X-rayed using an IMS Giotto mammography equipment (Giotto,
194 Pontecchio Marconi, BO, Italy), with 20 pixels per mm² resolution, exposure at 22 kV and 100
195 mAs. For gutted fish sampled at slaughter, X-rays were taken using a semi-digital computed
196 radiography system (Fuji Medical AS, Oslo, Norway). Prior to rib cage X-rays, frozen gutted
197 bodies were thawed at 4 °C for three days before cutting and trimming at room temperature.
198 Images were taken on coated photo-reactive phosphorous imaging plates Fujifilm Computed
199 Radiography (FCR) (Fujifilm, Tokyo, Japan), and read using FCR Profect Reader (Fujifilm,
200 Tokyo, Japan). Sample preparation and evaluation of rib morphology was performed according
201 to [Jiménez-Guerrero et al. \(2022\)](#). Evaluation of vertebrae morphology was done similarly to
202 [Bou et al. \(2017\)](#) and [Fjellidal et al. \(2007\)](#), but separating major morphological abnormalities
203 (e.g., compression, fusion, and cross-stitch) from vertebra X:Y ratio deviations and internal
204 structural bending of the vertebra body. The impaired mineralization score was performed
205 according to the scale in Supplementary 8. After X-ray analyses, fish sampled prior to seawater
206 transfer were pooled per original tank and stored at -20 °C for mineral analyses, while rib cage
207 skeleton and vertebrae from vertebra number 31 to 41 of slaughter fish were kept at 4 °C for
208 mechanical analysis.

209

210 **2.6 Bone dissection, strength measurement, and mineral content**

211 Rib numbers 1 – 22 from rib cages sampled at slaughter were dissected from the fish
212 peritoneum using metal pincers, and the remaining attached flesh was carefully removed. Ribs
213 number 12, 13, and 14 from the left and right sides were selected for mechanical analyses. Prior

214 to the mechanical test, ribs were kept for two hours on a dry surface at room temperature to
215 standardize moisture levels. Mechanical analyses were performed instrumentally (TA-XT2
216 Texture Analyzer, Stable Micro Systems, Surrey, UK), with a guillotine knife (70 mm width,
217 3 mm thickness) and well bottom surface at three different rib parts: proximal, mid, and distal
218 ([Jiménez-Guerrero et al., 2022](#)). The trigger force was 1 Newton at a traveling speed of 2 mm/s.
219 Strength values were recorded as breaking load (N) and the elasticity (slope) at 50 % of the
220 breaking load. Following the test, all ribs (approx. 44 per fish) were pooled per original tank in
221 freshwater (n = 4 per dietary treatment) and stored at -20 °C for mineral analysis.

222 Vertebrae were dissected and trimmed for neural (*arcus vertebrae* and *processus*
223 *spinosus*) and haemal spines (*arcus hemalis*) to minimize the contact between the knife and
224 those parts not belonging to the vertebrae body (*corpus vertebrae*). Two separated vertebrae
225 from each fish were latero-laterally compressed to emphasize the trabecular fraction
226 (*substantia spongiosa*) since it is naturally more active than the compact bone ([Gil Martens et](#)
227 [al., 2006](#); [Nordvik et al., 2005](#)). Analyses were performed using the same instruments and
228 guillotine knife as ribs but with a trigger load of 10 Newton at a traveling speed of 2 mm/s.
229 Strength values were collected from the given time-load graphs as load (N), elasticity (slope),
230 and area as work (N*mm) at 50 % of the compression depths due to the structural symmetry
231 of the vertebra body. Values from both vertebrae measurements per fish were averaged. After
232 the test, vertebrae were pooled per original tank in freshwater (n = 4 per dietary treatment) and
233 stored at -20 °C for mineral analysis.

234 Ribs and vertebrae from slaughter-sized fish were homogenized. Fish bodies sampled
235 prior to seawater transfer were gutted to exclude feces and homogenized. Excluding ribs,
236 homogenized samples were heated for dry matter ([ISO6496, 1999](#)) and ash content ([ISO5984,](#)
237 [2002](#)) determination. The concentrations of Ca, P, Mg, K, Na, Zn, Fe, Mn, and Cu were
238 determined spectrophotometrically after digestion with acid using an MP-AES. Due to the low

239 volume of pooled homogenized ribs, only total Ca, P, and Mg were analyzed. Ca and Mg
240 concentration was assessed using inductively coupled plasma mass spectrometry (ICP-OES)
241 after microwaved digestion. Total P concentration was estimated through an individual
242 spectrophotometrically method ([ISO6491, 1998](#)).

243

244 **2.7 Macroscopic muscle straits**

245 Fillet color was assessed using DSM SalmoFan™ (F. Hoffmann-La Roche AG, Basel,
246 Switzerland), and the severity of gaping was assessed by the average gaping score (from 0, no
247 gaping, to 5, severe gaping) ([Andersen et al., 1994](#)) of the left and right fillets. The mechanical
248 properties of fillets were determined as the firmness at the dorsal loin (epaxial skeletal muscle)
249 of the right fillet as the force required to break the fillet surface (breaking force, N) using the
250 same instruments as for bone, but with a flat-ended 12.5 mm probe at a traveling speed of 1
251 mm/s ([Mørkøre and Einen, 2003](#)). The presence of DS was evaluated according to their size
252 and color using a log-2 scoring system from 0 (no visible DS) to 8 (DS > 6 cm width) ([Mørkøre,](#)
253 [2012](#)).

254

255 **2.8 Serum chemistry**

256 Blood was extracted using 6 ml vacutainer tubes and centrifuged at 3700 RPM at ambient
257 temperature for 10 minutes, using an Avanti J-15R centrifuge (Beckman Coulter, Inc.,
258 Indianapolis, United States) with a radius rotor of 207.8 mm for serum extraction. Serum was
259 pooled in groups of five fish per original freshwater tank and stored at -20 °C for clinical
260 biochemistry analysis (Faculty of Veterinary Medicine, NMBU, Norway). Due to the high
261 dietary contrast, the concentration of several standard health parameters in serum was explored
262 to monitor different fish health indicators: alkaline phosphatase (ALP), a specific bone

263 formation marker ([Kuo and Chen, 2017](#)); creatine kinase (CK) as a marker for disruption of
264 cell membranes due to hypoxia or injury ([Baird et al., 2012](#)); creatinine as muscle development
265 indicator ([Patel et al., 2013](#)); inorganic phosphorous (Pi), calcium (Ca²⁺), sodium (Na⁺), and
266 potassium (K⁺) for available ions and electrolyte balance. Samples were analyzed using
267 Atellica[®] CH (Siemens Healthcare Diagnostics Inc., Deerfield Road Deerfield, United States).

268

269 **2.9 Statistics**

270 Statistical analyses were performed with R software (v. 4.0.3, R Core Team, Vienna,
271 Austria). The “lm()” R function was used in parametric traits, while “glm()” was adjusted for
272 Poisson or binomial distribution for non-parametric traits. Pairwise test of non-parametric
273 distributions was performed using the Wilcoxon rank sum test using the
274 “pairwise.wilcox.test()” function, with p.adjust.method = "BH". The models did not consider
275 random effects. Microsoft[®] Excel[®] software (v. 15128.20280, Microsoft Corporation,
276 Redmond, United States) was used to create figures. The significance level was set at $p \leq 0.05$,
277 and results were presented as mean \pm standard error (SEM).

278

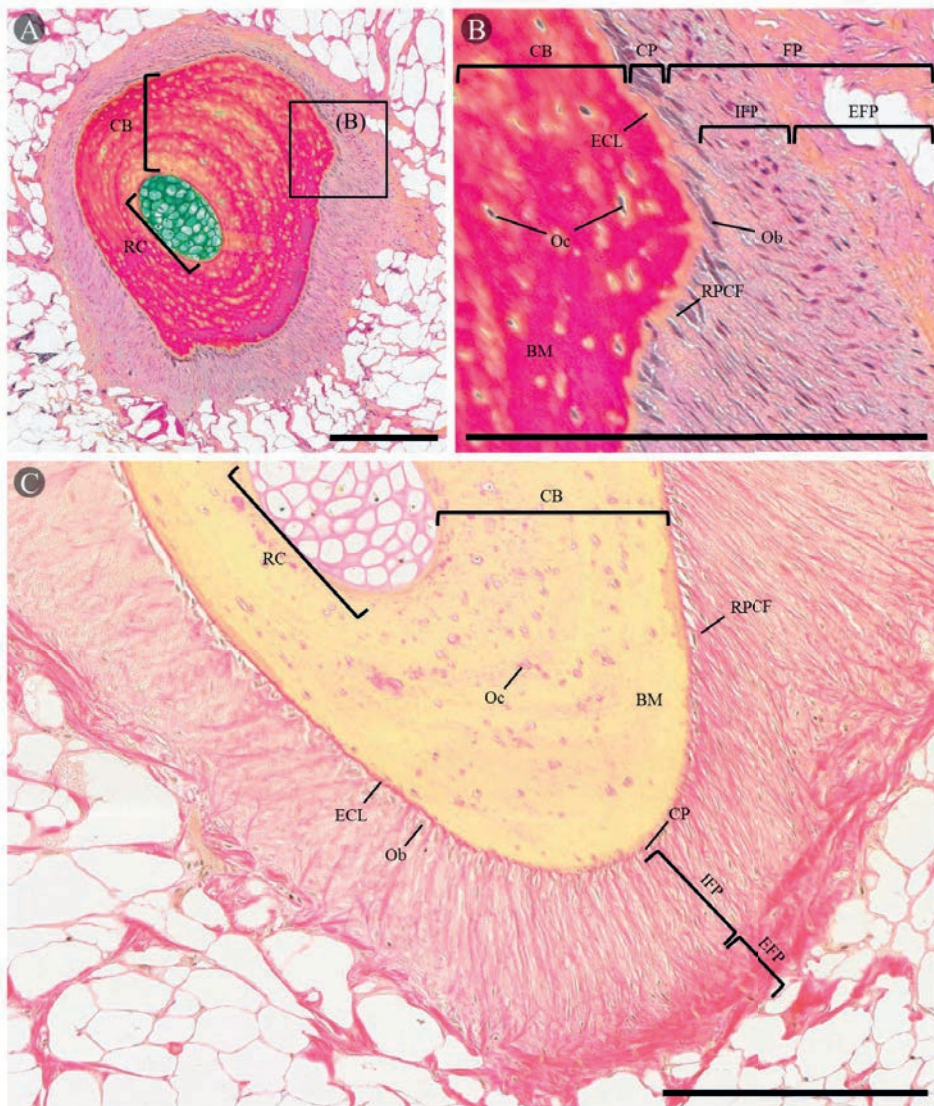
279 **3 Results**

280 **3.1 Rib histomorphology**

281 Most (71 %) rib's cross-sections showed normal histological traits viewed by light
282 microscopy, whereas a smaller proportion (29 %) displayed noticeable deviations regardless of
283 the dietary treatments before seawater transfer.

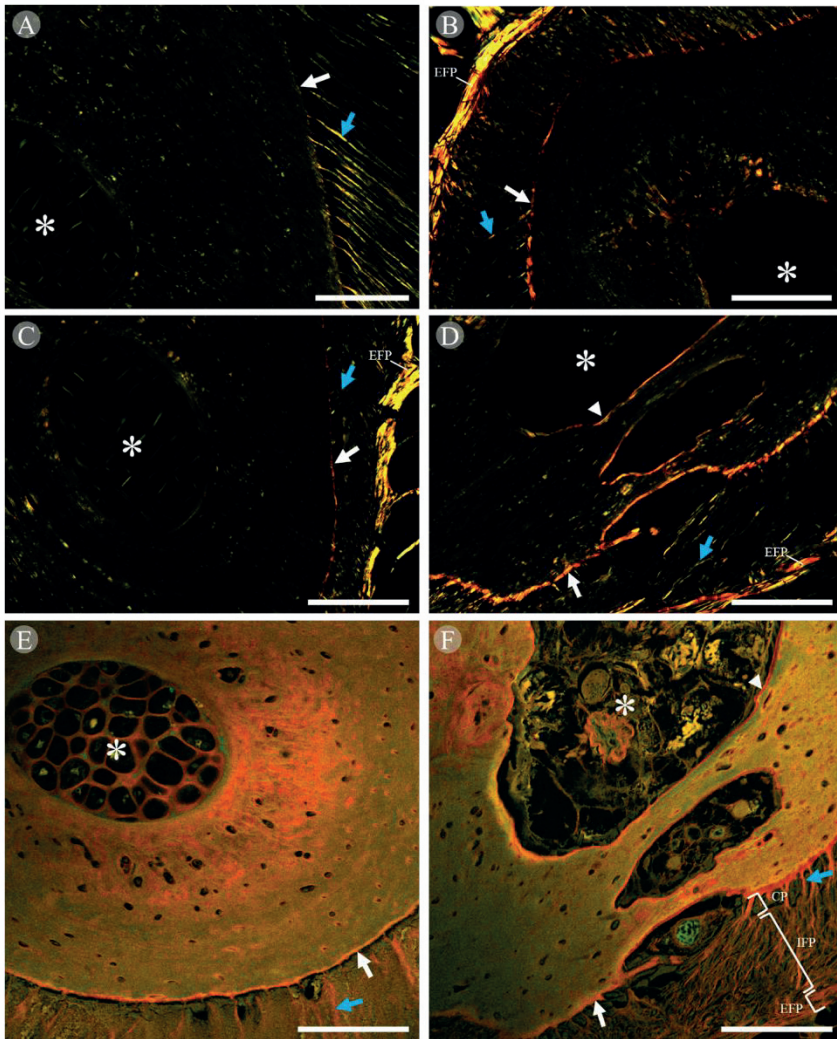
284 Normal ribs showed multiple concentric layers of osteocytes from the appositional
285 growth of the compact bone (*pars ossea*). The bone matrix presented collagen and non-collagen

286 proteins organized around a core (*pars cartilaginea*) with chondrocytes near the hypertrophic
287 phase of slight radiolucency. The rib core showed low birefringence collagen type III signal,
288 probably due to the disorganized distribution of the fibers (Figure 1. A; Figure 2. A and C).
289 Osteocyte density was around 0.003 cells/ μm^2 . Compact bone had a relatively low amount of
290 collagen, mainly type III (Figure 1. C; Figure 2. A and C). The rib periosteum presented an
291 irregular thickness on the internal and external fibrous fraction. Radial glycoproteins and
292 collagen type III (mainly) and I fibers were seen connecting the fibrous periosteum to the
293 outermost compact bone layer, occasionally forming a small shield of collagen type I under the
294 osteoblasts (Figure 1. B and C; Figure 2. C and E), exclusively found in the cellular periosteum.
295 The external fibrous periosteum layer surrounding the ribs had the richest content of collagen
296 type I and III fibers (Figure 1. B and C; Figure 2. A and C). No blood vessels were observed
297 in the periosteum. Both dietary groups shared common features in adjacent muscle areas,
298 indicating no abnormal glycogen accumulation nor significant signs of muscle necrosis or
299 fibrosis. In 8 % of the samples, sparse melanomachrophages without near inflammatory
300 processes or fibrosis were seen in deeper layers of the myocommata near blood vessels.



301

302 Figure 1. Cross-sectional morphology of normal mid rib (*costae*) parts of Atlantic salmon (3
 303 kg). For A) and B) Movat Pentachrome staining was used for proteoglycans and mucins (blue),
 304 collagen/reticular fibers (yellow), colocalization of collagen/reticular fibers and proteoglycans
 305 (green), muscle and osteoid (or decalcified bone matrix) (reddish-brown), nuclei and elastin
 306 (black) and active nucleus (osteoblast in cellular periosteum) (violet/purple). The box in image
 307 A) indicates the region of zoom of image B). Picro Sirius Red staining was used in C) to
 308 highlight the collagen fiber network (red) in the periosteum. CB, Compact bone (*substantia*
 309 *compacta; pars ossea*); RC, Rib core with hypertrophic chondrocytes (*pars cartilaginea*); Oc,
 310 Osteocytes; BM, Bone matrix, ECL; External collagen layer of the CB; Ob, Osteoblast; CP,
 311 Cellular periosteum with Ob; FP, Fibrous periosteum; IFP, Internal fibrous periosteum; EFP,
 312 External fibrous periosteum; RPCF, Radial periosteal collagen fibers. Black bars on the bottom
 313 right corner show the image scale, set to 250 µm. Color print.

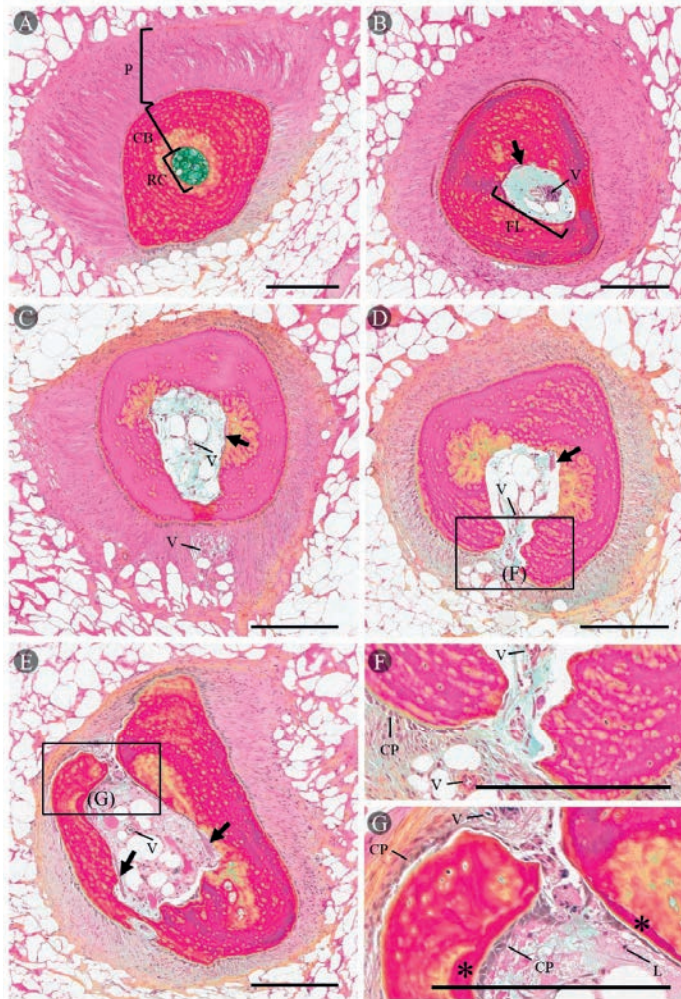


314

315 Figure 2. Collagen distribution in cross-sections of normal (left panel) and abnormal (right
 316 panel) mid ribs (costae) with generalized radiolucency of Atlantic salmon (3 kg). A) to D)
 317 under polarized light. E) and F) confocal microscope. Yellow-orange birefringence in polarized
 318 images stands for collagen type I (thick fibers), while green birefringence type III (thin fibers).
 319 C) and E), and D) and F) correspond to the same rib, respectively. Picro Sirius red staining.
 320 IFP, Interior fibrous periosteum; EFP, Exterior fibrous periosteum. White arrows indicate the
 321 external collagen layer of the compact bone (*substantia compacta; pars ossea*) under the
 322 cellular periosteum (CP). White asterisks indicate either rib core with hypertrophic
 323 chondrocytes (*pars cartilaginea*) (normal ribs) or a fibrous lumen. White arrowheads indicate
 324 the internal collagen layer in rib lumen. Blue arrows indicate radial periosteal collagen fibers.
 325 White bars on the bottom right corner of images show the image scale, set to 100 μ m. Color
 326 print.

327

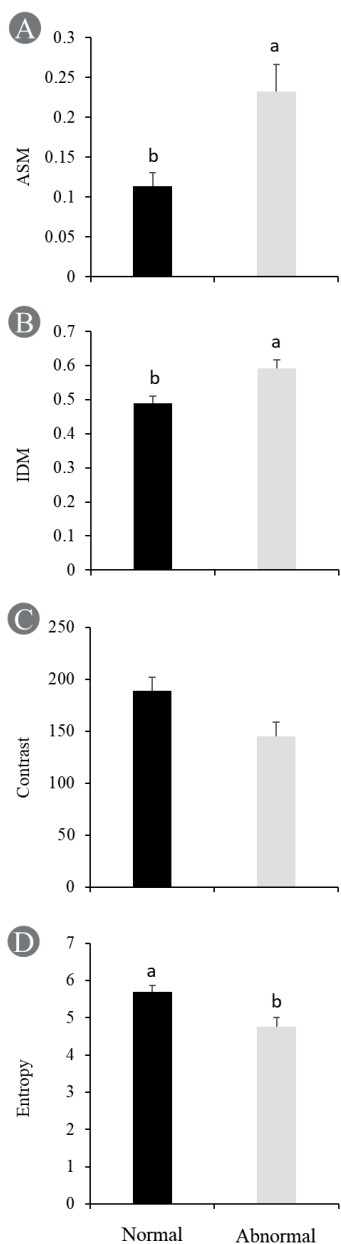
328 Ribs with abnormal histomorphology exhibited 18 - 20 % greater overall diameter than
329 those with normal histomorphology ($p = 0.04$), and there were no indications of acute or
330 chronic inflammation or melanisation of the ribs or the surrounding soft tissue. The cross-
331 sectional area of the compact bone and osteocyte density were similar for normal and abnormal
332 ribs. However, the rib core possibly transformed into an irregular osteolytic lumen of large
333 radiolucency with an amorphous fibroblasts/fibroblast-like cell network (fibrous rib lumen)
334 containing lipid vacuoles, blood vessels, osteoclasts, and sparse leucocytes (Figure 3). The rib
335 lumen was surrounded by a thick collagen type I layer in non-active osteolytic borders (Figure
336 2. B and D). Another wide collagen type I layer was also observed surrounding the outermost
337 compact bone in contact with the cellular periosteum.



338

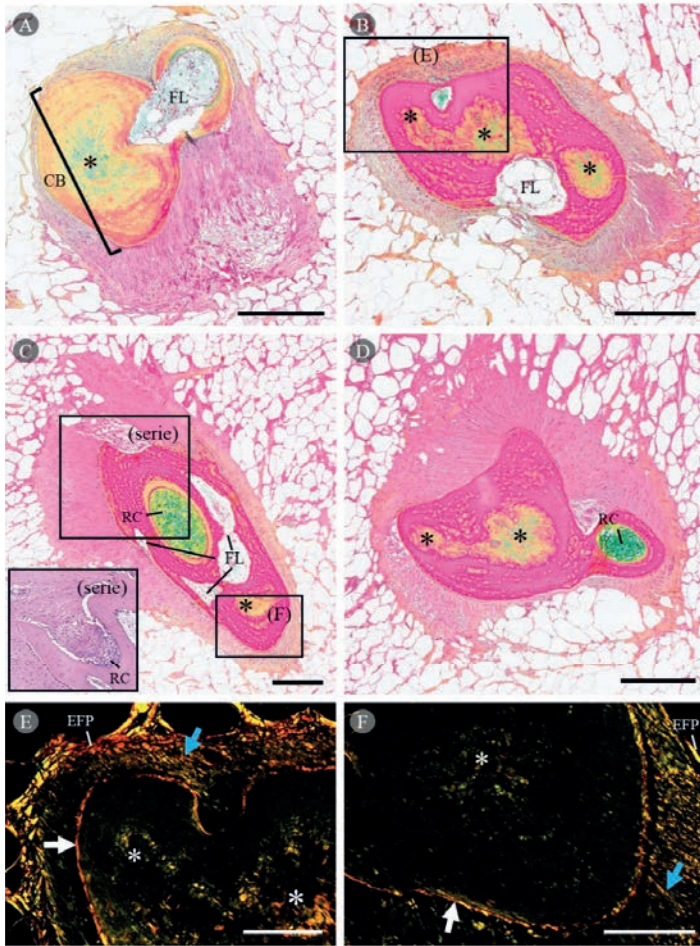
339 Figure 3. Proposed model for progressive cross-sectional morphological changes in
 340 generalized radiolucent ribs (*costae*) of Atlantic salmon (3 kg). A) Grade 0, normal rib; rib core
 341 (RC) with hypertrophic chondrocytes (*pars cartilaginea*). B) Grade 1; increase in thickness,
 342 rib with small fibrous lumen (FL), and mild osteolysis. C) Grade 2; thick rib with large FL, and
 343 advanced uneven osteolysis. D) Grade 3; thick rib with large FL and osteolytic opening to the
 344 periosteum (P). E) Grade 4; thick rib with large FL, advanced osteolytic opening to P, and
 345 infiltration of cellular periosteum (CP). Generalized radiolucency reaches its maximum in
 346 grade 4 as it generally depends on the extension and location of the osteolytic areas. Boxes
 347 with letters indicate the region of zoom of F) and G). Movat pentachrome staining for
 348 proteoglycans and mucins (blue), collagen/reticular fibers (yellow), colocalization of
 349 collagen/reticular fibers and proteoglycans (green), muscle and osteoid (or decalcified bone
 350 matrix) (reddish-brown), nuclei and elastin (black) and active nucleus (osteoblast in CP)
 351 (violet/purple). CB, Compact bone (*substantia compacta; pars ossea*); V, Blood vessels; L,
 352 Leucocytes. Black arrows indicate osteoclast. Black asterisks indicate regions with
 353 osteomalacia. Black bars on the bottom right corner show the image scale, set to 250 μm . Color
 354 print.

355 Image texture analyses of rib histology revealed that homogeneity values were found
356 higher in the compact bone of abnormal ribs than normal ribs (ASM, $p = 0.03$; IDM, $p = 0.02$),
357 while heterogeneity values were found lower (Contrast, $p = 0.058$; Entropy, $p = 0.02$) (Figure
358 4). Thus, compact bone was more uniform with less gray levels variation in abnormal than
359 normal ribs, hence less organized concentric osteocyte growth pattern. Notably, the collagen-
360 rich low mineralized osteoid halo of slight radiolucency around the chondroid core was reduced
361 in size or appeared with “polar” localization. This was further manifested as isolated islands of
362 disorganized collagen type I and III fibers (none or poor birefringence signal), and glycoprotein
363 composition were more visible in the most advanced phases (Figure 3 and Figure 5).



364

365 Figure 4. Quantitative concentric appositional growth pattern of the compact bone from normal
 366 and abnormal ribs (*costae*) in Atlantic salmon (3 kg). Data is generated through gray level co-
 367 occurrence matrix texture analysis of compact bone from histology sections. A) Angular
 368 second moment (ASM), B) inverse difference moment (IDM), C) contrast, and D) entropy.
 369 Data are presented as non-transformed mean \pm SEM, n = 4 and 6 for normal and abnormal ribs,
 370 respectively. Significant differences between groups are indicated by different letters over the
 371 SEM ($p \leq 0.05$).



374 Figure 5. Alternative cross-sectional morphologies for advanced stages of generalized
375 radiolucent ribs (*costae*) with cores (RC) of immature hyaline cartilage (*pars cartilaginea*) and
376 fibrous lumen (FL) in Atlantic salmon (3 kg). A) to D) Movat pentachrome staining for
377 proteoglycans and mucins (blue), collagen/reticular fibers (yellow), colocalization of
378 collagen/reticular fibers and proteoglycans (green), muscle and osteoid (or decalcified bone
379 matrix) (reddish-brown), nuclei and elastin (black) and active nucleus (osteoblast in cellular
380 periosteum) (violet/purple). Boxes with letters on images B) and C) indicate the region of zoom
381 of images E) and F). Serie histology image in Haematoxylin and Eosin. Black bars on the
382 bottom right corner from A) to D) show the image scale, set to 250 μm . E) and F) Picro Sirius
383 red staining under polarized light. Yellow-orange birefringence in polarized images stands for
384 collagen type I (thick fibers), while green birefringence type III (thin fibers). EFP, Exterior
385 fibrous periosteum. White arrows indicate the external collagen layer of the compact bone (CB)
386 (*substantia compacta; pars ossea*). Blue arrows indicate radial periosteal collagen fibers. Black
387 and white asterisks indicate regions of the CP rich in collagen and glycoproteins. White bars
388 on the bottom right corner of E) and F) images show the image scale, set to 100 μm . Color
389 print.

390 Given the common histology features of abnormal ribs, and variable generalized
391 radiolucency (70%) accompanied by thickening displayed by X-ray, they were designated as
392 generalized radiolucent ribs. Initial histological changes (Grade 1; Figure 3. B), included the
393 disappearance of chondrocytes, and the rib core – now termed the lumen – was filled with an
394 amorphous fibrotic substance with lipid vacuoles, accompanied by blood vessels and
395 osteoclasts. The osteolytic changes progressed (Grade 2; Figure 3. C), and the core penetrated
396 through to the periosteal area (Grade 3; Figure 3. D and F), accompanied by loss of linear
397 organization of the concentric appositional growth pattern. Then, cellular periosteum cells
398 infiltrated the osteolytic layer of the rib lumen, in an endosteum-like manner (Grade 4; Figure
399 3. E and G). The different degrees of histomorphology of the compact bone seemed to be
400 positively associated with homogeneity values (Angular second moment, $p = 0.08$; Inverse
401 difference moment, $p = 0.07$), while negatively with heterogeneity (Contrast, $p = 0.02$; Entropy,
402 $p = 0.07$) from the gray level co-occurrence matrix texture analysis. Progressive processes of
403 osteogenesis by appositional growth in the cellular periosteum and osteolysis in the rib lumen
404 likely contributed to the (abnormal) changes in cross-sectional rib morphology, giving a bi-
405 tubular appearance to ossify the opening by appositional growth (Figure 5. A). Osteoid was
406 observed in newly formed compact bone (Figure 3. E and G). Typically, the more advanced
407 the changes, the more visible the generalized radiolucency. Variations to what is described
408 included multiple fibrous rib lumens, and rib core (sometimes exposed to periosteum)
409 containing chondrocytes in the immature hyaline phase (Figure 5, B, C, and D). As no signs of
410 herniation of the exposed cartilage core were observed in response to internal pressure, it was
411 assumed to be invagination (Figure 5. C).

412 Histologically, red DS were characterized by the presence of intramuscular hemorrhage
413 with infiltration of erythrocytes and inflammatory cells, mainly macrophages. In some cases,
414 melanomacrophages were observed. Black DS presented dispersed melanomacrophages

415 mainly in myocommata (*intermyotomal fascia; epimysium*) and between myocytes in a lower
 416 number. Some necrotic myocytes were seen with macrophage infiltration. No major fibrotic
 417 areas were observed (Supplementary 11).

418

419 3.2 Dietary effects on fish performance and fillet quality

420 The body weight of the P-group was 28 % lower compared with the M-group prior to
 421 seawater transfer ($p < 0.001$), while the weight difference was 11% in favor of the M-group 10
 422 ten weeks after seawater transfer ($p = 0.003$). At harvesting, the weight of both dietary groups
 423 was similar (Table 1), but the condition factor of the P-group was slightly higher ($p = 0.02$).
 424 The mortality rate of both dietary groups was similar ($< 1\%$). Fillet quality analyses at harvest
 425 revealed comparable color intensity of both dietary groups (Score; 23.5 - 23.7), but the P-group
 426 had a higher gaping score ($p = 0.03$) and softer fillets ($p = 0.049$) than the M-group (Table 1).

427 Table 1. Biometric traits, fillet quality, and vertebrae morphology of Atlantic salmon prior, 10
 428 weeks after seawater transfer, and at slaughter, fed either a marine (M-group) or a plant-based
 429 diet (P-group) during smoltification.

Parameters	Prior to seawater transfer				After seawater transfer				Slaughter			
	M-group	P-group	p value	n	M-group	P-group	p value	n	M-group	P-group	p value	n
Biometric traits												
Body weight (g)	111.7 ± 3.6	81.3 ± 2.9	< 0.001	15	281 ± 3.9	250.8 ± 5.9	0.003	40	3046 ± 68	3132 ± 71	0.24	80
Condition factor	1.28 ± 0.03	1.29 ± 0.02	0.28	15	1.12 ± 0.01	1.15 ± 0.02	0.14	40	1.46 ± 0.01	1.48 ± 0.01	0.02	80
Fillet quality												
Firmness (N)	11.8 ± 2.7	10.5 ± 2.4	0.049	20
Gaping (score)	0.1 ± 0.1	0.4 ± 0.1	0.03	20
Vertebrae morphology												
Abnormal vertebrae (%)	0	8	0.33	15	20	10	0.56	10	17	23	0.52	40
Impaired mineralization score	0	0	.	15	0.76 ± 0.24	1.4 ± 0.19	0.049	10	0	0	.	20
Vertebra X:Y ratio	0.96 ± 0.01	0.93 ± 0.01	0.01	15	0.93 ± 0.01	0.90 ± 0.01	0.04	10	1.03 ± 0.01	1.02 ± 0.01	0.39	20
Intervertebral space (mm)	0.36 ± 0.01	0.34 ± 0.01	0.12	15	0.50 ± 0.03	0.50 ± 0.02	0.97	10	0.15 ± 0.03	0.16 ± 0.03	0.81	20

431 Significant differences between groups were set to $p \leq 0.05$. Data are presented as non-
 432 transformed mean ± SEM. Condition factor = $100 \times \text{body weight} / (\text{body length})^3$.

433

434 **3.3 X-ray**

435 At slaughter, the number of rib abnormalities increased from the proximal to distal rib
 436 parts. Rib abnormalities were mostly concentrated around rib number 9 for both dietary groups.
 437 However, the P-group showed 1.9 more abnormalities than the M-group in the central (ribs 8 -
 438 15) ($p = 0.02$) and 5 times more in mid areas ($p < 0.001$; Table 2) of the rib cage. These
 439 differences were contributed principally by two abnormality forms (Figure 6). Firstly, axis
 440 deviations in the form of several parallel rib bendings in a linear pattern and wrinkly
 441 deformations affecting 19 (M-group) and 26 % (P-group) of studied ribs ($p = 0.01$; Table 2) in
 442 a decreasing number from anterior (ribs 1 - 7) to posterior (ribs 16 - 22) areas of the rib cage.
 443 Mid rib parts of the P-group presented more axis deviations than the M-group ($p < 0.001$).
 444 Secondly, generalized radiolucency affecting 12 % (M-group) and 17 % (P-group) of studied
 445 ribs ($p < 0.001$) concentrated in central ($p = 0.061$) and mid-distal areas of the rib cage ($p <$
 446 0.001) in the P-group, contrasting to an even distribution from rib number 1 to 22 in the M-
 447 group (Table 2).

448 Table 2. Morphology, mechanical properties, and mineral composition of ribs (*costae*) of
 449 Atlantic salmon (3 kg), fed either a marine (M-group) or a plant-based diet (P-group) during
 450 smoltification.

Rib parameters	M-group	P-group	p value
Longitudinal morphology (rib abnormalities)			
Category I (no continuity break)	6 ± 0.9	11.5 ± 1.2	< 0.001
Generalized radiolucent	1.9 ± 0.4	5.0 ± 1	< 0.001
Axis deviations	4.0 ± 0.9	6.6 ± 1	0.01
Category II (continuity break)	3.0 ± 0.7	3.7 ± 0.4	0.36
Fracture	0 ± 0	0.1 ± 0.1	1.00
Supernumerary	0 ± 0	0 ± 0	1.00
Radiolucent callus	0.8 ± 0.2	0.7 ± 0.2	0.86
Radiopaque callus or hyperostosis	0.3 ± 0.2	0.2 ± 0.2	0.75
Radiolucent non-union	0.1 ± 0.1	0 ± 0	0.65
Shorter or missing parts	1.8 ± 0.5	2.7 ± 0.3	0.18
Total	9.0 ± 1.3	15.3 ± 1.4	< 0.001
Proximal	0.5 ± 0.2	0.7 ± 0.2	0.52
Mid	1.0 ± 0.5	5.0 ± 0.7	< 0.001
Distal	7.4 ± 0.9	9.5 ± 0.9	0.08

Cross-sectional morphology (mm)

Bone diameter	0.5 ± 0.03	0.5 ± 0.04	0.92
Periosteum width	0.2 ± 0.03	0.2 ± 0.01	0.74
Rib hub diameter	2.1 ± 0.22	2.0 ± 0.14	0.80

Mechanical properties**Breaking load (N)**

Proximal	10.8 ± 0.7	10.4 ± 0.6	0.65
Mid	7.1 ± 0.4	7.0 ± 0.3	0.87
Distal	5.5 ± 0.3	5.3 ± 0.2	0.70

Modulus of Elasticity (N mm⁻¹)

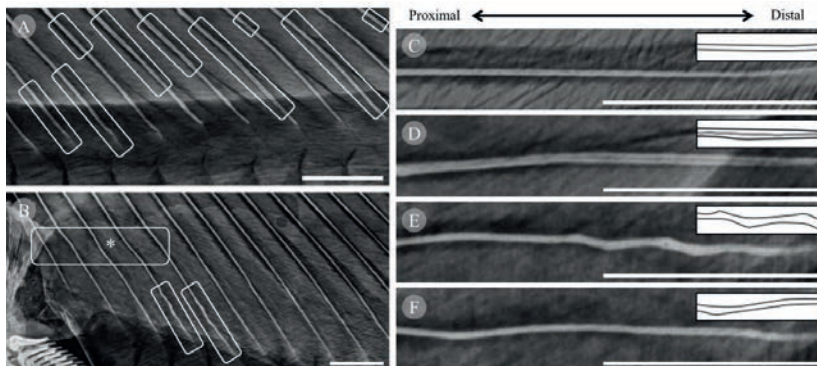
Proximal	39.4 ± 2.5	36.8 ± 1.9	0.43
Mid	30.6 ± 1.5	26.7 ± 1.4	0.06
Distal	32.5 ± 3.1	28.9 ± 1.2	0.27

Mineral composition (ww)

Ca (g kg ⁻¹)	137.5 ± 4.8	127.6 ± 2.5	0.11
P (g kg ⁻¹)	63.8 ± 2.9	55.3 ± 2.7	0.07
Ca:P ratio	2.2 ± 0.2	2.3 ± 0.1	0.51
Mg (g kg ⁻¹)	2.8 ± 0.3	3.0 ± 0.1	0.65

451 The longitudinal morphology is described as the number of rib abnormalities per rib cage
 452 (*cavea thoracis*) side. Significant differences between groups were set to $p \leq 0.05$. Data are
 453 presented as non-transformed mean ± SEM, n = 12 (morphology), 20 (mechanical properties),
 454 and 4 (mineral composition; pooled per tank) per dietary group. N, Newton; ww, Wet weight;
 455 Ca, Calcium; P, Phosphorus; Mg, Magnesium.

456



457

458 Figure 6. Typical rib (*costae*) morphologies of Atlantic salmon (3 kg). Lateral X-ray. A) Rib
 459 cage side (*cavea thoracis*) with examples of generalized radiolucent ribs (white frames). B)
 460 Rib cage side with examples of axis deviations in the form of parallel bent ribs in a linear
 461 pattern (white frame with an asterisk) and wrinkly morphology (white frames). C) Zoom in of
 462 normal rib, D) generalized radiolucency, E) axis deviation (wrinkly), and F) axis deviation
 463 (bending). A simplified illustration of the respective rib morphology from C) to F) is added in
 464 the top right corner. The white bars on the bottom right corner show the image scale, set to 12
 465 mm.

466

467 Prior to seawater transfer, virtually no vertebrae abnormalities nor clinical morphological
468 signs of impaired mineralization was observed. On the other hand, the vertebra X:Y ratio was
469 lower in the P-group than in the M-group ($p = 0.01$). Ten weeks after seawater transfer, fish
470 from both dietary treatments presented clear signs of impaired mineralization (likely P
471 deficiency). However, the severity was more pronounced for the P-group, as indicated by a
472 higher impaired mineralization score ($p = 0.049$) and a lower vertebra X:Y ratio ($p = 0.04$)
473 (Table 1). Numerically lower vertebra X:Y ratio and more fussed vertebrae were found in both
474 groups than before seawater transfer (). At slaughter, the vertebra X:Y ratio increased to normal
475 values, and no signs of residual dietary-induced internal deformations of the vertebra body
476 were observed. The prevalence of fish from the M-group with abnormal vertebrae (17 %) was
477 not significantly different from the P-group (23 %), nor was the magnitude. No differences
478 were observed in the width of the intervertebral space (*symphysis intervertebralis*) between the
479 dietary groups at any sampling time.

480

481 **3.4 Bone mechanical properties**

482 Mechanical tests of salmon ribs revealed a decreasing breaking load from proximal to
483 distal rib parts, with no differences between dietary groups (Table 2). The elasticity showed a
484 similar trend with lower values at the proximal than mid and distal rib parts. Mechanical rib
485 analyses showed no significant differences between the dietary fish groups, but the P-group
486 showed a numerically higher elasticity ($p = 0.06$) than the M-group in mid rib parts (Table 2).

487 The area and load of vertebrae were lower of the P-group than the M-group at 5, 10, 15,
488 and 20 % compression depth ($p < 0.04$). These values increased with compression depth for
489 both groups (Supplementary 10). Among all compression depths, only elasticity at 15 % was

490 different between dietary groups, with higher modulus in the P-group than M-group ($136.8 \pm$
491 5.1 vs. 121.9 ± 5 N/mm; $p = 0.045$).

492 Assuming no body weight and diet interaction, the most significant correlations with rib
493 morphology were between the number of axis deviations per rib cage side and either area ($r =$
494 -0.37 ; $p = 0.049$), load ($r = -0.38$; $p = 0.04$) at 5 %, or area ($r = -0.37$; $p = 0.04$) at 10 % of
495 compression depth of vertebrae. Regarding rib mechanical properties, the most significant
496 correlations were between the modulus of elasticity in mid rib parts and either area ($r = 0.36$;
497 $p = 0.02$) or load ($r = 0.32$; $p = 0.03$) at 15 % of the compression depth of vertebrae.

498

499 **3.5 Bone mineral content**

500 No differences were observed in the composition of macrominerals in ribs between the
501 dietary groups, although the P-group tended to have lower a P concentration than the M-group
502 ($p = 0.07$) (Table 2).

503 There were only relatively few differences in the mineral composition of vertebrae
504 between the dietary groups. Fish prior to seawater transfer showed a higher % of ash with a
505 higher Ca:P ratio ($p = 0.03$), Na ($p = 0.01$), and Mn levels ($p = 0.02$) in the P-group than in the
506 M-group (Supplementary 3). At slaughter, the mineral analysis revealed a higher Na content in
507 the P-group than in the M-group ($p = 0.002$) (Supplementary 10).

508

509 **3.6 Blood serum**

510 Prior to seawater transfer, the serum from the M-group showed higher levels of ALP (p
511 $= 0.01$), creatinine ($p < 0.001$), cholesterol ($p < 0.001$), and free fatty acids ($p = 0.02$) than the
512 P-group (Supplementary 12). Ten weeks after seawater transfer, only ALP levels differed

513 significantly between the fish group, being higher for the P-group than the M-group ($p < 0.001$).
514 At slaughter, all blood parameters were similar for the dietary groups (Supplementary 12).

515

516 **3.7 Focal dark spots**

517 At slaughter, DS were observed in large experimental land-based flow-through tanks. No
518 differences were observed in the prevalence of red (5 %) or black DS (3 – 12 %) between the
519 dietary groups. DS were primarily found in the form of petechial, focal hemorrhages, and mild
520 melanisation (score 0.5 - 1), which is generally not considered a cause for quality downgrading
521 (Supplementary 13).

522

523 **4 Discussion**

524 In the present study, we could confirm and describe the dominance of two subtypes of
525 rib abnormalities in Atlantic salmon. On the one hand, axis deviations such as parallel bending
526 of several mid rib parts resulting from mechanical deformations of the rib cage ([Jiménez-
527 Guerrero et al., 2022](#)) and wrinkly ribs, earlier associated with suboptimal (P-deficient) diet
528 ([Baeverfjord et al., 1998](#)). On the other hand, generalized radiolucent ribs previously related to
529 osteolytic secondary changes due to a local inflammatory process such as DS ([Jiménez-
530 Guerrero et al., 2022](#)). Generalized radiolucent ribs showed consistent histological
531 characteristics across our samples, where there was an absence of any surrounding local
532 inflammatory process or DS. Here, the observed expanded osteolytic and fibrotic lumen with
533 internal lipid vacuoles and vascularization possibly led to the increase in rib diameter through
534 compensatory appositional growth to preserve the mechanical properties. Internal
535 vascularization in salmon ribs has also been observed by [Brimsholm et al. \(2023\)](#). They
536 suggested that rib core erosion and vascularization could be mere anatomical variations in

537 salmon ribs because of the aquatic environment, similar to other marine species where bone
538 erosion may be expected in late growth phases ([Soliman, 2018](#)). We found that the erosion of
539 the rib core potentially represents the transformation or dedifferentiation of chondrocytes to
540 mesenchymal-like cells ([de la Fuente et al., 2004](#)) (e.g., fibroblast, adipocytes, and endothelial
541 cells). Blood vessels resulting from such a remodeling process would facilitate myeloid-like
542 cells (osteoclast and lymphocytes) ([Veis and O'Brien, 2023](#)) to enter the cores. Rib core erosion
543 and vascularization could be an essential step for the progression of generalized radiolucency
544 if osteoclasts are naturally absent in the inner compact bone and cartilage core of salmon ribs.

545 On the other hand, our findings indicate clear evidence of pathology in generalized
546 radiolucency, particularly in advanced stages where morphological alterations align with
547 discernible X-ray changes. [Jiménez-Guerrero et al. \(2022\)](#) found that generalized radiolucency
548 prevalence is notably low in adult wild fish, and it does not increase in later growth stages in
549 farmed fish, indicating that these changes are not associated with late growth phases. On the
550 contrary, there is a response to environmental factors and dietary contrasts. Combined with the
551 histopathological changes, altered rib development and osteomalacia are the likely diagnoses
552 of generalized radiolucent ribs when no associated inflammatory responses exist. Osteomalacia
553 was also supported by the increase of periosteal collagen, possibly in an attempt to compensate
554 for the observed higher elasticity and the lower P content in ribs. Softer ribs might also be
555 contributed by the relative increase of the fibrotic lumen, osteoid, and distortion of the
556 concentric mineralized layers or disorganized collagen-rich islands in the compact bone, which
557 would increase the risk of rib deformations (axis deviations), and, therefore, clinical relevance,
558 as our data shows. When selecting ribs for assessing elasticity and P deficiencies, we could not
559 discriminate between normal and abnormal ribs by visual inspection, which resulted in an
560 increased standard deviation that impacted significance levels between dietary groups. Since
561 distal rib parts that concentrate most rib abnormalities have the weakest breaking load and

562 relatively higher elasticity than proximal parts, it reinforces that mid and predominantly distal
563 areas of the rib cage are more susceptible to external mechanical stress ([Jiménez-Guerrero et](#)
564 [al., 2022](#)).

565 To understand the observed long-term effects of dietary contrast on rib morphology in
566 the broader musculoskeletal framework, we additionally explored the growth performance,
567 vertebrae, and skeletal muscle. Regarding growth performance, compared to [Kaushik et al.](#)
568 [\(1995\)](#) and [Drábiková et al. \(2021\)](#), we observed reduced growth in the P-group from
569 freshwater to 10 weeks after seawater transfer, at least. This poor growth was reflected in the
570 lower creatinine levels of the P-group, likely as a response to the lower muscle development.
571 The poor performance was unlikely due exclusively to a P deficiency ([Baeverfjord et al., 1998](#);
572 [Drábiková et al., 2021](#)), but possibly as a response to the suboptimal level of methionine in the
573 P-group diet (0.7 vs. 0.9 - 1.1 g/g) ([Hua and Bureau, 2019](#); [Mai et al., 2022](#)) among other
574 nutritional differences such as EPA and DHA, which were under recommended levels for
575 maximizing growth performance (< 0.1 - 0.2 vs. 0.5 g/100g of lipids) ([Qian et al., 2020](#)). Later,
576 the P-group experienced compensatory growth, allowing both groups to exhibit similar
577 slaughter traits (body weight and fillet color) and serum chemistry, which evidence exceptional
578 compensatory capabilities of salmon under dietary contrast during smoltification. Therefore,
579 the effects of dietary contrast in growth would not have been detected in our fish by standard
580 evaluations at the slaughterhouse.

581 As vertebrae are a proven marker of skeleton health in salmon, they were monitored in
582 the period prior to after seawater transfer and at slaughter. As expected in the short-term
583 ([Drábiková et al., 2021, 2022](#); [Fjellidal et al., 2012](#)), we found a similarly low number of
584 morphological vertebrae abnormalities prior to and after seawater in both salmon groups, which
585 aligned with the P_i concentrations between both groups, similar to fish fed a regular P diet in
586 [Drábiková et al. \(2021\)](#), suggesting that dietary P_i might have been absorbed and made

587 available at similar levels. The availability of P_i was further supported by the lack of observable
588 effects on the width of the intervertebral space, a short-term indicator of P deficiency
589 ([Drábiková et al., 2021](#)). Despite these similarities, we identified differences in bone
590 mineralization in response to dietary contrast, as indicated by the lower vertebra X:Y ratio in
591 the P-group before and after seawater transfer. Before the transfer, lower vertebra X:Y
592 differences did not correspond to variations in mineral composition (excluding Ca:P ratio, Na,
593 and Mn) or clinically observable impaired bone mineralization. Intriguingly, the gutted body
594 of the P-group had a higher ash content even though the fish were fed lower ash levels than the
595 M-group during smoltification. Since these mineral composition results are not specific to the
596 bone, it is important to consider other factors, such as a relatively lower mineral concentration
597 in fast-growing fish ([Baeverfjord et al., 2018](#)).

598 Ten weeks after seawater transfer, vertebra X:Y ratio and macroscopic evaluations
599 indicated that both groups went through a period in which they were in negative bone
600 mineralization balance. The effects of seawater transfer in vertebrae of both farmed and wild
601 salmon have already been reported ([Fjellidal et al., 2006](#); [Fjellidal et al., 2007](#)). Later, [Jiménez-](#)
602 [Guerrero et al. \(2022\)](#) also reported signs of negative mineralization balance in ribs after
603 seawater transfer. Here, we show that the observed short-term impaired mineralization
604 generally impacted the P-group more as they likely started with a subclinical lower mineral
605 status prior to seawater transfer. However, the impaired vertebrae mineralization was resolved,
606 and both groups presented similar normal vertebra morphology and mineral composition at
607 slaughter (excluding Na) ([Drábiková et al., 2021, 2022](#)), contrasting to what [Fjellidal et al.](#)
608 [\(2009\)](#) reported. Therefore, in contrast to ribs, the impaired mineralization did not cross the
609 point of no return, as the number of fish with vertebrae abnormalities did not differ between
610 the dietary groups in the long-term. Such bone development behavior was in line with serum
611 ALP (osteoblast activity), which showed lower values in the P-group than the M-group prior

612 to seawater transfer, followed by an inversion of the trend 10 weeks after seawater transfer.
613 The ALP pattern is probably a sign of compensatory skeleton growth with a recovery to similar
614 values at slaughter. Nevertheless, besides the lack of clinical evidence, there were subclinical
615 long-term effects on the mechanical properties of the trabecular fraction of vertebrae.

616 The higher concentration of Na in the vertebrae composition of the P-group at slaughter
617 was in accordance with our findings in body composition prior to seawater transfer, and it
618 establishes a link between high levels of Na in bone composition and long-term deterioration
619 of the mechanical properties, morphology, and composition of ribs and mechanical properties
620 of vertebrae trabeculae. Potential stimulatory effects of Na-based hydroxyapatite on bone
621 osteolysis and remodeling due to its higher instability likely affected the mechanical properties
622 of compact bone ([Yoo et al., 2021](#)). Unfortunately, we did not have enough material to
623 determine Na concentrations in rib bones, which would strengthen these findings. Factors
624 modulating Na concentrations in fish bones and their impact on skeleton health should be the
625 focus of future research.

626 Regarding the skeletal muscle, we present the first evidence for long-term effects
627 (beyond three weeks; [Kaushik et al. \(1995\)](#)) of dietary contrast during smoltification on muscle
628 quality in salmonids. Thus, we hypothesized a response of the diet near seawater transfer on
629 DS at slaughter, as [Sissener et al. \(2016\)](#) reported. However, although red and black DS of
630 lower prevalence and economic relevance than previously reported in commercial sea-cages
631 were found ([Bjørngen et al., 2019](#); [Jiménez-Guerrero et al., 2022](#)), the dietary contrast did not
632 modulate the prevalence and focal inflammatory response of these musculoskeletal injuries in
633 the long-term. The lack of DS modulation contrasted with dietary treatments in the early
634 seawater phase and of longer duration ([Dessen et al., 2019](#); [Lutfi et al., 2022](#)). Moreover, the
635 lack of effects in DS did not correspond to the modified number of axis deviations and
636 mechanical properties of ribs. Here, these rib axis deviations were mostly contributed by

637 wrinkly deviations resulting from impaired mineralization rather than traumatic events, which
638 may explain the lack of relationship. On the other hand, it is possible that a lower incidence of
639 damaging mechanical impacts on the rib cage in our experimental conditions made it difficult
640 to evaluate any difference between both dietary groups as the lower number of radiopaque
641 calluses in the M-group than in farmed salmon in commercial sea-cages from [Jiménez-
642 Guerrero et al. \(2022\)](#) indicates. Altogether, we cannot exclude the potential protective effects
643 of nutrition during smoltification on musculoskeletal health against DS in more challenging
644 environments.

645 Although the dietary contrast did not aim to be comparable to commercial diets, we found
646 the marine-based diet to have positive effects on rib development. Compared to a previous
647 study where wild and farmed fish in different environments from different life stages using the
648 same facilities, equipment, evaluation methods, and radiologist ([Jiménez-Guerrero et al.,
649 2022](#)), we observed a similar number for most rib abnormalities in M-group as wild fish. We
650 could also see a reduction of the characteristic concentration of rib abnormalities in central
651 parts of the rib cage in the M-group, drawing a similar pattern as wild fish. Moreover, the M-
652 group showed 1/3 and 1/2 of the number of axis deviations in farmed salmon fed a standard
653 diet and grown in land-based tanks or sea-cages.

654 Several factors may explain the positive effects of marine ingredients. Nutritional
655 deficiencies during smoltification would explain the observed increase in axis deviations in
656 ribs due to structural defects during early development. However, the long-term osteomalacia
657 in ribs after fish were fed commercial diets suggests persistent changes in either absorption of
658 nutrients or osteogenesis after the dietary treatment. The parallel affection of the mechanical
659 properties of skeletal muscle and bone suggest a generalized alteration of the extracellular
660 collagen matrix, which is known to be mediated by collagen type I alpha 1 chain (*coll1a1*)
661 ([Aubin, 1998](#)) and collagen type II alpha 1 chain (*col2a1*) ([Dale and Topczewski, 2011](#)) among

662 other genes. While *coll1a1* can be upregulated by n-3 PUFAs ([Abshirini et al., 2021](#); [Ytteborg](#)
663 [et al., 2015](#)), *col2a1* is downregulated when using plant-based protein concentrates in diet
664 ([Dhanasiri et al., 2020](#)). Transformation or dedifferentiation, feasible in mesenchymal lineage
665 cells, could be induced through dietary-dependent or mechanical factors ([Hall, 2015](#)); in fact,
666 n-3 PUFAs have been proven to suppress collagen matrix degradation in cartilage ([Abshirini](#)
667 [et al., 2021](#)), which would explain the lower fibrotic changes in cartilage rib cores in the M-
668 group. Thus, combining fish oil and non-plant-based protein concentrates probably had a
669 synergic effect on musculoskeletal health. We suggest further study of the potential nutritional
670 programming effects of high inclusion of marine-based ingredients in diets of farmed salmon,
671 at least during the smoltification phase.

672

673 **5 Conclusions**

674 Generalized radiolucency and axis deviation are the two major types of morphological
675 abnormalities in salmon ribs. Salmon rib morphology was more sensitive to the smoltification
676 diet than vertebrae. Generalized radiolucent ribs were characterized by different forms of
677 altered appositional growth with dedifferentiated chondrocytes, lumen osteolysis, and
678 osteomalacia.

679

680 **6 Acknowledgments**

681 The Norwegian Seafood Research Fund (FHF) and Norwegian University of Life
682 Sciences (NMBU) supported this study. The authors acknowledge the skillful assistance,
683 dedicated fish management, and excellent work provided by staff at the Research Station for
684 Sustainable Aquaculture (Nofima) and laboratories, with special thanks to Kjellrun Hoås
685 Gannestad. Thanks to Ph. D. Thomas Larsson and M.Sc. Sumeng Galdat, for your assistance

686 in processing part of the data. Thanks to Miroslava Hansen for the excellent work processing
687 and sectioning histology samples. Thanks to The Imaging Center (NMBU) for allowing the use
688 of its infrastructure and expertise.

689

690 **7 Declaration of funding**

691 The study was supported by the Norwegian Seafood Research Fund (FHF) (901487), and
692 the Norwegian University of Life Sciences (NMBU). Fish material belonged to the Nofima's
693 R&D licenses granted by the Norwegian Directorate of Fisheries for large-scale Industrial
694 Research.

695 8 References

- 696 Abshirini, M., Ilesanmi-Oyelere, B.L., Kruger, M.C., 2021. Potential modulatory mechanisms of action
697 by long-chain polyunsaturated fatty acids on bone cell and chondrocyte metabolism. *Prog. Lipid Res.*
698 83, 101113. <https://doi.org/https://doi.org/10.1016/j.plipres.2021.101113>
- 699 Akama, K., Ebata, K., Maeno, A., Taminato, T., Otsuka, S., Gengyo-Ando, K., Nakai, J., Yamasu, K.,
700 Kawamura, A., 2020. Role of somite patterning in the formation of Weberian apparatus and pleural rib
701 in zebrafish. *J. Anat.* 236(4), 622-629. <https://doi.org/10.1111/joa.13135>
- 702 Andersen, B.U., Steinsholt, K., Stroemsnes, A.N., Thomassen, M.S., 1994. Fillet gaping in farmed
703 Atlantic salmon (*Salmo Salar*). *Norwegian Journal of Agricultural Sciences* 8(3/4), 165-179.
- 704 AOCSBa6a-05, 2017. Official methods and recommended practices of the AOCS - Determination of
705 crude fiber.
- 706 Aubin, J.E., 1998. Bone stem cells. *J. Cell. Biochem. Suppl.* 30-31, 73-82.
- 707 Baeverfjord, G., Antony Jesu Prabhu, P., Fjellidal, P.G., Albrektsen, S., Hatlen, B., Denstadli, V.,
708 Ytteborg, E., Takle, H., Lock, E.-J., Berntssen, M.H.G., Lundebye, A.-K., Åsgård, T., Waagbø, R.,
709 2018. Mineral nutrition and bone health in salmonids. *Rev. Aquac.* 11(3), 740-765.
710 <https://doi.org/10.1111/raq.12255>
- 711 Baeverfjord, G., Asgard, T., Shearer, K.D., 1998. Development and detection of phosphorus deficiency
712 in Atlantic salmon, *Salmo salar* L., parr and post-smolts. *Aquacult. Nutr.* 4(1), 1-11.
713 <https://doi.org/10.1046/j.1365-2095.1998.00095.x>
- 714 Baird, M.F., Graham, S.M., Baker, J.S., Bickerstaff, G.F., 2012. Creatine-kinase- and exercise-related
715 muscle damage implications for muscle performance and recovery. *J. Nutr. Metab.* 2012, 960363.
716 <https://doi.org/10.1155/2012/960363>
- 717 Bjørgen, H., Haldorsen, R., Oaland, Ø., Kvellestad, A., Kannimuthu, D., Rimstad, E., Koppang, E.O.,
718 2019. Melanized focal changes in skeletal muscle in farmed Atlantic salmon after natural infection with
719 *Piscine orthoreovirus* (PRV). *J. Fish Dis.* 42(6), 935-945. <https://doi.org/10.1111/jfd.12995>
- 720 Bou, M., Berge, G.M., Baeverfjord, G., Sigholt, T., Østbye, T.K., Ruyter, B., 2017. Low levels of very-
721 long-chain n-3 PUFA in Atlantic salmon (*Salmo salar*) diet reduce fish robustness under challenging
722 conditions in sea cages. *J. Nutr. Sci.* 6, e32. <https://doi.org/10.1017/jns.2017.28>
- 723 Brimsholm, M., Fjellidal, P.G., Hansen, T., Trangerud, C., Knutsen, G.M., Asserson, C.F., Koppang,
724 E.O., Bjørgen, H., 2023. Anatomical and pathological characteristics of ribs in the Atlantic salmon
725 (*Salmo salar* L.) and its relevance to soft tissue changes. *Anat. Histol. Embryol.*
726 <https://doi.org/10.1111/ahc.12900>
- 727 Clarke, W.C., Saunders, R.L., McCormick, S.D., 1996. Smolt production, in: Pennel, W., Barton, B.A.
728 (Eds.), *Principles of salmonid culture*. CRC Press, Elsevier, Amsterdam, The Netherlands, pp. 517-567.
- 729 Cohen, L., Dean, M., Shipov, A., Atkins, A., Monsonego-Ornan, E., Shahar, R., 2012. Comparison of
730 structural, architectural and mechanical aspects of cellular and acellular bone in two teleost fish. *J. Exp.*
731 *Biol.* 215(11), 1983-1993. <https://doi.org/10.1242/jeb.064790>
- 732 Currey, J.D., 2003. The many adaptations of bone. *J Biomech* 36(10), 1487-1495.
- 733 Dale, R.M., Topczewski, J., 2011. Identification of an evolutionarily conserved regulatory element of
734 the zebrafish *col2a1a* gene. *Dev. Biol.* 357(2), 518-531. <https://doi.org/10.1016/j.ydbio.2011.06.020>
- 735 de la Fuente, R., Abad, J.L., García-Castro, J., Fernández-Miguel, G., Petriz, J., Rubio, D., Vicario-
736 Abejón, C., Guillén, P., González, M.A., Bernad, A., 2004. Dedifferentiated adult articular
737 chondrocytes: a population of human multipotent primitive cells. *Exp. Cell Res.* 297(2), 313-328.
738 <https://doi.org/10.1016/j.yexcr.2004.02.026>
- 739 Dessen, J.E., Mørkøre, T., Bildøy, J.I., Johnsen, S.N., Poppe, L.T., Hatlen, B., Thomassen, M.S.,
740 Rørvik, K.A., 2019. Increased dietary protein-to-lipid ratio improves survival during naturally occurring
741 pancreas disease in Atlantic salmon, *Salmo salar* L. *J. Fish. Dis.* 42(1), 21-34.
742 <https://doi.org/10.1111/jfd.12904>
- 743 Dhanasiri, A.K.S., Johnny, A., Xue, X., Berge, G.M., Bøgevik, A.S., Rise, M.L., Fæste, C.K., Fernandes,
744 J.M.O., 2020. Plant-Based Diets Induce Transcriptomic Changes in Muscle of Zebrafish and Atlantic
745 Salmon. *Front. Genet.* 11. <https://doi.org/10.3389/fgene.2020.575237>

746 Drábiková, L., Fjelldal, P.G., De Clercq, A., Yousaf, M.N., Morken, T., McGurk, C., Witten, P.E.,
747 2021. Vertebral column adaptations in juvenile Atlantic salmon *Salmo salar*, L. as a response to dietary
748 phosphorus. *Aquac.* 541, 736-776. <https://doi.org/https://doi.org/10.1016/j.aquaculture.2021.736776>
749 Drábiková, L., Fjelldal, P.G., De Clercq, A., Yousaf, M.N., Morken, T., McGurk, C., Witten, P.E.,
750 2022. What will happen to my smolt at harvest? Individually tagged Atlantic salmon help to understand
751 possible progression and regression of vertebral deformities. *Aquac.* 559, 738430.
752 <https://doi.org/https://doi.org/10.1016/j.aquaculture.2022.738430>
753 EC152, 2009. Commission Regulation (EC) No 152/2009 of 27 January 2009 laying down the methods
754 of sampling and analysis for the official control of feed (Text with EEA relevance). 130.
755 Fjelldal, P.G., Hansen, T., Albrektsen, S., 2012. Inadequate phosphorus nutrition in juvenile Atlantic
756 salmon has a negative effect on long-term bone health. *Aquac.* 334-337, 117-123.
757 <https://doi.org/https://doi.org/10.1016/j.aquaculture.2011.12.043>
758 Fjelldal, P.G., Hansen, T., Breck, O., Sandvik, R., Waagbø, R., Berg, A., Ørnstrud, R., 2009.
759 Supplementation of dietary minerals during the early seawater phase increase vertebral strength and
760 reduce the prevalence of vertebral deformities in fast-growing under-yearling Atlantic salmon (*Salmo*
761 *salar* L.) smolt. *Aquac. Nutr.* 15(4), 366-378. [https://doi.org/https://doi.org/10.1111/j.1365-](https://doi.org/https://doi.org/10.1111/j.1365-2095.2008.00601.x)
762 [2095.2008.00601.x](https://doi.org/https://doi.org/10.1111/j.1365-2095.2008.00601.x)
763 Fjelldal, P.G., Lock, E.-J., Grotmol, S., Totland, G.K., Nordgarden, U., Flik, G., Hansen, T., 2006.
764 Impact of smolt production strategy on vertebral growth and mineralisation during smoltification and
765 the early seawater phase in Atlantic salmon (*Salmo salar*, L.). *Aquac.* 261(2), 715-728.
766 <https://doi.org/https://doi.org/10.1016/j.aquaculture.2006.08.008>
767 Fjelldal, P.G., Nordgarden, U., Hansen, T., 2007. The mineral content affects vertebral morphology in
768 underyearling smolt of Atlantic salmon (*Salmo salar* L.). *Aquac.* 270(1), 231-239.
769 <https://doi.org/https://doi.org/10.1016/j.aquaculture.2007.03.008>
770 Gil Martens, L., Witten, P.E., Fivelstad, S., Huysseune, A., Sævareid, B., Vikeså, V., Obach, A., 2006.
771 Impact of high water carbon dioxide levels on Atlantic salmon smolts (*Salmo salar* L.): Effects on fish
772 performance, vertebrae composition and structure. *Aquac.* 261(1), 80-88.
773 <https://doi.org/https://doi.org/10.1016/j.aquaculture.2006.06.031>
774 Gislason, H., Karstensen, H., Christiansen, D., Hjelde, K., Helland, S., Bæverfjord, G., 2010. Rib and
775 vertebral deformities in rainbow trout (*Oncorhynchus mykiss*) explained by a dominant-mutation
776 mechanism. *Aquac.* 309(1), 86-95. <https://doi.org/https://doi.org/10.1016/j.aquaculture.2010.09.016>
777 Gray, J., 1957. How Fishes Swim. *Sci. Am.* 197(2), 48-55.
778 Hall, B.K., 2015. Chapter 30 - Initiating Skeletal Growth, in: Hall, B.K. (Ed.), *Bones and Cartilage*.
779 Academic Press, San Diego, pp. 475-486.
780 Hansen, T., Fjelldal, P.G., Yurtseva, A., Berg, A., 2010. A possible relation between growth and number
781 of deformed vertebrae in Atlantic salmon (*Salmo salar* L.). *J. Appl. Ichthyol.* 26(2), 355-359.
782 <https://doi.org/10.1111/j.1439-0426.2010.01434.x>
783 Haugarvoll, E., Bjerkas, I., Szabo, N.J., Satoh, M., Koppang, E.O., 2010. Manifestations of systemic
784 autoimmunity in vaccinated salmon. *Vaccine* 28(31), 4961-4969.
785 <https://doi.org/10.1016/j.vaccine.2010.05.032>
786 Horton, J.M., Summers, A.P., 2009. The material properties of acellular bone in a teleost fish. *J. Exp.*
787 *Biol.* 212(9), 1413-1420. <https://doi.org/10.1242/jeb.020636>
788 Hua, K., Bureau, D.P., 2019. Estimating changes in essential amino acid requirements of rainbow trout
789 and Atlantic salmon as a function of body weight or diet composition using a novel factorial requirement
790 model. *Aquac.* 513, 734440. <https://doi.org/https://doi.org/10.1016/j.aquaculture.2019.734440>
791 ISO5983-2, 2009. Animal feeding stuffs - Determination of nitrogen content and calculation of crude
792 protein content - Part 2: Block digestion and steam distillation method. 15.
793 ISO5984, 2002. Animal feeding stuffs - Specifies a method for the determination of crude ash of animal
794 feeding stuffs. p. 6.
795 ISO6491, 1998. Animal feeding stuffs - Determination of phosphorus content - Spectrometric method.
796 p. 7.
797 ISO6496, 1999. Animal feeding stuffs - Preparation of test samples - Determination of moisture and
798 other volatile matter content. p. 7.
799 ISO6878, 2004. Water quality - Determination of phosphorus - Ammonium molybdate spectrometric
800 method. p. 21.

801 ISO9831, 1998. Animal feeding stuffs - Determination of gross calorific value - Bomb calorimeter
802 method. 23.

803 ISO13903, 2005. Animal feeding stuffs - Determination of amino acids content. p. 17.

804 Jiao, Y.Y., Okada, M., Hara, E.S., Xie, S.C., Nagaoka, N., Nakano, T., Matsumoto, T., 2020. Micro-
805 architectural investigation of teleost fish rib inducing pliant mechanical property. *Materials* 13(22),
806 5099. <https://doi.org/https://doi.org/10.3390/ma13225099>

807 Jiménez-Guerrero, R., Bæverfjord, G., Evensen, Ø., Hamre, K., Larsson, T., Dessen, J.-E., Gannestad,
808 K.-H., Mørkøre, T., 2022. Rib abnormalities and their association with focal dark spots in Atlantic
809 salmon fillets. *Aquac.* 561, 738697. <https://doi.org/https://doi.org/10.1016/j.aquaculture.2022.738697>

810 Karki, R., 2022. Effect of dietary protein and lipid sources on technical quality of pellets for Atlantic
811 salmon, Department of Animal and Aquaculture Sciences. Norwegian University of Life Sciences, Ås,
812 p. 76.

813 Kaushik, S.J., Cravedi, J.P., Lalles, J.P., Sumpter, J., Fauconneau, B., Laroche, M., 1995. Partial or total
814 replacement of fish meal by soybean protein on growth, protein utilization, potential estrogenic or
815 antigenic effects, cholesterolemia and flesh quality in rainbow trout, *Oncorhynchus mykiss*. *Aquac.*
816 133(3), 257-274. [https://doi.org/https://doi.org/10.1016/0044-8486\(94\)00403-B](https://doi.org/https://doi.org/10.1016/0044-8486(94)00403-B)

817 Kryvi, H., Poppe, L.T., 2016. *Fiskeanatomi*. Fagbokforlaget, Bergen.

818 Kuo, T.-R., Chen, C.-H., 2017. Bone biomarker for the clinical assessment of osteoporosis: recent
819 developments and future perspectives. *Biomark. Res.* 5(1), 18. <https://doi.org/10.1186/s40364-017-0097-4>

820

821 Lutfi, E., Berge, G.M., Bæverfjord, G., Sigholt, T., Bou, M., Larsson, T., Mørkøre, T., Evensen, Ø.,
822 Sissener, N.H., Rosenlund, G., Sveen, L., Østbye, T.-K., Ruyter, B., 2022. Increasing dietary levels of
823 the n-3 long-chain PUFA, EPA and DHA, improves the growth, welfare, robustness and fillet quality
824 of Atlantic salmon in sea cages. *Br. J. Nutr.*, 1-19. <https://doi.org/10.1017/S0007114522000642>

825 Mai, K., Xue, M., He, G., Xie, S.Q., Kaushik, S.J., 2022. Chapter 4 - Protein and amino acids, in: Hardy,
826 R.W., Kaushik, S.J. (Eds.), *Fish Nutrition* (Fourth Edition). Academic Press, pp. 181-302.

827 Mørkøre, T., 2012. Mørke flekker i laksefilet – Kunnskapsstatus og tiltak for å begrense omfanget.
828 Nofima.

829 Mørkøre, T., Einen, O., 2003. Relating sensory and instrumental texture analyses of Atlantic salmon. *J.*
830 *Food Sci.* 68(4), 1492-1497. <https://doi.org/https://doi.org/10.1111/j.1365-2621.2003.tb09672.x>

831 Noble, C., Gismervik, K., Iversen, M.H., Kolarevic, J., Nilsson, J., Stien, L.H., Turnbull, J.F., 2018.
832 Welfare Indicators for farmed Atlantic salmon: tools for assessing fish welfare.

833 Nordberg, M., 2018. Seasonal variation in fillet quality of Atlantic salmon (*Salmo salar*), Department
834 of Animal and Aquaculture sciences. Norwegian University of Life Sciences, Ås, Norway.

835 Nordvik, K., Kryvi, H., Totland, G.K., Grotmol, S., 2005. The salmon vertebral body develops through
836 mineralization of two preformed tissues that are encompassed by two layers of bone. *J. Anat.* 206(2),
837 103-114. <https://doi.org/10.1111/j.1469-7580.2005.00372.x>

838 Patel, S.S., Molnar, M.Z., Tayek, J.A., Ix, J.H., Noori, N., Benner, D., Heymsfield, S., Kopple, J.D.,
839 Kovesdy, C.P., Kalantar-Zadeh, K., 2013. Serum creatinine as a marker of muscle mass in chronic
840 kidney disease: results of a cross-sectional study and review of literature. *J. Cachexia Sarcopenia*
841 *Muscle* 4(1), 19-29. <https://doi.org/10.1007/s13539-012-0079-1>

842 Qian, C., Hart, B., Colombo, S.M., 2020. Re-evaluating the dietary requirement of EPA and DHA for
843 Atlantic salmon in freshwater. *Aquac.* 518, 734870.
844 <https://doi.org/https://doi.org/10.1016/j.aquaculture.2019.734870>

845 Roberts, R.J., Hardy, R.W., Sugiura, S.H., 2001. Screamer disease in Atlantic salmon, *Salmo salar* L.,
846 in Chile. *J. Fish Dis.* 24(9), 543-549. <https://doi.org/10.1046/j.1365-2761.2001.00328.x>

847 Sissener, N.H., Waagbø, R., Rosenlund, G., Tvenning, L., Susort, S., Lea, T.B., Oaland, Ø., Chen, L.,
848 Breck, O., 2016. Reduced n-3 long chain fatty acid levels in feed for Atlantic salmon (*Salmo salar* L.)
849 do not reduce growth, robustness or product quality through an entire full scale commercial production
850 cycle in seawater. *Aquac.* 464, 236-245.
851 <https://doi.org/https://doi.org/10.1016/j.aquaculture.2016.06.034>

852 Soliman, A.S., 2018. The growth cartilage and beyond: Absence of medullary bone in silver carp ribs.
853 *Mathews J. Cytol. Histol.* 2(1).

854 Sullivan, M., Hammond, G., Roberts, R.J., Manchester, N.J., 2007. Spinal deformation in commercially
855 cultured Atlantic salmon, *Salmo salar* L.: a clinical and radiological study. J. Fish Dis. 30(12), 745-752.
856 <https://doi.org/10.1111/j.1365-2761.2007.00889.x>
857 Veis, D.J., O'Brien, C.A., 2023. Osteoclasts, Master Sculptors of Bone. Annu. Rev. Pathol.: Mech. Dis.
858 18(1), 257-281. <https://doi.org/10.1146/annurev-pathmechdis-031521-040919>
859 Vielma, J., Lall, S.P., 1998. Control of phosphorus homeostasis of Atlantic salmon (*Salmo salar*) in
860 fresh water. Fish Physiol. Biochem. 19(1), 83-93. <https://doi.org/10.1023/A:1007757321695>
861 Witten, P.E., Fjellidal, P.G., Huyseune, A., McGurk, C., Obach, A., Owen, M.A.G., 2019. Bone without
862 minerals and its secondary mineralization in Atlantic salmon (*Salmo salar*): the recovery from
863 phosphorus deficiency. J. Exp. Biol. 222(3). <https://doi.org/10.1242/jeb.188763>
864 Yoo, D.S., Cho, J.S., Chung, Y.-C., Rhee, S.-H., 2021. Defect structures of sodium and chloride co-
865 substituted hydroxyapatite and its osseointegration capacity. J. Mater. Sci. 56(9), 5493-5508.
866 <https://doi.org/10.1007/s10853-020-05645-9>
867 Ytteborg, E., Todorovic, M., Krasnov, A., Takle, H., Kristiansen, I., Ruyter, B., 2015. Precursor cells
868 from Atlantic salmon (*Salmo salar*) visceral fat holds the plasticity to differentiate into the osteogenic
869 lineage. Biol. Open 4(7), 783-791. <https://doi.org/10.1242/bio.201411338>
870 Zaletel, I., Milosevic, N.T., Todorović, V.N., Kovacevic-Filipovic, M., Puškaš, N., 2017. Fractal and
871 gray level co-occurrence matrix texture analysis of senescent and non-senescent deciduous teeth stem
872 cells: A pilot study. FGNAMB 2, 1-6.

873

874 **9 Supplementary**

875 **9.1 Supplementary**

876 Supplementary 1. Formulation and chemical composition of the marine- (M-group) and plant-
877 based diet (P-group) of salmon fed during smoltification.

	M-group	P-group
Formulation		
Fish meal (%)	61.0	0.0
Wheat (%)	20.7	8.4
SPC (%)	0.0	34.6
Wheat gluten (%)	0.0	22.0
Corn gluten (%)	0.0	10.0
Fish oil (%)	15.4	0.0
Rapeseed oil (%)	0.0	20.4
MgSO ₄ (500 ppm extra) (%)	0.2	0.2
K ₂ CO ₃ (500 ppm extra) (%)	0.1	0.1
Vitamin premix (%)	0.5	0.5
Monosodium phosphate (%)	2.5	2.5
Astaxanthin (%)	0.1	0.1
Mineral premix (%)	0.5	0.5
Chemical composition		
Protein (%)	46.1	46.5
Lipids (%)	21.2	18.2
Starch (%)	12.6	9.3
Energy (MJ kg ⁻¹)	21.2	22.2

878 SPC, Soy protein concentrate.

879

880 **9.2 Supplementary**

881 Supplementary 2. Amino acid and fatty acid composition of the marine- (M-group) and plant-
 882 based diet (P-group) of salmon fed during smoltification.

	M-group	P-group
Amino acid composition		
Aspartic acid (g g ⁻¹)	3.9	3.5
Glutamic acid (g g ⁻¹)	6.1	12.0
Hydroxyproline (g g ⁻¹)	0.4	<0.1
Serine (g g ⁻¹)	1.9	2.4
Glycine (g g ⁻¹)	2.7	1.8
Histidine (g g ⁻¹)	1.0	1.0
Arginine (g g ⁻¹)	2.6	2.3
Treonine (g g ⁻¹)	1.8	1.5
Alanine (g g ⁻¹)	2.6	1.9
Proline (g g ⁻¹)	1.9	3.9
Tyrosine (g g ⁻¹)	1.3	1.4
Valine (g g ⁻¹)	2.2	2.0
Methionine (g g ⁻¹)	1.3	0.7
Isoleucine (g g ⁻¹)	1.8	1.9
Leucine (g g ⁻¹)	3.2	4.0
Fenylalanine (g g ⁻¹)	1.7	2.4
Lysine (g g ⁻¹)	3.4	1.8
Fatty acid composition		
14:0 (g 100g lipids ⁻¹)	6.3	0.1
16:0 (g 100g lipids ⁻¹)	13.3	4.9
18:0 (g 100g lipids ⁻¹)	1.6	1.8
20:0 (g 100g lipids ⁻¹)	0.2	0.5
16:1 n-7 (g 100g lipids ⁻¹)	4.1	0.2
18:1 (n-9)+(n-7)+(n-5) (g 100g lipids ⁻¹)	11.8	56.6
20:1 (n-9)+(n-7) (g 100g lipids ⁻¹)	8.7	1.5
22:1 (n-11)+(n-9)+(n-7) (g 100g lipids ⁻¹)	13.5	0.4
18:2 n-6 (g 100g lipids ⁻¹)	2.5	20.4
18:3 n-3 (g 100g lipids ⁻¹)	1.2	7.8
18:4 n-3 (g 100g lipids ⁻¹)	2.9	<0.1
20:5 n-3 (EPA) (g 100g lipids ⁻¹)	7.0	0.1
22:6 n-3 (DHA) (g 100g lipids ⁻¹)	10.2	0.1
Sum of saturated fatty acids (g 100g lipids ⁻¹)	21.5	7.7
Sum of unsaturated fatty acids (g 100g lipids ⁻¹)	38.8	58.9

Sum of n-6 (g 100g lipids ⁻¹)	3.3	20.5
Sum of n-3 (g 100g lipid ^{s-1})	23.1	8.1
Sum of EPA + DHA (g 100g lipids ⁻¹)	17.2	0.2

883 Fatty acids results shown for values > 1 g 100g lipids⁻¹ in both dietary groups.

884 EPA, eicosapentaenoic acid; DHA, docosahexaenoic acid

885

886 **9.3 Supplementary**

887 Supplementary 3. Dry matter, ash, and mineral composition of the marine- (M-group) and
 888 plant-based diet (P-group) provided to Atlantic salmon during smoltification, and mineral
 889 composition of gutted bodies per dietary group at the end of the smoltification in freshwater.

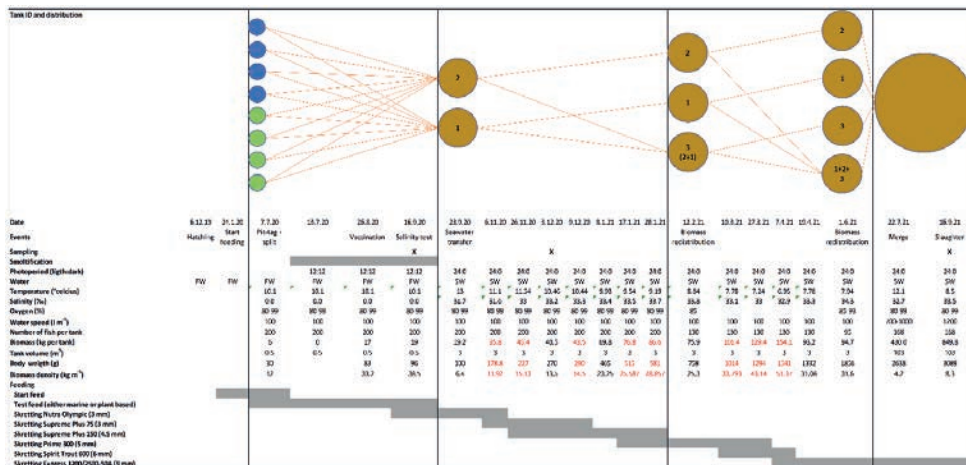
Composition	Diet		Gutted body		
	M-group	P-group	M-group	P-group	<i>p</i> value
Dry matter (%)	90.0	90.4	0.31 ± 0.0	0.30 ± 0.0	0.93
Ash (%)	9.5	5.0	7.7 ± 0.1	8.1 ± 0.1	0.02
Mineral (ww)					
Ca (g kg ⁻¹)	12.2	2.4	13.4 ± 1	15.8 ± 0.2	0.08
P (g kg ⁻¹)	17.7	10.5	15.3 ± 0.7	16.1 ± 0	0.29
Soluble P (g kg ⁻¹)	9.3	6.6	.	.	.
Ca:P ratio	0.7	0.2	0.9 ± 0	1 ± 0	0.03
K (g kg ⁻¹)	9.0	7.8	12.1 ± 0.2	11.9 ± 0.1	0.57
Na (g kg ⁻¹)	12.2	4.8	2.4 ± 0.1	2.8 ± 0.1	0.01
Mg (g kg ⁻¹)	2.7	2.5	1.1 ± 0	1.1 ± 0	0.98
Zn (mg kg ⁻¹)	158.1	172.0	61.4 ± 1.3	65.8 ± 1.1	0.11
Fe (mg kg ⁻¹)	266.7	265.4	24 ± 0.6	36 ± 7.1	0.16
Mn (mg kg ⁻¹)	59.9	86.9	3.9 ± 0.3	5.3 ± 0.1	0.02
Cu (mg kg ⁻¹)	16.7	20.9	2.6 ± 0.2	2.4 ± 0.1	0.50

890 Significant differences between groups were set to $p \leq 0.05$. Data are presented as non-
 891 transformed mean ± SEM, n = 15 fish per dietary group. ww, Wet weight; Ca, Calcium; P,
 892 Phosphorus; Mg, Magnesium; K, Potassium; Na, Sodium; Zn, Zinc; Fe, Iron; Mn, Manganese;
 893 Cu, Copper.

894

895 **9.4 Supplementary**

896 Supplementary 4. Experimental overview and feeding plan. Red values are theoretical
 897 estimations.



898

899 FW, Fresh water; SW, Seawater.

900

901 **9.5 Supplementary**

902 Supplementary 5. Analyzed chemical and mineral composition of the standard commercial

Feed	Skretting Nutra Olympic	Skretting Supreme Plus 75	Skretting Supreme Plus 150	Skretting Prime 300	Skretting Spirit Trout	Skretting Express 1200/2500-50A
Pellet size (mm)	3	3	4.5	5	6	9
Protein (%)	50.6	47.7	47.6	43.1	43.3	35.7
Dry matter (%)	93.8	92.1	91.8	92	92.1	92.6
Ash (%)	8.8	5.5	5.2	4.4	4.4	4.2
Mineral composition (ww)						
Total Ca (g kg ⁻¹)	19.5	7.3	6.4	3.5	3.4	3.5
Total Na (g kg ⁻¹)	6.8	2.1	2.0	1.7	1.7	1.4
Total Mg (g kg ⁻¹)	3.1	2.2	2.0	1.9	1.9	2.2
Total K (g kg ⁻¹)	11.1	10.1	8.9	7.9	7.9	7.3
Total P (g kg ⁻¹)	12.0	10.6	10.6	10.2	10.1	9.8
Soluble P (g kg ⁻¹)	2.5	5.2	5.3	5.9	6.0	4.9
Ca:P ratio	1.6	0.7	0.6	0.3	0.3	0.4
Total Fe (mg kg ⁻¹)	214	265	265	309	259	233
Total Mn (mg kg ⁻¹)	54	63	55	54	58	52
Total Cu (mg kg ⁻¹)	16	13	14	14	14	16
Total Zn (mg kg ⁻¹)	153	165	245	149	152	147
Fat (%)	22.8	24.5	26.5	27	27.7	36.2
Fiber (%)	2.1	2.1	1.8	2	2.2	2.4
Starch (%)	6.8	12.3	10.7	15.5	8.1	6.9
Free Astaxanthin (mg kg ⁻¹)	7.2	58	61	49	42	41
Energy (MJ kg ⁻¹)	22.4	22.8	23.2	23.5	23.5	24.9

903 diets during the seawater phase.

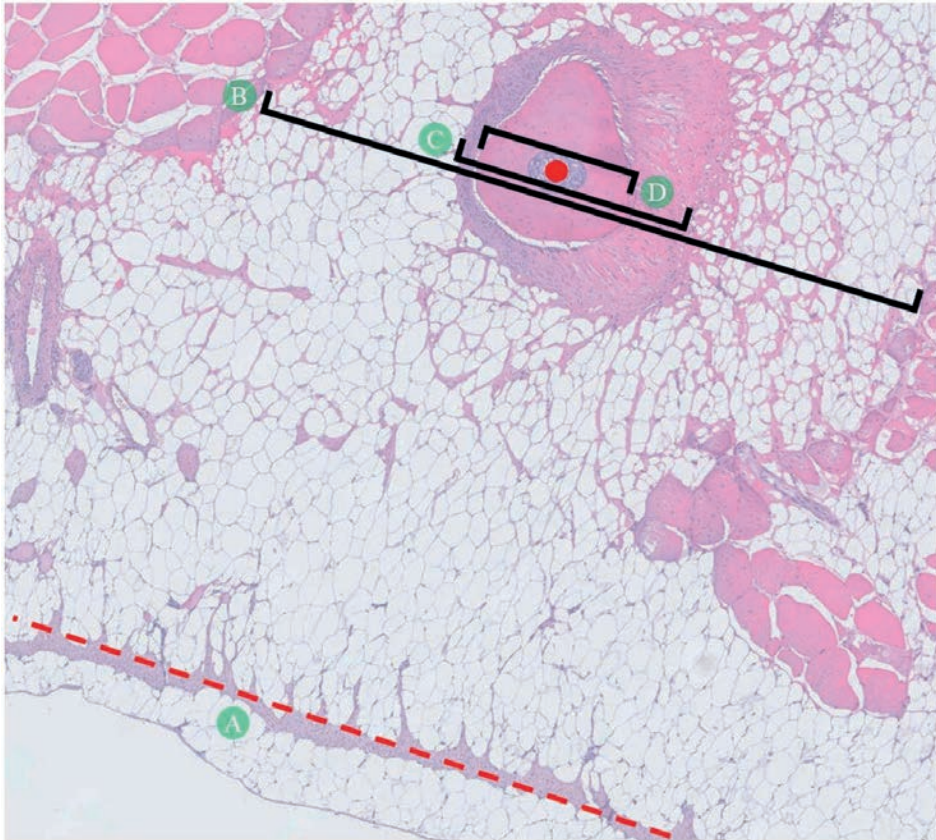
904 Ca, Calcium; P, Phosphorus; Mg, Magnesium; K, Potassium; Na, Sodium; Zn, Zinc; Fe, Iron;

905 Mn, Manganese; Cu, Copper.

906

907 **9.6 Supplementary**

908 Supplementary 6. Method for cross-sectional morphology evaluation of ribs (*costae*) and
909 associated tissues in histological sections of Atlantic salmon (3 kg). A) Perpendicular reference
910 of the transverse fascia to the center of the rib (red dot). Morphological estimations are
911 collected from cross-sections of different regions passing through the rib center, parallel to the
912 discontinuous reference line. B) Rib cluster thickness (cross-section including bone and
913 surrounding fat and periosteum). C) Rib and periosteum thickness. D) Rib thickness.
914 Haematoxylin and eosin staining.

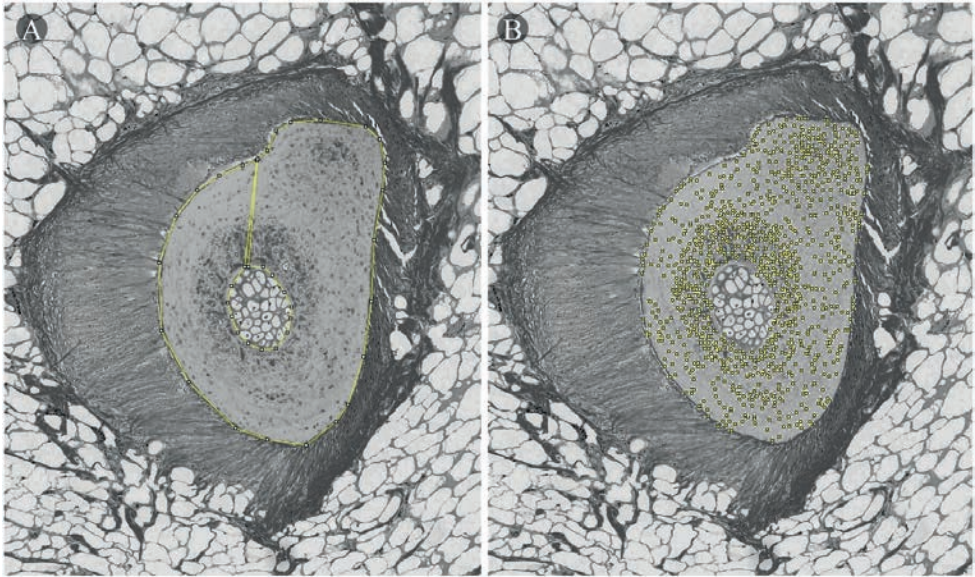


915

916

917 **9.7 Supplementary**

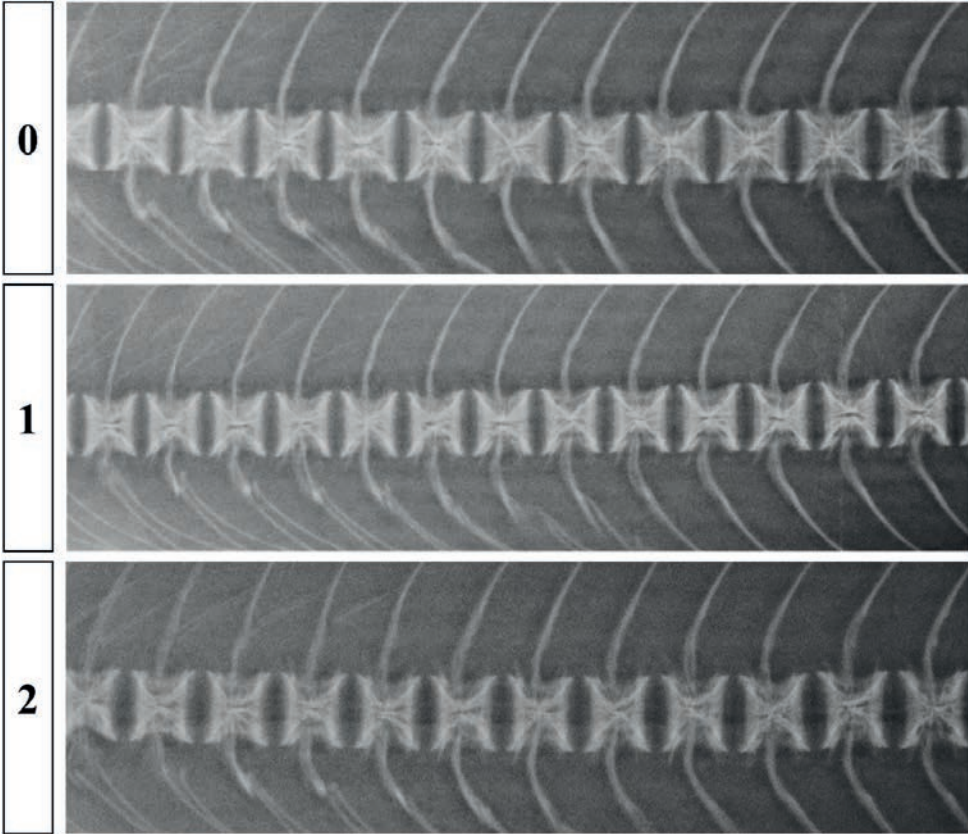
918 Supplementary 7. Selection of cross-sectional compact bone area (A) in gray scale Picro Sirius
919 Red-stained images for estimation of micro-organization and osteocyte density in ribs (*costae*)
920 (B). Dots in B) indicate the detection of osteocytes.



921

922 **9.8 Supplementary**

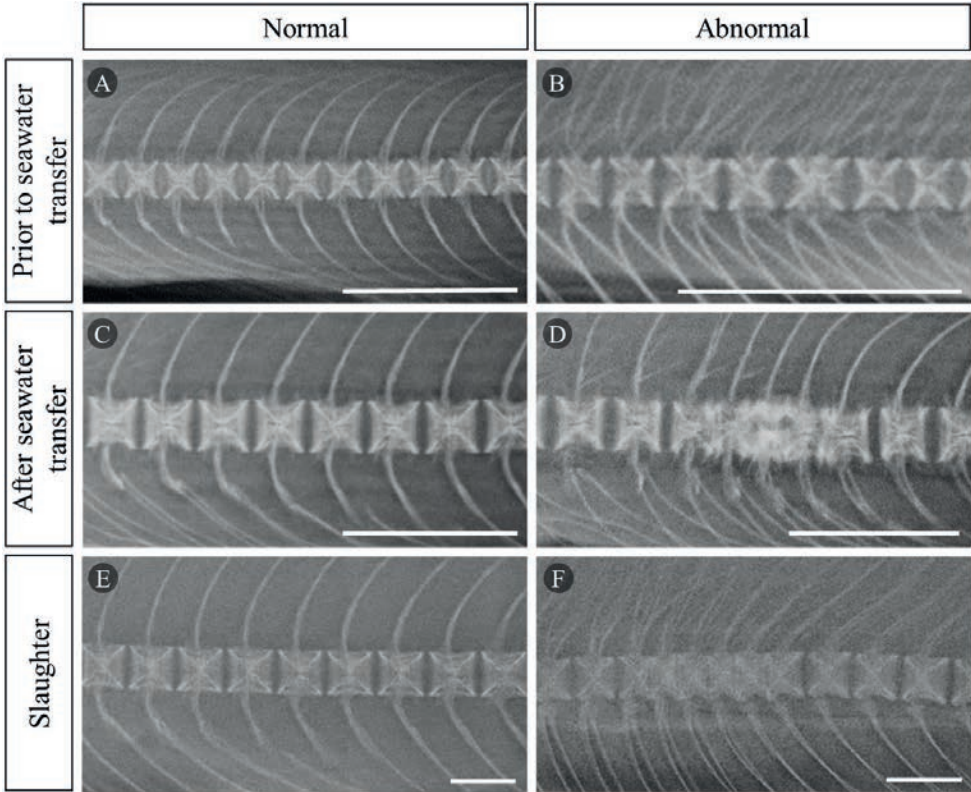
923 Supplementary 8. Scale for impaired mineralization score in salmon vertebrae from number 31
924 to 41. The score is determined according to the aspect ratio of vertebrae and the mineral density
925 around the intervertebral space (*symphysis intervertebralis*). Score 1, aspect ratio near 1 and
926 good mineral density around the intervertebral space; Score 2, aspect ratio near 0.9 and little
927 mineral density around the intervertebral space; Score 3, aspect ratio near 0.9 and very low
928 mineral density around the intervertebral space.



929

930 **9.9 Supplementary**

931 Supplementary 9. Vertebrae morphology of Atlantic salmon prior, 10 weeks after seawater
932 transfer, and at slaughter. Typical morphology of vertebra number 31 to 41 prior (A), 10 weeks
933 after seawater transfer (C) and slaughter (E). Abnormal vertebrae morphology in the form of
934 fusion prior (B), 10 weeks after seawater transfer (D) and slaughter (F). The white bars on the
935 bottom right corner show the image scale, set to 12 mm. X-ray images.



936

937

938 **9.10 Supplementary**

939 Supplementary 10. Mechanical properties and composition of vertebrae of Atlantic salmon (3
 940 kg) fed either a marine (M-group) or a plant-based diet (P-group) during smoltification.

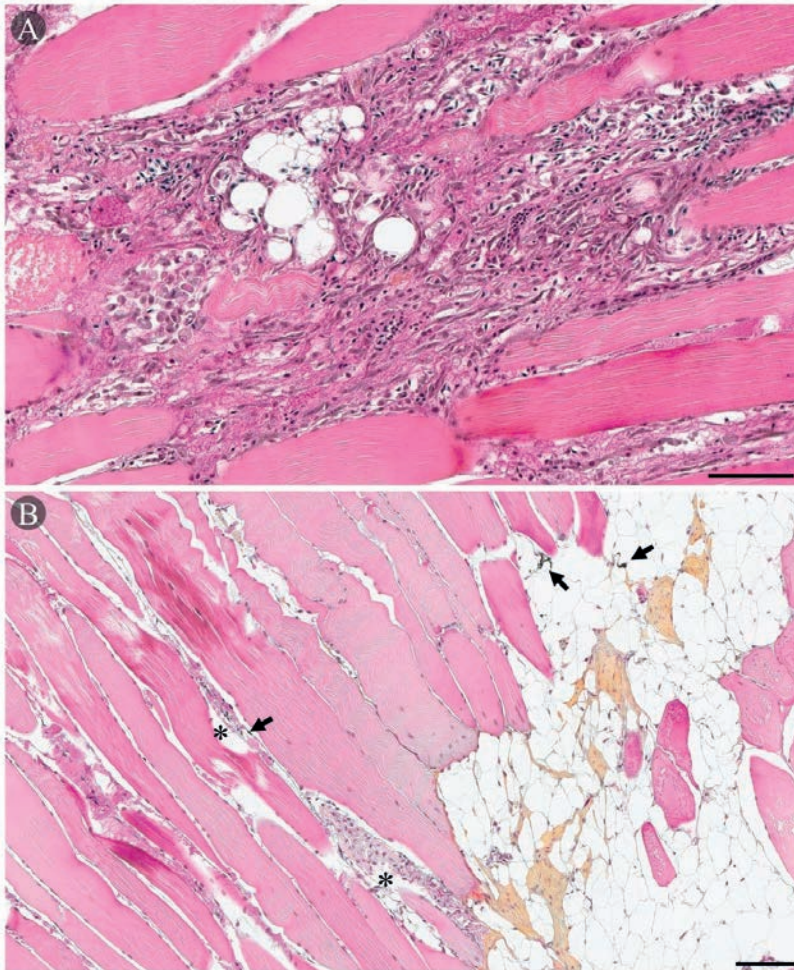
	M-group	P-group	<i>p</i> value
Mechanical properties of vertebrae			
Load (N)			
5 %	22.7 ± 0.5	19.6 ± 0.8	0.004
10 %	53.7 ± 1.4	46.4 ± 2.1	0.01
15 %	92.2 ± 2.8	81.5 ± 3.5	0.02
20 %	128.6 ± 4.4	115 ± 4.8	0.04
Area (N mm)			
5 %	4.9 ± 0.1	4.4 ± 0.2	0.01
10 %	20.2 ± 0.5	17.3 ± 0.8	0.01
15 %	50.3 ± 1.3	43.2 ± 2.2	0.01
20 %	96.6 ± 2.7	83.8 ± 4.3	0.02
Composition			
Dry matter (%)	0.56 ± 0.0	0.55 ± 0.0	0.76
Ash (%)	25.1 ± 0.4	24.7 ± 0.3	0.46
Mineral (ww)			
Ca (g kg ⁻¹)	78.1 ± 2.5	76.4 ± 1	0.56
P (g kg ⁻¹)	50.4 ± 1.8	49.3 ± 0.5	0.59
Ca:P ratio	1.5 ± 0	1.5 ± 0	0.89
K (g kg ⁻¹)	6.7 ± 0.2	6.4 ± 0.2	0.36
Na (g kg ⁻¹)	2.6 ± 0	2.7 ± 0	0.002
Mg (g kg ⁻¹)	1.6 ± 0.1	1.6 ± 0	0.64
Zn (mg kg ⁻¹)	52.1 ± 5.3	57.1 ± 5.2	0.53
Fe (mg kg ⁻¹)	7.7 ± 0.8	6.5 ± 0.3	0.25
Mn (mg kg ⁻¹)	38.1 ± 2.9	42.6 ± 1.7	0.23
Cu (mg kg ⁻¹)	0.5 ± 0.1	0.6 ± 0.1	0.49

941 Analyses were based on the vertebrae region from vertebra number 31 to 41. Significant
 942 differences between groups were set to $p \leq 0.05$. Data are presented as non-transformed mean
 943 ± SEM, n = 20 (mechanical properties), and 4 (mineral composition; pooled per tank) per
 944 dietary group. N, Newton; ww, Wet weight; Ca, Calcium; P, Phosphorus; Mg, Magnesium; K,
 945 Potassium; Na, Sodium; Zn, Zinc; Fe, Iron; Mn, Manganese; Cu, Copper.

946

947 **9.11 Supplementary**

948 Supplementary 11. Histology of focal dark spots (DS) of Atlantic salmon (3 kg). A)
949 Intramuscular hemorrhage with infiltration of inflammatory cells and degeneration of
950 myocytes; red DS. B) Disperse melanomacrophage infiltration (asterisks) in myocommata
951 (*epimysium*) and myomere (hypaxial *muscularis lateralis profundus*); black DS. Discrete
952 myocyte degeneration can be observed (black arrows). Black bars on the bottom right corner
953 show the image scale, set to 100 μm . Movat pentachrome staining.



954

955

956 **9.12 Supplementary**

957 Supplementary 12. Blood serum chemistry of Atlantic salmon fed either a marine (M-group)
 958 or a plant-based diet (P-group) during smoltification sampled prior, 10 weeks after seawater
 959 transfer, and at slaughter.

Serum parameters	Prior seawater transfer			After seawater transfer			Slaughter		
	M-group	P-group	<i>p</i> value	M-group	P-group	<i>p</i> value	M-group	P-group	<i>p</i> value
ALP (U L ⁻¹)	178 ± 9	124 ± 5	0.03	214 ± 3	264 ± 4	0.001	209 ± 7	192 ± 12	0.28
CK (U L ⁻¹)	7384 ± 3588	8753 ± 3460	0.60	3700 ± 1032	5563 ± 797	0.29	10999 ± 1702	12294 ± 779	0.51
Creatinine (µmol L ⁻¹)	51.3 ± 1.9	15.7 ± 1.3	< 0.001	19 ± 1	21 ± 1	0.29	< 13	< 13	.
Pi (mmol L ⁻¹)	4.5 ± 0	4 ± 0.2	0.15	3.1 ± 0.5	3.6 ± 0.4	0.51	6 ± 0.5	6.1 ± 0.5	0.95
Ca ²⁺ (mmol L ⁻¹)	3 ± 0.1	2.9 ± 0.1	0.87	2.9 ± 0.1	3 ± 0	0.1	3.3 ± 0	3.2 ± 0	0.67
Na ⁺ (mmol L ⁻¹)	158 ± 1	157 ± 1	0.75	164 ± 1	165 ± 1	0.1	170 ± 1	170 ± 1	0.39
K ⁺ (mmol L ⁻¹)	1.8 ± 0.3	2.1 ± 0.5	0.91	1.4 ± 0.6	1.3 ± 0.4	0.85	< 1	< 1	.

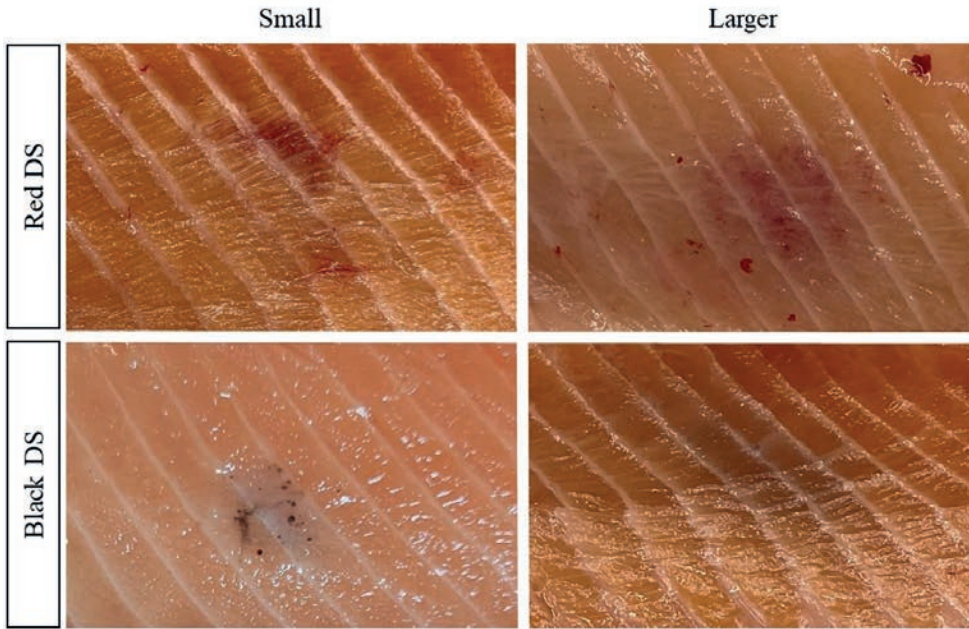
961 Significant differences between groups were set to $p \leq 0.05$.

962 Data are presented as non-transformed mean ± SEM, n = 10 - 15 per dietary group.

963 ALP, Alkaline phosphatase; CK, Creatine kinase; Pi, Inorganic phosphorous; Ca²⁺, Calcium
 964 ion; Na⁺, Sodium ion; K⁺, Potassium ion.

965 **9.13 Supplementary**

966 Supplementary 13. Focal dark spots (DS) morphology of Atlantic salmon (3 kg).



967

968

Paper III



Full length article

Differentiation and traffic of IgM⁺ B cells between focal dark spots in skeletal muscle of Atlantic salmon, lymphoid and adipose tissues

Raúl Jiménez-Guerrero^{a,*}, Christian Karlsen^b, Pierre Boudinot^c, Sergey Afanasyev^d,
Turid Mørkøre^a, Aleksei Krasnov^b

^a Department of Animal and Aquacultural Sciences, Norwegian University of Life Sciences, Ås, Norway

^b Department of Fish Health, Nofima, Ås, Norway

^c Université Paris-Saclay, INRAE, UVSQ, VIM, Jouy-en-Josas, France

^d Sechenov Institute of Evolutionary Physiology and Biochemistry, Saint Petersburg, Russia

ARTICLE INFO

Keywords:

Atlantic salmon
B-cell
Melanin spots
Healing
Gene expression
IgM repertoire

ABSTRACT

Focal dark spots (DS) in farmed Atlantic salmon filets contain a significant number of B cells as revealed by the high abundance of immunoglobulin (Ig) transcripts in transcriptome data. The immune response in DS remains unknown while they represent a major problem in commercial aquaculture. Here, we characterized the diversity and clonal composition of B cells in DS. Sixteen gene markers of immune cells and antigen presentation were analyzed with RT-qPCR. All genes expression showed a positive correlation with DS area and intensity. The flatter the DS, the higher the expression of *cd28*, *csfr*, *ctla*, *igt*, and *sigm*, the lower expression of *cd83* and *bta*, and the larger the cumulative frequency within DS. The expression of most of the analyzed immune genes, including three Ig types and markers of B cells was lower in DS than in the lymphatic organs, head kidney and spleen, but significantly higher compared to skeletal muscle. High levels of *ctla4* and *cd28* in DS might indicate the recruitment of T cells. Sequencing of IgM repertoire (Ig-seq) assessed migration of B cells by co-occurrence of identical CDR3 sequences in different tissues. The combination of gene expression and Ig-seq revealed the presence of several stages of B cell differentiation in DS. B cells at the earliest stage, with high ratio of membrane to secretory IgM (*migm* and *sigm*), showed minor Ig repertoire overlap with other tissues. Further differentiation stage (increased *sigm* to *migm* ratio and high expression of *pax5* and *cd79*) was associated with active movement of B cells from DS towards lymphatic organs and visceral fat. Traffic and expression of immune genes decreased at later stages. These B cells could be involved in a response directed against viruses, pathogenic or opportunistic bacteria in DS. Seven of eight fish were positive for salmon alphavirus, and levels were higher in DS than in unstained muscle. PCR with universal primers to the 16S rRNA gene did not detect bacteria in DS. Although the evolution of DS most likely implies local exposure to antigens, neither this nor previous studies have found a necessary association between DS and pathogens or self-antigens.

1. Introduction

Focal dark spots (DS) are red and black discolorations responsible of the major quality problem in farmed Atlantic salmon (*Salmo salar* L.), affecting about 16–18% of harvest size salmon [1]. Transcriptome profiling of DS suggested trauma as a possible etiology [2], and a recent study found a relationship between DS and damaging incidents in the rib cage [3]. Hemorrhages or red (early) DS are changes associated with a pro-inflammatory micro-environment and M1 type macrophages, while M2 type macrophages were dominating in black DS [4]. Histopathology

of DS finds varying numbers of erythrocytes, inflammatory cells, and fibrous infiltrations in different forms of chronic-active inflammatory processes [5]. Moreover, black DS typically contain abundant T cells, and MHC class I and II⁺ cells [4,6]. Transcriptome analysis revealed the presence of many B cells [2], which besides from antibody/immunoglobulin (Ig) production, might be involved in immunoregulation [7] and tissue repair [8]. The co-localization of immune responses with *Piscine orthoreovirus*-1 (PRV-1) [4,5] suggests possible intervention of pathogens in DS development.

B cells are defined as antibody-producing cells. In human and mouse,

* Corresponding author. Department of Animal and Aquacultural Sciences, Norwegian University of Life Sciences, NO-1430, Ås, Norway.

E-mail address: raul.jimenez.guerrero@nmbu.no (R. Jiménez-Guerrero).

<https://doi.org/10.1016/j.fsi.2023.108858>

Received 13 March 2023; Received in revised form 12 May 2023; Accepted 28 May 2023

Available online 10 June 2023

1050-4648/© 2023 The Authors. Published by Elsevier Ltd. This is an open access article under the CC BY license (<http://creativecommons.org/licenses/by/4.0/>).

following activation by antigen, B cells can differentiate into antibody-secreting cells, specifically, short lived plasmablasts that divide and long lived plasma cells that do not proliferate [9], as well as memory B cells, which are long-lived membrane-bound Ig cells that quickly respond to antigen upon recall [10]. In the last decade, different subsets of regulatory B cells have also been identified. In particular, plasma cells with immune regulatory functions have been described as producing interleukin-10 or interleukin-35 [7]. A first wave of B cell response against pathogens often occurs in a T-independent way, followed by a T-dependent immune response in the spleen (S) and lymph nodes, with the development of the germinal center reaction and production of antibody-secreting cells and memory cells that largely locate in the S and bone marrow [11]. However, other populations of memory B cells are located in multiple tissues with specific signatures, and the role of these tissue-resident memory B cells in protection and adaptive responses has been recently reevaluated [12]. In fish, and in particular in salmonids, both involvement of B cells in inflammatory mechanisms and circulation of responding antibody-secreting cells are poorly understood. In absence of lymph nodes, hematopoietic bone marrow and clear division of S into white and red pulp, the specialized niches of B cells are different [13]. Sequential expression of key transcription factors strongly suggest that B cell differentiation occurs in the pronephros [14], which seems to be also a niche for plasma cells. However, as very few B cell markers are targeted by available monoclonal Igs, it remains very complicated to track B cells involved in responses and inflammatory mechanisms. In this context, IgHmu repertoire comparison across different organs provides an interesting approach.

We previously developed an Ig-seq protocol – sequencing of the junctional region of IgM heavy chain transcripts (i.e., the Complementarity Determining Region (CDR)-3) [15], which led us to discover a migration pattern of B cells assessed by co-occurrence of IgHmu CDR3 sequences expressed in different tissues of the same individual [16]. Each IgHμ CDR3 sequence can be considered as a barcode for a B cell clone. Indeed, a very large diversity of junctional sequences is produced in developing B cell populations by recombination of V, D, and J genes with enzymatic insertions and deletions at joints [17]. Hence, the probability of independent production of identical CDR3 sequences is low. Such events may occur mainly for rearrangements in which no or very few nucleotides are added to the germline sequences [18]. Therefore, co-occurrence of IgHμ CDR3 sequences in different tissues or sites is generally explained by the migration of B cells belonging to the same clone, i.e., deriving from a common precursor. Our previous reports suggested that traffic increases under various conditions, such as smoltification [19], vaccination, and viral infections [20].

In this work, we propose to use IgHmu CDR3 sequences (i.e., the region encoding IgHm CDR3) to track B cell clones across different tissues, which are potentially relevant for the development of DS. Combined with other markers, including the three Ig isotypes, master regulators of B cell differentiation, markers of antigen presentation, T cells, and macrophages analyzed with RT-qPCR, we present the first geographic analysis of B cells recirculation between DS and other niches for lymphocytes that are potentially important in the development/evolution of the event. We also attempted to detect and characterize bacteria and viruses in DS.

2. Materials and methods

2.1. Fish material

Non-sexually mature and externally healthy Atlantic salmon (average weight 4.5 kg) from a commercial-scale research and development (R&D) facility were used [3]. The salmon were sampled immediately after slaughtering (electrical stunning and bleeding), and eight fish were selected for further analyses based on clearly visible DS through the parietal peritoneum. Each selected fish was sampled for head kidney (HK), S, and visceral peritoneum fat (VF) (one sample per

tissue from each fish). Samples were stored in RNAlater solution (Thermo Fisher Scientific, Waltham, MA, USA). Pictures of the DS were taken before and after the removal of the parietal peritoneum and ribs, using a Canon PowerShot G7 X Mark II (Canon Inc., Tokyo, Japan), 5472 × 3648 resolution, “Auto” mode, flash off, and ambient lighting. Dark-stained tissue from each DS was sampled (three different samples per DS from each fish). Normal skeletal muscle (SM) was sampled from the same anatomical region on the opposite fillet side to the DS (three different samples per opposite side from each fish). Samples were stored in RNAlater solution. The same DS and SM samples were used for RT-qPCR, IgM sequencing, and PCR amplification. DS were visually evaluated using a log - 2 score system based on diameter (1, grey DS < 3 cm; 2, DS < 3 cm; 4, DS 3 – 6 cm), and estimating the relative focal area (myomere²), intensity level (relative area*darkness), and shape (aspect ratio; horizontal length/vertical length) [3].

2.2. RNA extraction and RT-qPCR

Sixteen selected and a reference gene for RT-qPCR were selected with preference to the markers of antigen presentation (*cd40* and *mhc2*) and cell lineages. Analysis included the three isotypes of salmon Ig: *igd*, *igt* and *igm*. The transition from a membrane to a secretory isoform (*migm* and *sigm*) marks the beginning of antigen-dependent differentiation of naïve B cells into antibody-secreting cells. *Pax5* is essential for commitment of progenitors to B cells [21], while *blimp1* controls their terminal differentiation [22]. The temporal expression patterns of these genes in salmonid fish support their roles [23]. *Cd79* is involved in signaling after binding of antigens by B cell receptors [24]. Tyrosine kinase *blk* is expressed in differentiating and mature B cells, but not in plasma cells [25]. *Btla* (also known as *cd272*) is a negative regulator of B and T cells [26], while *cd28* and especially *ctla* are specific for activated T cells [27]. *Cd83* is a marker of dendritic cells [28], activated B cells and peripheral Tregs, *csfr* and *marco* were included in analysis as markers of macrophages. We used published primers to *blimp1* [29], *cd40*, *mhc2* [30], *cd83* [31], *csfr* [32], *igt*, *igd*, *migm* and *sigm* [33], *marco* [34] and reference gene *ef1a* [35] (Supplementary 1). Other primers were designed using OligoPerfect Primer Designer (Thermo Fisher Scientific, Waltham, MA, USA) from the same provider.

Gene expression was analyzed in the DS, SM, HK, and S samples. Tissues (5–10 mg) were placed in tubes with 400 μL lysis buffer (Qiagen, Düsseldorf, Germany) and beads, and 20 μL proteinase K (50 mg/mL) was added to each tube. Samples were homogenized in FastPrep 96 (MP Bio-medicals, Eschwege, Germany) for 120 s at maximum shaking speed, centrifuged, and incubated at 37 °C for 30 min. RNA was extracted on Biomek 4000 robot using Agencourt RNAdvance Tissue kit according to the manufacturer's instructions. RNA concentration was measured with NanoDrop One (Thermo Fisher Scientific, Waltham, MA, USA), and quality was assessed with Bioanalyzer 2100 (Agilent, Santa Clara, CA, USA). RNA was treated with DNase I (Thermo Fisher Scientific, Waltham, MA, USA) and cDNA was synthesized using TaqMan Reverse Transcription Reagent (Applied Biosystems, Waltham, MA, USA) and random hexamers. PCR was run in QuantStudio5 real-time quantitative PCR system (Applied Biosystems, Waltham, MA, USA), the reaction mixture contained 4 μL (21 μg/μL) of diluted cDNA, 5 μL SYBR™ Green Master Mix (Applied Biosystems, Waltham, MA, USA), and 1 μL of the forward and reverse primer. The program included heating for 1 min at 95 °C, amplification (1 s at 95 °C, 20 s at 60 °C) and melting curve stage. Each biological sample was run in duplicates for all genes to ensure reproducibility. After subtraction the Ct values of the reference gene, the average ΔCt was calculated for each gene in the entire data set and subtracted from each datapoint.

2.3. IgM sequencing

Analyses were performed in DS, SM, VF, S and HK samples. Synthesis of cDNA was primed with oligonucleotide to the constant region of

Atlantic salmon IgM (TAAGAGACGGGTCTGCAG), using SuperScript IV reverse transcriptase (Thermo Fisher Scientific, Waltham, MA, USA) according to the manufacturer's instructions. Libraries were prepared with two PCR reactions. The first PCR amplified cDNA with a degenerate primer TCGTCGGCAGCGTCAGATGTGTATAAGAGACAGTGARGACWCWGCWGTGTATTAYTGTG, which aligns to the 3'-end of all Atlantic salmon VH genes and a primer GTCTCGTGGGCTCGGAGATGTGTA-TAAGAGACAGGGAACAAGTCGGAGCAGTTGATGA to the 5'-end of CH. Both primers are complementary to Illumina Nextera adaptors. Reaction mixtures (20 μ L) included 10 μ L 2X Platinum™ Hot Start PCR Master Mix (Thermo Fisher Scientific, Waltham, MA, USA), 0.5 μ L of each primer (10 μ mol/ μ L), 8 μ L water, and 1 μ L template. The second PCR used Nextera™ XT Index Kit v2 (Illumina, San Diego, CA, USA), and the reaction included 2 μ L of each primer and 2 μ L product of the first PCR. PCR program included heating: 1 min at 94 °C, amplification: 10 s at 94 °C, 20 s at 53 °C, and 20 s at 72 °C (30 cycles in first PCR and 9 cycles in second PCR) and extension: 5 min at 72 °C. DNA concentration of the amplified product was measured with Qubit (Thermo Fisher Scientific, Waltham, MA, USA). Aliquots of libraries were combined and purified twice with PCR clean-up kit (Qiagen, Düsseldorf, Germany). Sequencing was carried out using Illumina MiSeq™ Reagent Kit v3, 150-cycle (Illumina, San Diego, CA, USA). Libraries were diluted to 4 nM and PhiX control was added to 0.8 nM. After the trimming of Illumina adaptors and primers and removal of low quality reads, CDR3 sequences were identified in IgH μ sequences according to the IMGT standards and definition [36], and transferred to a relational database. The frequencies of unique CDR3 sequences represented with at least two reads per 10⁵ reads were evaluated. Cumulative frequencies (CF), i.e. the sums of frequencies of the 50, 100, and 500 most expressed CDR3 were calculated. The traffic of B cells was assessed by pairwise comparison of tissues or samples from the same tissue (DS and SM). CF of CDR3 sequences detected in both compared tissues or samples were calculated. The sequences were registered in NCBI SRA (PRJNA966774).

2.4. Targeting prokaryotic DNA and RNA by PCR amplification

Samples from the RT-qPCR were used, both cDNA and a pooled sample of the corresponding RNA. The amplification of 16S rRNA gene was performed in two ways. The first used degenerate versions of the universal bacterial 16S rRNA gene primers 27F (5'-AGRGTITGATYMTGGCTACG) and 1492R (5'-GGYTACCTTGTACGACTT), with an expected amplicon of ~1400 bp. The second was with degenerate versions of primers 341F (5'-CCTACGGGNGGCWGCAG) and 785R (5'-GACTACHVGGGTATCTAATCC), with expected amplified fragments of ~440 bp. PCR of the 16S rRNA gene was performed using 150 ng and diluted 15 ng samples, 1 \times Phusion Master Mix, 0.5 μ mol/L 16S-F primer, 0.5 μ mol/L 16S-R primer, in a 50 μ L reaction volume. Extracted bacterial genomic DNA was used as positive control. Negative controls included master mix and primers without template, and reagent mix of cDNA. Samples were prepared on ice and amplified in the thermocycler with the block preheated to 98 °C. The reactions were performed using the following cycling conditions: preincubation at 98 °C for 2 min, followed by 32 cycles of denaturation at 98 °C for 10 s, annealing at 55 °C for 15 s, elongation at 72 °C for 60 s, and a final extension step at 72 °C for 3 min. Aliquots of 8 μ L of each reaction were visualized on 1.5% (w/v) agarose gel in TBE buffer using SYBR Safe stain (Edvotek Corp. USA). Absence of distinct positive 16S bands indicated low abundance or no live bacteria, except from the positive control of bacterial genomic DNA.

A further attempt used the same sample material but new \leq 10 mg tissue from DS (trimmed to include melanin clusters or granulomas), SM, S and HK. Tissue was added to ZR BashingBead Lysis Tubes (0.1 & 2.0 mL, Zymo Research) pre-filled with DNA/RNA Shield™ and homogenized with the mechanical bead beater device Precellys®24 (Bertin Technologies) for 1 \times 20 s at 5,000 rpm. Further extraction of DNA was performed using the Quick-DNA/RNA Pathogen Miniprep kit (Zymo Research, Irvine, CA) according to the manufacturer's specifications.

The DNA was eluted in ZymoBIOMICS™ DNase/RNase-Free Water and the concentration determined using a Thermo Scientific Nanodrop 2000c. PCR amplification and visualization of the 16S rRNA gene product with primers 27F/1492R was performed as described above using 1 μ L of normalized 21 ng/ μ L concentration of the extracted DNA as template. The reactions were performed using the following cycling conditions: preincubation at 98 °C for 60 s, followed by 32 cycles of denaturation at 98 °C for 10 s, annealing at 59 °C for 15 s, elongation at 72 °C for 60 s, and a final extension step at 72 °C for 2 min.

2.5. Detection of viruses by RT-PCR

Analyses were performed in DS, and SM samples. The presence of viruses infecting skeletal muscle of Atlantic salmon was checked (PatoGen AS, Ålesund, Norway) using RT-PCR. Analyses included piscine myocarditis virus (PMCV), PRV-1, and salmonid alphavirus (SAV).

2.6. Statistics

Data was analyzed with TIBCO Statistica® (v. 14.0, TIBCO Software Inc., Palo Alto, USA), R software (v. 4.0.3, R Core Team, Vienna, Austria), and Microsoft® Excel® software (v. 16.0.12527.21294, Microsoft Corporation, Redmond, USA). Correlation was assessed between gene expression ($\Delta\Delta$ Ct values) and squared root of DS characteristics: visual score, relative area, intensity level, and shape. Gene expression in tissues was analyzed with ANOVA followed by Tukey test. SAV levels (Ct values) were compared with paired *t*-test. The significance level was set at $p < 0.05$. The missing values (not detected) were set to 37.

3. Results

3.1. DS description

Sampled fish with visible peritoneum discoloration presented DS of different morphologies with a visual color score ranging from 1 to 4 (Fig. 1). All fish presented black DS, excluding fish #4, which presented an apparent combination of red and black DS. The relative area of DS ranged from 0.8 to 4.2 myomere². When including the color score, the intensity levels of DS ranged from 2.7 to 16.8. The shape of DS ranged from round (aspect ratio = 1) to very flat (aspect ratio = 8).

3.2. Correlation between gene expression, DS morphology, and CF Spot-Spot

All analyzed immune genes showed a positive correlation ($r \geq 0.42$; $p < 0.05$) between gene expression and DS area and intensity level, especially *mhc2* ($r = 0.88$ and 0.82 respectively; $p < 0.001$), *cd83* ($r = 0.81$ and 0.71 respectively; $p < 0.001$) and *igt* ($r = 0.79$ and 0.71 respectively; $p < 0.001$). The flatter the DS, the higher the expression of *cd28*, *csfr*, *ctla*, *igt* ($r \geq 0.22$; $p < 0.05$), and especially *sigm* ($r = 0.57$; $p = 0.02$), the lower expression of *cd83* ($r = -0.34$; $p = 0.01$) and *btlA* ($r = -0.31$; $p = 0.04$), and the larger the CF Spot-Spot ($r = 0.5$; $p = 0.02$). There was a positive relationship between *sigm* ($r = 0.85$; $p = 0.005$), *blimp1* expressions ($r = 0.66$; $p = 0.045$), and the CF Spot-Spot.

3.3. Tissue expression of immune genes

Overall, the expression levels of the 16 selected immune genes in DS were intermediate between the lymphatic tissues and SM. Expression of 12 genes was significantly lower in DS than in HK and S and differences were greatest in Ig (*mign*, *sigm*, *igd*, and *igt*) and four genes specific for B cells: *pax5*, *blimp1*, *blk* and *cd79* (Fig. 2). Possibility of massive recruitment of activated T cells to DS was indicated by expression of *cd28* (higher than in HK) and *ctla4* (increased in comparison with both

















ID	PARIETAL PERITONEUM DS	SKELETAL MUSCLE DS	VISUAL SCORE	RELATIVE AREA	INTENSITY LEVEL	SHAPE
1			1	1.4	3.5	5.0
3			2	0.8	2.7	1.0
4			1	3.1	7.9	1.0
5			4	3.6	10.7	8.0
6			2	4.2	16.8	3.0
7			2	2.6	10.2	1.2
8			2	2.7	8.0	4.7
9			4	3.6	14.5	7.8

Fig. 1. Visualization of focal dark spots (DS) in skeletal muscle through parietal peritoneum used for RT-qPCR and Ig-seq. DS are characterized according to visual score (1, grey DS < 3 cm; 2, DS < 3 cm; 4, DS 3–6 cm), relative area (myomere²), intensity level (relative area*darkness), and shape (aspect ratio; horizontal length/vertical length). DS are ordered according to their ID. Color print.

lymphatic organs). Transcripts of 11 genes including the membrane form of IgM (*migm*), *igd* and *pax5* were more abundant in DS than in SM of the same individual and only *cd40* was expressed at higher levels in SM. The expression of *mhc2* showed no difference between tissues (not included in Fig. 2). Though melanomacrophages are believed to play an important part in the development of DS, expression of *csfr* and *marco* in these areas was not higher than in SM.

3.4. Differentiation stages of DS B cells

Ig-seq in combination with RT-qPCR (Fig. 3) was used to investigate the circulation of B cells at different differentiation stages between DS and other (lymphoid) organs. A total of 90 libraries were sequenced (Supplementary 2). The number of high quality reads, and unique CDR3 nucleotide sequences per samples were respectively 128945 ± 28628 and 5666 ± 1686 (mean \pm SD). By CF100, which is inversely related to the repertoire diversity, tissues were divided in two groups: S and HK (6.40‰ and 8.75‰) on the one hand, and VF, DS and normal SM (15.55 – 19.58‰) on the other hand; CF100 in DS was $17.66 \pm 1.36\%$. As a guide for the assessment of B cells traffic, we suggest a model (Fig. 4. A) that integrates our results with those of our previous studies. The model defines a source tissue (the donor) and a target tissue (the recipient) based on the kinetics of Ig repertoire modifications. In this model, under basal conditions in the absence of recent immunization, the Ig

repertoires are different in each site, i.e., the CF of shared junctional sequences is low. The traffic is stimulated shortly after B cell expansion in the donor (source) tissue. Because migration to a recipient tissue begins with a lag, initial CF is higher in donor tissue. The CF of co-expressed CDR3 sequences gradually grows in the recipient tissue, while in donor tissue the frequency of the corresponding clones decreases. Egress of B cells from donor tissue continues and co-occurrence of junction sequences returns to the basal level. The B cells can reside in recipient tissues for a long time, but their connection with the original organs is not detectable anymore.

The DS from different individual fish were classified according to the stage of differentiation of their B cells (Fig. 3). High level of *migm* and low levels of *sigm* were expressed in DS of fish #4 (Fig. 3. A), suggesting that most B cells had not entered antigen-dependent differentiation into antibody-secreting cells. This was in line with higher expression of genes promoting B cell differentiation (*pax5* and *cd79*). In DS from fish #7 and 9, expression of *migm* was higher or equal to expression of *sigm* and expression of B cells-specific genes (*igd*, *igt*, *pax5* and *cd79*) was relatively high. These DS contained B cells which had started an antigen-dependent differentiation into antibody-secreting cells. Fish #5 was most likely at a subsequent stage characterized by an increased *sigm* to *migm* ratio, and lower expression of B cell-specific genes. DS from fish #1, 6, 3 and 8 (Fig. 3. B), ordered by decreasing expression level of *sigm*, still expressed more *sigm* than *migm*, and overall low levels of B cell

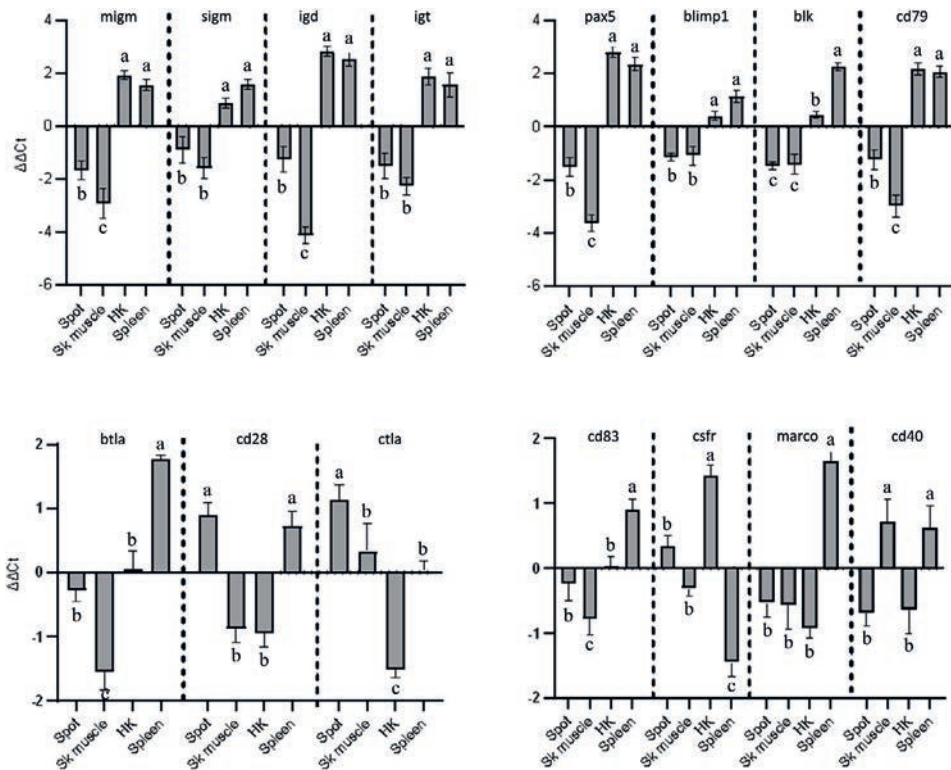


Fig. 2. Expression of immune genes (RT-qPCR). The panel presents genes with differences between tissues. Bars not sharing common letters are significantly different (ANOVA, Tukey test, $p < 0.05$).

markers (*migm*, *igd*, *igt*, *pax5* and *cd79*) suggesting a reduced amount of B cells likely due to egress.

3.5. CDR3 sharing between organs shed light on B cell recirculation pattern

The abundance of shared IgHm CDR3 between DS and other tissues was used to assess the circulation of B cells within each individual fish. To do so, we identified CDR3 in DS detected in other organs and calculated the cumulative frequencies of shared CDR3, which are represented as bar plots in Fig. 3 (right panels). These CF provide an overview of the fraction of the expressed IgM repertoire corresponding to clones shared by different organs. Sharing across DS from studied fish was analyzed following the differentiation gradient described above.

Spot/spot: The CF of shared CDR3 between the two independent samples from each DS were analyzed as a good measure of the fraction of the whole repertoire they represent. In fish #4, it is the lowest (10%), in a diverse repertoire in which Top frequent CDR3 do not represent a large fraction; The proportion is much higher in DS of fish #9, 7, 5, 1, and 6 (ranging from 30 to 60%), during B cell response while decreased in DS from fish #3 and 8 containing much fewer B cells due to egress towards other sites.

Spot/VF-HK-Spleen: CDR3 from DS of fish #4 are present at very low frequency in other tissues, while they are abundant in VF, HK, and spleen in fish #9, 7, and 5. Interestingly, these clones are particularly frequent in VF, suggesting that this tissue is an important recipient for expanded B cells migrating out of DS. The CF of DS CDR3 present in other tissues is around 10 – 15% in fish #1, 6, 3, and 8, likely

representing the situation post DS B cell responses and egress.

VF-HK-Spleen/Spot: Most frequent CDR3 sequences expressed in VF or HK or spleen were overall less frequent in DS, than CDR3 from DS were in the other organs. An interesting observation, which looks consistent across the putative developmental stages of DS B cells (hence, with fish order in Fig. 3), was that the highest sharing was between VF and DS (see fish #4, 5, 1, 6, 3), suggesting privileged B cell circulation between these tissues.

Overall, our analysis suggests that B cells can expand and mature into antibody-secreting cells within DS, then egress towards lymphoid organs, possibly with a preference for VF (Fig. 4).

3.6. Prokaryotic RNA and DNA, viral RNA

PCR analyses with universal primers found no evidence of bacterial RNA or DNA in DS and SM. All fish were free from PMCV. PRV-1 was detected in fish #5 (normal muscle and DS) and #6 (DS). Fish #6 and normal muscle of fish #2 were SAV negative. SAV was detected in all other samples and in DS its level was significantly higher: 3.9 ± 1.4 (Ct \pm SE), $p = 0.03$, paired *t*-test (Supplementary 3). No relationship was observed between SAV Ct values and DS morphology parameters (score, area, level, and shape), expression of immune genes, and CF Spot-Spot.

4. Discussion

Different hypotheses have been proposed to explain the development of DS in Atlantic salmon. Red DS are most likely initiated by damaging events in the rib cage [3], but the transition from red to black DS still

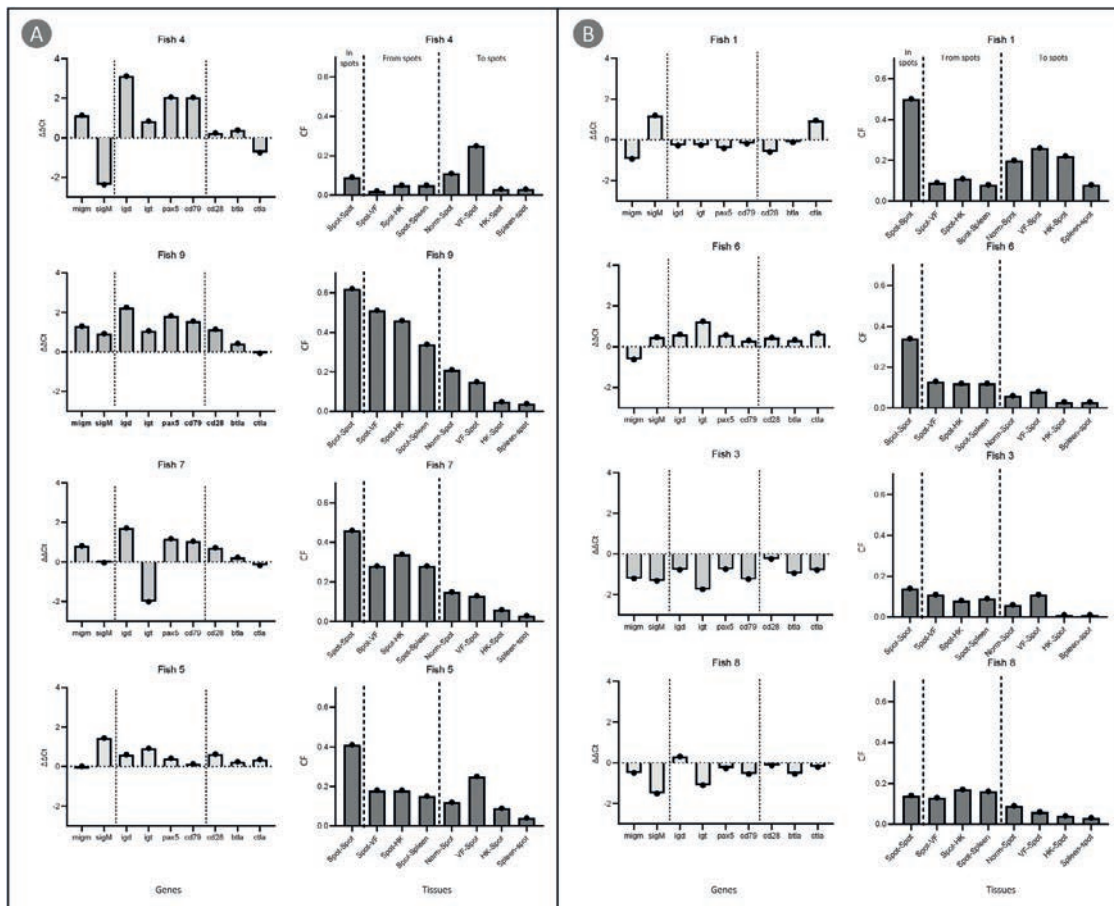


Fig. 3. Association between gene expression in focal dark spots (spots) and co-occurrence of IgM sequences in spots and tissue samples from the same individuals. Fish at early (A), mid and late stages (B) of B cells differentiation in spots: gene expression in spots (left) and cumulative frequencies (CF) of CDR3 sequences detected in spots replicates and pairs of tissues (right). VF – visceral peritoneum fat. HK – head kidney, Norm – normal skeletal muscle. The right panels represent averaged cumulative frequency of CDR3 sequences from a tissue that are expressed in another site. For example, Spot-VF and VF-Spot are cumulative frequencies of CDR3 present in both tissues are calculated in respectively spots and VF. As two independent samples have been sequenced from each spot, the first bar (Spot-Spot) corresponds to the mean of pairwise comparisons of samples from the same spot.

remains unclear. Accumulations of activated B and T cells in DS could be induced by exogenous antigens due to presence of opportunistic bacteria and/or viruses in the lesion. Previously, parallel sequencing detected higher numbers of bacterial 16s RNA transcripts in DS compared to SM from the same fish [2], supporting this first hypothesis. Infection with the PRV-1 has also been involved in the development of DS. However, given the ubiquity of this virus, the absence of DS after experimental inoculation, and the presence of DS in PRV-1 negative fish in this and previous studies [5], the PRV-1 hypothesis is put in doubt. For the same reasons, higher levels of SAV in DS shown in the present study do not mean that this virus is the causative agent, as proven by similar Ct values in all DS phases in different phases, although the presence of SAV may predispose to the development of DS. In another model, traumatic conditions might stimulate macrophages to migrate from the peritoneum to the musculoskeletal injury. These migrating macrophages could be loaded with vaccine antigens and mineral adjuvants coming from the injection site and participate in the maturation of DS [3]. Since DS can develop in non-vaccinated fish [37,38], aberrant processing of vaccine

components as a prerequisite for the development of DS can be also ruled out. Overall, the mechanisms of DS development remain poorly understood. It is possible that different antigens can cause reactions leading to the accumulation of melanin.

In the present work, we analyzed DS from healthy salmon from a commercial population aged 14 months (4.5 kg) after seawater transfer. From these DS samples, we failed to amplify any bacterial RNA or DNA with PCR, indicating there were not association to ongoing bacterial infection. It might be possible that melanomacrophages had remained in skeletal muscle after an infection had been eliminated. Gene expression profiles revealed that DS contained several populations of B cells with different proportions of naïve and Ab-secreting cells and different levels of IgHmu (*sigm/migm*) expression. IgHm CDR3 sequencing further showed that B cells present in DS belong to many clones, and circulate to other issues including VF, S, and HK. Thus, B cells represent an important and complex cellular component of these inflammatory events, with potential consequences on both DS fate and B cell repertoire.

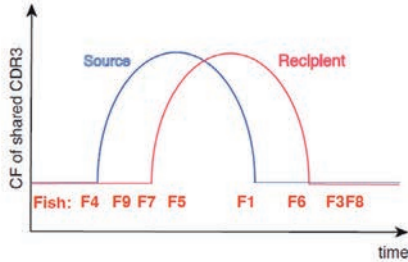
The local environment of DS is characterized by a high density of

A Model of B cell trafficking between tissues during the immune response

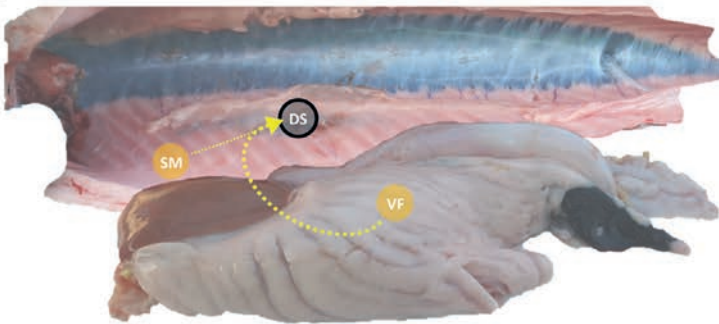
Definitions:
 «Source» or «donor» tissue: from which B cells egress during the response
 «Recipient» tissue: into which B cells traffic during the response

Model:
 Evolution of CF of most frequent CDR3 (for example, Top100 or shared CDR3) in both source and recipient tissues typically follows a bell shape trajectory during the response. The curve in the recipient tissue is shifted (delayed) from the source tissue by about two days, and the model predicts that B cells move from source to recipient.

The panel below illustrates the model and the trade off between source and recipient tissues. Each analysed fish is also placed at the stage of the response suggested by the repertoire analysis.



B B cell traffic from tissues to DS



C B cell traffic from DS to other tissues

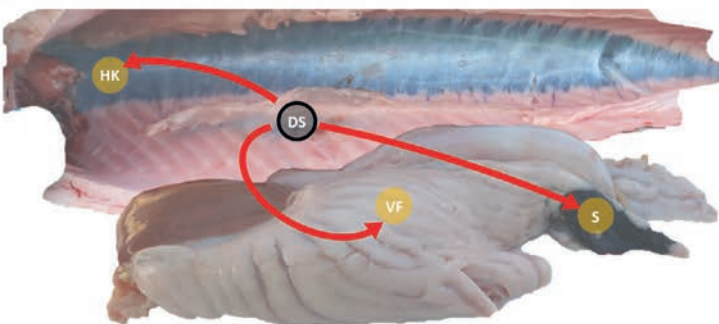


Fig. 4. Model of B cell traffic in Atlantic salmon between focal dark spots (DS) and other tissues. (A) Model of B cell traffic between a “source” tissue and “recipient” tissue. CF – cumulative frequency. (B) Schematic illustration of B cell traffic. Discontinuous yellow arrows illustrate the likely B cell traffic between tissues before the formation of DS. SM – normal skeletal muscle. VF – visceral peritoneum fat. (C) After exposure to antigens, B cells migrate from DS to other tissues including head kidney (HK), VF and spleen (S) indicating systemic immunization. Continuous red arrows represent the traffic between B cells resident organs or tissues, and DS. The thickness of the arrows indicates the order of shared CF. Based on Fig. 3. Color print.

melanomacrophages, which are involved in antigen processing and presentation [39]. The role of these cells in fish B cell activation and differentiation seems to be complex. In lymphoid organs, it has been proposed that aggregates of melanomacrophages are associated with B

cells that express activation-induced cytidine deaminase and undergo somatic hypermutation [40], reminiscent of mammalian germinal centers. However, melanomacrophages are also found in other tissues, especially in the liver in fish, amphibians, and reptiles, and those do not

express activation-induced cytidine deaminase. Incidentally, melano-macrophage centers may also function as focal depositories for intracellular pathogenic bacteria [41], which might explain the associations with bacteria previously reported.

We consider that our data are more in favor of an endogenous path scenario for DS formation [42]. Firstly, there seemed to be an association between DS morphology and the phase of the process, being the CF Spot-Spot and *sigm* expression larger the flatter the DS. Therefore, this points to more B cell activity in flatter DS, which is a link between the type/degree of the initial damage and the immune microenvironment. Secondly, flatter, larger, more intense DS, which is associated with recurrent injury processes [3], also showed higher expression of both innate (macrophage, antigen presentation) and adaptive (B cells, and T helper and cytotoxic cells) immune response genes. Thus, it seems reasonable that continuous mechanical stress in damaged muscle and ribs generates cell damage that may expose lymphocytes to a constant source of autoantigens [43,44] in a pro-activating context leading to melanomacrophage aggregates, where B cells may also acquire a regulatory phenotype driven by local inflammation [45], or respond to tissue regeneration with myoblasts expressing high levels of myositis autoantigens [43,46]. Activation of the immune response in DS in absence of pathogens is in line with the “danger model” proposed by Matzinger [47]. B cells and Ig isolated from DS could be useful for identifying key (auto)antigens involved in DS development in future research. Further transcriptome analysis of DS antibody-producing B cells (with a focus on key factors like BAFF, transcription factors like HIF and TRAF3) might provide insights into their autoimmune phenotype, as reviewed in Mubarki and Vadasz [48].

To gain insight into the involvement of B cells in DS biology, we studied differentiation and traffic of B cells. B cells could enter the antigen-dependent differentiation in the lymphatic tissues and later migrate to DS. Alternatively, B cells might be activated locally, in developing DS in skeletal muscle, and either reside at the site of antigen deposition or migrate to other tissues. We expected preferential migration of B cells from the HK and S to peripheral tissues, including DS. However, our analyses suggested that an antigen stimulated differentiation was rather initiated in DS followed by subsequent migration of cells, a typical finding in inflammatory myopathies in humans [42,49].

We propose here a model (Fig. 4. A) that integrates the conclusions of our data with previous studies [15,19,20]. B cells would recognize their cognate antigen in the DS, start differentiating into antibody-secreting cells and move from DS to other tissues. This model predicts low co-occurrence of clones in different tissues under basal condition and higher CF of shared CDR3 sequences in donor at early phase, and in recipient tissue at late phases. The IgM repertoire in DS with the highest *migm* to *sigm* ratio showed minor overlap with other tissues and co-occurrence of CDR3 sequences was very low even in the replicates from the same area (fish #4 in Fig. 3. A). In fish with relatively high expression of both membrane and secreted IgM in DS, CF of shared CDR3 sequences was greater in DS than in other tissues including the S and HK; this suggested co-ordination between antigen stimulated differentiation and traffic of B cells. CF in non-DS samples was higher than in DS in only one individual in concordance with decreased *migm* to *sigm* ratio in DS (fish #1 in Fig. 3. B). Low expression of B cell-specific genes corresponding to the late phase of B cells development coincided with limited sharing. Co-occurrence of CDR3 sequences in DS and VF was greater than in the lymphatic organs indicating that adipose tissue serves as a depot of lymphocytes and can be a transition point in their migration. B cells residing in VF and their responses to vaccination have been characterized in rainbow trout [50] and may constitute a particular B cell population. It will be interesting to investigate the origin and fate of this population, and its relationship with DS B cells. Taken together, our results suggest a local exposure to antigens initiated in melanized foci, which may lead to systemic responsiveness of fish due to active migration of B cells. Thus, if the development of DS is triggered with muscle autoantigens, this might pose a risk of immune-mediate

inflammatory myopathies [42]. The phenotype of B cells relocated from DS to other tissues will have to be further characterized to understand their functionality.

5. Conclusion

We show here that B cells traffic between melanized foci and other tissues, implying systemic spreading of clones involved in local DS responses. While the role of DS B cells in the formation of black DS remains unknown, our data provide a new frame to associate B cell responses and maturation with DS evolution. Longitudinal studies starting from the first detection of DS to complete maturation will be important to better understand the mechanisms underlying the development.

Funding

The study was supported by the Norwegian Seafood Research Fund (FHF) (901487), the Norwegian University of Life Sciences (NMBU), the Agence Nationale de la Recherche (ANR) (ANR-21-CE35-0019), and the Sechenov Institute of Evolutionary Physiology and Biochemistry of RAS (No. 075-00967-23-00). Fish material belonged to the Nofima's R&D licenses granted by the Norwegian Directorate of Fisheries for large-scale Industrial Research.

CRedit authorship contribution statement

Raúl Jiménez-Guerrero: Investigation, Validation, Formal analysis, Data curation, Resources, Visualization, Writing – original draft, Writing – review & editing. **Christian Karlsen:** Investigation, Validation, Resources, Visualization, Supervision, Writing – original draft. **Pierre Boudinot:** Methodology, Validation, Investigation, Resources, Visualization, Supervision, Formal analysis, Funding acquisition, Writing – original draft, Writing – review & editing. **Sergey Afanasyev:** Investigation, Resources, Validation, Formal analysis, Investigation, Data curation, Funding acquisition, Software. **Turid Mørkøre:** Validation, Formal analysis, Investigation, Resources, Visualization, Supervision, Project administration, Conceptualization, Funding acquisition, Writing – original draft. **Aleksei Krasnov:** Conceptualization, Methodology, Validation, Investigation, Formal analysis, Investigation, Visualization, Supervision, Software, Writing – original draft, Writing – review & editing.

Data availability

Data will be made available on request.

Acknowledgments

The authors acknowledge the skillful assistance and dedicated fish management of the technicians at Leroy Midt AS, with special thanks to Helge Endresen. The authors remark on the excellent work during sampling provided by Dr. Jens-Erik Dessen and Håkon Torsvik. We wish to thank Vibeke Voldvik and Marianne Hansen for their help during RT-qPCR analyses and Ig sequencing.

Appendix A. Supplementary data

Supplementary data to this article can be found online at <https://doi.org/10.1016/j.fsi.2023.108858>.

References

- [1] T. Mørkøre, T. Larsson, R. Jiménez-Guerrero, H.M. Moreno, J. Borderias, B. Ruyter, I.B. Standal, A. Sarno, Ø. Evensen, J.-E. Dessen, K.-A. Rørvik, K. Hamre, Ø. Andersen, K. Wakamatsu, S. Ito, K.H. Gannestad, C. Xu, T.-K. Østbye, B. Hillestad, J.S. Torgersen, G. Bæverfjord, EX-Spot, Mørke flekker i laksefilet, Nofima, 2022, p. 78.

- [2] A. Krasnov, H. Moghadam, T. Larsson, S. Afanasyev, T. Mørkøre, Gene expression profiling in melanized sites of Atlantic salmon filets, *Fish Shellfish Immunol.* 55 (2016) 56–63.
- [3] R. Jiménez-Guerrero, G. Baeverfjord, Ø. Evensen, K. Hamre, T. Larsson, J.-E. Dessen, K.-H. Ganestad, T. Mørkøre, Rib abnormalities and their association with focal dark spots in Atlantic salmon filets, *Aquac* 561 (2022), 738697.
- [4] M.S. Malik, H. Bjørgen, I.B. Nyman, Ø. Wessel, E.O. Koppang, M.K. Dahle, E. Rimstad, PRV-1 Infected macrophages in melanized focal changes in white muscle of Atlantic Salmon (*Salmo salar*) correlates with a pro-inflammatory environment, *Front. Immunol.* 12 (2021), 664624.
- [5] H. Bjørgen, R. Haldorsen, Ø. Oaland, A. Kvellestad, D. Kannimathu, E. Rimstad, E. O. Koppang, Melanized focal changes in skeletal muscle in farmed Atlantic salmon after natural infection with *Piscine orthoreovirus* (PRV), *J. Fish. Dis.* 42 (6) (2019) 935–945.
- [6] H.A. Larsen, L. Austbø, T. Mørkøre, J. Thorsen, I. Hordvik, U. Fischer, E. Jirillo, E. Rimstad, E.O. Koppang, Pigment-producing granulomatous myopathy in Atlantic salmon: a novel inflammatory response, *Fish Shellfish Immunol.* 33 (2) (2012) 277–285.
- [7] D. Catalán, M.A. Mansilla, A. Ferrier, L. Soto, K. Oleinika, J.C. Aguilón, O. Aravena, Immunosuppressive mechanisms of regulatory B cells, *Front. Immunol.* 12 (2021).
- [8] R.F. Sîrbulescu, A. Mamidi, S.-Y.C. Chan, G. Jin, M. Boukhali, D. Sobell, I. Ilies, J. Y. Chung, W. Haas, M.J. Whalen, A.E. Sluder, M.C. Poznansky, B cells support the repair of injured tissues by adopting MyD88-dependent regulatory functions and phenotype, *Faseb. J.* 35 (12) (2021), e22019.
- [9] S.L. Nutt, P.D. Hodgkin, D.M. Tarlinton, L.M. Corcoran, The generation of antibody-secreting plasma cells, *Nat. Rev. Immunol.* 15 (3) (2015) 160–171.
- [10] I. Dogan, B. Bertocci, V. Vilmont, F. Delbos, J. Mégret, S. Storck, C.A. Reynaud, J. C. Weill, Multiple layers of B cell memory with different effector functions, *Nat. Immunol.* 10 (12) (2009) 1292–1299.
- [11] E. Paramithiots, M.D. Cooper, Memory B lymphocytes migrate to bone marrow in humans, *Proc. Natl. Acad. Sci. U. S. A.* 94 (1) (1997) 208–212.
- [12] C. Chen, B.J. Laidlaw, Development and function of tissue-resident memory B cells, *Adv. Immunol.* 155 (2022) 1–38.
- [13] H. Bjørgen, E.O. Koppang, Anatomy of teleost fish immune structures and organs, in: K. Buchmann, C.J. Secombes (Eds.), *Principles of Fish Immunology* : from Cells and Molecules to Host Protection, Springer International Publishing, Cham, 2022, pp. 1–30.
- [14] B. Abós, C. Bailey, C. Tafalla, Adaptive immunity, in: K. Buchmann, C.J. Secombes (Eds.), *Principles of Fish Immunology* : from Cells and Molecules to Host Protection, Springer International Publishing, Cham, 2022, pp. 105–140.
- [15] A. Krasnov, S.M. Jørgensen, S. Afanasyev, Ig-seq: deep sequencing of the variable region of Atlantic salmon IgM heavy chain transcripts, *Mol. Immunol.* 88 (2017) 99–105.
- [16] A.F. Bakke, H. Bjørgen, E.O. Koppang, P. Frost, S. Afanasyev, P. Boysen, A. Krasnov, H. Lund, IgM+ and IgT+ B cell traffic to the heart during SAV infection in Atlantic salmon, *Vaccines* 8 (3) (2020).
- [17] C.H. Bassing, W. Swat, F.W. Alt, The mechanism and regulation of chromosomal V (DJ) recombination, *Cell* 109 (Suppl) (2002) S45–S55.
- [18] M. Yasuike, J. de Boer, K.R. von Schalburg, G.A. Cooper, L. McKinnel, A. Messmer, S. So, W.S. Davidson, B.F. Koop, Evolution of duplicated IgH loci in Atlantic salmon, *Salmo salar*, *BMC Genom.* 11 (1) (2010) 486.
- [19] H. Lund, A. Bakke, P. Boysen, S. Afanasyev, A. Rebl, F. Manji, G. Ritchie, A. Krasnov, Evaluation of immune status in two cohorts of Atlantic salmon raised in different aquaculture systems (case study), *Genes* 13 (5) (2022).
- [20] A.F. Bakke, H. Bjørgen, E.O. Koppang, P. Frost, S. Afanasyev, P. Boysen, A. Krasnov, H. Lund, IgM+ and IgT+ B cell traffic to the heart during SAV infection in Atlantic salmon, *Vaccines* 8 (3) (2020) 493.
- [21] C. Cobaleda, A. Schebesta, A. Delogu, M. Busslinger, Pax5: the guardian of B cell identity and function, *Nat. Immunol.* 8 (5) (2007) 463–470.
- [22] S.L. Nutt, K.A. Fairfax, A. Kallies, BLIMP1 guides the fate of effector B and T cells, *Nat. Rev. Immunol.* 7 (12) (2007) 923–927.
- [23] P. Zwollo, Dissecting teleost B cell differentiation using transcription factors, *Dev. Comp. Immunol.* 35 (9) (2011) 898–905.
- [24] P.G. Chu, D.A. Arber, CD79: a review, *Appl. Immunohistochem. Mol. Morphol.* 9 (2) (2001) 97–106.
- [25] S.M. Dymecki, P. Zwollo, K. Zeller, F.P. Kuhajda, S.V. Desiderio, Structure and developmental regulation of the B-lymphoid tyrosine kinase gene *blk*, *J. Biol. Chem.* 267 (7) (1992) 4815–4823.
- [26] C. Zeng, T. Wu, Y. Zhen, X.P. Xia, Y. Zhao, BTLA, a new inhibitory B7 family receptor with a TNFR family ligand, *Cell. Mol. Immunol.* 2 (6) (2005) 427–432.
- [27] D. Bernard, A. Six, L. Rigottier-Gois, S. Messiaen, S. Chlmonczyk, E. Quillet, P. Boudinot, A. Benmansour, Phenotypic and functional similarity of gut intraepithelial and systemic T cells in a teleost fish, *J. Immunol.* 176 (7) (2006) 3942–3949.
- [28] R.M. Steinman, M. Pack, K. Inaba, Dendritic cells in the T-cell areas of lymphoid organs, *Immunol. Rev.* 156 (1997) 25–37.
- [29] B. Abós, R. Castro, J. Pignatelli, A. Luque, L. González, C. Tafalla, Transcriptional heterogeneity of IgM+ cells in rainbow trout (*Oncorhynchus mykiss*) tissues, *PLoS One* 8 (12) (2013), e82737.
- [30] L.X. Lagos, D.B. Iliev, R. Helland, M. Roseblatt, J.B. Jørgensen, CD40L–a costimulatory molecule involved in the maturation of antigen presenting cells in Atlantic salmon (*Salmo salar*), *Dev. Comp. Immunol.* 38 (3) (2012) 416–430.
- [31] D.B. Iliev, G. Strandskog, M. Sobhkhz, J.A. Bruun, J.B. Jørgensen, Secretome profiling of Atlantic salmon head kidney leukocytes highlights the role of phagocytes in the immune response to soluble β -glucan, *Front. Immunol.* 12 (2021), 736964.
- [32] M.M.D. Peñaranda, I. Jensen, L.G. Tollersrud, J.A. Bruun, J.B. Jørgensen, Profiling the Atlantic salmon IgM(+) B cell surface proteome: novel information on teleost fish B cell protein repertoire and identification of potential B cell markers, *Front. Immunol.* 10 (2019) 37.
- [33] T.M. Tadisó, K.K. Lie, I. Hordvik, Molecular cloning of IgT from Atlantic salmon, and analysis of the relative expression of τ , μ , and δ in different tissues, *Vet. Immunol. Immunopathol.* 139 (1) (2011) 17–26.
- [34] Y.A. van der Wal, S. Jenberie, H. Nordli, L. Greiner-Tollersrud, J. Kool, I. Jensen, J. B. Jørgensen, The importance of the Atlantic salmon peritoneal cavity B cell response: local IgM secreting cells are predominant upon *Piscirickettsia salmonis* infection, *Dev. Comp. Immunol.* 123 (2021), 104125.
- [35] K. Julin, L.H. Johansen, A.I. Sommer, Reference genes evaluated for use in infectious pancreatic necrosis virus real-time RT-qPCR assay applied during different stages of an infection, *J. Virol. Methods* 162 (1–2) (2009) 30–39.
- [36] M.-P. Lefranc, **The immunologist**. <https://www.imgt.org/IMGTScientificChart/Nomenclature/IMGT-FCRDRdefinition.html>, 1999. (Accessed 7 May 2023).
- [37] T. Mørkøre, Mørke Flekker I Laksefeltet – Kunnskapstatus Og Tiltak for Å Begrense Omfanget, 2012. Nofima.
- [38] A. Berg, A. Yurtseva, T. Hansen, D. Lajus, P.G. Fjellidal, Vaccinated farmed Atlantic salmon are susceptible to spinal and skull deformities, *J. Appl. Ichthyol.* 28 (3) (2012) 446–452.
- [39] A.E. Ellis, M. de Sousa, Phylogeny of the lymphoid system. I. A study of the fate of circulating lymphocytes in plaice, *Eur. J. Immunol.* 4 (5) (1974) 338–343.
- [40] D. Waly, A. Muthupandian, C.W. Fan, H. Anzinger, B.G. Magor, Immunoglobulin VDJ repertoires reveal hallmarks of germinal centers in unique cell clusters isolated from zebrafish (*Danio rerio*) lymphoid tissues, *Front. Immunol.* 13 (2022), 1058877.
- [41] C. Agius, R.J. Roberts, Melano-macrophage centres and their role in fish pathology, *J. Fish. Dis.* 26 (9) (2003) 499–509.
- [42] A. Farini, C. Villa, L. Tripodi, M. Legato, Y. Torrente, Role of immunoglobulins in muscular dystrophies and inflammatory myopathies, *Front. Immunol.* 12 (2021).
- [43] N. Kimura, S. Hirata, N. Miyasaka, K. Kawahata, H. Kohsaka, Injury and subsequent regeneration of muscles for activation of local innate immunity to facilitate the development and relapse of autoimmune myositis in C57BL/6 Mice, *Arthritis Rheumatol.* 67 (4) (2015) 1107–1116.
- [44] C. Sciorati, E. Rigamonti, A.A. Manfredi, P. Rovere-Querini, Cell death, clearance and immunity in the skeletal muscle, *Cell Death Differ.* 23 (6) (2016) 927–937.
- [45] S. Fillatreau, Natural regulatory plasma cells, *Curr. Opin. Immunol.* 55 (2018) 62–66.
- [46] T.L. Suber, L. Casciola-Rosen, A. Rosen, Mechanisms of disease: autoantigens as clues to the pathogenesis of myositis, *Nat. Clin. Pract. Rheumatol.* 4 (4) (2008) 201–209.
- [47] P. Matzinger, Tolerance, danger, and the extended family, *Annu. Rev. Immunol.* 12 (1994) 991–1045.
- [48] R. Mubarik, Z. Vadász, The role of B cell metabolism in autoimmune diseases, *Autoimmun. Rev.* 21 (7) (2022), 103116.
- [49] M. Salajegheh, J.L. Pinkus, A.A. Amato, C. Morehouse, B. Jallal, Y. Yao, S. A. Greenberg, Permissive environment for B-cell maturation in myositis muscle in the absence of B-cell follicles, *Muscle Nerve* 42 (4) (2010) 576–583.
- [50] R. Simón, A. Martín-Martín, E. Morel, P. Díaz-Rosales, C. Tafalla, Functional and phenotypic characterization of B cells in the teleost adipose tissue, *Front. Immunol.* 13 (2022).

ISBN: 978-82-575-2097-7

ISSN: 1894-6402



Norwegian University
of Life Sciences

Postboks 5003
NO-1432 Ås, Norway
+47 67 23 00 00
www.nmbu.no